INTERACTION OF ANTICANCEROUS DRUG DAUNOMYCIN WITH NUCLEIC - ACIDS

A THESIS

submitted in fulfilment of the requirements for the award of the degree of

DOCTOR OF PHILOSOPHY

By

UMA SHARMA

DEPARTMENT OF BIOSCIENCES AND BIOTECHNOLOGY
UNIVERSITY OF ROORKEE
ROORKEE-247 667 (INDIA)

FEBRUARY, 1996

CANDIDATE'S DECLARATION

I hereby certify that the work which is being presented in this thesis entitled **"INTERACTION OF ANTICANCEROUS DRUG DAUNOMYCIN WITH NUCLEIC-ACIDS"** in fulfilment of the requirements for the award of the Degree of **DOCTOR OF PHILOSOPHY**, submitted in the Department of Biosciences and Biotechnology of the University is an authentic record of my work carried out during a period from August, 1990 to February, 1996 under the supervision of Dr. (Mrs.) Ritu Barthwal, Head and Reader, Department of Biosciences and Biotechnology, University of Roorkee, Roorkee.

The matter presented in this thesis has not been submitted by me for the award of any other degree of this or any other University.

Uma Sharma

Date : 15.02.96 **(UMA SHARMA)**

This is to certify that the above statement made by the candidate is correct to the best of my knowledge.

Ritu Barthwal

(RITU BARTHWAL) 15/02/96

Head & Reader, Deptt.
of Biosciences & Biotechnology

The Ph.D. Viva-Voce examination of Ms. UMA SHARMA Research Scholar, has been held on NOV 16, 1996

Signature of Supervisor & Signature of Head of the Department

Ritu Barthwal

Professor & Head
Deptt. of Biosciences and
Biotechnology
University of Roorkee
Roorkee

Signature of External Examiner

C. L. Khetrapal

(C. L. KHETRAPAL)
Professor & Head SIF
Indian Instt of Science
Bangalore

ABSTRACT

Nature has evolved a diverse set of antibiotics that bind to DNA in a variety of ways, but with the common ability to act as potent inhibitors of DNA transcription and replication. As a consequence, these natural products have been of considerable interest as potential anti cancer agents. Many synthetic compounds have been added to this list in the search for more potent drugs for use in chemotherapy. While it is appreciated that DNA is a primary target for many potent antitumor agents, data that pin-point the exact mechanism of action are generally unavailable. A substantial body of research has been directed towards understanding the molecular basis for DNA sequence specificity for binding, by identifying the preferred binding sequences of many key drugs with DNA. Structural tools such as x-ray crystallography and NMR spectroscopy, coupled with molecular modelling techniques have had considerable impact in advancing our understanding of the microscopic structural heterogeneity of DNA and the molecular basis for drug-DNA interactions.

Daunomycin is an anticancer antibiotic isolated from *Streptomyces peucetius*; active mainly against acute lymphocytic leukemia. It inhibits in vitro growth of both normal and cancer cell lines and as a consequence nuclear damage occurs. Chromosomal and genetic aberrations of several types are produced by daunomycin.

The present study has been undertaken to get a new insight of the conformational features of daunomycin in solution using one-dimensional and two-dimensional NMR techniques at 500 MHz. The three-dimensional structure obtained by spin-spin coupling constraints, interproton distances has been compared with that obtained by x-ray crystallography. The conformation of deoxyhexanucleotide d-$(TGATCA)_2$ is investigated in D_2O. Geometry of the deoxyribose sugar of each residue is deduced using double quantum filter COSY (DQF) cross peak patterns, spin-spin coupling constants and sums of couplings obtained from one-dimensional NMR. The relative intensities of cross peaks obtained in NOESY spectra recorded at various mixing times have been used independently to deduce the geometry of deoxyribose sugar. The base to sugar proton NOE connectivities have been used to get information on glycosidic bond rotation.

The complex of daunomycin and d-$(TGATCA)_2$ has been obtained at various drug to DNA concentration ratio by adding daunomycin to d-$(TGATCA)_2$ in steps to achieve 2:1 complex. Titration studies have been carried out using 1D proton NMR. While two-dimensional NMR technique serves as a tool to assign all proton NMR signals unambiguously and determine the conformational features such as sugar puckering, helix sense, glycosidic bond rotation in complexed form. The changes in chemical shifts are attributed to stacking, alterations in base-base overlap etc. The NOE connectivities within the drug and DNA molecules are used to obtain the change in conformation of DNA and daunomycin due to

interaction. Several intermolecular NOEs between protons of ring D and base protons of 5′-3′ d-TpG step are direct proof of intercalation of aglycon chromophore of the drug between base pairs.

Several intermolecular NOEs between daunosamine sugar protons and A3 and T4 residues of d-$(TGATCA)_2$ indicate the proximity of sugar protons to the third base pair in the sequence. The results are discussed with a view to understand the implications of binding.

ACKNOWLEDGEMENTS

I wish to express my sincere thanks and gratitude to Dr. Ritu Barthwal, Head and Reader, Department of Biosciences and Biotechnology, University of Roorkee, Roorkee for providing her supervision, valuable criticism, expert guidance and constant encouragement throughout the completion of this work.

I wish to express my appreciation and thanks to my senior Dr. Anwer Mujeeb, for his timely help and support. It would have been very difficult to complete my work without his help.

I am most grateful to all the members of FT-NMR National facility at TIFR, Bombay for extending their cooperation during my stay. I take this oppurtunity to thank Mamta, Devidas and Mr. Ranpura for providing friendly atmosphere and helping me.

I thank Prof. V.S. Chauhan, ICGEB New Delhi and Prof. K.B. Roy, JNU New Delhi for providing me all required research facilities for synthesis and purification of DNA samples. I acknowledge the help provided by Tapas. He worked hard along with me during synthesis and purification of DNA samples.

Financial assistance rendered by Department of Science and Technology and University Grants Commision, Government of India, is gratefully acknowledged.

Now at this moment when I stop and ponder I recall many friends who have been a great help to me. I thank Neerja, Shoma and Dr. Neeti for helping me in more ways than I recount. I don't find words to express my feelings for Nandana, who was with me in my most difficult times. Her assistance and support helped me see through this long period. I enjoyed working with Sadhna, Rashmi, Ritu, Shalini, Ramesh and Jignesh.

My parents and in-laws have contributed much to this thesis, they have provided love and affection, to bring this dissertation to fruition. My husband Vyom has provided love support and has been with me throughout this tenure.

I acknowledge Mr. Seva Ram for carefully typing this thesis.

(UMA SHARMA)

LIST OF PUBLICATIONS

1. Barthwal R., Srivastava N., Sharma U. and Govil G. A 500 MHz proton NMR study of the conformation of adriamycin. J. Mol. Struc., 1994, 327, 201.

2. Barthwal R., Mujeeb A., Srivastava N. and Sharma U. A proton nuclear magnetic resonance investigation of the conformation of daunomycin. Chemico-Biol. Interact., 1996, (in press).

CONTENTS

CHAPTER - i

INTRODUCTION

A large number of antibiotics exert their effect primarily by interacting directly with the genetic material of cells i.e. with DNA. In doing so, these compounds impair the ability of DNA to act as a template for the processes of nucleic-acid expression and synthesis. Owing to DNA's central role in biological replication and protein biosynthesis, modification by such interaction greatly alters cell metabolism, diminishing and in some cases terminating the cell growth. There is much pharmacological evidence from cytological, antimitotic and mutagenic effects and the inactivation of viruses, indicating that DNA is the principal cell target for many antitumor agents.

Interaction of antitumor agents with DNA has been the subject of intensive and increasing study over a period of time for two principal reasons ; firstly, one of the most important lines of drug development and of current chemotherapy against cancer, viral, and some parasitic diseases involves drugs which interact reversibly with nucleic-acids. These are widely used in clinical treatment of a variety of neoplastic diseases for example - daunomycin, adriamycin, nogalamycin, etc. Much of the drive to understand drug-DNA interactions has come from the interest in understanding the mode of action of existing medicinal agents and from the desire to develop a new generation of superior drugs.

Secondly, because of their relative simplicity, the interactions of drug molecules with nucleic-acids have provided much of our most accurate information about nucleic-acid binding specificity, ligand-induced conformational transitions, the molecular basis of cooperativity in binding, the interaction of aromatic amino acid side chains with nucleic-acid bases, and other similar critical features of nucleic-acid interactions and chemistry.

Anticancer agents both naturally occurring and synthetic, employed in treatment of cancer interact with double-stranded DNA primarily by:

(i) Covalent interactions e.g. aziridine antibiotics, pyrrolo (1,4) benzodiazepines and spirocyclopropane.

(ii) Reversible interactions e.g. groove binding drugs and intercalating drugs.

AGENTS INTERACTING WITH DNA COVALENTLY

There are wide variety of anticancerous agents which form covalent bonds to nucleic-acids. These are either electrophiles or generate electrophiles in vivo including carbonium ions or their kinetic equivalents (such as chloronium ions or alkyl diazotates) which may attack electron-rich sites in biological macromolecules, adding alkyl groups to nitrogen, sulphur or oxygen atoms. An extensive list of these agents includes dimethyl sulphate (DMS), methyl methanesulphonate (MMS) and their ethyl homologs, β-propiolactone, 2-methyl aziridine, 1,3 propanesulfonate, nitrogen mustard, sulphur mustard.

A large number of 'first generation' anticancer drugs were designed to combine a simple alkylating function such as a nitrogen mustard, an aziridine, or an alkanesulfonate ester with another function designed to direct the agent towards the target tissue. Most of these compounds turned out to be less tumor selective than one might have hoped and, what is worse, many of them have proved to be carcinogens which have given rise to new tumors some time after the termination of chemotherapy for the original cancer. As a result, their general use is now viewed with some suspicion.

A group of 'second generation' compounds has emerged, many of them are natural products, but now augmented by a growing number of rationally designed, synthetic drugs. Their common feature is that they appear to form an initial physical complex with DNA before covalently binding to it. This heterogenous group of compounds includes aziridines, such as mitomycin C, several pyrrolo (1,4) benzodiazepines, and spirocyclopropanes such as CC-1065.

Aziridine antibiotics

An assortment of naturally occurring antibiotics, each having an aziridine ring, has been isolated from *Streptomyces caespitonis*. The most interesting of them in clinical terms is mitomycin C. The enzymatic reduction of quinone ring of mitomycin C initiate the processes that cause alkylation of DNA. It interacts with DNA at $O^6G > N^6A > N^2G$ and forms one cross-link for about every ten monocovalent links. Another example of an

aziridine antibiotic is carzinophilin A, which is an antitumor metabolite produced by *Streptomyces sahachiroi*. It has two aziridine functions and produces cross-links in DNA.

Pyrrolo (1,4) benzodiazepines, P(1,4) Bs

Anthramycin and tomamycin along with sibiromycin and neothramycins A and B, are members of the potent P(1,4)Bs antitumor antibiotic group produced by various actinomycetes. The first three of these compounds bind physically in the minor groove of DNA where they form covalent bonds to N^2-G, showing a DNA sequence specificity for 5'-purine-G-purine sequences.

Spirocyclopropane antibiotics

The spirocyclopropane antibiotic CC-1065 is an extremely potent cytotoxin, its biological activity is due to sequence selective binding in the minor groove of DNA followed by covalent binding. CC-1065 can not be used as an antitumor agent because of its unacceptable toxic side effects, while its synthetic analog, U-71184, has enhanced antitumor activity and diminished side effects.

AGENTS INTERACTING WITH DNA REVERSIBLY

This class comprises of many anticancerous agents which are being widely used in cancer chemotherapy. These agents interact with DNA either by binding to it via major or minor groove or by intercalating between base pairs of DNA. This interferes in biological functions of DNA in cancerous cells.

Groove binding agents

Typically, minor groove binding molecules have several aromatic rings such as pyrrole, furan, or benzene connected by bonds with torsional freedom. This creates compounds which, with the appropriate twist, can fit into the helical curve of the minor groove with displacement of water from the groove. These molecules form van der Waals contacts with the edges of base pairs on the floor of the groove. Substituents at aromatic rings of these molecules may form hydrogen bonds with C-2 carbonyl oxygen of thymine or the N-3 nitrogen of adenine. However, hydrogen bonding of groove binding agents with the amino group of guanine and the carbonyl oxygen of cytosine in G.C base pairs is sterically unfavourable. A possibility with groove binding molecules, which does not exist with intercalators, is that they can be extended to fit over many base pairs along the groove and have very sequence specific recognition of nucleic-acids. This class of anticancer agents includes netropsin, distamycin, Hoechst 33258 and SN6999.

Intercalating agents

Typical intercalators are planar, aromatic cations which bind by insertion of the aromatic ring system between DNA base pairs. They may have non-planar substituents, either cationic or neutral, which protrude into one of the DNA grooves. Generation of the intercalation site causes extension of the DNA duplex, local unwinding of the base pairs, and other possible distortions in the DNA backbone (such as bends) which are characteristics of the

intercalator species. A great variety of substances, including several agents of importance in chemotherapy are known to bind to DNA by intercalation e.g. ellipticine, acridines, naturally occurring anthracycline antibiotics : daunomycin, adriamycin, nogalamycin, carminomycin, aclacinomycin, quinoxaline antibiotics: echinomycin, triostin A and synthetic agents amsacrine and mitoxantrone etc. Mitoxantrone represent a novel, completely synthetic substance with a basic functionalized anthraquinone structure. Mitoxantrone and its dedihydroxy analog ametantrone are less cardiotoxic and being used against phase I trials of human breast cancer. Quinoxaline antibiotics, echinomycin and triostin A are bisintercalators having two potential intercalating ring systems connected with linkers which can vary in length and rigidity. The interaction of the ring systems with DNA base pairs is controlled to a large extent by the characteristics of the linker.

Daunomycin : An anthracycline antibiotic

Objective of the present study is the investigation of interaction of anthracycline antibiotic daunomycin with specific DNA sequences. Daunomycin is a highly cytotoxic compound isolated from strains of *Streptomyces peucetius*. It is being used in the treatment of acute lymphocytic and myelogenous leukemia. Daunomycin inhibit the in vitro growth of both normal and cancer cell lines, and as a consequence, nuclear damage is characteristically observed [31]. A number of studies have demonstrated that daunomycin function primarily at DNA level and

both RNA and DNA synthesis are inhibited [37,81,83,136]. Subcellular localization of daunomycin in cultured fibroblast has shown exclusive uptake in nuclei and lysosomes. Daunomycin molecule typically possess an aglycon chromophore containing four fused rings (A-D) and daunosamine sugar (Fig. 1.1). This structure has three principal functional parts of anthracycline antibiotics : the intercalator (rings B-D), the anchoring function associated with ring A, and the amino sugar. Each component of the daunomycin plays an important role in the biological activity of the drug. Chemical substituents on the fused ring system , and on the amino sugar attenuate the therapeutic properties of daunomycin and the various members of the anthracycline family of drugs [47,81,83]. In fact the slight changes in chemical structure resulted in the significant changes in clinical properties, for example- adriamycin is closely related structurally to daunomycin. It has an extra hydroxyl group at C-14 position, is effective in the treatment of a number of tumors that are quite distinct from those against which daunomycin is active and is less cardiotoxic than daunomycin. One recently developed anticancerous compound 4′- epiadramycin differs from adriamycin only by an inversion of the stereochemistry at the 4′- position of the amino sugar. It has reduced cardiotoxicity than daunomycin and adriamycin. Thus for designing of anticancerous drugs with reduced side effects and wide spectrum of anticancerous activity, knowledge of molecular basis of interaction of anticancerous anthracyclines with nucleic-acids is required.

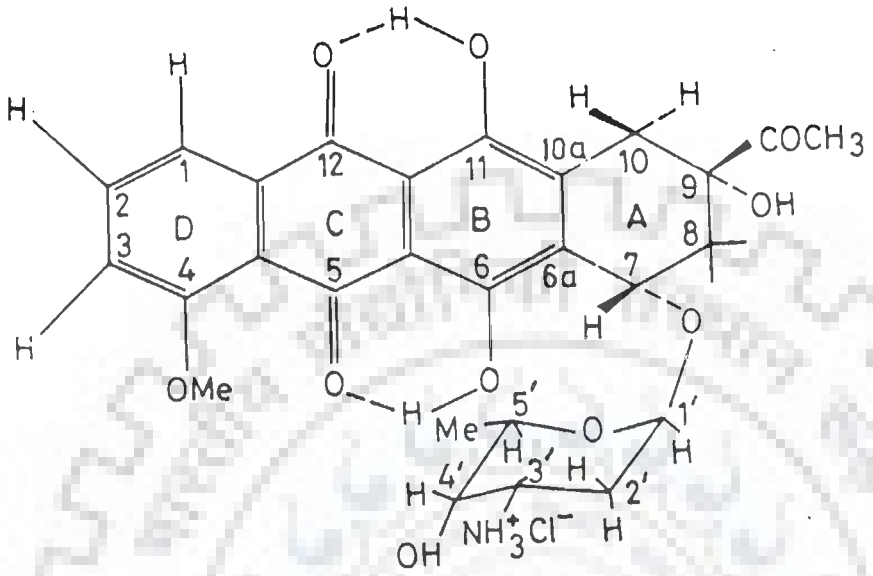

Fig. 1.1 : Structure of daunomycin

THE INTERMOLECULAR FORCES BETWEEN ANTICANCER DRUGS AND NUCLEIC-ACIDS

Intermolecular forces between drug and nucleic acids determine the mechanism by which adrug specifically interacts with nucleic-acids. One must consider not only the forces between the two molecules, but also the effects of the solvent and ions in the solution. The forces between drugs and nucleic-acids can be classified into four types.

Electrostatic forces : salt bridges

In drug-DNA complexes electrostatic forces occur between the ionized phosphates of the DNA and positively charged groups of drugs. Electrostatic interactions are influenced by the concentration of salt in solution : as it increases, the strength of the electrostatic forces decreases. These interactions are much stronger when there are no water molecules between the two ionized groups because water has a high dielectric constant.

Dipolar forces : hydrogen bonds

Hydrogen bonds occur between the substituents on drug and the bases of the nucleic-acid, both of which also form hydrogen bonds to water. Since all linear hydrogen bonds have similar free energies, they make little net contribution to the favourable free energy change when the drug and nucleic-acid interact in solution. By contrast, formation of poorly aligned hydrogen bonds, or absence of some of them on complex formation, carries a free energy penalty of about 4 k J mol^{-1}. Thus hydrogen bonds are one of the most important means of making sequence specific

interaction of drug with nucleic-acids e.g. in case of daunomycin-DNA complexes, the two hydrogen bonds formed between the 9OH group of ring A of daunomycin and amino group of gunanine, determine the sequence specificity of daunomycin.

Entropic forces : the hydrophobic effect

The hydrophobic effect is due to the behaviour of water at an interface. A non-polar molecule such as aromatic rings of drugs, in water creates a sharply curved interface region where there is a layer of ordered water molecules. When these non-polar molecules aggregate, the ordered water molecules which were at the interface are released and become part of the disordered bulk water. This stabilizes the aggregate by increasing the entropy of the system and hence decreasing its free energy.

Therefore, the surface of the non-polar planar aromatic chromophore of drugs exactly complement the surface of nucleic-acid, it binds to, so that there are no unnecessary bound water molecules left in the interface when the drug-DNA complex forms.

Base stacking : dispersion forces

Base stacking is caused by two kinds of interactions : the hydrophobic effect mentioned above and dispersive forces. Molecules with no net dipole moment can attract each other by a transient dipole-induced dipole interaction. Such dispersion forces decrease with the inverse sixth power of the distance separating the two dipoles, and so are very sensitive to the thermal motion of the molecules involved.

Despite their extreme distance dependence, dispersion forces are important in the maintenance of the structure of double-stranded nucleic-acids for they help to cause base stacking. Further more, base stacking help in binding of drugs because aromatic planar rings of drugs stack in between the bases of nucleic-acids in an intercalated fashion.

STRUCTURE OF NUCLEIC-ACIDS

Nucleic-acids are very long, thread-like polymers, made up of a linear array of monomers called nucleotides. Ribonucleic acid (RNA) and deoxyribonucleic acid (DNA) (Fig. 1.2) are two major nucleic-acids. Monomeric unit of RNA is ribonucleotide while that for DNA it is deoxyribonucleotide. All nucleotides are constructed from three components a nitrogen heterocyclic base, a pentose sugar, and a phosphate residue. The major bases are monocyclic pyrimidines or bicyclic purines. Adenine (A) and guanine (G) are purine bases and thymine (T) and cytosine (C) are pyrimidines. The base adenine pairs with thymine through two hydrogen bonds and base guanine pairs with cytosine through three hydrogen bonds in double helical DNA (Fig. 1.3). Pentose sugar occurs in furanose form in nucleic-acids. It is ribose in RNA and deoxyribose in DNA (Fig. 1.4 (a, b)). Pentose sugar is linked through a N-glycosyl linkage to bases. Purines are covalently bonded to C1′ of sugars through N9 atom and pyrimidines are linked through N1 atom (Fig.1.4(c)). Further nucleotide units are covalently linked through phosphodiester bridges formed between 5′-hydroxyl units of one nucleotide and 3′-OH group of the next

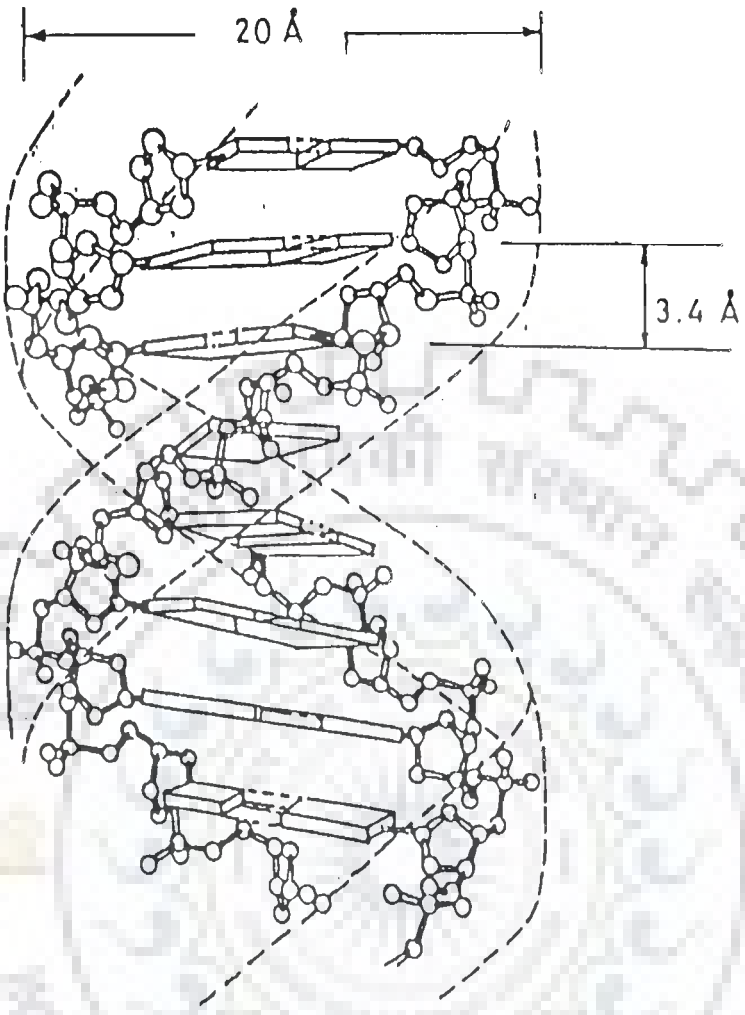

Fig.1.2 : Schematic representation of the DNA double helix. The sugar-phosphate backbones run at the periphery of the helix in antiparallel orientation. Base pairs are stacked along the center of the helix.

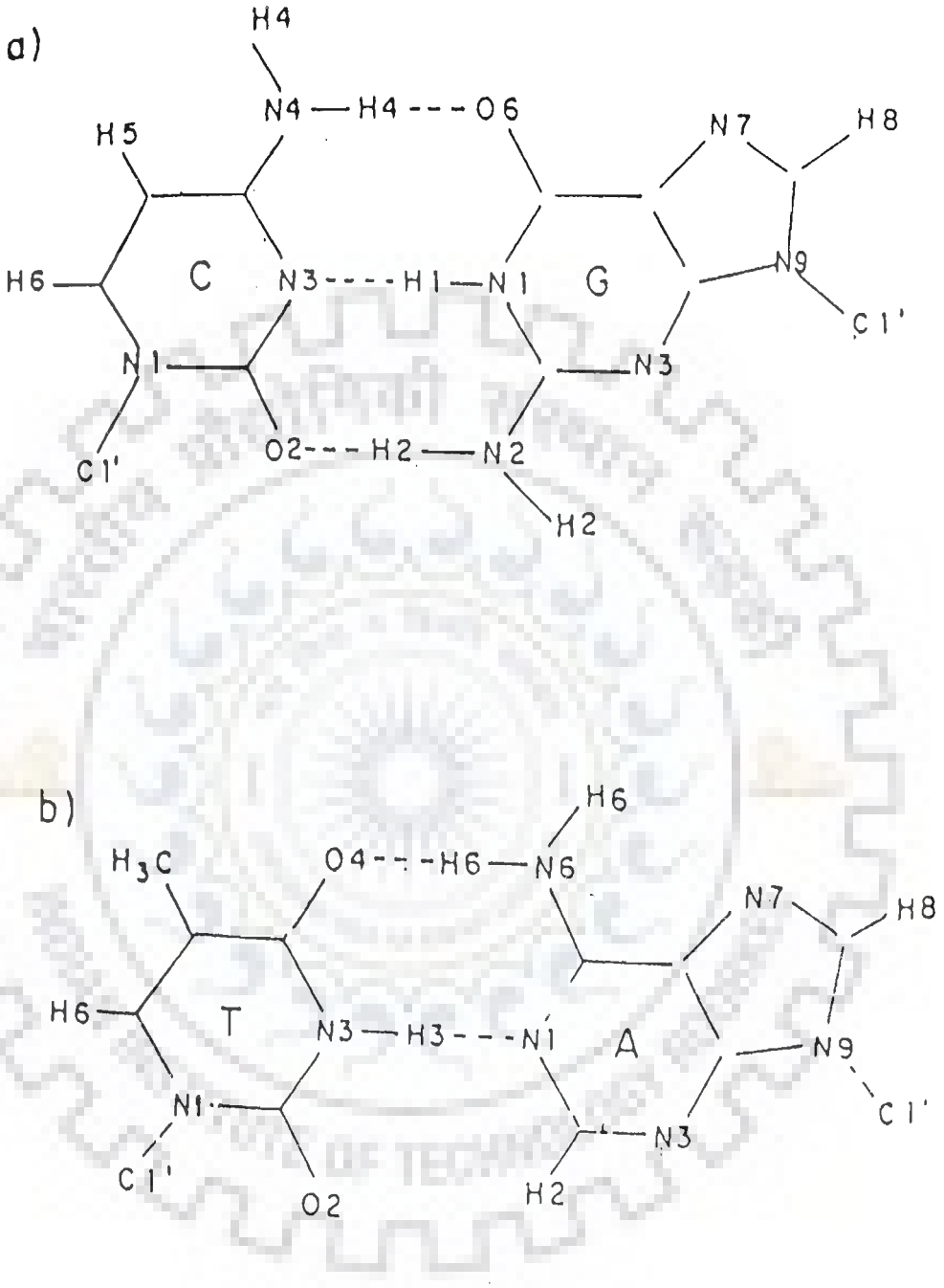

Fig.1.3 : Watson and Crick base pairs showing the hydrogen bonding arrangement in double helical DNA.

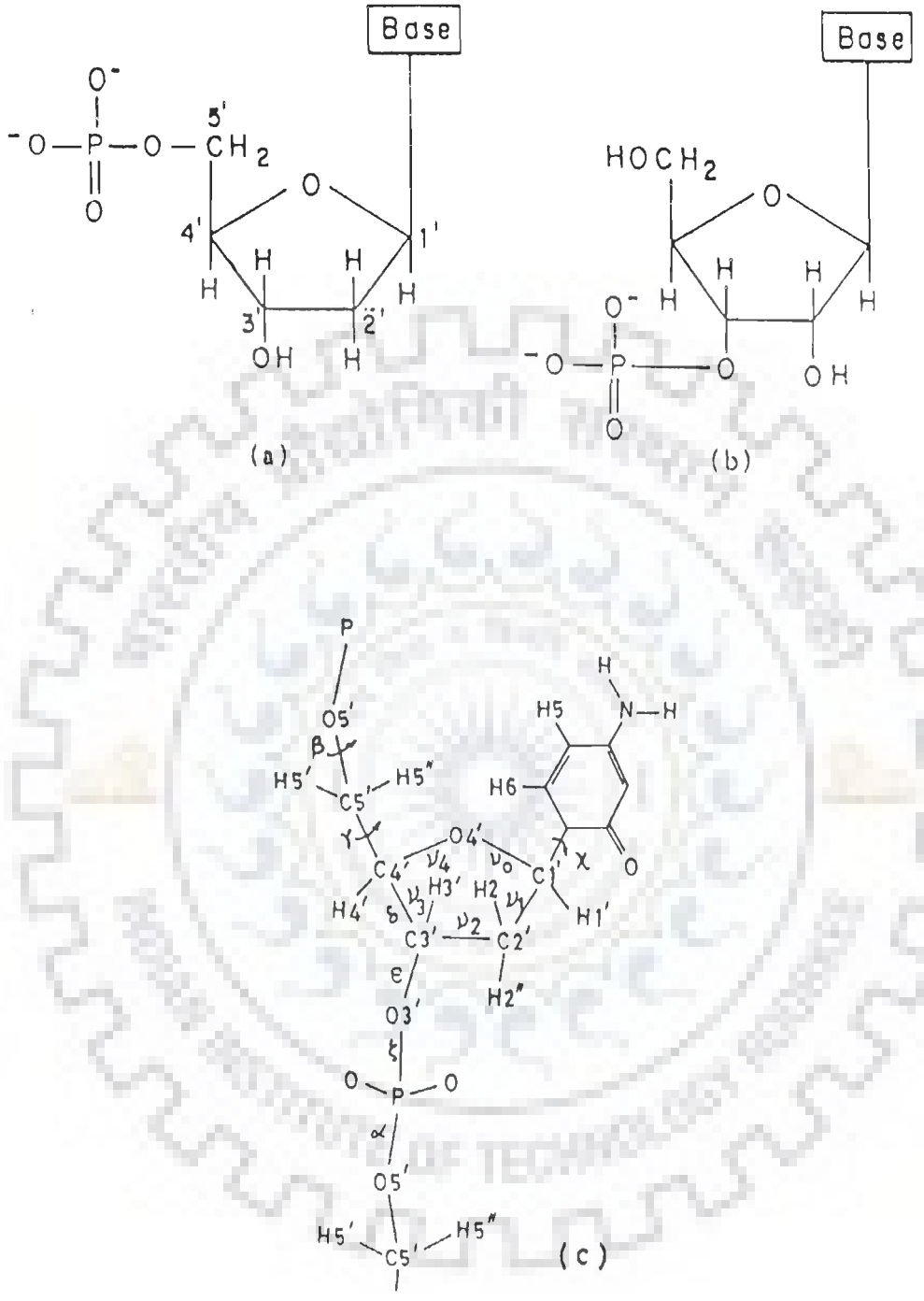

Fig. 1.4 : Five membered furanose ring (a) deoxyribose and (b) ribose found in DNA and RNA, respectively (c) A nucleotide unit showing the numbering of the atoms in the furanose ring and the backbone torsion angles.

(n+1) unit.

Torsional angles and their ranges in nucleic-acids

The three-dimensional structure of a molecule is characterized by bond lengths, bond angles, and rotation of groups of atoms about bonds. These rotations about a central bond B-C are described by torsion angles involving four atoms in sequence A-B-C-D. The torsion angle, θ , is defined as the angle between projected bonds A-B and C-D when looking along the central bond either in direction B $\longrightarrow$ C or in the opposite sense C $\longrightarrow$ B. It is defined as 0° if A-B and C-D are eclipsed (cis and coplanar) and the sign is positive if the far bond is rotated clockwise with respect to the near bond. The torsion angle is usually reported either in the range 0° to 360° or -180° to $+180^{\circ}$.

In molecules with rotational freedom about single bonds, usually not all feasible torsion angles are assumed but rather certain sterically allowed conformations are preferred. Therefore, it is often convenient to describe a structure with torsion angle ranges. The ranges commonly used are those proposed by Klyne and Prelog, viz. syn ($\sim 0^{\circ}$), anti ($\sim 180^{\circ}$), synclinal ($\sim \pm 60^{\circ}$) and anticlinal ($\sim \pm 120^{\circ}$).

The conformation of the sugar-phosphate backbone following the sequential numbering of atoms P $\longrightarrow$ O5′ $\longrightarrow$ C5′ $\longrightarrow$ C4′ etc. is defined by torsion angles α, β, γ, δ, ε, ξ. Angles ν_0, ν_1, ν_2, ν_3 and ν_4 decide the geometry of sugar ring (Fig. 1.4(c)). The different families of DNA structures are characterized by the values of these torsion angles.

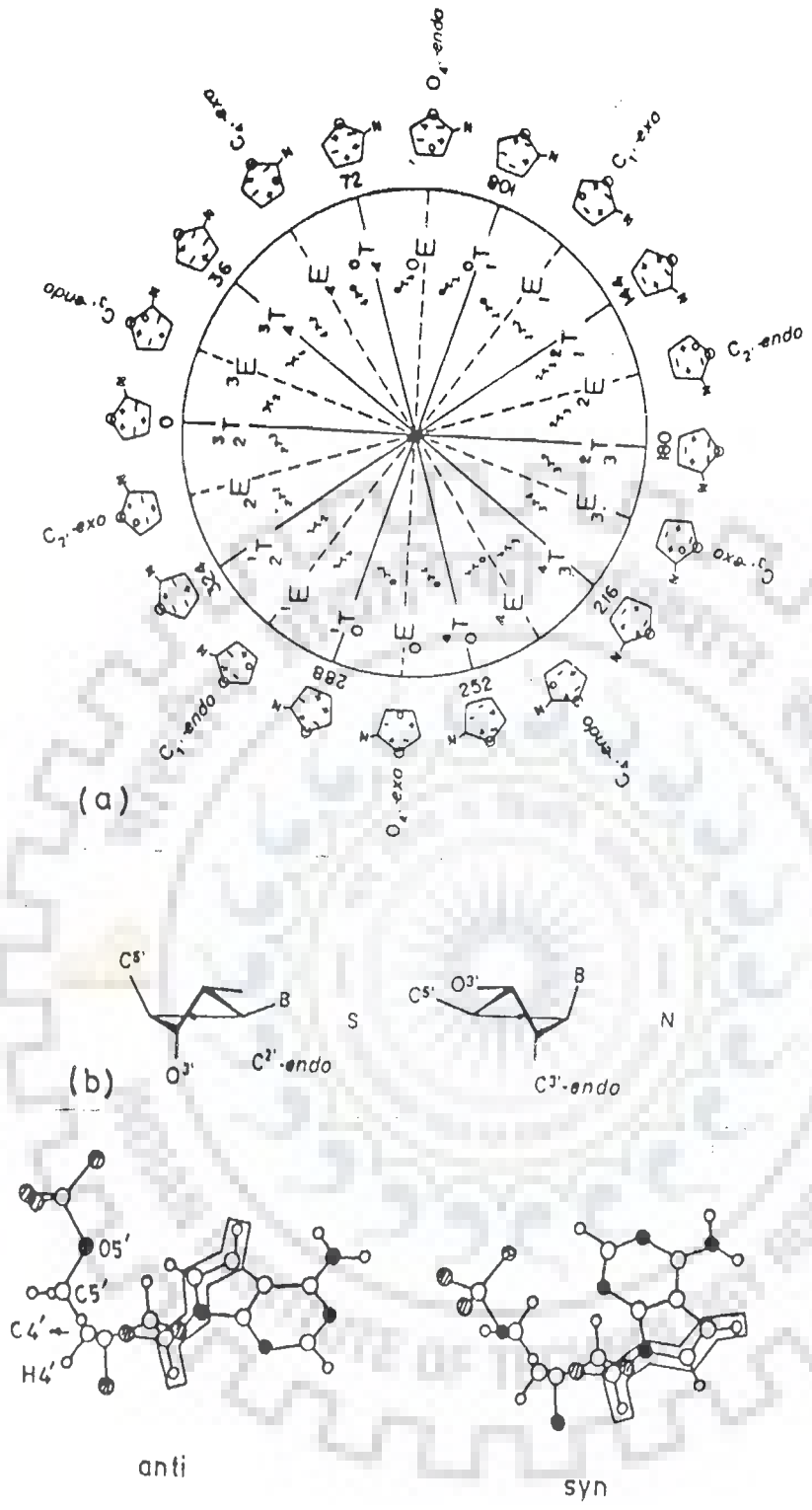

Fig. 1.5 : (a) Pseudorotation cycle of the furanose ring in nucleosides (b) Preferred conformations C2'-endo and C3'-endo of sugar pucker (c) Anti and syn orientations about the glycosyl bond.

Sugar puckers : The pseudorotation cycle

The five membered furanose ring is generally non-planar. Sugar puckering is described by identifying major displacement of carbon-2′ and -3′ from the median plane of C1′-O4′-C4′. Thus if the endo-displacement of C-2′ is greater than the exo displacement of C-3′, the conformation is called C2′-endo and so on. Sugar puckering modes are defined accordingly.

Pseudorotation cycle

The preceeding methods for describing sugar puckering are only approximate and if intermediate twist modes are considered, they are inadequate. In furanose ring maximum pucker rotates virtually without potential energy barriers, giving rise to an "infinite" number of conformations. These can be described in terms of the maximum torsion angle (degree of pucker), ν_{max}, and the pseudorotation phase angle P (Fig. 1.5(a)) [1,2,111,121,122].

In nucleotides, the pseudorotation phase angle P is calculated from the endocyclic sugar torsion angles according to [2] :

$$\tan P = \frac{(\nu_4 + \nu_1) - (\nu_3 + \nu_0)}{2.\ \nu_2\ (\mathrm{Sin}\ 36^\circ + \mathrm{Sin}\ 72^\circ)}$$

Given the phase angle P, the five torsion angles are related by :

$$\nu_j = \nu_{max} .\ \mathrm{Cos}\ (P + j.\ \psi)$$

where j = 0 to 4 and $\psi = 720^\circ/5 = 144^\circ$. The maximum torsion angle, ν_{max} is derived by setting j = 0.

$$\nu_{max} = \nu_0 \ /\ \mathrm{Cos}\ P$$

Fig. 1.5(a) displays the theoretical changes of the five torsion angles during one full pseudorotation cycle [63]. At every phase angle P, the sum of the positive torsion angles equals that of the negative torsion angles, i.e. the sum of the five angles is zero.

$$\nu_0 + \nu_1 + \nu_2 + \nu_3 + \nu_4 = 0$$

In nucleotide structure analysis, two ranges of pseudorotation phase angles are preferred C3'-endo at $0^\circ \leq P \leq 36^\circ$ (in the "north" of the cycle, or N conformer) and C2' endo at $144^\circ \leq P \leq 190^\circ$ ("south", or S conformer) (Fig. 1.5(b)).

Glycosidic bond rotation

Orientation of pyrimidine or purine bases relative to sugar ring is defined by glycosidic bond angle (χ). Measurements of angle is made either with respect to the position at C6 in pyrimidine nucleotides and C8 in purine nucleotides.

$$\chi \begin{cases} O4' - C1' - N9 - C4 \text{ (Purine nucleotide)} \\ O4' - C1' - N1 - C2 \text{ (Pyrimidine nucleotides)} \end{cases}$$

Relative to the sugar moiety, the base can adopt two main orientations, called anti and syn. They are shown in Fig. 1.5(c). In anti, the six membered ring in purines and O2 in pyrimidines, is pointing away from the sugar, and in syn it is over or towards the sugar. High anti is a variant of anti, in which the bond C1' - C2', is nearly eclipsed with N1-C6 in pyrimidine or N9-C8 in purine nucleosides. The term high anti actually denotes a torsion angle lower than anti.

Polymorphism in DNA structures

Various studies on DNA/oligonucleotides in solid state and in solution have shown the existence of primarily three families of nucleic-acid double helix. These are the right-handed B-family with anti glycosidic bonds and C3'-exo/C2'-endo sugar pucker; the right-handed A-family with anti glycosidic bonds and C3'-endo sugar pucker; and the left-handed Z-family with alternating syn-anti glycosidic bonds and alternating C3'-endo-C2'-endo sugar pucker. The characteristic features of these are summarised in Table 1.1. The RNA-RNA duplexes always exist as A-type and right-handed because the 2'-OH group prevents a B-type conformation. DNA-RNA hybrids also adopt an A-type structure. Native DNA is found to exist in B-DNA form.

The left-handed structures have been observed only in alternating GC oligodeoxynucleotides. Cooperative transitions between families can be induced by salt, alcohol or humidity changes.

ROLE OF NMR SPECTROSCOPY IN THE STUDY OF DRUG -DNA INTERACTIONS

NMR method has the potentialities for studies of structure, conformation and dynamics of molecules such as drugs, proteins and nucleic-acids and intermolecular interactions between molecules. The great advantage of NMR technique is that being in solution form, molecular structure determined is close to actual biological conditions and even structural and biochemical changes in intact cells (in vivo NMR) can be monitored. In drug - DNA interaction

Table 1.1 : Structural Characteristics of A, B, and Z-type double helices.

Family Type	A-Type	B-Type	Z-Type
Bases per turn	11	10	12
Rotation per nucleotide	30° to 32.7°	36° to 45°	-60°
Base pair tilt	10° to 20.2°	- 5.9° to 16.4°	-7° TO 9°
Helix pitch (nm)	3.09 to 3.60	3.38	4.56
Rise per residue	0.20	0.34	0.76/2
Helix diameter (nm)	2.30	1.93	1.81
Helix sense	Right-handed	Right-handed	Left-handed
Glycosidic bond rotation	Anti	Anti	Anti (Cytosine) Syn (Guanosine)
Sugar pucker	C3'-endo	C2'-endo	C2'-endo (Cytosine) C3'-endo (Guanosine)

studies, the structure and conformation of free drug molecule as well as DNA fragments can be established by NMR. The parallel studies on complexed form of both drug and DNA moleculeprovide an insight of specific changes occurring in conformation and chemical behaviour of these molecules due to interaction. Sequence specific ^{1}H NMR experiments in the complex provide spectroscopic probes for distinguishing between different modes of drug binding. Quantitative analysis of intermolecular ^{1}H-^{1}H NOEs provide direct intermolecular distances for distinguishing between intercalating drugs and drugs binding to the major or minor groove of DNA. Since the interacting species may undergo reversible associations and the stability of the complexes may vary over a wide range, depending on solution conditions such as pH, ionic strength and temperature. NMR may be used to monitor the thermodynamic and kinetic stability of the complexes formed under different experimental conditions and to define optimised solution conditions.

Thus, it can be well justified that nuclear magnetic resonance (NMR) spectroscopy provides a powerful probe and outstanding potentialities for studies of drug-DNA interactions.

CHAPTER - II

LITERATURE REVIEW

GENERAL REVIEW

Many antitumor drugs are known to interact with DNA molecules to exert their biological activities. Some form covalent linkages with DNA, while others form complexes with the DNA double helix using noncovalent interactions. Over the years a large number of studies were carried out using spectroscopic, NMR, theoretical computations and x-ray crystallographic techniques to understand the molecular mechanism of action of these antitumor agents.

Lerman [62] has proposed the model on intercalation of molecules like proflavine or ethidium bromide into DNA base pairs. It has been demonstrated that basic change which has to be made in the structure of the DNA helix to allow the intercalation of a flat molecule like proflavine or ethidium bromide is the formation of a cavity between two base pairs. The size of the cavity must be such that an intercalating molecule would fit in, that is the distance between the two base pairs along the helix axis within the cavity must be 6.8 A°. Intercalation of these molecules leads to unwinding of helix. Paoletti and Le Pecq [88] performed computer simulation of energy transfer between ethidium bromide molecules bound to DNA. Since the energy transfer is very dependent on orientation, the angle between two ethidium molecules

and, therefore the local change in the winding angle of the DNA helix caused by intercalation, can be determined. It has been inferred that the DNA helix is wound by $13^{\circ} \pm 4^{\circ}$, and not unwound on intercalation of ethidium bromide as previously assumed [62] . Paoletti and Le Pecq [89] proposed an alternative model of intercalation. The main difference between the Lerman model and this model is the change of the torsion of the helix. The Lerman model permits only unwinding of the helix, the unwinding angle being included between 45° and 15°. The model proposed here permits either an unwinding of the helix, the unwinding angle is then included between 15° and 0° or a winding of the helix up to 16°. Further to understand the change in the torsion of the DNA helix caused by intercalation, Saucier and Le Pecq [113] studied the interaction of ethidium bromide, proflavine, quinacrine and daunomycin with supercoiled DNA from PM2 bacteriophage by viscometry. It was found that change of the torsion of the DNA helix vary with the drug intercalated. The change of torsion angle found for proflavine, quinacrine were 8° to 9° and for daunomycin 4°.

The interaction of ethidium bromide with the self-complementary ribonucleoside monophosphates CpG, GpC, ApU, UpA as well as with mixtures of complementary and non-complementary ribonucleoside monophosphates has been investigated by circular dichroism, fluorescence and nuclear magnetic resonance and visible spectroscopy techniques [59]. It was observed that ethidium bromide form a complex with all four of the dinucleotides but

exhibit a definite preference for binding to dinucleosides that have a pyrimidine (3'-5') purine sequence. Nuclear magnetic resonance study [90] on the binding of ethidium bromide to dC-dG-dC-dG self-complementary duplex has shown that ethidium bromide phenanthridine ring protons shift upfield by 0.9 ppm on complex formation. On the basis of these upfield shifts it was suggested that phenanthridine ring of ethidium bromide intercalates into the dC-dG-dC-dG duplex in solution.

Neidle et al. in 1977 [80] studied the crystal structure of 3:2 complex of proflavine with dinucleoside phosphate cytidylyl-3'5'-guanosine. It was reported that one of the proflavine molecule symmetrically intercalates between the base pairs and protrude into the minor groove. Each amino group of this proflavine participated in a hydrogen bond to a phosphate oxygen on either side of the duplex. The other two proflavine molecules were found to stack symmetrically above and below the miniature double helix. Patel and Canuel [91] reported the binding of mutagen proflavine with dC-dC-dG-dG and dG-dG-dC-dC self-complementary tetranucleotide duplexes by NMR spectroscopy and UV-vis spectrophotometry . An overlap geometry was proposed between the proflavine ring and nearest neighbor base pairs at the intercalation site from a comparison between experimental chemical shifts and those calculated for various stacking orientations.

Three-dimensional structure of the 9-aminoacridine . 5 -iodo-cytidylyl (3'-5') guanosine complex was solved by x-ray

crystallography [112]. The structure demonstrated two distinct intercalative binding modes. The first of these involve a pseudosymmetric stacking interaction between 9-aminoacridine molecules and G.C base pairs. The second configuration involved an asymmetric interaction between acridine and guanine rings. Ribose sugar puckering was found as C3′-endo (3′-5′) C2′-endo. These conformational changes, along with alterations in the glycosidic torsional angles permit base pairs to separate 6.8 A° and give rise to the twist between base pairs above and below 9-aminoacridine molecules.

The crystal structure of a complex containing deoxycytidylyl (3′-5′) deoxyguanosine and a terpyridine platinum (TPH) compound was reported [124]. TPH compound was found to intercalate between two Watson-Crick GC base pairs. The deoxyguanosine at the 3′- end of the molecule was found to have a deoxyribose with the C2′-endo pucker, however, the deoxycytidine at the 5′-end have C3′-endo sugar pucker.

In order to design intercalating agents that intercalate in an optimum manner, Miller and Newlin [69] performed computational analysis. Binding of fundamental moieties, protonated pyridine, aniline, phenol, quinone, and 4H-thiopyran-4-one was studied. Ideal intercalants proposed contain three and four fused ring system, having protonated ring nitrogen atoms to maximize the electrostatic interactions with DNA, hydroxy and amino groups that can hydrogen bond to the O2 and O5′ phosphate backbone atoms, and

carbonyl and sulfur groups in the central position of the ring system to provide variations in the chromophore and to interact with the relatively positive region in the intercalation site.

One and two-dimensional NMR studies on the oligomer d-(A_1T_2-$G_3C_4G_5C_6A_7T_8$), with and without actinomycin D were performed [116]. 1D NMR and 2D COSY studies have shown that two 1:1 unsymmetric complexes form in unequal proportions with the phenoxazone ring intercalated at a GpC site. The oligomer was found to remain in a right-handed helix, but the extreme conformational changes both at and adjacent to the binding site were observed. The deoxyribose conformation of T_2, C_4, and C_6 were found to shift from C2'-endo in the free duplex to an increased amount of C3'-endo in the 2:1 complex. It was suggested that cyclic peptide rings of actinomycin D bind in the minor groove of the DNA with the peptide ring on the quinoid side of the phenoxazone ring pointing toward the end of the duplex and the benzenoid side pointing into the center of the duplex. The conformation of a DNA oligomer d(TCGCGTTTTCGCGA), which has adopted a hairpin structure and its complexes with the actinomycin D were characterized using homo and heteronuclear NMR techniques [10]. Two distinct actinomycin D-oligonucleotide complexes were formed in unequal concentrations. These complexes differ by the orientation with which the asymmetric drug chromophore intercalates into the d(GC) step. Interestingly, the large changes were not observed at the intercalation site (G3, C4, G11, C12) but rather for the flanking cytosines, C2 and C10.

Arora in 1983 [4] studied the structure of nogalamycin by x-ray crystallography. It was reported that B, C and D were planar rings. The ring A adopted half chair conformation, while nogalose and glucopyranose were in normal chair conformations.

NMR studies on the interaction of the antibiotic nogalamycin with the hexa-deoxyribonucleotide duplex d-$(GCATGC)_2$ were carried out [117]. Observed NOE contacts indicated that nogalamycin intercalates at the 5'-CA and 5'-TG steps with the major axis of the anthracycline chromophore aligned approximately at right angles to the major axis of base pairs. Major determinants of sequence specificity were found as hydrogen bonding interactions between the O6 and N7 atoms of the guanine in the intercalation site and the two hydroxyl groups of the bicyclic sugar of the antibiotic coupled with hydrogen bonding/electrostatic interaction between the protonated dimethyl amino group and the O6 carbonyl of the terminal guanine. Robinson et al. [108] studied the interaction between nogalamycin and DNA hexamer d-(CGTACG) by proton NMR. Two sets of NOE cross peaks were observed, one set was found to associate with the protons in nogalose and ring A of the chromophore interacting with the DNA protons in the minor groove. Another set was of the aminoglucose sugar protons interacting with the ring protons (H5 and H6) of cytosine C1 residue in the major groove.

Zhang and Patel [134] studied the interaction of nogalamycin with d(A-G-C-A-T-G-C-T) in aqueous solution using two-dimensional

NMR techniques and molecular dynamics calculations. It was found that aglycon chromophore of nogalamycin intercalates at (C-A).(T-G) steps with the long axis of the aglycon approximately perpendicular to the long axis of the flanking C3.G6 and A4.T5 base pairs. The ring A of nogalamycin has adopted a half chair conformation such that the C9 atom of ring was out the plane of the aglycon aromatic ring system and on the same side as the nogalose and bicyclic amino sugar rings. The OH-2", and OH-4" protons on the bicyclic sugar were directed toward the helix axis. The aglycon A ring and nogalose sugar of nogalamycin were found in the minor groove of the duplex with the intermolecular alignments stabilized by a large set of van der Waals contacts.

The structure of carminomycin I and stereochemistry of ring D substituents has been investigated by x-ray crystallography [95]. The six chiral centers were found as C7(S), C9(S), C1'(R), C3'(S), C4'(S) and C5'(S). The configuration of the daunosamine unit of carminomycin I was found same as that for daunomycin.

Murdock et al. [76] synthesized several new compounds and tested for their antitumor activity. Among these compounds, mitoxantrone was found as more effective anticancerous agent against L-1210 leukemia, B-16 melanoma and colon tumor 26 than adriamycin. Binding of the mitoxantrone, ametantrone and related structures to DNA has been studied by viscometry, topoisomerase and spectrophotometric assay [66]. Mitoxantrone and compounds which have the similar hydroxy substitution pattern on the

aromatic ring and with side chain hydroxy groups were found to have higher binding constant with DNA than other compounds. Capranico et al. in 1993 [12] reported the DNA sequence dependent action of mitoxantrone on topoisomerase II DNA cleavage in SV40 DNA fragments and short oligonucleotides, in comparison to VM-26, 4-demethoxydaunorubicin and amsacrine (mAMSA). It was observed that mitoxantrone and 4-demethoxydaunorubicin share 7% of cleavage sites. A pyrimidine and particularly a cytosine was found as the required base at the 3′ terminus of the break site for mitoxantrone stimulation of DNA cleavage.

Wang et al. [125] studied the molecular structure of triostin A-d(CGTACG) complex by x-ray crystallography. It was found that triostin A molecule, has the form of a bisintercalator with the quinoxaline rings bracketing the two CG base pairs at either end of the hexamer. The backbone NH of both alanines participated in hydrogen bonds with N-3 of G2 and G12. Carbonyl group of alanine has formed a hydrogen bond with the amino group at N-2 of G12. The Watson-Crick base pairing between two central AT base pairs has changed to Hoogsteen base pairing due to interaction. NMR studies were carried out on interaction of echinomycin with DNA octamers $[d(ACGTACGT)]_2$ and $[d(TCGATCGA)]_2$ [40]. In the saturated complexes two echinomycin molecules bind to each octamer by bisintercalation of the quinoxaline moieties on either side of each CpG step. At the low temperatures, both the internal and terminal A.T base pairs adjacent to the binding site in the $[d(ACGTACGT)]_2$-2 echinomycin complex were Hoogsteen base paired,

however, as the temperature was raised, the internal A.T Hoogsteen base pairs destabilized and were observed to be exchanging between the Hoogsteen base paired and Watson-Crick base paired state. In contrast, in the $[d(TCGATCGA)]_2$ - 2 echinomycin complex, no A.T Hoogsteen base pairs were observed.

Gao and Patel [38] has investigated the sequence selectivity and metal ion specificity in chromomycin-DNA oligomer complexes d(A1-A2-G3-G4-C5-C6-T7-T8) and d(A1-G2-G3-A4-T5-C6-C7-T8) in the presence of divalent cations by NMR. It was reported that chromomycin prefer (G-G) step as binding site due to the hydrogen bonding potential of acceptor N3 and donor NH_2 groups of guanosine that line the minor groove. Results indicated that monomers in the chromomycin dimer align through coordination of the divalent cation to the C1 carbonyl and the C9 enolate anion on the hydrophobic edge of each aglycon ring.

Aclacinomycin A and B are anthracycline antibiotics. Each consists of an alkavinone aglycon chromophore and a trisaccharide (rhodosamine-deoxyfucose-cinerulose A or B) attached at the C7 of ring A of alkavinone. 2D NMR studies on 2:1 aclacinomycin-d-(CGTACG) complex [133] indicated that the elongated alkavinone of aclacinomycin intercalates between the CpG steps and the trisaccharide lie in the minor groove. Possibility of several hydrogen bonds was found to exist between aclacinomycin and DNA. Intercalation geometry of aclacinomycin was found as hybrid between those of daunorubicin and nogalamycin. Multiple molecular

species coexisted in the solution of 1:1 mixture of aclacinomycin and d-CGTACG due to the slow rate of drug binding to DNA.

NMR spectroscopy combined with molecular modelling was used to characterize a heterodimeric complex of distamycin (Dst) and 1-methylimidazole-2-carboxamide-netropsin (2-ImN) with d(GCCTAACAA GG).d(CCTTGTTAGGC) DNA sequence [39]. In heterodimeric complex NOE cross peaks between DNA protons and the pyrrole protons H3-2, H3-3 and NH protons supported that the imidazole-pyrrole-pyrrole-pyrrole ring system of 2-ImN spans the 5'-G16-T17-T18-A19-3' of the TAACA.TGTTA binding site with the imidazole nitrogen specifically recognizing the amino group. This geometry was further confirmed by cross peaks between the imidazole H4-1 proton and C1'H and amino protons of G16. Likewise, the pyrrole-pyrrole-pyrrole ring system of distamycin span the 5'-A5-A6-C7-A8-3' sequence. Titrations of the same site with Dst or 2-ImN alone yielded homodimeric complexes (2:1 ligand.DNA) of lower stability than the 1:1:1 2-ImN.Dst.DNA complex. Dst and 2-ImN binding to d(CGCAACTGGC).d(GCCAGTTTGCG) was also investigated. The 1:1:1 2-ImN.Dst.DNA complex was again the most stable complex with the AAACT.AGTTT site and was similar to the TAACA.TGTTA complex.

Momparler et al. [70] investigated the effect of adriamycin on DNA, RNA, and protein synthesis in cell free systems and intact cells. It was observed that adriamycin produces a greater inhibition of DNA-dependent DNA polymerase than the RNA

polymerase. Nakata and Hopfinger [77] performed conformational analysis of doxorubicin by energy calculations using the molecular mechanics potential functions. The major finding from this work was that the stable conformation of doxorubicin and daunomycin computed was different from the crystal conformation. This new conformation was characterized by a stabilising bifurcated hydrogen bond involving the 5-oxygen and 6-hydroxyl group of the anthraquinone ring and the 5'-oxygen of the sugar ring. The molecular mechanics energy calculations have been carried out for doxorubicin interacting with two dinucleotide dimer sequences d(CpG) and (dTpC-ApG) [78]. The results suggested that the preferred mode of binding was such that anthraquinone ring intercalates in the minor groove and was nearly perpendicular to the base pairs of the (CpG) sequence having alternate C3'endo-C2'endo sugar ring puckering.

Pachter et al. [87] studied the interaction of adriamycin and its analogs to calf thymus DNA and closed circular PM-2 DNA by fluorimetry and viscometry techniques. Results suggested that intercalative and electrostatic interactions were both important in the DNA binding of these analogs. It was demonstrated that the presence of second and third sugars on the anthracycline side chain did not effect the ability of the drug to distort DNA upon intercalation. Graves and Krugh [43] used the phase partition technique to measure the binding of the adriamycin and daunorubicin to various DNAs. Both drugs were found to bind cooperatively at ionic concentrations comparable to the

physiological levels. However, at ionic concentrations of 0.01 and 1 M NaCl, both drugs were shown to interact with DNA in a noncooperative manner. It was suggested that properties of the DNA helix, such as base pair stacking, play a role in the cooperative binding phenomenon. Chen et al. [23] studied the effect of adriamycin on B to Z transition of poly (dGm^5dC).poly (dGm^5dC) by circular dichroism and ^{31}P NMR spectroscopy. The results showed that adriamycin inhibits the Mg^{2+} - induced B to Z conformational transition of poly (dGm^5dC).poly (dGm^5dC) and reduces the degree of cooperativity of the transition.

Chen et al. in 1986 [25] investigated the structural and energetical factors involved in the sequence selective binding of adriamycin to five self-complementary double-stranded hexanucleotides by theoretical computations. The intrinsically preferred sequence for adriamycin binding was found as the one comprising two GC base pairs at the intercalation site flanked at the down-stream side by an adjacent AT base pair. Jones et al. in 1987 [54] determined the site specificities for intercalation of steffimycin B, adriamycin, echinomycin and ethidium bromide with DNA by CD first-order neighbor analysis. It was reported that steffimycin B, adriamycin and echinomycin exhibit preferential binding to sites comprised of guanine and cytosine. Pohle et al. [100] reported studies based on infrared spectroscopy and quantum-chemical calculations. It was found that adriamycin molecule intercalates between the base pairs of DNA and anchored by hydrogen bonding of its C14 hydroxyl group to the phosphate

group of DNA. Williams et al. [130] have cocrystallized the 4'-epiadriamycin with the DNA hexamer d-(CGATCG) and solved the structure using x-ray crystallography. It was observed that one drug molecule binds at each CpG step of the hexamer duplex. The 9-OH group formed two hydrogen bonds with base G2 as observed in adriamycin-d-(CGATCG) complex [34]. One feature of the complex which was distinctly different from the other anthracycline - DNA complexes was a direct hydrogen bond from the 4'-hydroxyl group of the anthracycline sugar to the N3 of A(3). This hydrogen bond resulted directly from inversion of the stereochemistry at the 4'-position of 4'-epiadriamycin.

Cirilli et al. [27] have used truncated driven nuclear overhauser effect difference spectra to ascertain the conformational characteristics of the glycosidic linkage of adriamycin in solution. Interproton distances 5'H-4'H, 5'H-8eqH, 7H-1'H were determined as 2.37 A°, 2.49 A° and 2.16 A°, respectively. The conformational angles defining glycosidic linkage were calculated. Langlois et al. in 1992 [60] determined the structure of the complex between d(TGATCA) and 4'-epiadriamycin. The chromophore was intercalated between base pairs d(TpG) with the amino sugar positioned in the minor groove. Amino group of daunosamine sugar formed direct hydrogen bonds to N3 of A(9), O2 of T(4) and O4' of C(5). The direct hydrogen bond between O4' of sugar and N3 atom of adenine was observed.

STUDIES ON DAUNOMYCIN AND ITS COMPLEXES

The investigations on structure of antitumor antibiotic - daunomycin and its interaction with nucleic-acids cover a wide range of spectrum of techniques and approaches used so far. Calendi et al. [11] reported that daunomycin binds to double-stranded DNA. Certain physicochemical changes such as changes in the sedimentation coefficient and viscosity of DNA were observed on binding to drug. UV absorption spectrum, fluorescent emission and polarographic behaviour of daunomycin were also affected on interaction with DNA. It was suggested that daunomycin binds with RNA as well. Iwamoto et al. [52] studied the structure of daunomycin in chloroform by NMR spectroscopy at 220 MHz. Position of the glycosidic bond and stereochemistry of the substituents at C-7 and C-9 was reported. It was observed that anomeric proton H1'is equatorially oriented and the daunosamine sugar exists as α-L form.

Waring [128] studied the variation of the supercoils in closed circular ϕX174 RF DNA on binding with antibiotics and drugs by observing changes in sedimentation coefficient. It was observed that ethidium bromide, proflavine, hycanthone, daunomycin, nogalamycin, chloroquine and propidium all believed to intercalate, affect the supercoils in the similar fashion. For proflavine, hycanthone, daunomycin and nogalamycin, the values of unwinding angle ϕ were found to be significantly less than 12°. Non-intercalating substances tested include spermine, streptomycin, methylglyoxal-bis-(gyanylhydrazone), berenil,

chromomycin and mithramycin, have not removed and reverse the supercoiling.

X-ray diffraction studies were carried out on DNA-daunomycin complex [98]. It was found that drug molecule intercalates between base pairs and leads to unwinding of DNA by 12° per drug molecule at the point of intercalation. Intercalation of drug separated two base pairs by an extra distance of 3.4 A°. Interaction between ionized amino group and the second DNA phosphate away from the intercalation site was suggested. A hydrogen bond between the first phosphate and the hydroxyl attached to the saturated ring was also proposed. The interaction of daunomycin and its derivatives with calf thymus DNA was studied by visible absorption spectrophotometry, equilibrium dialysis, low shear viscometry and thermal denaturation of the complex [135]. The importance of amino sugar residue in the binding reaction was emphasized by experiments in which substitution of daunosamine by N-guanidine acetamide daunosamine or D-glucosamine considerably reduced the apparent binding constant. The effects of daunomycin and its derivatives on thermal denaturation of the complex indicated that in the same experimental conditions adriamycin was most effective in stabilising the structure of DNA.

The circular dichroism spectra of complexes of the antibiotics daunomycin, nogalamycin and chromomycin with calf thymus DNA was measured over a wide range of drug/DNA ratios [29]. It was found that chromomycin and mithramycin have similar binding

sites whereas the binding site for nogalamycin and daunomycin on DNA was found to be different. Four stereoisomeric daunomycin derivatives, characterized by the absence of the methoxyl group in position 4 were examined for effects on the thermal denaturation of calf thymus DNA and for their ability to bind to DNA [137]. It was observed that the most characteristic effects of the interaction with DNA on 4-demethoxydaunomycin were similar to those of daunomycin. Gabbay et al. [36] studied the interaction specificity of salmon sperm DNA with various derivatives of daunorubicin. It was noted that complex formation with daunorubicin and/or the C-9 analogs adriamycin and rubidazone leads to a larger increase in the specific viscosity of DNA solution as compared to the N-peptide derivatives. On the basis of circular dichroism and flow dichroism data, it was suggested that the anthracycline ring intercalates between base pairs in a plane perpendicular to the helical axis of DNA. Specific hydrogen bonding between amino group of daunosamine and DNA was suggested which was in accord with earlier report [98]. Shafer [118] studied the interaction of daunomycin with yeast transfer RNA (t-RNA) using UV-visible spectroscopy, thermal denaturation and fluorescence. It was observed that at a nucleotide to drug ratio, of 2.7, daunomycin increases the T_m of t-RNA by about nine degrees. Fluorescence of daunomycin was measured at a fixed wavelength in solutions of varying concentrations of t-RNA and calf-thymus DNA. Addition of t-RNA was found to result in a significant amount of quenching, but somewhat lesser than the

addition of DNA. It was suggested that t-RNA interacts with daunomycin in a manner similar to DNA.

Plumbridge and Brown [99] studied the changes in the visible absorption spectrum and the degree of fluorescence polarization of daunomycin and mepacrine on binding to DNA and poly (I.C) and compared the results with that obtained for the intercalating agent ethidium. It was reported that fluorescence of both daunomycin and mepacrine quenched and fluorescence polarization increased on binding to DNA in a manner to that for interaction of DNA with ethidium indicating intercalation as the possible mode of interaction. On interaction with poly (I.C), only ethidium showed effects characteristic of intercalation. Neither daunomycin nor mepacrine intercalated into the poly (I.C) helix. Bohner and Hagen [9] studied the effect of quinacrine, 9-aminoacridine, proflavine and daunomycin on the activity of DNA polymerase I. The enzyme kinetics were followed at various concentrations of DNA 3'OH primer end groups and constant concentrations of deoxynucleoside triphosphates. It was observed that binding of acridines prevent the action of DNA polymerase.

Crystal structure of daunomycin was reported by Neidle and Taylor [79] in 1977. Ring A, B and C were planar. Methyl carbon atom of methoxy substituent at ring A deviates from the plane of other atoms by about 0.26 A°. Cyclohexane ring D was in half chair conformation. Atom C-8 of ring D deviates out of plane from other five atoms by 0.58 A°. An intramolecular hydrogen bond

between O (7) of daunosamine sugar and H-(09) of ring D was observed. The distance was found as 2.12 A°. It was predicted that 9-OH group of ring D play an important role in binding of dauomycin to DNA. Amino sugar (N3') may form close contact with phosphate of DNA. The helix-to-coil transition of the synthetic DNA poly (dA-dT) in the presence of daunomycin has been investigated by 1D NMR spectroscopy [92]. The changes in chemical shift in 1H, 2H, 3H and $4OCH_3$ protons on complex formation suggested that either ring B and/or C of chromophore of daunomycin overlap with adjacent nucleic-acid base pairs. Ultraviolet / visible melting studies of daunomycin complexes with a series of synthetic DNAs- substituted with halogen atoms (Br, I) at position 5 were carried out. It was observed that substitution of a bulky halogen atom at position 5 of the pyrimidine ring of synthetic DNA did not perturb the intercalation of the antibiotic into poly (dA-dU). A comparison of the melting curves for the daunomycin. poly (dA-dT) complex with an analog of the antibiotic where the NH_3^+ group was replaced by dimethylglycine was made and it was demonstrated that the contributions of electrostatic interactions between the amino sugar and backbone phosphate stabilize the complex. In another investigation Patel [93] studied the interaction between the daunomycin and the dG-dC-dG-dC duplex as a function of temperature by NMR spectroscopy. The complex formation of daunomycin with DNA in 0.1 M phosphate buffer was found to result in stabilization of the duplex. The

Intercalation geometry was deduced on the basis of upfield shift in 1H, 2H, 3H and 4OCH_3 protons of daunomycin due to complexation.

Courseille et al. [28] studied the structure of daunomycin by x-ray crystallography. The main feature of the structure was that the aromatic part of the molecule was planar. The cyclohexane ring had the monoplanar or half chair form. The sugar daunosamine was protonated on the amino group. It had the chair form of conformation and its mean plane was almost perpendicular to the tetracyclic plane (83°). A short intramolecular distance O(9)-H(9)....O(7) of 2.84 A° was observed. Existence of hydrogen bonds was proposed, the distances of which were O(5)-H(5)... O(6) = 2.53 A° and O(12)-H(12)...O(11) ≈ 2.47 A°. Neidle and Taylor [82] investigated some conformational properties of the daunomycin and several of its derivatives using semi empirical energy calculations. It was reported that conformation corresponding to the minimum energy was close to, but not identical with, the experimentally determined ones. Deletion of the O9 hydroxyl group and -$COCH_3$ was not found to result in any appreciable shift of the global energy minimum. It was suggested that deletion of O6 would result in a therapeutically improved derivative. The structure of the crystalline daunomycin - d(CGTACG) complex was solved by x-ray diffraction analysis [101]. It was observed that DNA forms a right-handed double helix with two daunomycin molecules intercalated in the 5'-d(CpG)-3' sequence. The daunomycin aglycon chromophore oriented at right angles to the long dimension of the DNA base pairs and the cyclohexene ring was in the minor groove.

Unwinding of DNA helix by 8° followed by distortions of the backbone occurred on intercalation. Mixed sugar puckering was observed i.e. C1 sugar as C2′-endo; G2 as C1′-exo; T3 as O1′-endo; A4 as C2′-endo; C5 as C2′-endo and G6 as C3′-exo. Atom C9 of daunomycin was found to be farthest from the plane of the unsaturated ring system. A strong hydrogen bond between O9 atom of ring A and the nitrogen N3 of guanine (G2) was observed. In addition, the amino group N2H of the same guanine was also found within hydrogen bonding distance of O9 atom. The amino sugar was found to lie in the minor groove of the double helix without bonding to the DNA.

Nuss et al. [86] reported the NMR study of the interaction of daunomycin with dinucleotides d-pApT, d-pTpA, d-pGpC, d-pCpG and d-pCpC. It was observed that daunomycin does not bind to all sequences of the dinucleotides with equal strength. A molecular model based on results obtained from the daunomycin/nucleotide titrations was proposed. Interaction of the 3′-amino group with the phosphate group belonging to the base adjacent to the intercalation site was proposed. It was observed that the conformation of ring A remains unaltered upon binding to dinucleotides, but the conformation of daunosamine sugar moiety was altered.

The helix-coil transition of the self-complementary hexanucleotide $d(pTpA)_3$ has been studied in 1 M NaCl by NMR spectroscopy [96]. It was found that daunomycin interacts with

hexanucleotide at 5 °C and stabilizes it by 21 °C at a drug/nucleotide ratio of 0.063. The cooperative release of daunomycin from the hexanucleotide duplex was monitored by observing the change in chemical shifts of daunomycin protons on increasing the temperature. On melting the helix, the H(1′) and aromatic proton signals shift downfield by ≥ 0.21 and 0.14 ppm, respectively. The changes in chemical shift of the drug protons suggested that ring D of daunomycin does not overlap significantly with the central base pair of the hexanucleotide and that it extends out from the helix. Patel et al. [94] deduced the structural aspects of the intercalation complex of the daunomycin and its analog 11-deoxydaunomycin with the synthetic DNA poly (dA-dT) by ^{1}H and ^{31}P NMR in high salt solution. 11-deoxydaunomycin has the non exchangeable proton in place of exchangeable hydroxyl group at position 11 of anthracycline ring B. A very large upfield shift (≃ 1.42 ppm) was observed in 11OH proton on complex formation as compared to the much smaller upfield shifts (0.15-0.35 ppm) observed at H-1, H-2, H-3 and OCH_3-4. Results indicated that ring B must be located in the shielding region of the base pairs and ring D does not overlap with the adjacent base pairs.

Chaires et al. [14] studied the self association of daunomycin in aqueous solution. Sedimentation results showed that daunomycin aggregates beyond a dimer with an association constant of 1500 M^{-1}. NMR data have shown that the aromatic protons i.e. 1H, 2H, 3H of the anthracycline portion of the drug are most affected by

self association, probably due to stacking of the anthracycline rings. Effect of self association on drug binding to DNA was assessed. These results suggested that at low salt concentration the self association does not interfere with the drug binding. It was observed that at 200 mM ionic strength, daunomycin bind to DNA with an association constant of around 10^6 M^{-1}. Equilibrium dialysis and fluorescence titration were used to study daunomycin - DNA interactions [15]. Kinetics of the complex monitored at different temperatures indicated the binding to be exothermic. Dialysis experiments have shown that GC base pairs were preferred more as binding sites for the drug. Daunomycin binds tightly to DNA and show the negative cooperativity. The intrinsic binding constant was found to drop from 7.0×10^5 M^{-1} to 1.8×10^5 M^{-1}, as the Na^+ concentration changes from 0.2 to 1.0. An exclusion parameter was determined as n = 3.5 base pairs.

Fritzsche et al. [35] studied the interaction of daunomycin and iremycin with DNA by transient electric dichroism and sedimentation analysis of supercoiled closed duplex DNA. The apparent length increase of sonicated calf thymus DNA (150 ± 20 base pairs) in 2.5 mM sodium cacodylate buffer (pH 7.0) at 12 °C was found to be 0.40 ± 0.02 nm/bound iremycin and 0.31 ± 0.02 nm/bound daunomycin. Unwinding induced by iremycin was observed as 15.0 ± 1.5°. Under similar conditions daunomycin has induced an unwinding of 15.4 ± 1.5°.

Chaires [16] reported that daunomycin has an allosteric effect on the B to Z equilibrium. It is an effective inhibitor of the B to Z transition in poly d(G-C) in 4 M NaCl. Both the rate and extent of B to Z transition were found to decrease by the presence of drug. Equilibrium dialysis hydrodynamic and electric dichroism studies were carried out on the complex of daunomycin with H1-depleted 175 base pairs nucleosomes [17]. It was reported that daunomycin binds with higher affinity to free DNA than to nucleosomes while ethidium binds 10 times more strongly with nucleosomes than with free DNA. The inhibition of the RNA polymerase - catalysed synthesis of RNA by daunomycin was examined [58]. It was found that the saturation binding of daunomycin to the template leads to complete inhibition of RNA synthesis as a result of daunomycin interference with enzyme - template interactions. Beraldo et al. [7] reported that iron complexes of daunomycin and adriamycin display antitumor activity against P 388 leukemia that compares well with that for the free drug. Iron complex of adriamycin unlike adriamycin does not participate in NADH dehydrogenase mediated free-radical redox cycles, to any significant extent. It was suggested that it could be an effective non-cardiotoxic alternative to other currently available anthracycline anticancer agents.

The interaction of daunomycin with B and Z helices of a self-complementary DNA fragment d(CGm^5CGCG) in solution was studied by ^{1}H-NMR spectroscopy [84]. The results showed that B to Z transition kinetics was not affected by addition of daunomycin.

Daunomycin was found to bind exclusively to the B form of d(CGm^{5}CGCG).

Chaires [18] studied the binding of daunomycin to poly [d(G-C)] and poly [d(G-m^{5}C)] under a variety of solution conditions using spectrophotometric and flurometric methods. It was observed that nearly 1 bound drug molecule per 3 base pairs is required for conversion of poly [d(G-C)] from the Z to the B form in 3.5 M NaCl, while only one bound drug molecule per 20 base pairs is required in 2.4 M NaCl. Chaires [19] studied the thermodynamics of daunomycin - DNA interactions. The results indicated that the interaction is sensitive to temperature and ionic strength. The binding was found to be exothermic over the range of NaCl concentration 0.1 M to 1.0 M and the favourable free energy for the binding of the drug to DNA was reported to arise primarily from the large negative enthalpy. An overall negative enthalpy was found to be derived largely from the molecular interactions at the intercalation site, in particular from 3-5 hydrogen bonds. Kinetics of the interaction of daunomycin with calf thymus DNA were studied using stopped-flow and temperature-jump relaxation methods [20]. It was proposed that interaction mechanism has three steps. First step is the rapid "outside" binding of daunomycin to DNA, followed by intercalation of the drug which is then followed by either conformational adjustment of the drug or DNA binding site or redistribution of bound drug to preferred sites.

Chen et al. [24] performed theoretical computations on the interaction of daunomycin to six self-complementary double-stranded hexanucleotides; $d(CGTACG)_2$, $d(CGATCG)_2$, $d(CITACI)_2$, $d(TATATA)_2$, $d(CGCGCG)_2$ and $d(TACGTA)_2$. Results indicated that a distinct preference was manifested by the 9-hydroxyl group for sequences $d(CGATCG)_2$, $d(CGTACG)_2$ and $d(CGCGCG)_2$, that is, for intercalation sites between two GC base pairs. This preference was due to a favourable interaction of 9-OH group with G2 base by hydrogen bonding interaction between the hydroxyl oxygen and a hydrogen of the 2-amino group of G2. Interaction with daunosamine sugar favoured A or T at position 3. It was suggested that the sequence specificity of daunomycin in its interaction with oligo - or polynucleotides could not be described in terms of the two base pairs which compose the intercalation site of the chromophore and should rather be defined in terms of three base pairs. Among the six oligomer sequences investigated, the strongest complexes were those obtained for the mixed hexanucleotides $d(CGATCG)_2$ and $d(CGTACG)_2$. Mclennan et al. [68] studied the self association of daunomycin and adriamycin in D_2O and methanol using NMR spectroscopy at 400 MHz. It was reported that these antibiotics self associate as dimers in solution in contrast to results reported earlier [14]. At room temperature the association constant for the dimerization process was found as $4.0 \times 10^5\ M^{-1}$. Islam et al. [51] studied the interaction of substituted anthraquinones based on doxorubicin and mitoxantrone in solution and by computer graphics modelling of their intercalation into the

self-complementary deoxydinucleotide d(CpG). It was observed that 1-substituted compound can bind from either groove, the 1, 8-disubstituted compound binds with both substituents in the major groove. Mondelli et al. [71] investigated the conformational properties of daunomycin and its several analogs such as adriamycin by ^{1}H NMR in different solvents, $CDCl_3$, D_2O, DMSO, dioxane and pyridine. On the basis of $J_{7,8}$ and iong range coupling constants, it was reported that daunomycin and adriamycin prefer a single conformation of ring A as half chair, $^{0}H_{8}$, in D_2O. Intramolecular hydrogen bonding between 9(OH) and O(7); low steric interactions between substituents at C(7), C(10) and the peri hydroxy groups of ring B, were recognized as the stabilising factors for $^{9}H_{8}$ conformation.

The conformation of the daunosamine sugar with respect to the aglycon moiety has been investigated for N-acetyl daunomycin in $CDCl_3$ solvent by nuclear overhauser experiments [72]. Strong positive NOE effects were measured for H(1') (15%) and H(7) (13%) following irradiation of H(7) and H(1'), respectively. Interproton distances reported for H(5')-H(8eq), H(7)-H(8ax), H(7)-H(8eq), H(1')-OH(6) were 2.40, 2.30, 2.45 and 3.26 A° respectively. The glycosidic angles ϕ and ψ were calculated as $40^{\circ} \pm 5$ and $-5^{\circ} \pm 5$ respectively.

The site and sequence specificity of the daunomycin - DNA interaction was examined by deoxyribonuclease I foot-printing studies [21]. Preferred binding site for daunomycin was found as

triplets containing adjacent GC base pairs at their 5′ side flanked by an AT base pair. The crystal structure of a daunomycin-d(CGTACG) complex has been solved by x-ray diffraction analysis [126]. It was reported that daunomycin molecules intercalate their aglycon chromophores between CpG sites at both ends of the hexamer duplex. The DNA molecule in the complex adopted a distorted right-handed double helical structure with Watson - Crick base pairing. The daunomycin aglycon chromophore was oriented at right angles to the long dimension of the DNA base pairs, and the cyclohexene ring A was found to rest in the minor groove of the double helix. O9 hydroxyl group of the daunomycin formed two hydrogen bonds with N3 and N2 of an adjacent guanine base. Intramolecular hydrogen bond between O7 and O9 hydroxyl group of daunomycin was not found to exist in complex in contrast to that observed in x-ray crystal structure of the drug alone [79]. The C1 residue was found to have a normal anti-glycosyl torsion angle, $\chi = -154^{\circ}$, while that for the other three residues were all in high anti range. Amino sugar was found to lie in the minor groove. Sugar N3′ atom of the daunomycin molecule was strongly hydrogen bonded to two water molecules, the W2 and W13, and possibly to the O2 of residue C11. Skorobogaty et al. [119] investigated the DNA-sequence specificity of daunomycin by DNase I footprinting and E. coli RNA polymerase transcription - inhibition assay. The 5′-CA sequence was identified as being the highest affinity binding site.

Xodo et al. [132] studied the interaction of daunomycin with calf thymus DNA and six alternating purine-pyrimidine sequences by fluorimetric and UV-visible absorption methods. Binding affinity of drug for the various alternating copolymers considered was found to decrease in the following order : Gm^5C>AT>AC-GT>IC>GC> AU. On the basis of this trend it was suggested that not only the type of the base pairs immediately downstream of the intercalation site was important for the complex stabilization, but also the presence of a 5-group in the pyrimidine residue of the intercalation site play an important role for the drug - DNA interaction.

Ragg et al. [102] studied the interaction of daunorubicin with the self-complementary DNA fragment d(CGTACG) by ^{31}P NMR. The large downfield shift observed for C5pG6 with respect to the others indicated strong helical deformation at the level of C5pG6 sequences as a consequence of interaction. Daunomycin was found to intercalate in the d(CG) sequences at both ends of the helix. The local mobility of the complex between the daunomycin and a DNA hexanucleotide duplex of sequence d(CGTACG) was determined by anisotropic refinement of x-ray diffraction data [46]. It was reported that intercalation of daunomycin reduced the mobility of the base pairs (C.G) bracketing it. The intercalated daunomycin ring system (aglycon) was rigidly fixed in the base stack, while amino sugar was highly flexible. The intercalated ring system was considered as an anchor for the amino sugar segment of the drug. It was suggested that high flexibility of amino sugar may be

important for inhibition of replication and transcription not only by sterically blocking the minor groove, but also by allowing non productive interactions to be formed with various polymerase or other DNA binding proteins. Gorenstein and Lai [42] studied the conformational changes in phosphate ester backbone of RNA duplex poly (A).poly (U) and calf thymus DNA upon binding of the ethidium, quinacrine and daunomycin by ^{31}P NMR. It was observed that addition of a saturating ratio of daunomycin produced a 0.11 ppm downfield shift in the ^{31}P signal of DNA. Downfield shift in ^{31}P signal was attributed to change in backbone torsional angle from gauche, gauche (g,g) conformation to a more extended conformation.

In 1989, Moore et al. [73] studied the crystal structure of daunomycin complexed with self-complementary DNA sequence d(CGATCG). It was found that d(CGATCG) forms a distorted right-handed helix with a daunomycin molecule intercalated at each d(CpG) step. The position of the daunomycin aglycon chromophore was found to be similar as in case of daunomycin-d(CGTACG) complex [126]. The d(A3pT4) step in d(CGATCG)-daunomycin complex showed favourable intrastrand stacking in contrast to that observed for the d(T3pA4) steps in the daunomycin-d(CGTACG) complex. O9 atom of ring A of daunomycin was in hydrogen bonding distances with N-3 (2.9 A°) and N-2 (3.3 A°) of base G2 of d(CGTACG). In the major groove, N-7 of G12 and the two chromophore substituents O-4 and O-5 were geometrically positioned to provide the correct environment to chelate either a sodium atom or a

water molecule. The amino sugar N_3^+ has formed a hydrogen bond with O-2 of the neighboring thymine.

In 1990, Fredrick et al. [34] studied the structure of adriamycin-d(CGATCG) and daunomycin-d(CGATCG) by x-ray crystallography and compared them with the structure of daunomycin - d(CGTACG) solved by Wang et al. in 1987 [126]. In these complexes the chromophore was intercalated at the CpG steps at either of the DNA helix with the amino sugar extended into the minor groove. In each complex, one end of the aglycon is anchored by two direct hydrogen bonds between the drug O9 to N2 and N3 of residue G2 of DNA. In comparison with daunomycin - d(CGTACG), the amino sugars in the two daunomycin-d(CGATCG) and adriamycin-(CGATCG) complexes form more favourable interactions with the DNA. The van der Waals and hydrogen bond distances were significantly shorter. The structures of daunomycin and adriamycin with d(CGATCG) were found to be very similar to each other. However, additional solvent interactions between the C14 hydroxyl of adriamycin and DNA were observed. Under the influence of the altered solvation, there was considerable difference in the conformation of spermine in these two complexes. A switch of the base pair from TA to AT was found to increase the stability of complex. Cieplak et al. [26] studied the base specificity of drug-DNA interactions by free energy calculations. Free energy difference between the two complexes d(CGTACG).daunomycin and d(CGCACG).daunomycin was found as 3.6 kcal/mol. These results indicated that daunomycin preferably binds to a base pair sequence

that has a TA base pair close to the daunosamine sugar i.e. in the position next to the intercalation site. Chaires et al. [22] studied the preference of daunomycin binding site within the 160 base pair tyr T DNA fragment by deoxyribonuclease I (DNase I) footprinting titration procedure. The triplets 5' $\begin{matrix}A\\T\end{matrix}$ GC and 5' $\begin{matrix}A\\T\end{matrix}$ CG were identified as the preferred binding sites.

In 1991, Nunn et al. [85] studied the interaction of daunomycin with the hexanucleotide duplex sequences d(TGATCA) and d(TGTACA) by x-ray crystallography. Binding was found to occur via. intercalation of the drug chromophore at the d(TpG) step in both hexamers. The amino sugar was found to be situated in the minor groove in both the complexes. The hydroxyl atom O-9 was within the hydrogen bonding distance of residue G2. However, the hydrogen bonding interactions of the amino sugar group and the conformation of ring A were different in the two complexes. In daunomycin - d(TGTACA) complex, amino group has formed hydrogen bonds with two water molecules. These water molecules in turn interact with O-2 of residue T3 and O-4' of residue A4. In daunomycin -d(TGATCA) complex the amino group has formed hydrogen bonds via its three hydrogen atoms to oxygen atoms in the neighboring residues T4 and C5. Wang et al. in 1991 [127] reported that when daunomycin was mixed with DNA hexamer, in presence of formaldehyde, it forms stable covalent adducts with DNA. The structure of these adducts were determined by x-ray crystallography. The overall structure of each complex was found to be very similar to daunomycin-d(CGTACG) complex [126]. It was

proposed that new type of potential anticancer drug could be synthesized by attaching a reactive functional group at the N3′ amino position of daunorubicin/doxorubicin. Remeta et al. [106] reported the binding enthalpies for the complexation of monomeric daunomycin with a series of 10 polymeric DNA duplexes. It was observed that magnitude and even the sign of the enthalpy change for daunomycin binding was strongly dependent on the base composition and sequence of the host duplex. The binding of daunomycin to alternating purine-pyrimidine sequence that contained G.C base pairs was characterized by large exothermic enthalpies. Removal of a purine amino group that projects into the minor groove was found to result in a significant decrease in the magnitude of the daunomycin binding enthalpy. The structures of two hexanucleotide-anthracycline complexes d(CGGCCG)/daunomycin and d(TGGCCA)/adriamycin have been determined using single-crystal x-ray diffraction techniques. In both cases the anthracycline molecule is bound to non-preferred d(YGG) base pair triplet sites [61].

In 1994, Roche et al. [109] examined the binding properties of daunomycin using double helical oligonucleotides that were 16 base pairs long. Four major sequences examined contained six base pair core : CGTACG, TAGCTG.TCATCC and $(TA)_3$ which were flanked on the 5′ and 3′ ends by tracts of adenines. Fluorometric, absorption, calorimetric and stopped-flow techniques were used to examine the binding. Appreciable binding to the flanking adenine tracts was also observed. The strongest core binding sequence

found was CGTACG, but its affinity was only 2-fold larger than that for other core sequences. Roche et al. [110] have also tested the binding affinity of a series of daunomycin analogs to a group of oligonucleotides that contained binding sites specific for daunomycin using spectrophotometric techniques. The series of drugs selected differed from daunomycin in the sugar moiety, including substitution of a hydroxyl group for the charged amino group and replacement of the 2'-OH by an iodo substituent. It was found that the compounds with hydroxyl substituted for the amino group in the sugar ring bound less well to the oligonucleotides by factors of upto several hundred than daunomycin. Changing the iodo-substituted sugar from the natural L-form to the D-form has diminished the binding by 6-50 fold, depending on the sequence. This result implied a stereospecific interaction of the natural sugar with DNA chain. Recently Lipscomb et al. [64] studied the hydration and dynamics of daunomycin-d(CGATCG) and adriamycin - d(CGATCG) complexes by x-ray crystallography. Quantitative assessment of relationship between water ring size and frequency of occurrence in the vicinity of nucleic-acid interfaces was made. The results showed that five-membered water rings were not preferred over other ring sizes. Thermal mobility of the amino sugar of daunomycin and adriamycin was found to be significantly greater than that of the rest of the complex.

Recently in 1994, Barthwal et al. [6] studied the interaction of daunomycin with deoxydinucleotide d(CpG) in D_2O by two-dimensional proton magnetic resonance techniques at 500 MHz. It

was observed that ring D protons 1H, 2H, 3H and $4OCH_3$ shift upfield upto 0.23 ppm on complexation. Base protons GH8, CH6 and CH5 have also shown upfield shift of about 0.26 ppm. The T_m value of duplex d-CpG has increased by about 10 °C on complexation. The conformation of deoxyribose sugar was determined on the basis of coupling constants, Σ1′, Σ2′, Σ2", and Σ3′. It was found that sugar was predominantly in the S conformational state for both cytosine and guanine residues. The conformational parameters obtained were : P_S = 153°, ϕ_S = 36°, P_N = 18°, ϕ_N = 36° and χ_S = 0.65, and P_S = 135°, ϕ_S = 36°, P_N = 18°, ϕ_N = 36° and χ_S = 0.68 for G and C residues, respectively. The glycosidic bond rotation, χ was found as anti for both G and C residues. Conformation of daunomycin was found to alter on complexation. The spin - spin couplings: J(1′H-2′eqH), J(1′H-2′axH), J(4′H-5′CH_3), J (7H-8axH), and J(7H-8eqH), interproton distances: 1′H-2′axH, 7H-8axH, 7H-8eqH, 5′H-8axH, and 5′H-8eqH were altered significantly on complexation. Several intermolecular NOE contacts were observed between the drug and dinucleotide protons in the NOESY spectra of daunomycin - d(CpG) complex. The 1H and 2H protons of ring D were found close to CH6 protons.

SCOPE OF THESIS

As we gather from the available literature that various aspects of daunomycin and its interaction with DNA has been studied extensively using various techniques. Till 1980, several physicochemical techniques; UV-vis spectroscopy, fluorescence,

circular dichroism have been used to study the kinetics of binding, sequence specificty etc. These studies could predict that daunomycin intercalates between 5'-3' d-(CpG) and d-(TpG) DNA sequences. Later in 1985, preference for AT and TA as third base pair is also indicated [24]. However, the molecular basis of interaction of daunomycin, intermolecular forces involved in binding and complete three-dimensional structure of daunomycin - DNA complexes could not be ascertained. Recently, progress in instrumentation of x-ray and NMR techniques provided a new insight in determining the three-dimensional structure of a molecule. Then from 1987, onwards, several research groups used x-ray crystallography techniques to understand the molecular basis of daunomycin-DNA interactions. Molecular structure of daunomycin-hexanucleotide complexes is determined in solid-state. Several features of daunomycin-DNA interactions are determined at the molecular level. However, there is no such detailed study in solution state which is much closer to biological conditions in vivo. Further studies in solution state will be more relevant, as we know that electrostatic interactions, H_2 bonding interactions and stacking interactions which dictate the conformation of molecules and interactions occurring between them are more evident in aqueous solutions than in crystalline state. Recently we have reported [6] the two-dimensional NMR studies on interaction of daunomycin with deoxydinucleotide d-CpG in solution. Several features of daunomycin - DNA interactions occurring in solution conditions are determined. Further to understand these

interactions we have selected another oligonucleotide d-(TGATCA), which has two binding sites for daunomycin, and is a better representative of duplex DNA. High resolution two-dimensional NMR techniques are used to determine the three-dimensional conformation of daunomycin, hexanucleotide d-TGATCA, their complexes and thereby molecular basis of anticancerous action of daunomycin. The analysis of this model system will provide a guideline for change of substituents in designing of drug which will have less side effects and wide spectrum of anticancerous activity. Further, these studies will provide a basis to understand the interaction of aromatic amino acid side chains of proteins with nucleic-acid bases, the molecular mechanism of protein - DNA interactions.

MATERIALS AND METHODS

MATERIALS

The deoxyoligonucleotide 5'-3' d-$(TGATCA)_2$ is purchased from DNA Chemical International U.S.A. Deuterium oxide (D_2O) and chloroform ($CDCl_3$) with 99.96 % isotopic purity and daunomycin are purchased from Sigma Chemical Co. U.S.A. Sodium 2, 2-dimethyl-2-silapentane-5-sulfonate (DSS), internal NMR reference is purchased from Merck Sharp and Dohme Canada Ltd., Canada. Sodium dihydrogen phosphate (NaH_2PO_4), disodium hydrogen phosphate (Na_2HPO_4) and ethylene diamine tetra acetic acid (EDTA) are of analytical grade and purchased from E. merck, India Ltd. Drug and DNA samples are used without further purification.

Further, d-$(TGATCA)_2$ sample is also synthesized for routine 1D NMR experiments. Synthesis is carried out on 10 μmole scale on an Applied Biosystems DNA synthesizer (model 381 A) using cyanoethyl phosphoramidites in Dr. K.B. Roy's laboratory at J.N.U., Delhi. However, all 2D experiments are conducted on the sample purchased from DNA Chemical International, U.S.A.

The starting material is a solid support derivatized with a nucleoside which will become the 3'-hydroxyl end of the oligonucleotide. The 5'-hydroxyl is blocked with a

dimethoxytrityl (DMT) group. The steps of the DNA synthesis cycle are as follows :

(i) The treatment of the derivatized solid support with acid removes the DMT group and thus frees the 5′-hydroxyl for the coupling reaction. An activated intermediate is created by simultaneously adding the phosphoramidite nucleoside monomer and tetrazole, a weak acid, to the reaction column. The intermediate is so reactive that addition is complete within 30 seconds.

(ii) The next step, capping, terminates any chains which did not undergo addition. Capping is done with acetic anhydride and 1-methylimidazole. Capping minimizes the length of the impurities and thus facilitates their separation from the final product.

(iii) During the last step, oxidation, the internucleotide linkage is converted from the phosphite to the more stable phosphotriester. Iodine is used as an oxidising agent and water as oxygen donor. This reaction is complete in less than 30 seconds.

After oxidation, the dimethoxytrityl group is removed with trichloroacetic acid, the cycle is repeated until chain elongation is complete. Treatment with concentrated ammonium hydroxide for one hour removes the β-cyanoethyl protecting groups and also cleaves the oligonucleotide from the support. The benzoyl and isobutyryl base protecting groups are removed by heating at room

temperature in ammonia for 8 to 15 hours. Purification is carried out using RPLC and ion-exchange chromatography. RPLC is performed on ABI HPLC instrument with acetonitrile and triethyl ammonium acetate (0.01 M) buffer system (pH-7.0). The buffer system used for ion-exchange chromatogrpahy is 1 M NaCl in 10 mM NaOH and 10 mM NaOH (pH 12.0). Desalting is also carried out after purification using biogel column. The purified d-$(TGATCA)_2$ is annealed by heating it in a water bath up to 70 $^{\circ}C$ and then allowing it to cool until it attains room temperature. Thus a duplex of d-$(TGATCA)_2$ is prepared.

SAMPLE PREPARATION

Daunomycin solution (11.0 mM) is prepared by dissolving a known quantity of sample in D_2O. It is lyophilised and redissolved in D_2O and the process is repeated twice. The final concentration is checked by taking the absorbance of the sample at wavelength 480 nm using the value of extinction coefficient $\varepsilon = 9.8 \times 10^3\ M^{-1}\ cm^{-1}$. In a separate experiment 0.4 ml daunomycin solution (6.5 mM) is prepared by the same procedure in $CDCl_3$ solvent. HDO and $CDCl_3$ signals are used as internal NMR reference in these experiments. Solution of deoxyoligonucleotide d-$(TGATCA)_2$ (3.68 mM, duplex concentration) is prepared by dissolving a known quantity of it in deuterated phosphate buffer (16.25 mM) of pH 7.0 having 15 mM sodium salt. The sample is lyophilised and redissolved in D_2O and process is repeated twice. The final sample solution is prepared by adding 0.4 ml of D_2O to it just prior to

recording NMR experiments. Its concentration is checked at 260 nm by absorbance measurements at DU-6 spectrophotometer (Beckman). Value of extinction coefficient used is $\varepsilon = 11.4 \times 10^3\ M^{-1}\ cm^{-1}$. Typically 1 µl of 0.1 M DSS is added to the solution as internal NMR reference. Further 0.1 mM EDTA is added to solution in order to suppress paramagnetic impurities which causes line broadening during NMR measurements.

Preparation of daunomycin-d-$(TGATCA)_2$ complex

3.68 mM d-$(TGATCA)_2$ and 32.66 mM daunomycin solution are taken as the stock solution for preparation of complex. A complex of d-$(TGATCA)_2$ and daunomycin is prepared by titration. 90 µl of 32.66 mM daunomycin is added in steps of 10 µl to 0.4 ml of 3.68 mM d-$(TGATCA)_2$ sample during titration in order to make 2:1 complex of daunomycin : $d(TGATCA)_2$. The concentration of d-$(TGATCA)_2$ (N_1) in total volume of 0.41 ml is determined as follows :

$$N_1V_1 = N_2V_2$$

$$N_1 \times 0.41 = 3.68 \times 0.4$$

$$N_1 = 3.59\ mM$$

The concentration of daunomycin (N_3) in this solution is determined as follows :

$$N_3V_3 = N_4V_4$$

$$N_3 \times 0.41 = 32.66 \times 0.01$$

$$N_3 = 0.80\ mM$$

Likewise other daunomycin-d-$(TGATCA)_2$ complexes at different drug/nucleotide (D/N) ratio are prepared. The concentration of daunomycin (D), d-$(TGATCA)_2$ (N) and drug/DNA (D/N) are shown in Table 3.1.

NMR METHODS

Theory

Nuclear magnetic resonance spectroscopy (NMR) is an analytical technique and is based on the absorption of radiofrequency (rf) electromagnetic radiation by atomic nuclei, mainly protons but also other nuclei having an odd number of protons. A nucleus having magnetic moment I in a magnetic field B_0 takes up (2I+1) orientations which are characteristic of energies dependent on the magnitudes of magnetic moment μ and magnetic field B_0. For protons having I = 1/2, it is restricted to two possible orientations m_I = +1/2 and -1/2. The two orientations correspond to two energy states and it is possible to induce transitions between them. The frequency of the electromagnetic radiation which will effect such a transition is given by the equation :

$$\nu = \frac{\gamma B_0}{2\pi}$$

where ν is the linear resonance frequency, γ is the gyromagnetic ratio of the nucleus.

In order to interpret any NMR spectrum, it is essential to have an understanding of the various factors that influence the

Table 3.1 : Various concentration ratios (D/N) for the complex formed between daunomycin and d-$(TGATCA)_2$

Nucleotide Conc. (mM) = N	Drug Conc. (mM) = D	D/N
3.68	0	-
3.59	0.80	0.22
3.50	1.56	0.45
3.42	2.28	0.67
3.35	2.97	0.89
3.27	3.63	1.10
3.20	4.26	1.33
3.13	4.86	1.55
3.07	5.44	1.77
3.00	6.00	2.00

frequency, area and shape of the NMR signal. The NMR parameters are as follows :

Chemical shift

It was noted that an applied field B_0 induces electronic currents in atoms and molecules and that these produce an additional small field $B_0\sigma$ at the nucleus which is proportional to the B_0. The total effective field at the nucleus can therefore be written as :

$$B_{eff} = B_0 - B_0\,\sigma$$

$$= B_0\,(1 - \sigma)$$

σ, is called the shielding or screening constant. The screening constant σ is sensitive to the chemical environment of the nuclei, and therefore nuclei in different chemical environments experience different fields and hence produce signals at different frequencies. Thus position of a resonance signal on an NMR scale is defined by chemical shift. The chemical shift δ expressed in parts per million (ppm) is defined as :

$$\delta = 10^6 \times \left\{ \frac{\delta_{ref} - \delta_{obs}}{\delta_{ref}} \right\}$$

where, δ_{ref} is the position observed for a reference compound and δ_{obs} is the position of the signal of interest.

Spin - spin coupling constant

Spin-spin coupling arises from the effects of neighboring nuclei on the field felt by the nucleus of interest. The interaction is mediated by bonding electrons and depends on the distance between nuclei, the type of chemical bond, the bond angle and nuclear spin. The most important parameter in determining three-dimensional conformation of biological macromolecules is the vicinal or three-bond coupling constant (^3J) between nuclei A and D in the fragment A-B-C-D. These couplings are related to the dihedral angle θ between plane A-B-C and B-C-D by Karplus relationship [55,56] given as follows :

$$^3J = 8.5\ Cos^2\theta - 0.28 \qquad 0^\circ < \theta < 90^\circ$$

$$^3J = 9.5\ Cos^2\theta - 0.28 \qquad 90^\circ < \theta < 180^\circ$$

The dihedral angle (θ) can thus be obtained between a pair of coupled protons.

Relaxation time

The relaxation time is a measure of the time that spin system takes to return to its equilibrium value after it has been excited. The spin-lattice relaxation time (T_1) is a measure of the rate with which the Z component of magnetization, M_z, approaches thermal equilibrium. The rate at which a Boltzman distribution of population is set up among energy levels is $1/T_1$. The term spin-lattice is used because the processes involve an exchange of energy between the nuclear spins and their molecular frame work. It depends on several factors, e.g. internuclear dipole-dipole

interaction, chemical shift anisotropy, scalar coupling, spin rotation, electron-nuclear relaxation etc.

The spin-spin relaxation time (T_2) is a measure of the rate at which the M_{xy} component of magnetization returns to its equilibrium. The term spin-spin is used because the relaxation processes involve interactions between neighboring nuclear spins without any exchange of energy with the lattice. The relaxation time T_2 is reflected in the NMR line shape and line width. The line width at half height is related to T_2 by the following formula :

$$(\Delta\omega)_{1/2} = \frac{1}{\pi T_2}$$

where, $\Delta\omega_{1/2}$ correspond to line width at half height.

In practice $(\Delta\omega)_{1/2} = \frac{1}{\pi T_2^*}$

where T_2^* is the effective relaxation time which has contributions from the true relaxation time and from field inhomogeneities, so that T_2^* is always less than T_2.

In order to carry out a NMR experiment one needs a static magnetic field B_0 for the alignment of the nuclear spins, a radiofrequency field to stimulate absorption and a detector to record the resonance signals. In an FT-NMR spectrometer the sample is excited by a short radiofrequency pulse which contains all the frequencies in the range of possible chemical shifts in a given nucleus.

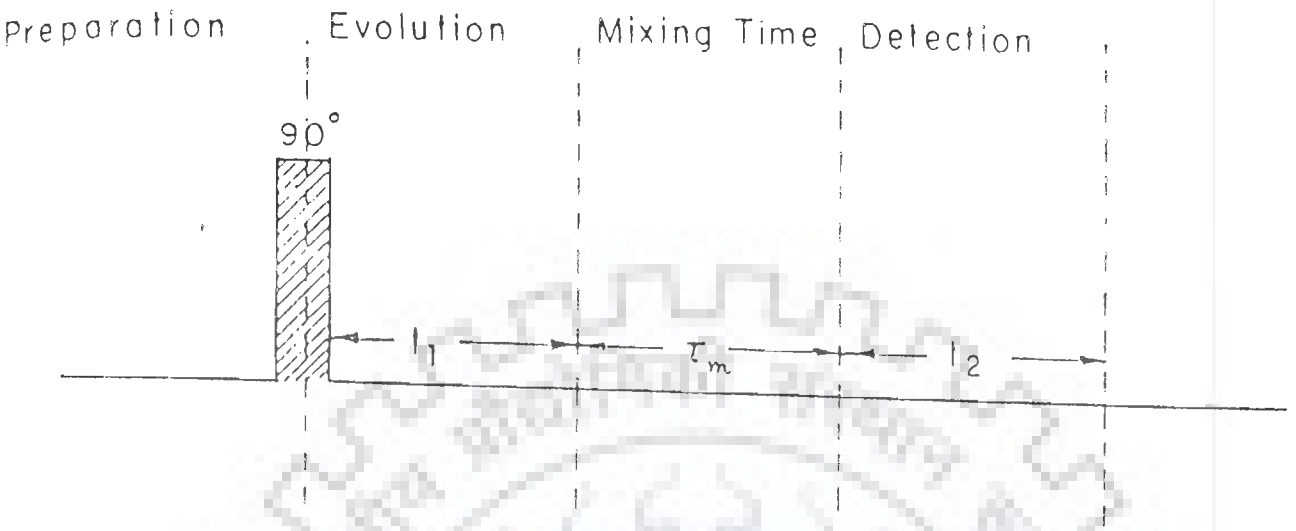

Fig.3.1 : Four different time segments of a 2D NMR experiment namely (i) preparation period (ii) evolution period (t_1) (iii) mixing period (τ_m) and (iv) detection period (t_2).

A normal one-dimensional (1D) NMR experiment provides information on the chemical shifts and spin-spin couplings but the spectra of biological macromolecules and large organic molecules are often too complex and it may not be possible to obtain complete resonance assignments and unambiguous structural information on the basis of 1D NMR. The advent of two-dimensional (2D) NMR, which was first proposed by Jeener in 1971 [53] and later developed by Aue et al. [5] has helped a lot in solving such problem.

TWO-DIMENSIONAL (2D) NMR TECHNIQUES

The two-dimensional spectrum has two frequency axis (ω_1, ω_2) and the intensities are represented along the third axis. Thus each peak in a 2D spectrum occupies volume as against an area in the 1D spectrum. The two frequency dimensions, ω_1 and ω_2 of a two-dimensional NMR are obtained after a fourier transformation with respect to a time domain function $S(t_1, t_2)$. The 2D NMR experiment consists, in effect, of a series of one-dimensional experiments in which the time interval t_1 is incremented and free induction decay for each experiment is recorded during the time interval t_2 as in one-dimensional NMR. The two time variables are generated by suitable segmentation of the time axis of the FT-NMR experiment. In all two-dimensional experiments, four different time segments can be distinguished namely preparation period, evolution period (t_1), mixing time (τ_m) and detection period (t_2) (Fig. 3.1).

(i) Preparation period

This consists of delay time followed by one or several radio frequency pulses. During this period thermal equilibrium is attained.

(ii) Evolution period (t_1)

During the evolution period the coherence evolves and at the end of this interval system assumes a specific state, which depends on the elapsed time t_1. The various spins are frequency labelled during this period. During this period, further radiofrequency puises may be applied according to the type of experiment being performed.

(iii) Mixing time (τ_m)

The mixing period may include one or several radiofrequency pulses and delay intervals. During the mixing period coherence is transferred between spins.

(iv) Detection period (t_2)

The amplitudes of signals are detected as a function of evolution time (t_1) during this period.

The kinds of interactions observed in a two-dimensional NMR experiment depend on the exact pulse sequence used (i.e. the number, length and phases of the pulses within and between the three time periods). The purpose of the variety of 2D NMR techniques is to establish a correlation between the behaviour of the spin system during the two periods - t_1 and t_2 which is

achieved by mixing period (τ_m).

Two-dimensional correlation spectroscopy (2D-COSY)

The pulse sequence for COSY experiment given by Jeener [53] is shown in Fig. 3.2. In the pulse scheme the spin system is allowed to relax to equilibrium during preparation period, at the end of which a 90° pulse converts the longitudinal magnetization into transverse magnetization. During the evolution period t_1 the magnetizations precess at their resonant frequencies just as in a normal free induction decay. The second 90° pulse acts as a mixing pulse and transfers magnetization between J-coupled spins in the system. Some spins do not exchange magnetization and these spins give rise to peaks along the diagonal in the 2D-COSY spectrum. Both diagonal and off diagonal cross peaks have multiplet structures characteristic of the spins from which they originate.

COSY experiment can be carried out with special phase cycling and data processing to change the 2D line shape into pure 2D absorption mode, allowing the use of a phase-sensitive display. There are two different methods in use, the first requires the results of two complete COSY experiments with different phase cycling to be added [120] and the second known as TPPI (Time proportional phase incrementation) method uses a single experiment with phase cycling which changes with t_1 increment [8,57,67,104] . The phase-sensitive COSY spectra has cross peaks in antiphase. The antiphase multiplet structure of a cross peak only occurs in

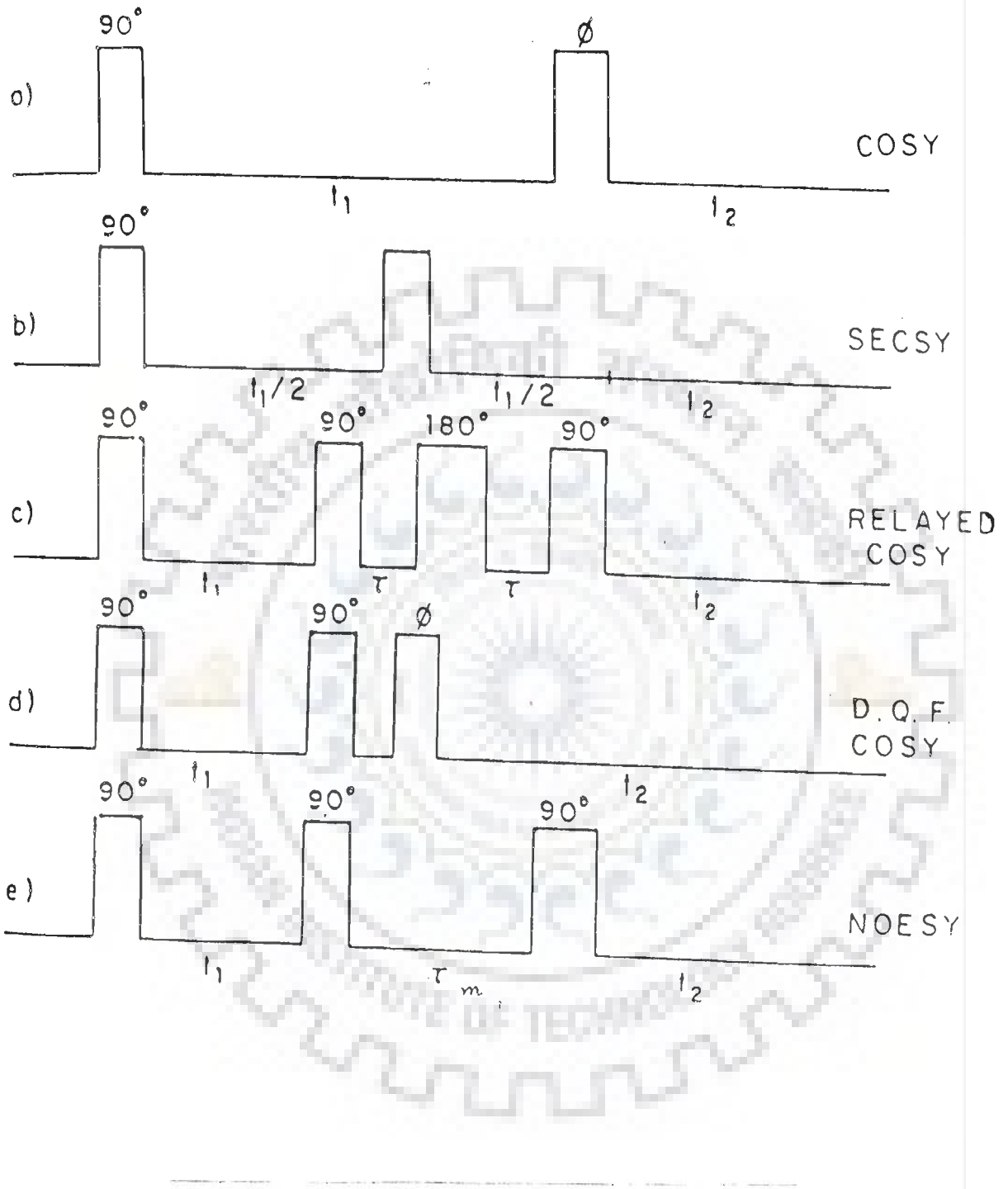

Fig.3.2 : Pulse schemes of various 2D NMR techniques.

the active coupling giving rise to cross peak. Extra splittings present in multiplet but, which do not give rise to cross peaks are called passive couplings and appear inphase. Thus, the advantage of phase-sensitive COSY is that the phase relation between peaks can be used for accurate assignment and calculation of coupling constants.

In a three spin system e.g. AMX with spin-spin coupling constants J_{AM}, J_{AX} and J_{MX} (Fig. 3.3(a)), the AX pattern is split into identical arrays [30]. The coupling between the protons connected by the cross peaks are active couplings while all others between these protons and any other proton are passive couplings. For example, the AX cross peak at $\omega_1 = \delta_X$ and $\omega_2 = \delta_A$ manifests along ω_2 the antiphase (+ -) splitting J_{AX} and inphase (+ +) splitting J_{AM}. Along ω_1 axis, it manifests antiphase splitting J_{AX} and inphase splitting J_{MX}. A typical phase-sensitive COSY [30] for an AMX system with positive and negative contours in black and red is shown in Fig. 3.3(b). In the cross peak pattern B, the smaller coupling is the active coupling J_{AX} (along both ω_1 and ω_2 axis) and the larger ones along ω_2 and ω_1 axis are passive couplings J_{AM} and J_{MX}, respectively. It is readily apparent from the Fig. 3.3 (a, b) that the appearance of the cross peaks including the order in which positive and negative components are arranged depends critically on the relative size of the individual coupling constant.

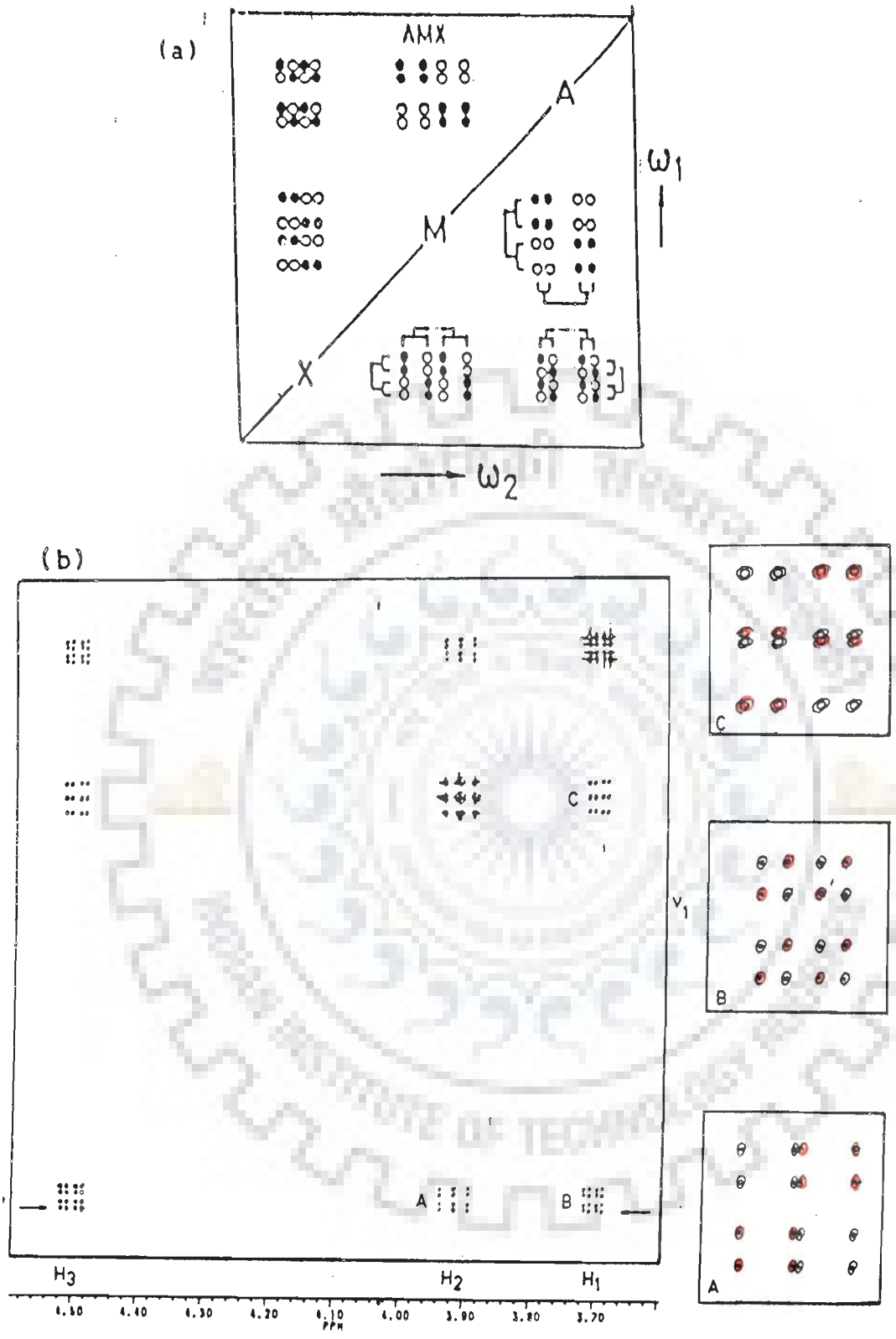

Fig.3.3 : (a) Schematic COSY spectrum of a three spin system, AMX. Filled circles represent positive signals, open circles represent negative signals. (b) A typical phase-sensitive COSY spectrum for an AMX system. Negative peaks are shaded with red colour.

Double quantum filter COSY (DQF-COSY)

The experiment uses the pulse sequence 90_{ϕ}-t_1-90_{ψ}-90_{ξ}-t_2 where ϕ, ψ and ξ are the appropriate phase cycles [97] (Fig. 3.2). In ^{1}H NMR spectra methyl singlets are often very intense and split into many lines due to spin-spin coupling. This creates problem in COSY and other spectra because multiplet responses of interest are sometimes buried beneath t_1 noise and spinning side bands from the singlets. INADEQUATE sequence specifically excludes singlets from the spectrum by creating multiple quantum coherence and forcing the phase cycling to follow the latter rather than the single quantum coherences. In double quantum filter COSY experiment, the responses from a COSY experiment are passed through a double quantum filter, thereby removing methyl and other singlets from the final spectrum. The short delays, Δ, immediately before and after the final pulse, are of the order of microseconds. Twice as many transients are needed in this experiment to achieve the same signal-to-noise ratio than in conventional COSY. Another advantage of DQF-COSY is that it converts the phase of COSY diagonal signals from dispersive antiphase to absorptive antiphase. These signals then do not interfere with the cross peaks. So, the cross peaks lying close to diagonal can be observed in double quantum filtered phase-sensitive COSY. Double filter COSY spectra can be used to determine the coupling constants [13,41].

Two-dimensional nuclear overhauser enhancement spectroscopy (2D NOESY)

Information about the proximity of atoms in space is obtained from 2D NOESY experiment. The NOE cross peak in a NOESY spectrum arises from cross-relaxation, a phenomenon due to dipole-dipole interaction between two or more protons which are close in space. Thus exact three-dimensional conformation of molecule can be deduced by 2D NOESY. The pulse sequence for making correlation through dynamic NOE is shown in Fig. 3.2.

The first 90° pulse creates transverse magnetization. During the evolution period t_1 the various magnetization components precess with their characteristic precession frequency in the X-Y plane of the rotating frame, are thus frequency labelled. After the second 90° pulse cross-relaxation leads to incoherent magnetization exchange during the mixing time τ_m. The signal is recorded immediately after the third pulse as a function of t_2. The experiment is repeated for a set of equidistant t_1 values. For adequate signal-to-noise ratio, n transients are accumulated for each value of t_1. Two-dimensional fourier transformation of the data matrix $S(t_1, t_2)$ then produces the desired frequency domain spectrum $S(\omega_1, \omega_2)$.

NMR EXPERIMENTAL PARAMETERS

All proton NMR experiments are carried out at National FT-NMR facility located at TIFR, Bombay and are recorded on 500 MHz, high resolution Bruker AM 500 FT-NMR spectrometer equipped with aspect

computer. Typical NMR parameters used for one-dimensional experiments are pulse width 10-12.5 μs (60°pulse), number of data points 8-16 K, spectral width 4000 Hz, number of scans 64-128 and digital resolution of 0.25-0.5 Hz/point. Receiver gain (RG) value is optimised in each case to obtain best possible signal to noise ratio. In temperature variable experiments, constant temperature is maintained in the range 277-350 K using temperature controller accessory. Phase-sensitive 2D COSY and NOESY experiments are carried out at 297 K for daunomycin and at 295 K for deoxy-oligonucleotide d-$(TGATCA)_2$ and daunomycin-d$(TGATCA)_2$ complex. 2D NOESY experiments are recorded at different mixing times (τ_m) 400, 500, 600, 700, 800 ms for daunomycin; 75, 150, 200, 250 ms for DNA hexamer d-$(TGATCA)_2$ and 50, 75, 150, 200, 350 ms for drug-DNA complex respectively. Typical parameters used for 2D experiments are 1024-2048 data points along t_2 dimension, 512 free induction decays in t_1 dimension, pulse width 9.5 - 12 μs, spectral width 4000 Hz, number of scans 64-128, digital resolution of 2.30-4.60 Hz/point, and relaxation delay of 1.0 s.

STRATEGIES USED FOR CONFORMATIONAL ANALYSIS OF NUCLEIC-ACIDS

The first step in determination of the structure of nucleic-acids is to obtain unambiguous resonance assignments of the individual protons. Once the assignments have been made, the quantitative estimation of various cross peaks in the 2D J-correlated and NOE correlated spectra can be used to derive

information about sugar geometry, glycosidic bond rotation and backbone structure along the entire sequence of the molecule.

Spectral assignment

From the NMR point of view, the protons in nucleic-acid can be classified into two groups namely the exchangeable NH protons of the bases which resonate between 10-16 ppm and the non-exchangeable base and sugar protons which resonate between 7-9 ppm and 2.0 - 6.5 ppm, respectively with the exception of methyl protons which resonate between 0.5 - 2.0 ppm.

Comprehensive sequential resonance assignment strategies for nucleic-acids have been put forward by a number of groups [32,33,45,48,49,50,65,75,104,114] based on the known structures of DNA and RNA.

The strategy basically consists of two steps. In the first step, a COSY spectrum is used to identify the sugar protons belonging to the individual networks of coupled spins following the intranucleotide J-connectivity pathways; H1'-(H2', H2"), H3'-(H2', H2"), (H3'-H4'), H4'-(H5', H5"). The cytosine and thymine base protons are identified by J(H5-H6) and J(CH_3-H6) correlations. Distinction between H2' and H2" protons can be made from the NOESY spectrum, which in view of the interproton distances, will show a stronger NOE between H1' and H2" protons as compared to H1' and H2' protons. In right-handed B-DNA structures, base-H2", H2' NOE cross peaks are much more intense than the base - H1' cross peaks. In the second step, the spin

system so identified are assigned to particular nucleotides along the sequence of the molecule by making use of the NOESY spectrum.

For right-handed structures with sugars in C2′-endo/O1′-endo pucker and glycosidic angle in the anti domain, a convenient strategy for sequential assignment is :

(GH8/TH6)n ⟶ (H2′, H2", H1′)n
intra-residue NOE

(GH8/TH6)n ⟶ (H2′,H2", H1′) n-1
inter-residue NOE

where n stands for nth residue in 5′-3′ oligonucleotide sequence. Schematically these are shown in Fig. 3.4(a).

In the case of left-handed Z-DNA conformations, however, strategies [103] are different and are as follows (Fig. 3.4(b)):

(GH8)	⟶	H1′	intra-residue NOE
(CH6)	⟶	H5", H2′	--do--
(GH8)n	⟶	(H5")n-1	inter-residue NOE
(CH6)n	⟶	(H2′)n-1, (H3′)n-1	--do--
(CH5)n	⟶	(H2′)n-1	--do--

Conformation of deoxyribose sugar

There are six proton-proton coupling constants (J) in each of the deoxyribose ring of a DNA duplex, namely ^{2}J(H2′-H2"), ^{3}J(H1′-H2′), ^{3}J(H1′-H2"), ^{3}J(H2′-H3′), ^{3}J(H2′-H3′) and ^{3}J(H3′-H4′). One of these ^{2}J(H2′-H2") is a geminal coupling which does not show significant conformational dependent variation. The

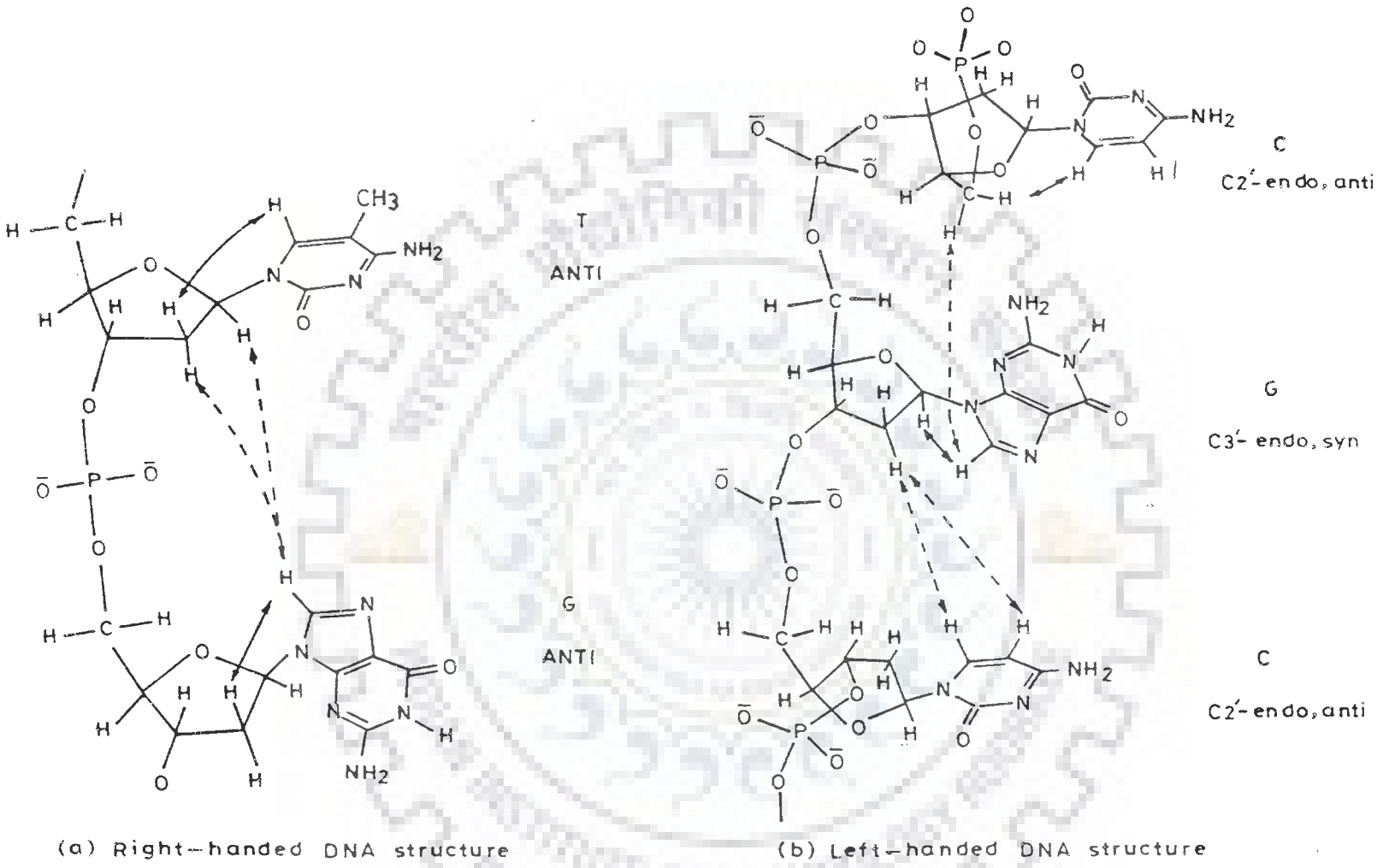

Fig 3.4 : Short interproton distances between adjacent nucleotide units in (a) right-handed DNA (b) left-handed DNA which can be used for sequential assignment

other five J values are vicinal couplings which show a strong dependence on the conformation of the deoxyribose ring [49]. Thus the knowledge of these coupling constants can be translated into the conformation of the deoxyribose rings. Values of coupling constants H1'-H2" and H2'-H3' vary within a narrow range of 6-10 Hz and are comparatively insensitive to the sugar geometry (Fig. 3.5). On the other hand, values of H2"-H3', H3'-H4' and H1'-H2' coupling constants vary in the range 0-10 Hz and can be utilised in fixing the domains of sugar geometries. Under the conditions of low resolution, the intensities of the cross peaks depend directly on the magnitudes of the coupling constants. So depending upon the sugar geometries, certain cross peaks in the COSY spectrum will be more prominent than others and peaks corresponding to low J values may even be absent. Fig. 3.6 shows typical COSY spectra expected for various sugar conformations. In C2'-endo sugar conformation H1'-H2' cross peak is more intense (J $\simeq$ 10 Hz) than H1'-H2" (J $\simeq$ 5.5 Hz) and H3'-H4' (J $\simeq$ 0.9 Hz) cross peak would be absent. However, in the C3' endo sugar geometry H1'-H2" cross peak is more intense (J $\simeq$ 8.0 Hz) than H1'-H2' cross peak (J $\simeq$ 1.4 Hz). The H3'-H4' cross peak is also intense (J $\simeq$ 8.6 Hz). Thus, the information on vicinal coupling constants can lead to important conclusions about the sugar geometry.

Phase-sensitive COSY/DQF-COSY spectra can be utilised to obtain the coupling constants information directly from separation between positive (+) and negative (-) components of a cross peak. But, even for a simple AX doublet, both line width and digital

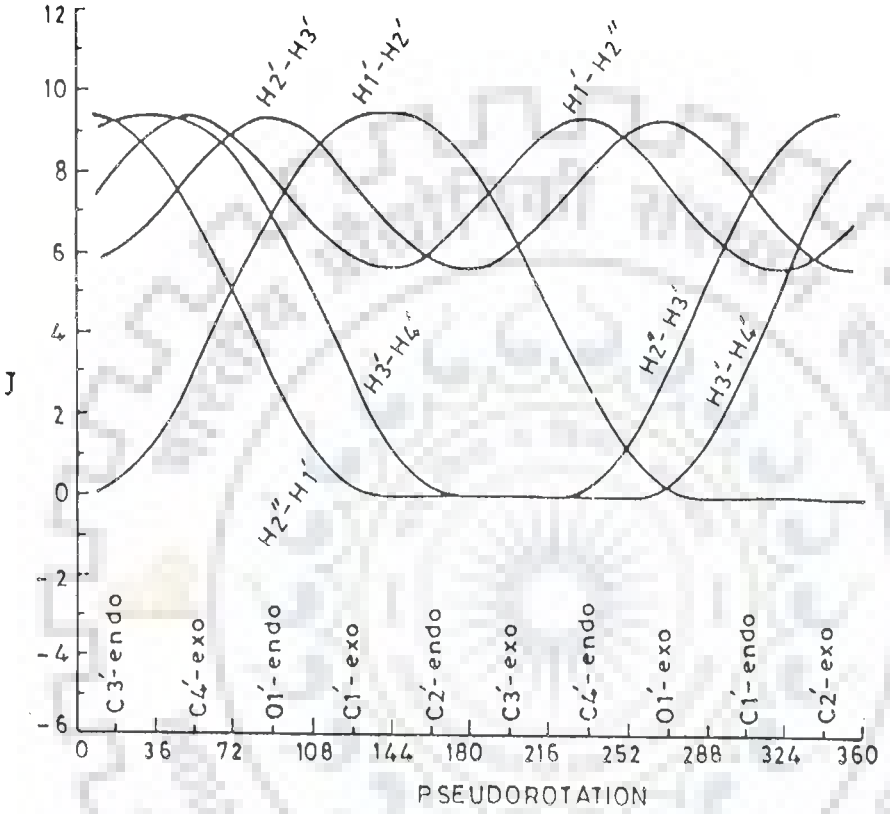

Fig 3.5 : Variation of the vicinal coupling constants in the deoxyribose ring as a function of the ring geometry.

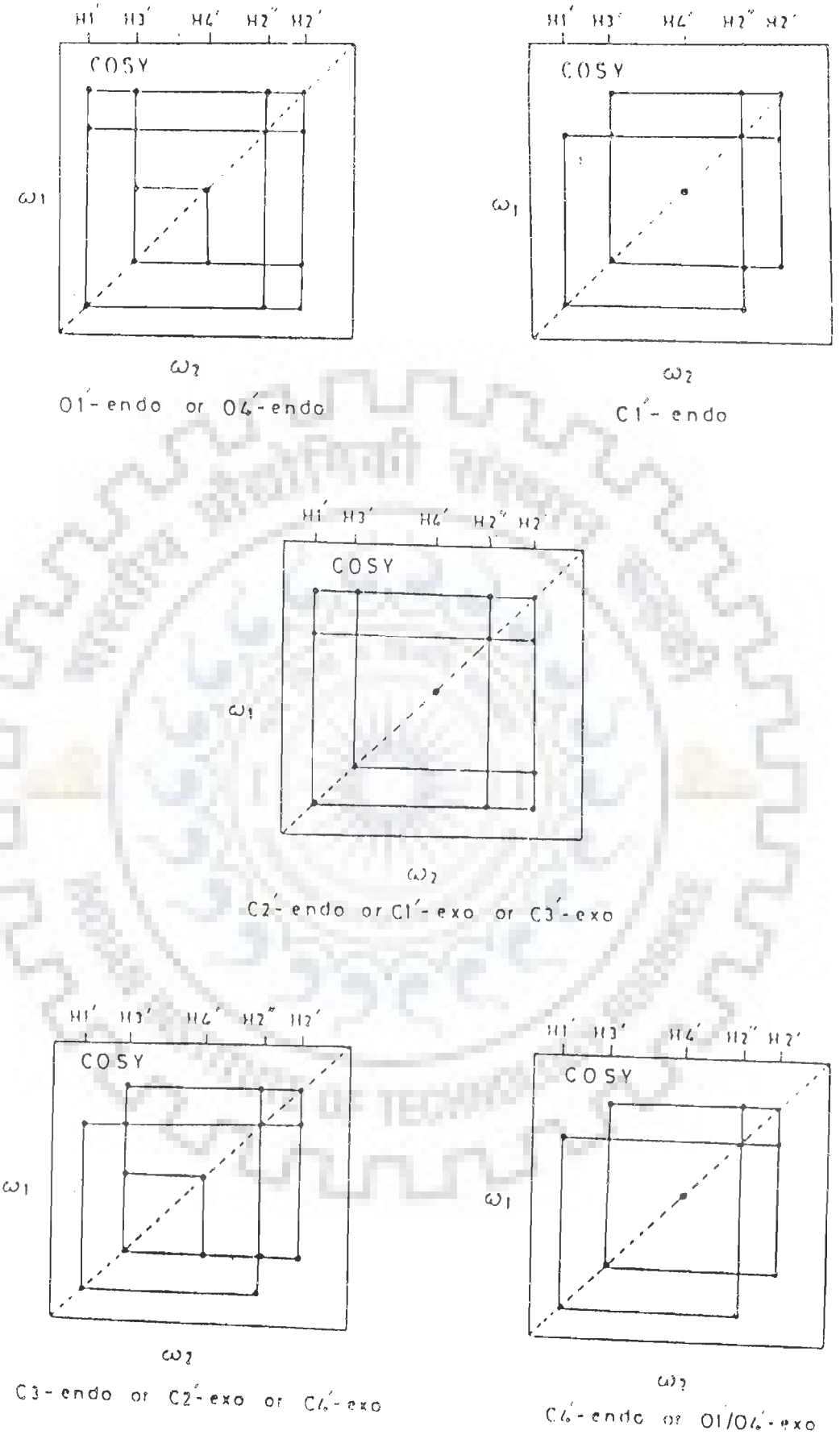

Fig 3.6 : Typical COSY spectra expected for various sugar geometries.

resolution significantly affect the actual separation between these components. Separation of positive and negative components in a cross peak is directly dependent on magnitude of coupling constant.

The strategy used to determine the sugar conformation is analysis of cross peak patterns of H1'-H2', H1'-H2", H2'-H3", H2"-H3', coupled connectivities and spin-spin coupling constants measured using phase-sensitive DQF COSY spectra. Second approach used for determination of sugar geometry is based on interpretation of intrasugar proton-proton distances.

It has been observed that in crystal structures of nucleosides and nucleotides, usually a single pure N or S-type conformer is found but, situation is different in aqueous solution where stacking behaviour plays a more prominent role. N and S-type sugar conformer might be present in equilibrium composition interconverting in solution. Several research groups [107,115,123,129] have developed the strategy to explain the dynamic behaviour of sugar conformers. Complete conformational analysis of a given interconverting furanose in the ideal cases involves the determination of five independent parameters : P_S, ϕ_S, P_N, ϕ_N, χ_N and χ_S, where P_S and P_N are pseudorotation angle for S and N-type conformer, ϕ_S and ϕ_N represent the amplitude of sugar pucker for S and N-type conformer, χ_S is the mole fraction of S-conformer and χ_N is the mole fraction for N-conformer . The mole fraction of S-conformer (χ_S) and N-conformer (χ_N) have been

calculated for each residue using this strategy and is discussed in Chapter V.

Conformation about the glycosidic bond

It has been already established that the torsional angle χ, defining the orientation of a base ring with respect to the deoxyribose ring falls into two categories designated as syn and anti conformation. A quantitative analysis of NOESY data can be used to discriminate between anti, high-anti and syn conformations of glycosidic angle [48,103]. For a syn conformation, a strong NOE between base (H8/H6) and H1′ proton should be observed. At the same time the NOEs from base to H2′, H2" protons will be relatively weak and will have different intensities. In the anti conformation, NOEs from base (H8/H6) to H2′, H2" protons of the same nucleotide will have different intensities. However, the proton corresponding to the weaker NOE will show a strong NOE to the base proton of the next nucleotide. In the high-anti conformation, the NOEs from base (H8/H6) to H2′, H2" will have similar intensities for C2′-endo sugar geometry and will have different intensities for C3′-endo sugar geometry. Further, the H2" proton which would show a strong NOE to base protons of the same nucleotide would also show a strong NOE to the base proton of the following nucleotide on 3′-end.

Among these intranucleotide distances, the (H6/H8)-H1′ distance only depends on χ, while other distances depend both on χ and P. Iso-distance contours have been calculated by Wuthrich

[131] in (P, χ) space for H6/H8-(H2', H2", H3', H4', H5') distances. In principle P and χ can be estimated using observed NOE intensity iso-distance contour plots as discussed in detail in Chapter V.

ESTIMATION OF INTERPROTON DISTANCES

The NOE cross peak in a NOESY spectrum arises from cross relaxation, a phenomena due to dipole-dipole interaction between two or more protons which are close in space (< 5 A°). The interproton distances can therefore be estimated from NOESY spectrum. For large molecules which satisfy the condition $\omega\tau_c > 1$, where τ_c is the effective correlation time and ω is the spectrometer frequency, cross relaxation is very efficient. Spin diffusion among protons leads to quick diffusion of magnetization. The extent of diffusion depends on the length of the mixing time (τ_m) used in the NOESY experiment. For short τ_m (< 50 ms), the magnetization transfer is restricted to a single step and under such conditions the intensity of a cross peak (I_{ij}) is proportional to a single cross-relaxation rate σ_{ij} (where i and j are the relaxing protons).

$$I_{ij} = \sigma_{ij} \tau_m \qquad \ldots(1)$$

Initially the intensity of the cross peak in equation (1) varies linearly with mixing time, and therefore this condition is referred to as "linear regime", but on higher mixing times, this condition does not exist due to multispin relaxation. Interproton distances can be estimated by measuring the intensities of cross

peaks in the "linear regime". Two-spin approximation is used in NOE distance measurements in which only the rate of dipolar magnetization transfer between proximal spins i and j is monitored and all other spins are ignored. For two-spin approximation, the intensity I_{ij} can be written as :

$$I_{ij} = \frac{\gamma^4 \hbar^2 \tau_c \tau_m}{10\, r_{ij}^6} \quad \text{when } \omega \tau_c >> 1 \qquad \ldots(2)$$

where γ is the magnetogyric ratio and $\hbar$, is planck's constant divided by 2π.

In order to determine the accurate value of τ_m for estimation of interproton distances, NOE build up curves should be obtained as a function of τ_m for several cross peaks, since spin diffusion can be different for different protons. Correlation times, τ_c, can be obtained from T_2 and T_1 measurements, according to the equation :

$$\tau_c = 2\omega^{-1}(3\, T_2/T_1)^{-1/2} \qquad \ldots(3)$$

which holds good for $\omega\tau_c >> 1$

If protons i, j, k, l have similar τ_c values and if r_{ij} is a known distance, then the unknown distance r_{kl} can be calculated by comparing the intensities I_{ij} and I_{kl} in a single spectrum.

$$\frac{I_{ij}}{I_{kl}} = \frac{r_{kl}^6}{r_{ij}^6} \qquad \ldots(4)$$

The choice of known distance is important in light of the mobility associated with different atoms in the nucleic-acid. Gronenborn et al. [44] have expressed the opinion of using different yardsticks for NOEs involving different group of protons. The r(CH5-CH6) and r(H2'-H2") have different effective correlation times and can be used as reference depending on the cross peak being compared. The thymidine ($H6-CH_3$) distance of 3.0 A° can be used as a reference for all NOEs involving CH_3 protons, the sugar H2'-H2" distance of 1.84 A° for all NOEs involving sugar H2', H2" protons and for the rest, cytidine H5-H6 distance of 2.45 A° can be used. Reid et al. [105] examined 2'H-2"H and H5-H6 cross-relaxation at 15, 30, 60, 90 and 100 ms in dodecamer DNA duplexes. Results indicate that sugars and bases have the same correlation times, therefore, all proton-proton distances in short DNA duplexes can be determined by scaling the initial NOE build up rate to the slope for the cytosine H5-H6 cross peak, as 2'H-2"H NOE cross peaks are close to diagonal and are usually unresolved.

ANTICANCER DRUG : DAUNOMYCIN

In this chapter we present the conformational properties of daunomycin. Proton NMR studies are carried out in D_2O as a function of temperature in the range 277-355 K on 11.0 mM daunomycin. Typical one-dimensional spectra of daunomycin at three different temperatures are shown in Fig. 4.1 (a-c). In addition the integral plot of daunomycin at 355 K is also shown (Fig. 4.1(d)). The changes in chemical shift of daunomycin protons with varying temperature in the range 277-355 K are shown in Fig. 4.2(a, b). Two-dimensional phase-sensitive COSY spectra and phase-sensitive NOESY spectra for τ_m = 400 ms, recorded at 297 K, are shown in Fig. 4.3(a, b) and Fig. 4.4 (a, b), respectively. Expansions of particular regions of phase-sensitive COSY spectra showing specific interproton connectivities used for calculations of coupling constants are given in Fig. 4.5 (a-j). 1D and 2D phase-sensitive NOESY spectra recorded in $CDCl_3$ at 297 K are shown in Fig. 4.8 and Fig. 4.9, respectively.

Spectral assignment

The protons of ring D 1H, 2H and 3H are observed around 7.3 - 7.7 ppm (Fig. 4.1(b)). The most downfield doublet appearing around 7.55 ppm at 325 K is assigned to aromatic 1H proton and the doublet at 7.46 ppm is therefore assigned to 3H proton [14]. The COSY spectra (Fig. 4.3(b)) shows the connectivity of 2H proton

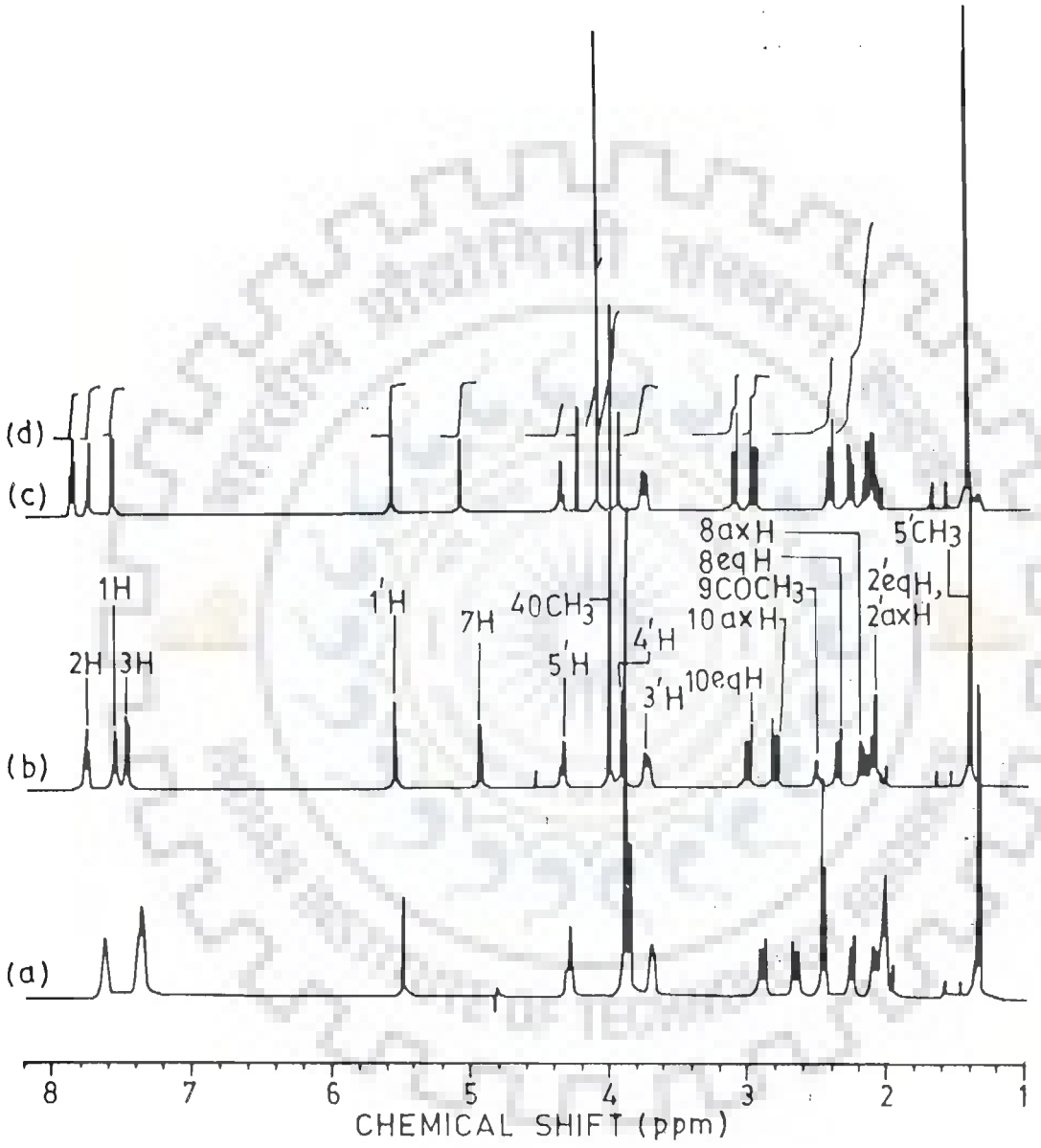

Fig 4.1 : 500 MHz proton 1D NMR spectra of 11.0 mM daunomycin in D_2O at (a) 297 K (b) 325 K (c) 355 K (d) An integral plot of 1D NMR spectra at 355 K. The HDO signal is used as an internal reference in all spectra.

with 1H and 3H protons of ring D, as expected. This confirms the assignment of 1H, 2H and 3H protons. As evident from the integral plot of daunomycin (Fig. 4.1(d)), the sharp intense peak at 3.88 ppm is due to three protons. This resonance gives strong NOE cross peaks with 2H and 3H protons (Fig. 4.4(b)) and is therefore assigned to $4OCH_3$ protons of ring D.

Ring A (Fig. 1.1 of Chapter I), has a pair of protons, 8axH, 8eqH and 10axH, 10eqH which are coupled through strong geminal couplings (^2J). The pairs of protons appearing as doublets at 2.08 and 2.25 ppm give strong intense cross peak in the COSY spectra. Similarly, the pairs of protons resonating at 2.65 and 2.89 ppm give COSY cross peak. These are assigned to the pairs of 8axH, 8eqH and 10axH, 10eqH protons, respectively. Due to ring current effects of aromatic chromophore 8axH and 10axH protons are shifted upfield with respect to their 8eqH and 10eqH protons, respectively [86]. The 8axH and 8eqH protons give COSY cross peak with 7H proton resonating at 4.8 ppm. The resonance at 2.46 ppm due to three protons (Fig. 4.1(d)) gives NOE contact with 10eq proton (Fig. 4.4(a)) and is therefore assigned to $9COCH_3$ protons of ring A.

The protons resonating at 1.33 ppm is assigned to $5'CH_3$ protons of daunosamine sugar. This resonance is strongly coupled to 5'H proton which is further coupled to 4'H proton. In the same way the COSY cross peaks 4'H-3'H, 3'H-2'axH, 3'H-2'eqH, 1'H-2'axH and 1'H-2'eqH assign these resonances. The chemical shift of various resonances of daunomycin are listed in Table 4.1. These

Table 4.1 : Chemical shift, δ (in ppm) of various protons of daunomycin and comparison with that reported in literature by Mondelli et al. [71].

Proton	Present work	Literature
2H	7.62	7.71
1H	7.37	7.53
3H	7.34	7.43
1'H	5.48	5.48
7H	4.80	4.82
5'H	4.29	4.26
$4OCH_3$	3.89	3.93
4'H	3.86	3.81
3'H	3.69	3.66
10eqH	2.89	2.92
10axH	2.65	2.67
$9COCH_3$	2.46	2.43
8eqH	2.25	2.22
8axH	2.08	2.10
$5'CH_3$	1.34	1.28
2'axH	2.04	2.00
2'eqH	2.04	1.96

spectral assignments are in accord with the results available in literature [71].

Changes in chemical shift with temperature

We have monitored self association of daunomycin by the changes in chemical shift with a view to ascertain the chemical shift values for monomeric drug useful for further binding studies. The chemical shift of various protons at different temperatures in the range 277-355 K are listed in Table 4.2. Most of the resonances of daunomycin are found to shift gradually with increase in temperature (Fig. 4.2(a, b)). The ring D protons 2H, 1H, 3H and $4OCH_3$ shift downfield by 0.32-0.51 ppm with temperature. It has been reported [14] that the protons 2H, 1H, 3H and $4OCH_3$ shift upfield by 0.20, 0.26, 0.33 and 0.18 ppm, respectively on increasing the concentration from 10 μM to 7 mM in D_2O solvent. This has been attributed to self association of several drug molecules by stacking of their aromatic rings at higher concentrations [14]. The self association of adriamycin and daunomycin has also been monitored from concentration dependence of ^2H line widths [68]. The changes in chemical shift due to stacking interactions have been reported in literature for drug.nucleic-acid complexes [92,93,96]. In our case daunomycin is present in a self associated form at 277 K and destacking of conjugated aromatic ring takes place with increase in temperature as manifested by downfield shift of proton resonances. The drug gradually changes to the monomeric form as the changes in chemical shift saturate. Therefore, the chemical shift at highest

Table 4.2 : Chemical shifts (in ppm) of daunomycin protons in D_2O at different temperatures.

Temp. (K)	2H	1H	3H	1'H	7H	5'H	4OCH$_3$
277	7.49	7.23	7.23	5.41	4.67	4.21	3.77
287	7.57	7.30	7.30	5.45	4.74	4.26	3.84
297	7.62	7.37	7.35	5.48	4.80	4.29	3.89
305	7.66	7.43	7.38	5.50	4.84	4.30	3.93
315	7.71	7.50	7.43	5.53	4.89	4.34	3.96
325	7.75	7.55	7.46	5.54	4.93	4.35	4.00
335	7.77	7.59	7.48	5.53	4.95	4.33	4.00
345	7.82	7.67	7.53	5.56	5.02	4.34	4.06
355	7.87	7.75	7.57	5.57	5.08	4.36	4.09

Temp. (K)	4'H	3'H	10eqH	10axH	9COCH$_3$	8eqH	8axH
277	3.77	3.63	2.78	2.51	2.37	2.14	2.00
287	3.82	3.67	2.84	2.59	2.42	2.20	2.05
297	3.86	3.69	2.89	2.65	2.46	2.25	2.08
305	3.88	3.71	2.93	2.70	2.49	2.29	2.12
315	3.91	3.73	2.98	2.77	2.52	2.33	2.17
325	3.92	3.74	3.01	2.81	2.52	2.35	2.18
335	3.91	3.72	3.02	2.83	2.49	2.35	2.18
345	3.93	3.75	3.07	2.90	-	2.39	2.23
355	3.94	3.76	3.11	2.97	-	2.42	2.27

Temp. (K)	2'axH	2'eqH	5'CH_3
277	1.98	1.98	1.25
287	1.98	1.98	1.29
297	2.04	2.04	1.34
305	2.07	2.07	1.36
315	2.10	2.10	1.40
325	2.09	2.09	1.40
335	2.09	2.09	1.39
345	2.11	2.11	1.42
355	2.13	2.13	1.43

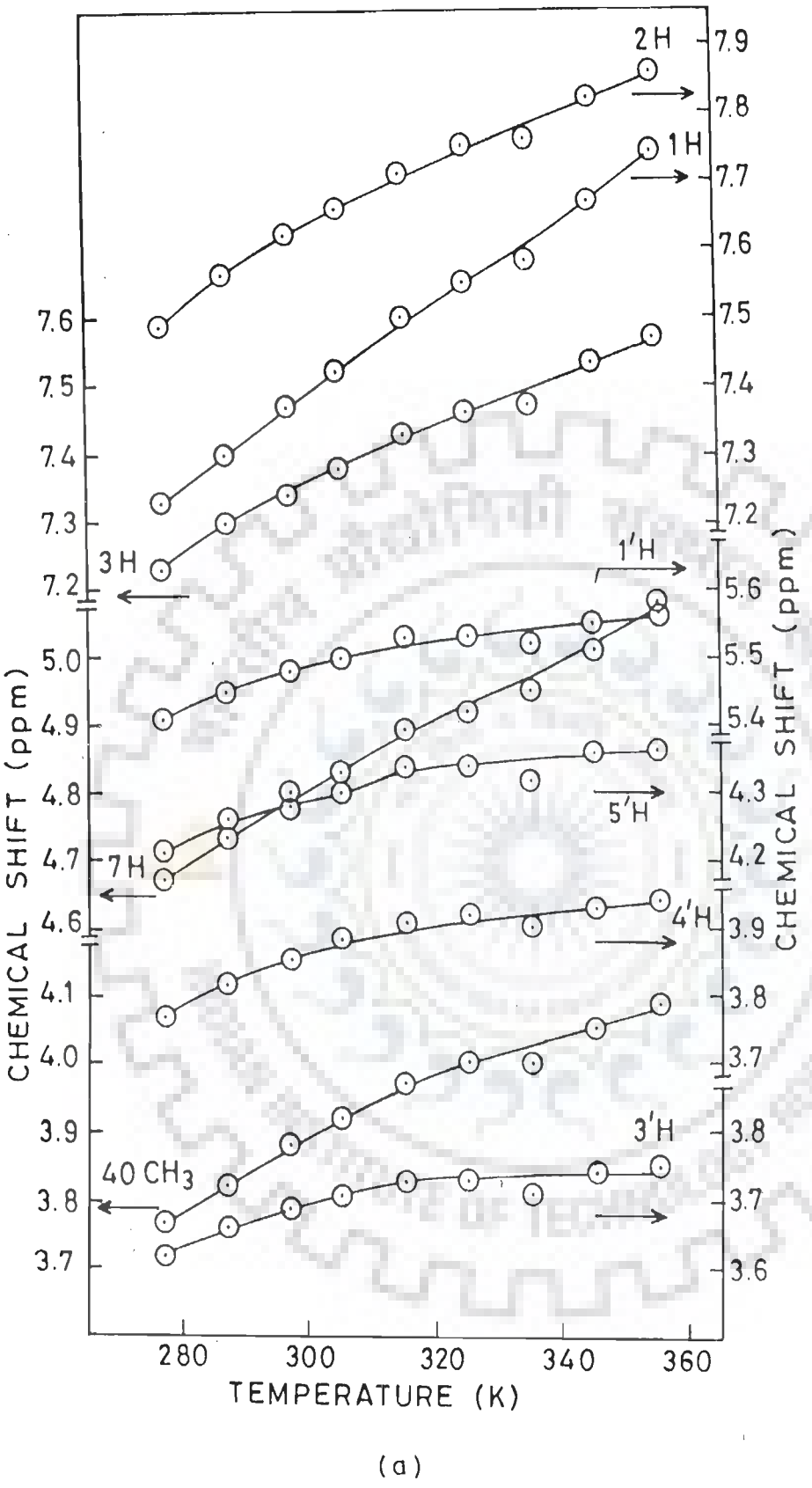

(a)

Fig 4.2 : Chemical shifts of daunomycin protons with varying temperature in the range 277-355 K. (a) Resonances appearing between 3.6-7.9 ppm (b) resonances appearing between 1.2-3.1 ppm.

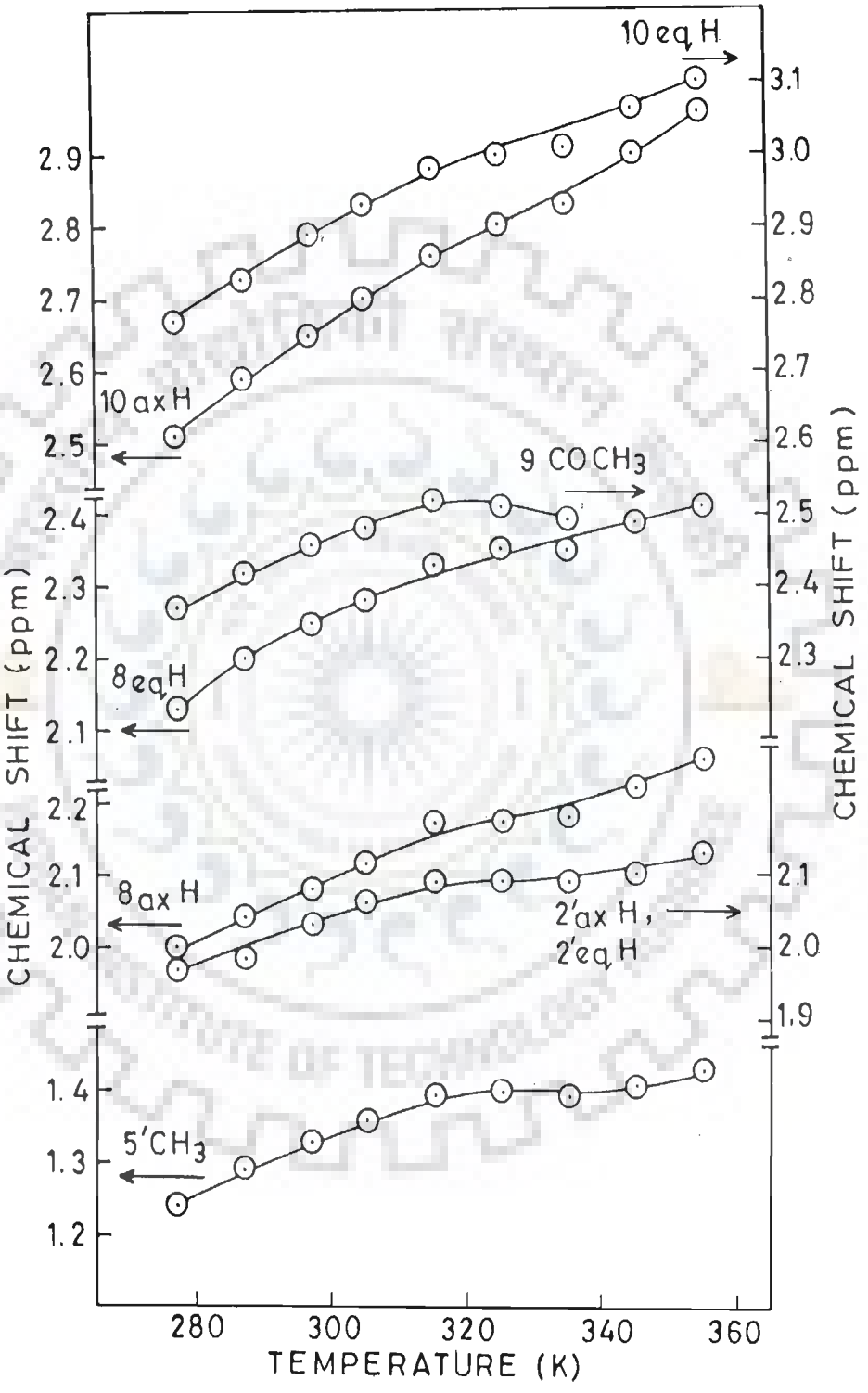
10 eq H
10 ax H
9 COCH3
8 eq H
8 ax H
2'ax H,
2'eq H
5'CH3
CHEMICAL SHIFT (ppm)
CHEMICAL SHIFT (ppm)
TEMPERATURE (K)
280
300
320
340
360

(b)

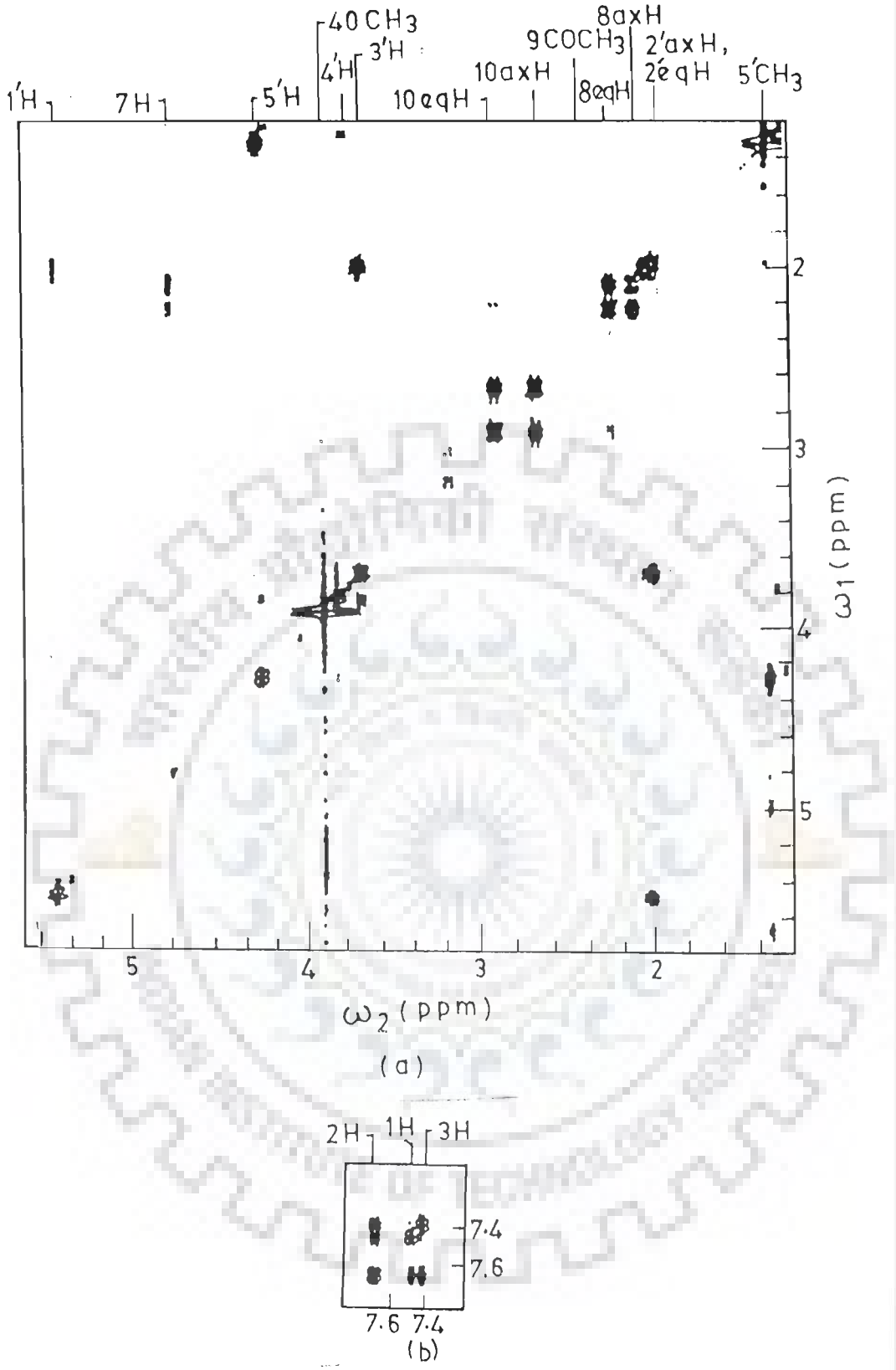

Fig 4.3 : The phase-sensitive COSY spectrum of 11.0 mM daunomycin in D_2O at 297 K showing the COSY connectivities between pairs of protons : (a) within the daunosamine sugar moiety and within ring A (b) within ring D.

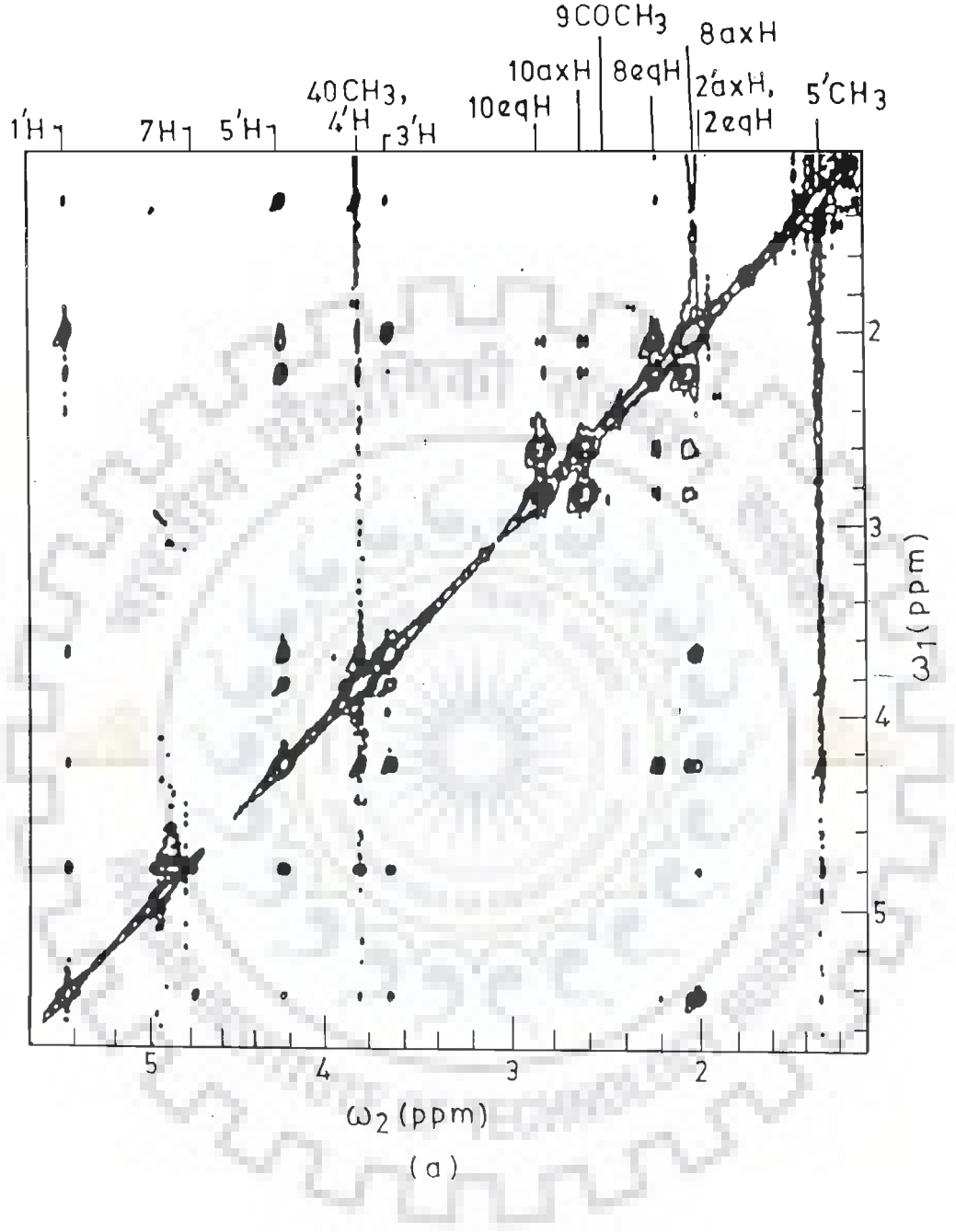

Fig 4.4 : The phase-sensitive NOESY spectrum of 11.0 mM daunomycin in D_2O at 297 K showing the NOE cross peaks between pairs of protons : (a) within ring A and within daunosamine sugar moiety, between ring A and daunosamine sugar moiety (b) within ring D protons.

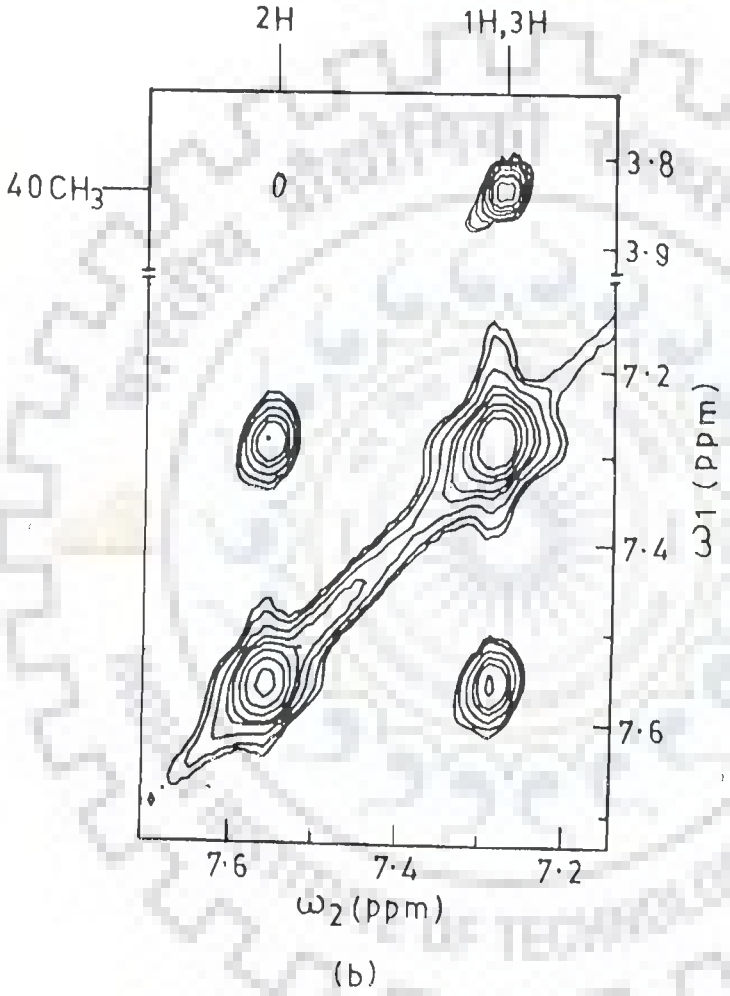

(b)

temperature, 355 K, may be attributed to that of the daunomycin monomer.

The 7H proton of ring A shifts downfield by 0.41 ppm with temperature suggesting the pseudoequatorial position of 7H with respect to rings B, C and D. A relatively small downfield shift of ≃ 0.12 ppm is observed for $9COCH_3$ protons and it is found to broaden at 355 K (Fig. 4.1(c)). The 8axH, 8eqH, 10axH and 10eqH protons shift downfield by 0.27-0.46 ppm, with 10axH showing large downfield shift ≃ 0.46 ppm. This is expected since being in the axial position, this proton is placed nearer to the adjacent stacked ring.

The daunosamine sugar protons show relatively small downfield shift, 0.13 - 0.18 ppm with temperature. The chemical shift of various protons of daunomycin at varying temperatures are shown in Table 4.2.

Coupling constants and torsional angles

The geminal (^2J) and vicinal coupling (^3J) constants are obtained from phase-sensitive COSY spectra. The spin-systems are identified for various coupled protons and active coupling is read off directly as separation between the positive and negative contours in the cross peak. The 8eqH is coupled to both 10eqH and 8axH proton. Since, $\Delta\delta$ (8eqH-10eqH) > J(8eqH-10eqH), this pair of protons belongs to AMX spin system. The splitting pattern along ω_2 axis are expected to be as shown in (a) below :

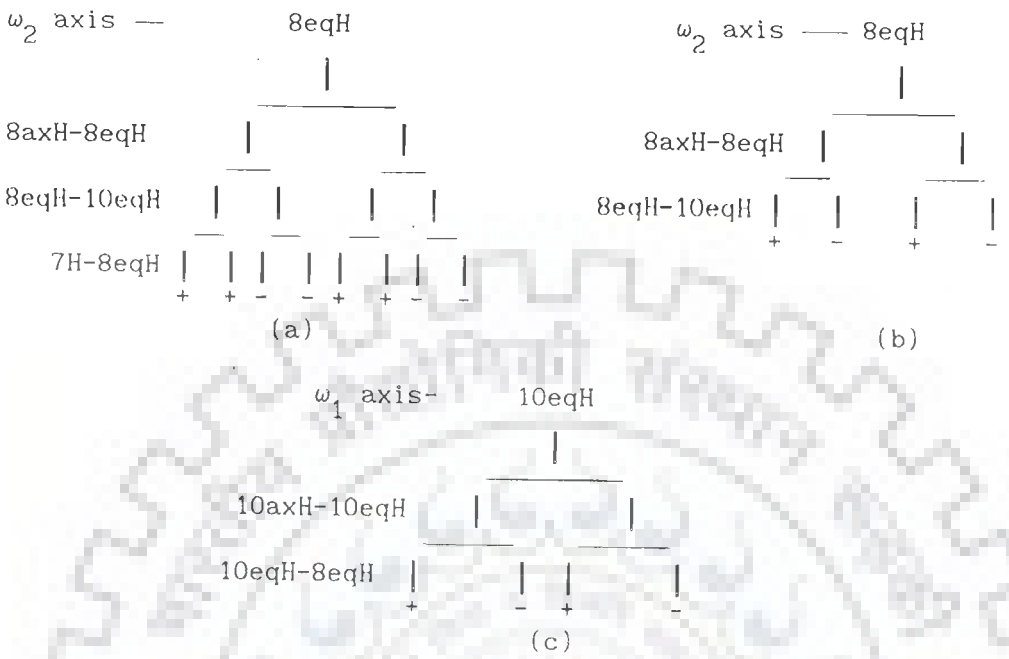

Since the 7H-8eqH coupling is small, the splittings along ω_2 axis may effectively be considered as shown in (b). In a similar way the 10eqH proton splits along ω_1 axis as shown in (c). Fig. 4.5(a) shows the experimentally observed contours of the phase-sensitive COSY spectra showing cross peaks of 8eqH with 10eqH. The negative components are differentiated from the positive ones by its red colour as shown in Figs. 4.5(a-j). The active coupling constant J(8eqH-10eqH) is obtained as the separation between + and - contours along the ω_2 axis as 5.2 Hz. The larger coupling wherein phase remains constant is due to coupling of 8eqH with 8axH protons and therefore gives a value of J(8axH-8eqH). Along ω_1 axis the passive coupling constant J(10axH-10eqH) is read off directly. However these strong geminal couplings J(8axH-8eqH) and J(10axH-10eqH) are more

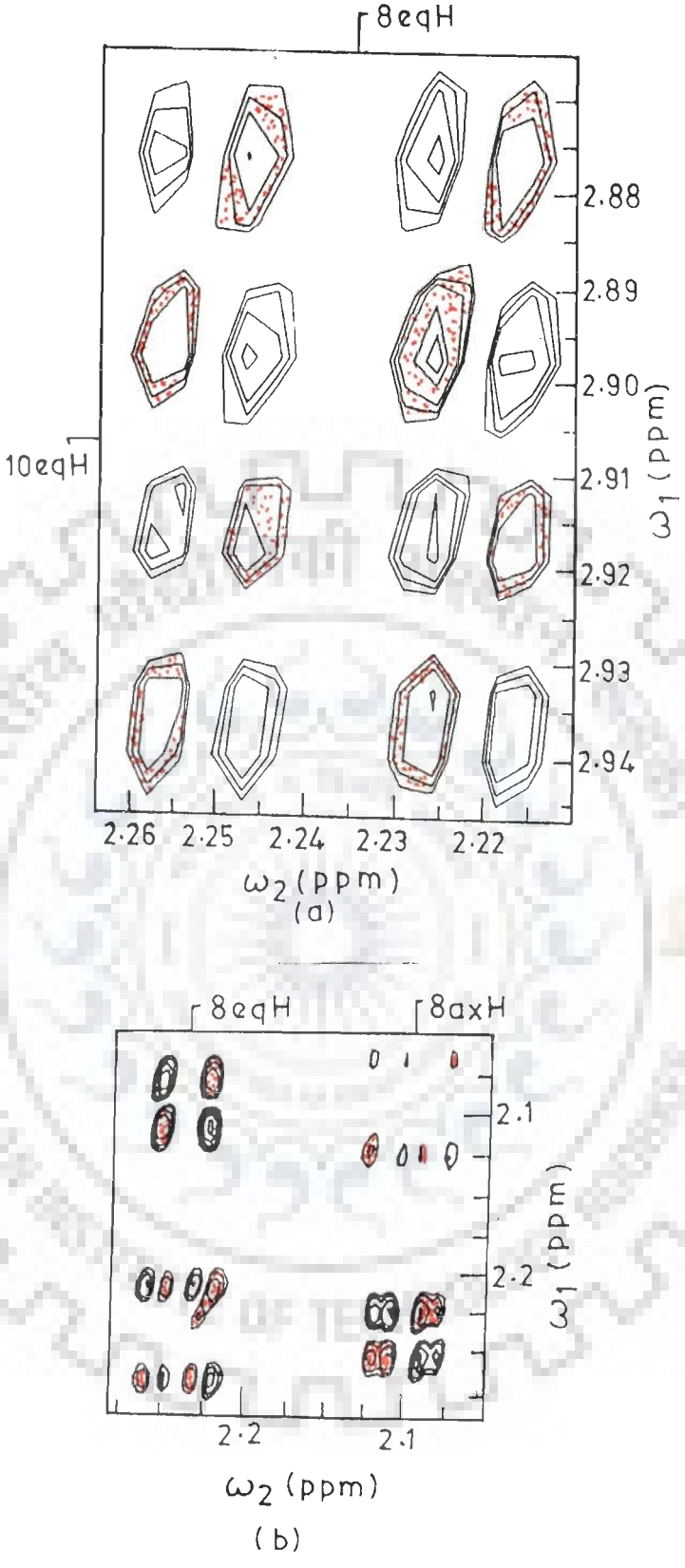

Fig 4.5 : Expansions of the phase-sensitive COSY spectrum (a-j) showing antiphase components along the ω_1 and ω_2 axis of various cross peaks connecting J-coupled protons.

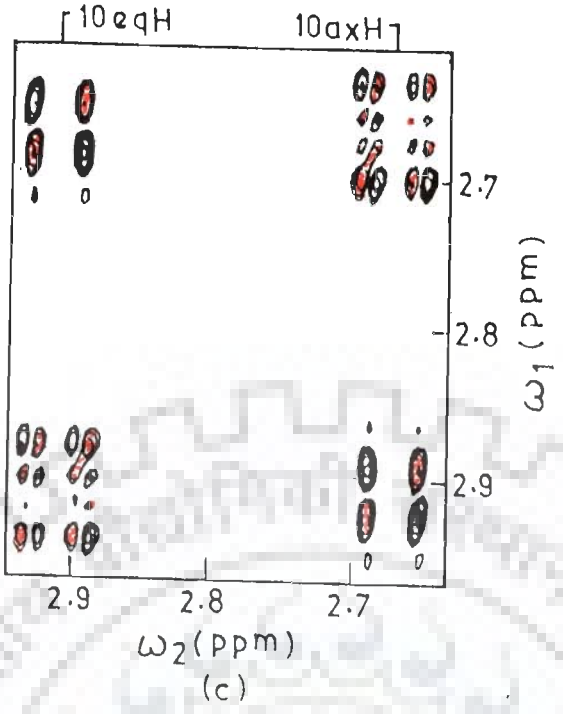
10eqH
10axH
2.7
2.8
2.9
ω_1 (ppm)
2.9
2.8
2.7
ω_2(ppm)
(c)

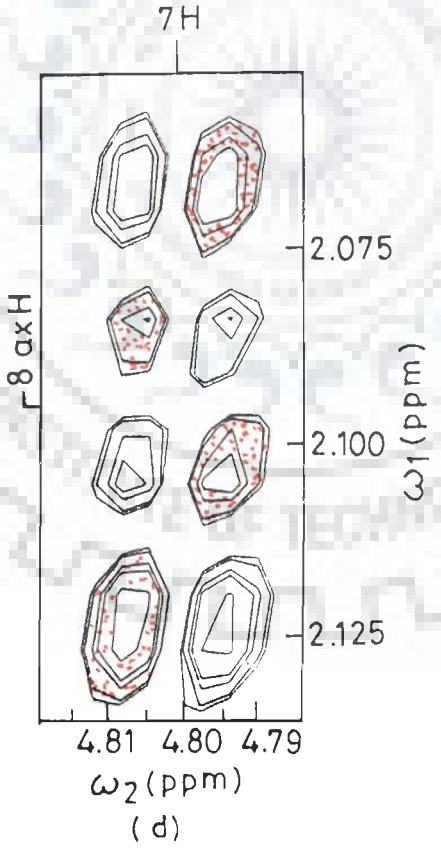
7H
8axH
2.075
2.100
2.125
ω_1(ppm)
4.81
4.80
4.79
ω_2(ppm)
(d)

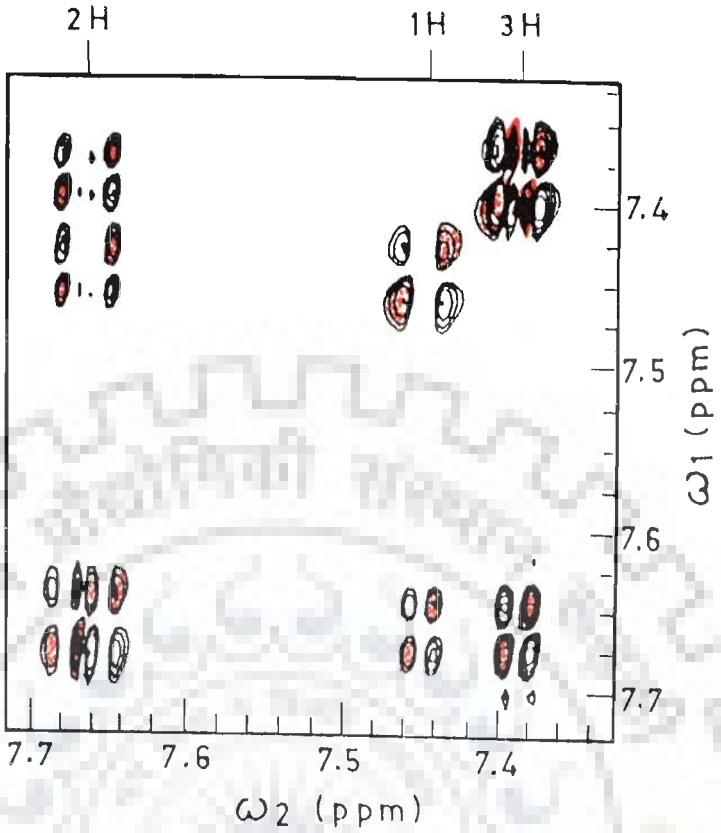
2H
1H
3H
7.4
7.5
7.6
7.7
ω1 (ppm)
7.7
7.6
7.5
7.4
ω2 (ppm)

(e)

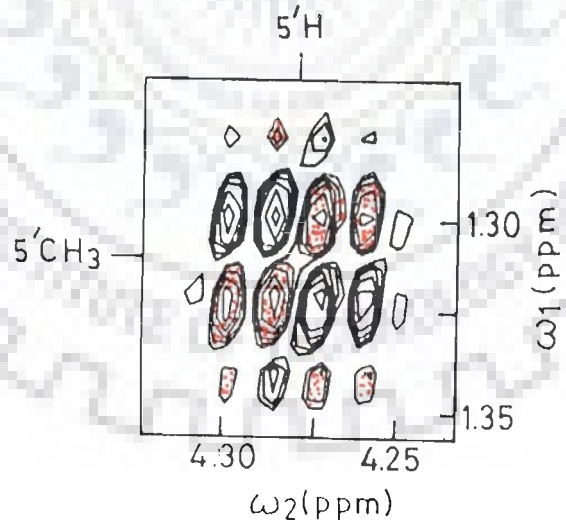
5'H
5'CH3
1.30
1.35
ω1 (ppm)
4.30
4.25
ω2(ppm)

(f)

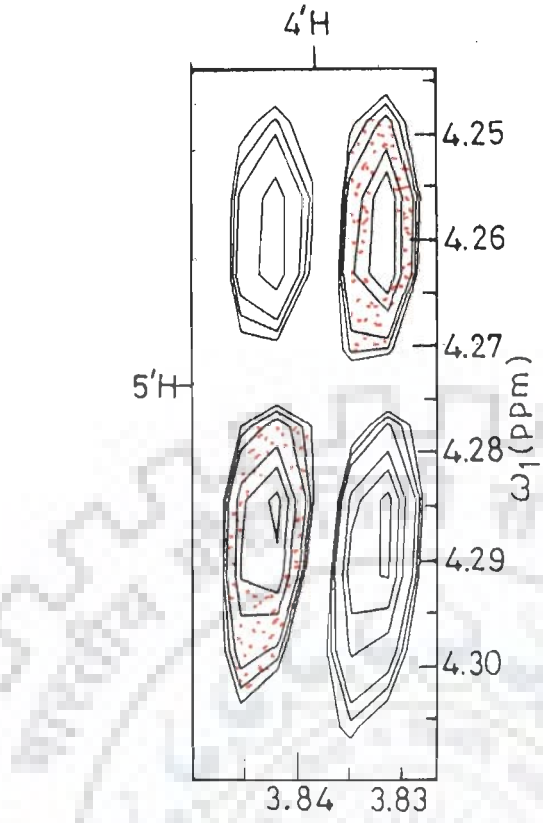
4'H
5'H
4.25
4.26
4.27
4.28
4.29
4.30
ω1(ppm)
3.84
3.83
ω2(ppm)

(g)

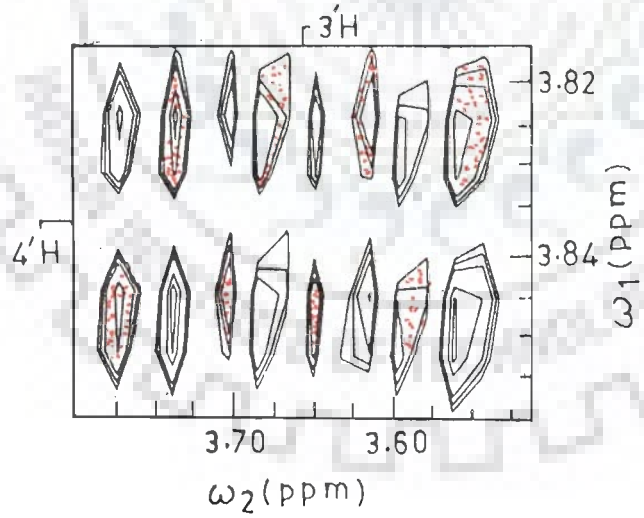
3'H
4'H
3.82
3.84
ω1(ppm)
3.70
3.60
ω2(ppm)

(h)

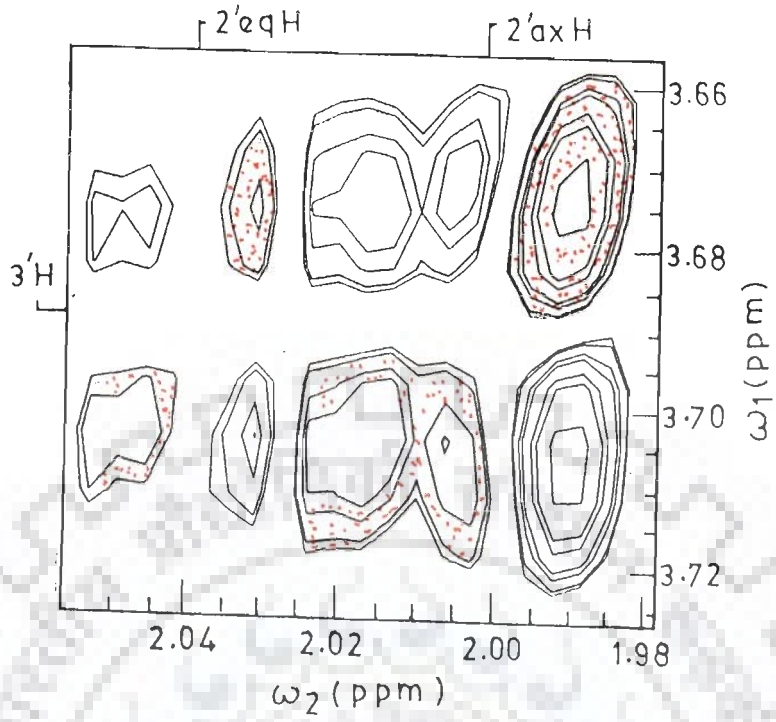
2'eqH
2'axH
3'H
3.66
3.68
3.70
3.72
ω1(ppm)
2.04
2.02
2.00
1.98
ω2(ppm)

(i)

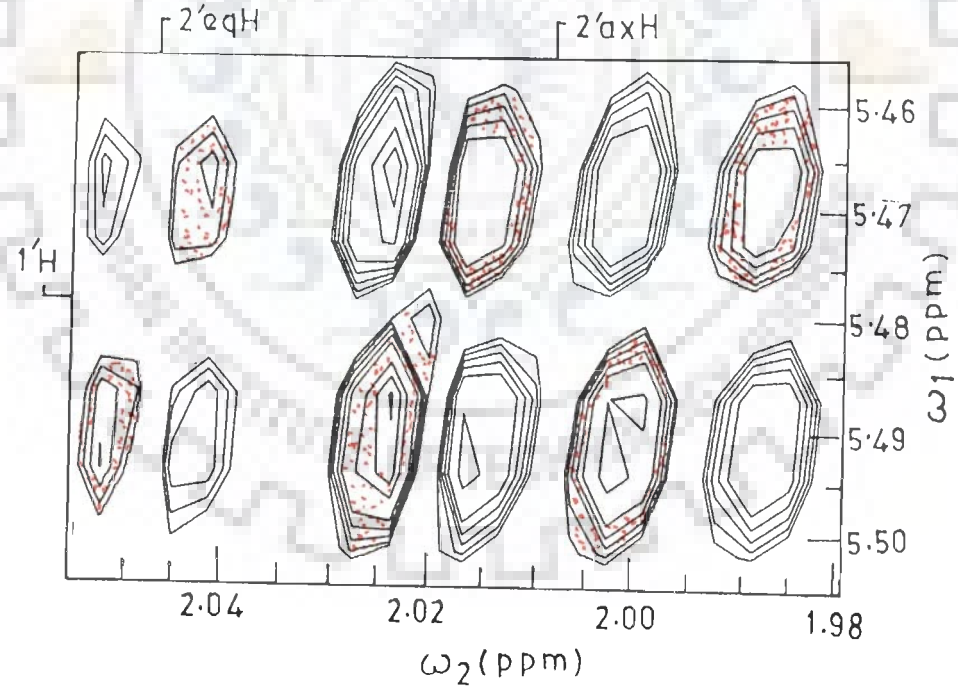
2'eqH
2'axH
1'H
5.46
5.47
5.48
5.49
5.50
ω1(ppm)
2.04
2.02
2.00
1.98
ω2(ppm)

(j)

Table 4.3 : Coupling constants, J (in Hertz) and torsional angle θ (in degrees), of daunomycin and for comparison the results of Mondelli et al. [71] from literature are also shown here.

Connectivities	Present work		Literature	
	J	θ	J	θ
1H-2H	8.0	~ 0	-	-
2H-3H	8.7	~ 0	-	-
1'H-2'axH	7.3	14.8	3.9	47.5
1'H-2'eqH	4.7	40.1	1.3	63.3
3'H-4'H	3.3	50.0	2.8	54.1
4'H-5'H	5.4	35.0	1.4	63.3
2'axH-3'H	11.3	180.0	13.0	-
2eqH-3'H	6.3	131.6	4.7	40.1
2'axH-2'eqH	13.4	-	13.1	-
5'H-5'CH_3	13.6	-	-	-
7H-8axH	5.4	126.7	5.0	39.2
7H-8eqH	w	60-100	-	-
8axH-8eqH	15.6	-	15.0	-
10axH-10eqH	18.5	-	18.3	-
8eqH-10eqH	5.2	-	2.0	-

w- cross peak weak in intensity

accurately obtained directly from the AX type spin system along the ω_2 axis (Fig. 4.5(b, c)) as 15.6 Hz and 18.5 Hz, respectively.

Proceeding in a similar way, we find that proton 7H is coupled to both 8ax and 8eq protons, which are coupled to each other by strong geminal coupling. The observed cross peak pattern of 7H with 8axH (Fig. 4.5(d)) gives the active coupling J(7H-8axH) read along ω_2 axis as 5.4 Hz. This pattern repeats due to passive coupling J(8axH-8eqH) along ω_1 axis. On the other hand, the cross peak of 7H with 8eqH is found to be very weak in intensity. The resolution used by us is not sufficient to resolve the coupling J(7H-8eqH) along ω_2 axis which is therefore inferred to be less than 2.30 Hz.

Similarly we find that both 1H and 3H protons of ring D of daunomycin are coupled to 2H proton. In daunosamine sugar, 5'CH_3 protons are coupled to 5'H proton which is further coupled to 4'H. The 4'H proton is coupled to 3'H which is coupled to 2'axH and 2'eqH. By identifying the specific spin systems, we obtained the J values from phase-sensitive COSY spectra which are listed in Table 4.3. We have calculated the torsional angle (Table 4.3) for all vicinal couplings using Karplus relationship [55,56].

NOE connectivities and interproton distances

The phase-sensitive NOESY spectra showing the pair of coupled protons in space through dipolar interaction is shown in Fig. 4.4 (a, b). The NOESY spectra are recorded at different mixing times (τ_m) in the range of 400-800 ms. NOE build-up curves are obtained as a function of τ_m for each cross peak to determine the

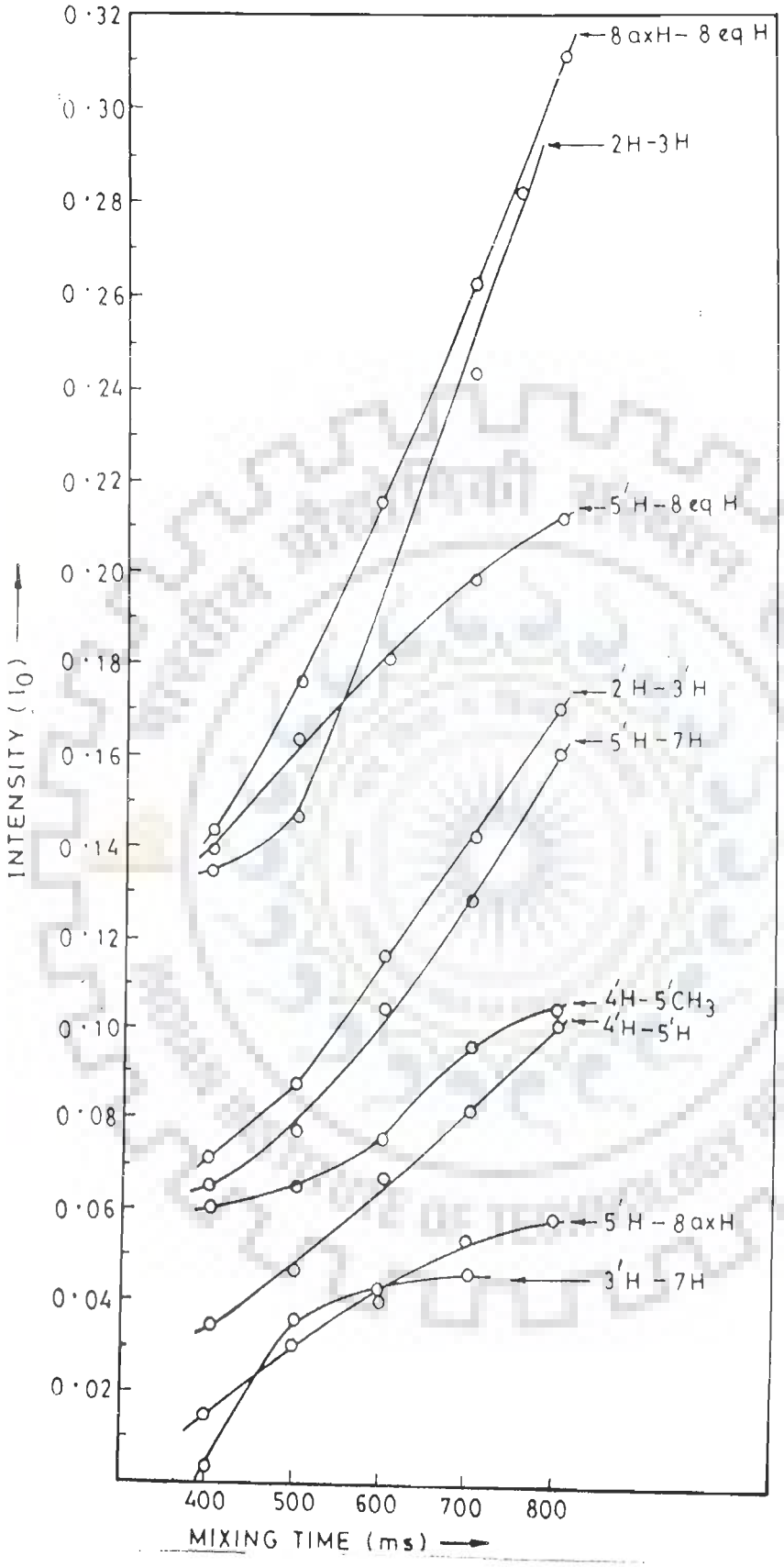

Fig 4.6 : NOE build up curves for various pairs of protons of daunomycin as a function of mixing time (τ_m) in the range 400-800 ms.

acceptable value of τ_m for interproton distance calculation. The NOE build up curves of some of the pairs of protons are shown in Fig. 4.6. It is found that intensity of the cross peak increases linearly with mixing time. Thus, the NOESY spectra recorded at lowest mixing time (τ_m = 400 ms) is selected for distance measurements. We have used the distance r(1H-2H) = 2.36 A° as an internal reference obtained from x-ray crystal structure analysis of daunomycin reported by Courseille et al. [28]. The interproton distances are calculated by integrating the volume of each cross peak which gives us intensity. The distance values thus calculated are shown in Table 4.4. All pairs of protons at distance < 5.0 A° are expected to give NOE cross peaks. It is observed that the pairs of protons correlated by spin-spin coupling give NOE cross peaks and have interproton distances < 3.5 A°. The distance 2'axH-2'eqH could not be ascertained due to overlap of resonances in this region.

The distance of 7H-8eqH pair of protons could not be obtained due to weak intensity of the signal. As it is evident from NOESY spectra (Fig. 4.7(b)), the resonance position of 2'ax, 2'eq and 8ax protons are very close to each other, so the distances 1'H - 2'axH, 1'H-2'eqH and 1'H-8axH can not be ascertained accurately. x-ray crystal structure analysis [79] has shown that the distance 1'H-2'axH, 1'H-2'eqH and 1'H- 8axH are 2.56, 2.53 and 4.47 A°, respectively. Assuming these distances to be in the ratio of the distances determined from x-ray structure analysis it is found that the observed intensity of NOE cross peak (1'H-2'axH)/

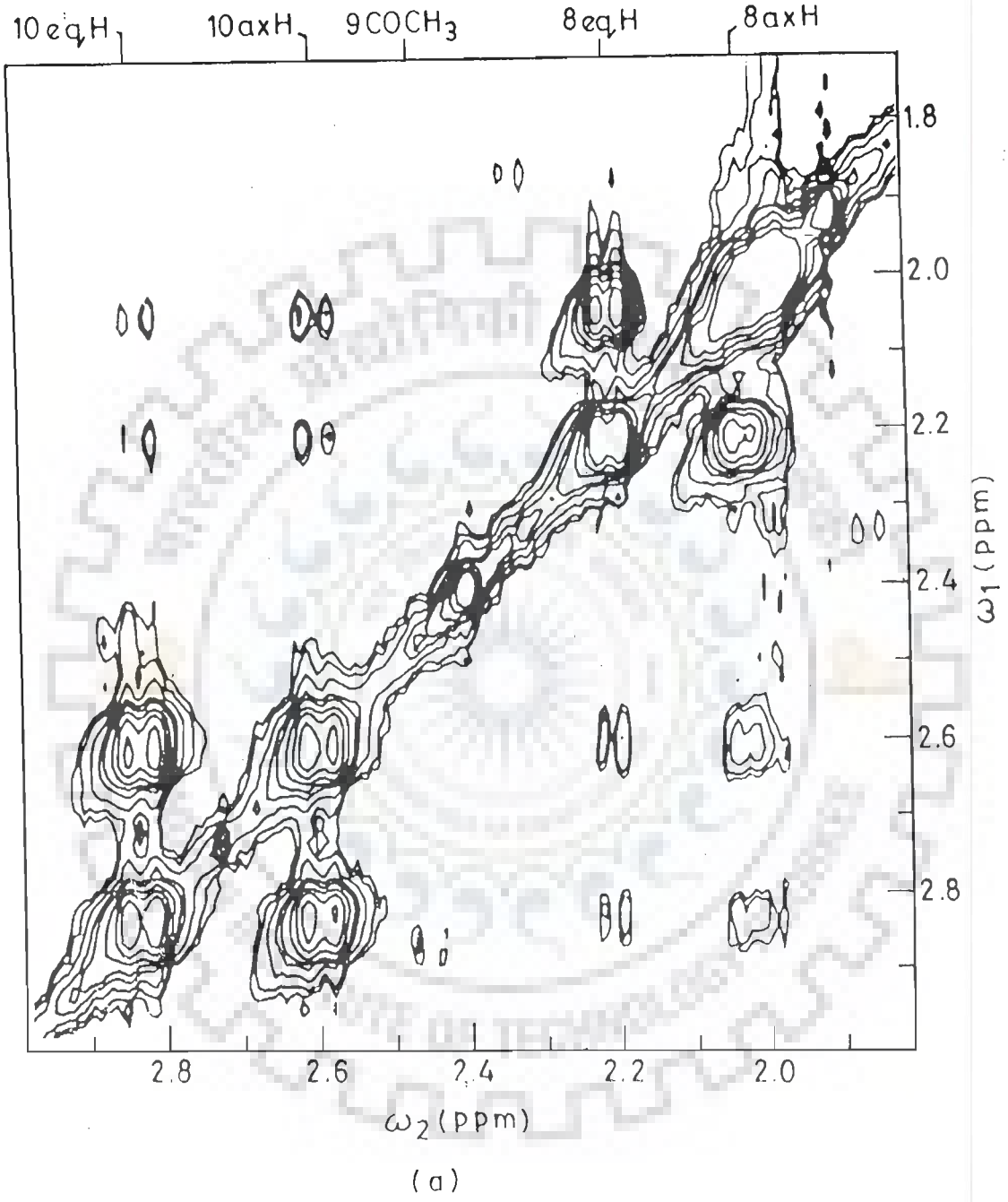

Fig 4.7 : Portions of the phase-sensitive NOESY spectrum (a-c) on an expanded scale showing specific NOE connectivities.

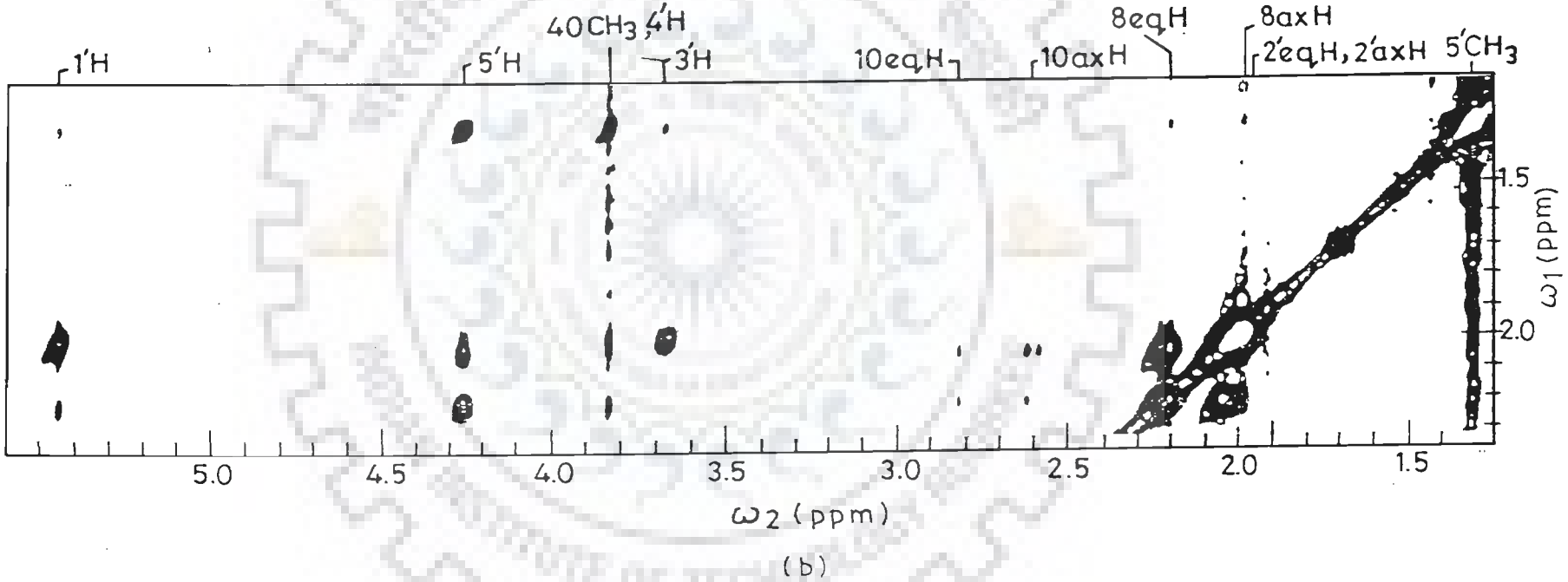
1'H
5'H
4'CH3, 4'H
3'H
10eqH
10axH
8eqH
8axH
2'eqH, 2'axH
5'CH3
5.0
4.5
4.0
3.5
3.0
2.5
2.0
1.5
ω2 (ppm)
1.5
2.0
ω1 (ppm)

(b)

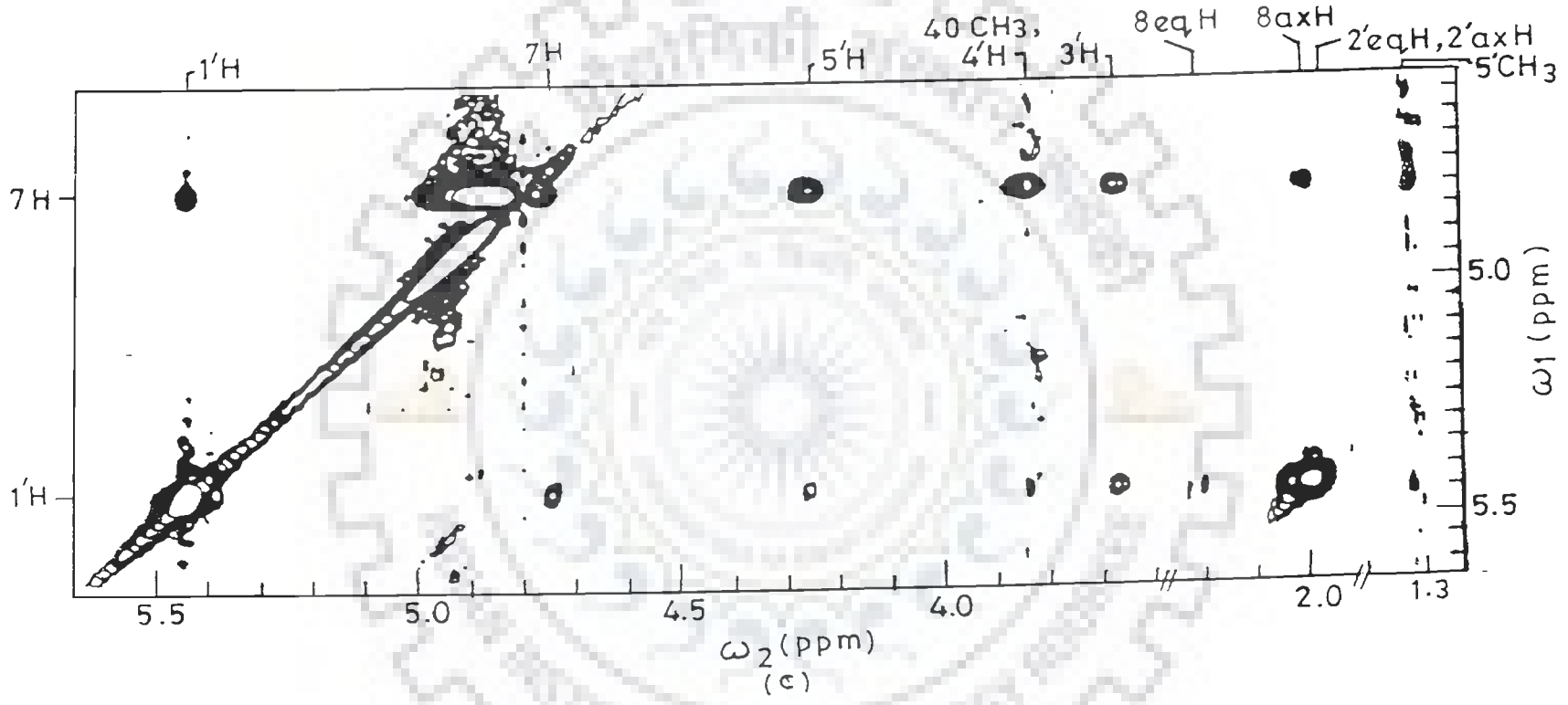
1'H
7H
5'H
4'H
3'H
8eqH
8axH
2'eqH,2'axH
5'CH3
7H
1'H
5.0
5.5
ω1 (ppm)
5.5
5.0
4.5
4.0
2.0
1.3
ω2 (ppm)
(c)

(1'H-2'eqH)/(1'H-8axH) corresponds to distances of 2.33, 2.30 and 4.07 A°, respectively (Table 4.4). Similarly, the distances 2'axH-3'H and 2'eqH-3'H are found to be 3.89 and 2.95 A° respectively in x-ray structure [79]. These distances are estimated as 3.21 and 2.44 A° (Table 4.4), respectively from the intensity of NOE cross peak (3'H-2'axH)/(3'H-2'eqH). Due to the unavoidable inaccuracy in the estimated interproton distances 1'H-2'axH; 1'H-2'eqH; 1'H-8axH; 3'H-2'axH and 3'H-2'eqH having overlapping , 2'axH, 2'eqH and 8axH resonances are used in further analysis as a guideline only. Apart from the spin-spin coupled protons, NOE contacts between protons within daunosamine sugar, within ring A as well as between ring A and daunosamine sugar, are observed. The interproton distances corresponding to these NOE connectivities are given in Table 4.4. It is observed that the $4OCH_3$ protons are close to 3H and 2H protons. Within ring A, the 8ax and 8eq protons are oriented with respect to 10ax and 10eq protons in a specific way so that their relative distances are fixed within 2.5 - 3.0 A°. Among sugar protons 1'H is in proximity of 3'H, 5'H and $5'CH_3$ protons. Further 3'H and 4'H protons are close in space to 5'H and $5'CH_3$ protons. NOE contacts obtained between ring A and daunosamine sugar protons give the proximity of specific ring A protons to the daunosamine sugar protons. It is observed that 7H atom is close to 1'H, 3'H, 4'H, 5'H and $5'CH_3$ protons, the distances being in the range 2.44 - 3.27 A°. Further 8eq proton is close to 1'H, 3'H, 4'H, 5'H and $5'CH_3$ while 8ax proton is close to 1'H, 5'H and $5'CH_3$ with their distances varying in the range 2.44-3.77 A°. Since, 2'ax and 2'eq

Table 4.4 : Interproton distances (A°) of daunomycin obtained form 2D NOESY spectra and comparison with that reported by x-ray structure analysis (a) [79] and NMR investigations (b) [72]. The distance between 1H and 2H protons is used as an internal reference.

Connectivity	Present work	a	b
Spin-spin coupled protons			
1H-2H	2.36	-	-
2H-3H	2.12	-	-
1'H-2'axH	2.33^{O}	2.56	2.21
1'H-2'eqH	2.30^{O}	2.53	2.35
3'H-4'H	2.37	2.55	-
4'H-5'H	2.27	2.45	2.35
3'H-2'axH	3.21^{O}	3.89	-
3'H-2'eqH	2.44^{O}	2.95	-
2'axH-2'eqH	0	1.76	-
5'H-5'CH_3	3.41, 2.75, 2.73	3.00, 2.41, 2.40	-
7H-8axH	3.46	2.36	2.30
7H-8eqH	w	2.40	2.45
8axH-8eqH	1.85	1.81	-
10axH-10eqH	1.76	1.77	-
8eqH-10eqH	2.98	4.25	-

Within ring D			
2H-4OCH$_3$	3.46	-	-
3H, 1H-4OCH$_3$	2.08	-	-
Within ring A			
8axH-10axH	2.50	2.64	-
8eqH-10axH	2.85	3.86	-
8axH-10eqH	2.71	3.71	-
10eqH-9COCH$_3$	3.53, 4.84, 3.57	3.25, 4.45, 3.28	-
Within sugar			
1'H-3'H	3.40	3.76	-
1'H-4'H	4.58	4.90	-
1'H-5'H	3.54	3.66	-
1'H-5'CH$_3$	5.18, 4.47, 4.34	5.36, 4.63, 4.49	-
3'H-5'H	2.41	2.40	-
3'H-5'CH$_3$	4.00, 4.48, 4.54	4.24, 4.61, 4.67	-
4'H-2'eqH	4.24	3.72	-
4'H-5'CH$_3$	2.34, 2.89, 3.54	2.43, 3.01, 3.68	-
Sugar with ring A			
7H-1'H	2.88	2.22	2.19
7H-3'H	3.27	4.67	-
7H-4'H	2.44	5.78	-
7H-5'H	2.70	3.65	-
7H-5'CH$_3$	4.29, 3.98, 3.23	5.41, 5.03, 4.08	-
8axH-1'H	4.07^{O}	4.47	-
8axH-5'H	2.63	4.35	-

8axH-5'CH_3	3.65,3.77,2.87	6.05,6.24,4.75	-
8eqH-1'H	3.49	3.94	-
8eqH-3'H	3.51	4.30	-
8eqH-4'H	3.01	5.07	-
8eqH-5'H	2.44	2.61	2.40
8eqH-5'CH_3	3.75,4.95,5.41	4.33,4.74,3.28	-

w- Cross peak weak in intensity

O- Overlapping peaks, since 2'axH, 2'eqH and 8axH peaks are very close to each other and are being used as guideline only (see text).

protons resonate at positions that are very close to the corresponding position for 8axH, the connectivity of 1'H proton with 8axH may well be due to its connectivity with 2'ax or 2'eq proton. The 5'H and 5'CH_3 are expected to be at a distance > 4.0 A° from 2'axH and 2'eqH. However, the distance of 5'H with 8axH and 8eqH are 2.63 and 2.44 A°, respectively. Therefore, these NOE contacts correspond to connectivity with 8axH rather than 2'ax, 2'eq protons. This corroborates with our model discussed later.

It is observed that the interproton distances estimated from NOE cross peaks are in agreement with the J-couplings obtained from COSY spectra. The J(2H-3H) obtained as 8.7 Hz gives torsional angle as 0° or 140°. In a planar ring it is well known that the relative orientation of ortho protons is in cis configuration and thus the torsional angle is about 0°. The torsional angle 0° corresponds to a distance of 2.2 A° which is in agreement with r(2H-3H) as 2.12 A° observed experimentally (Table 4.4). The J (4'H-5'H) of 5.4 Hz corresponds to torsional angle 36.7° or 126.7°. The distance 4'H-5'H is estimated as 2.27 A°, therefore the θ value is confirmed as 36.7°. Similarly, the distance 7H-8axH = 3.46 A° which is in accord with J(7H-8axH) = 5.4 Hz giving θ = 126.7° (Table 4.3 and 4.4).

Exchangeable protons and their connectivities

The resonances of all the exchangeable and non-exchangeable protons are observed in the spectra recorded in $CDCl_3$. Fig. 4.8 and 4.9 shows 1D and 2D NOESY spectra of daunomycin in $CDCl_3$. The 6OH and 11OH protons of ring B resonate in the region 13-14 ppm

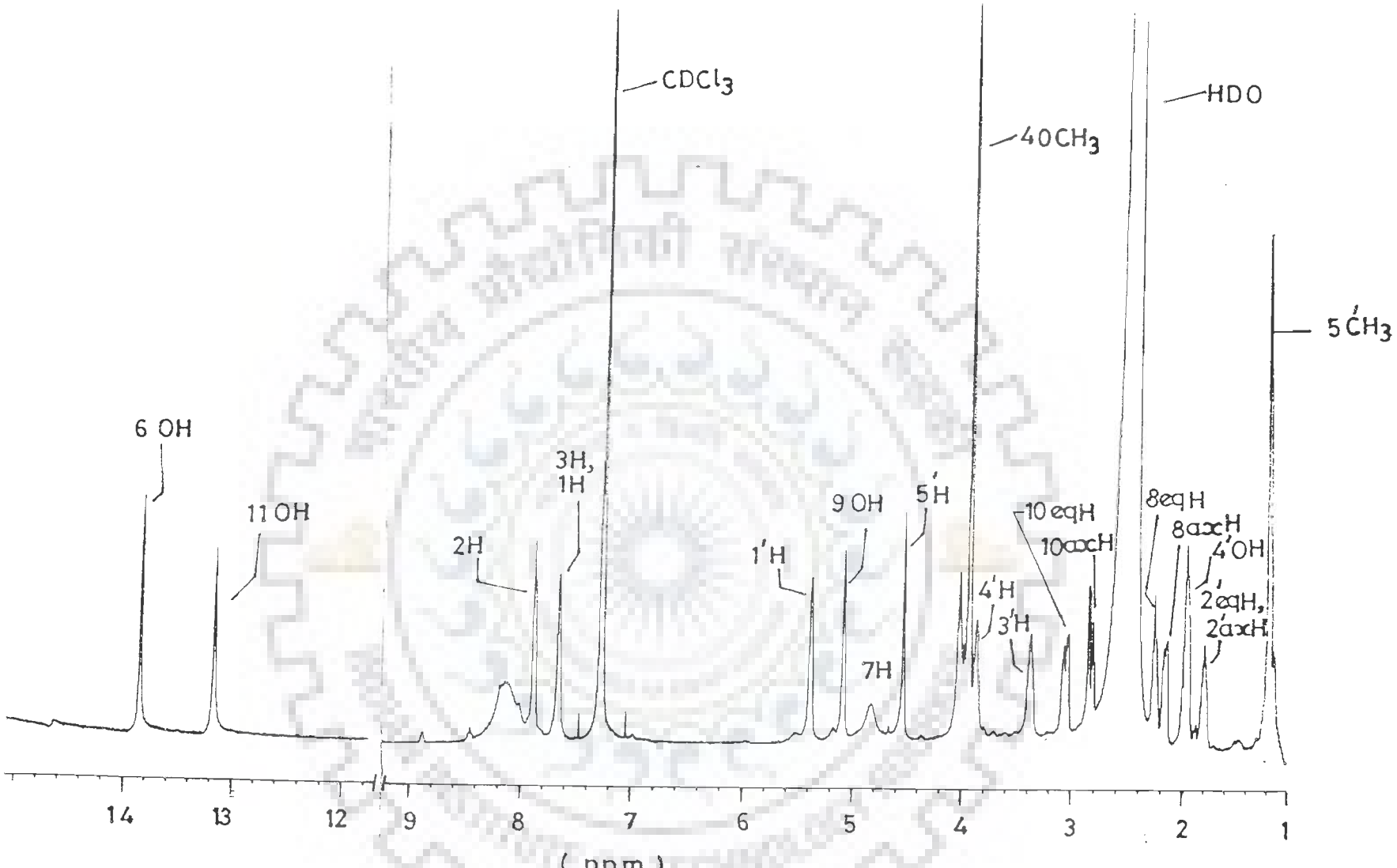

Fig 4.8 : 1D NMR spectra of 6.5 mM daunomycin in $CDCl_3$ at 297 K.

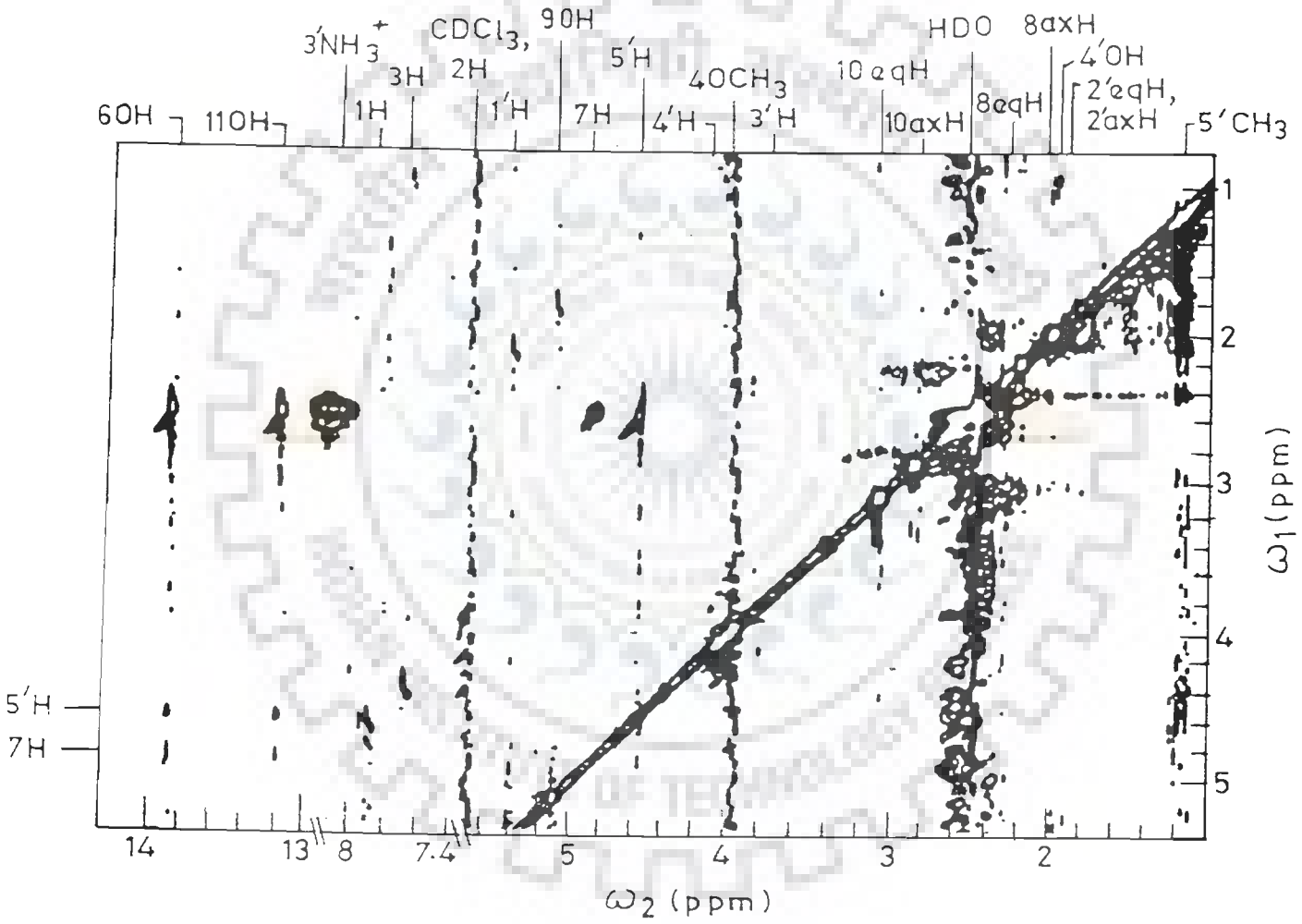

Fig 4.9 : Portion of phase-sensitive NOESY spectrum of 6.5 mM daunomycin in $CDCl_3$ at 297 K.

[71]. The resonance at 13.85 ppm gives NOE cross peak with 5'H proton of daunosamine sugar and 7H of ring A, and is therefore assigned to 6OH proton and the other resonance at 13.17 ppm is assigned to 11OH proton. Resonances at 5.08 ppm and 1.97 ppm are assigned to 9OH and 4'OH protons, respectively. The non-exchangeable protons of daunomycin are shifted downfield in $CDCl_3$ with respect to their position in D_2O. The chemical shifts of various protons of daunomycin as observed in $CDCl_3$ are listed in Table 4.5. The NOE connectivities 3'H -4'H, 10axH-10eqH, 8axH-8eqH, 1'H-2'axH; 1'H-2'eqH are clearly seen in the NOESY spectra (Fig. 4.9). These NOE cross peaks are fairly strong and may well correspond to distance $\simeq$ 1.8-2.4 A°. The distance r(6OH-7H) connectivity may be taken as $\simeq$ 2.4 A°.

CONFORMATION OF DAUNOMYCIN

The present investigation is the first attempt to obtain all interproton distances in aqueous solution. The other investigation available gives only few interproton distances of n-acetyl daunomycin [72] in chloroform. On comparing our results with that in literature, we find that the distances 1'H-2'axH, 1'H-2'eqH, 4'H-5'H, 5'H-8eqH are nearly same as that obtained for n-acetyl daunomycin in $CDCl_3$. However, the distances 7H-8axH and 1'H-7H observed as 3.46 and 2.88 A° are significantly different from the corresponding distances of 2.30 and 2.19 A°, observed by Mondelli et al. [72].

The distance 5'H-8axH and 5'H-8eqH was reported as > 4.0 A° whereas we observe the distance 5'H-8axH and 5'H-8eqH to be 2.63

Table 4.5 : Chemical shift (in ppm) of daunomycin protons in $CDCl_3$ at 297 K.

Protons	Chemical shift	Protons	Chemical shift
6OH	13.85	4'H	3.87
11OH	13.17	3'H	3.38
2H	7.88	10eqH	3.05
1H	7.66	10axH	2.83
3H	7.65	8eqH	2.25
1'H	5.38	8axH	2.16
9OH	5.08	4'OH	1.97
7H	4.80	2'axH	1.79
5'H	4.54	2'eqH	1.79
$4OCH_3$	3.94	$5'CH_3$	1.16

and 2.44 A° [72]. This suggests that the position of hydrogen atoms in daunomycin in present investigation is not identical to that of n-acetyl daunomycin as observed by Mondelli et al. [72].

Comparing the observed results with those obtained by x-ray crystal structure analysis [79], we find that interproton distances are similar in the two investigations, (within ± 0.5 A°). However the distances of 7H proton from 1'H, 3'H, 4'H, 5'H and 8axH; distances 5'H-8axH, 1'H-8eqH, 3'H-8eqH, 4'H-8eqH and 1'H-4'H are found to be different. It may be noted that distances i.e. 7H-8axH, 5'H-8axH, 1'H-7H are also found to differ from the corresponding results of Mondelli et al. [72]. In order to understand how these interproton distances will be reflected in the conformation of daunomycin, we have constructed a model of daunomycin by using dreiding stereo model. The rings B, C and D are planar. The carbon and oxygen atoms in ring A and daunosamine sugar are positioned in such a way that the torsional angle within ring A and amino sugar are same as that obtained by Neidle and Taylor [79] in the crystal structure of daunomycin. The protons attached to these atoms are then oriented so as to satisfy the observed torsional angles. Finally subtle changes are made in the positions of various atoms so that all observed interproton distances from NOESY spectra are consistent with the model. The torsional angle between 7H-8axH and 7H-8eqH are fixed as 126.7° and 60-100° with 8axH perpendicular and 8eqH parallel to ring A. The 1'H atom is placed relative to 7H so that it is at a distance of 2.88 A°. Assuming this position of 1'H we have fixed the

position of 2'axH and 2'eqH using torsional angle of 14.8 and 40.1° and hence corresponding J of 7.3 Hz and 4.7 Hz, as well as NOEs of 2.32 and 2.29 A°, respectively. Subsequently we have placed 3'H atom relative to 2'axH and 2'eqH; 4'H relative to 3'H; and so on. The glycosyl linkages are readjusted to get distances of 7H, 8axH and 8eqH atoms from daunosamine sugar protons to be in accord with the observed distances from NOESY spectra. It is found that it is possible to reach at a single specific geometry of the drug molecule. The various torsional angles in the final conformation of drug thus obtained differ from Neidle's x-ray crystal structure [79] by ± 15°. This is in accord with the observation that in the x-ray structure determined for similar drugs such as carminomycin [95], n-bromoacetyl daunomycin [3] the torsional angles within ring A and daunosamine sugar differ by 0 to 17°. It has also been found that on complexation of daunomycin with d-CGTACG [126], d-CGATCG [73], d-TGTACA and d-TGATCA [85] the torsional angles within ring A and daunosamine sugar change by ± 15° and glycosidic linkage differ by ± 25°. Thus it may be presumed that the position of all carbon and oxygen atoms in daunomycin and related drugs do not differ very much. Further, all these structures correspond to minimum energy conformation. The position of hydrogen atoms are however quite different in solution structure and are best known directly from NOESY spectra as shown in the present investigations. It may be noted that the torsional angles, ϕ, ψ defined as H1'-C1'-O7-C7 and C1'-O7-C7-H7 in n-acetyl daunomycin [72] in $CDCl_3$ were found to be 40° and 0°, respectively as compared to the corresponding crystal structure

[3] value of 41° and 18° suggesting that placement of hydrogen atoms is different in these two structures. This observation corroborates our results. Thus we arrive at a solution conformation specified by the spin-spin couplings and interproton distances from NOE contacts having positions of C, N and O atoms as dictated by bond angle - bond distance constraints as in x-ray crystal structure. These structural constraints have direct implications on the binding action of drugs.

CONFORMATION OF DEOXYHEXANUCLEOTIDE d-$(TGATCA)_2$

The conformation of deoxyhexanucleotide d-$(TGATCA)_2$ is investigated in D_2O by proton NMR at 500 MHz. We present here the assignment of various resonances of protons in d-$(TGATCA)_2$, followed by changes in chemical shifts of nucleotide protons as a function of temperature in the range 277-325 K. Then the conformational analysis of deoxyribose sugar and glycosidic bond rotation (χ) of the various nucleotide residues based on 2D phase-sensitive DQF COSY and NOESY spectra recorded at τ_m 75, 150, 200 and 250 ms at 295 K, is discussed.

RESONANCE ASSIGNMENTS

The bases of self-complementary d-$(TGATCA)_2$ are numbered as follows :

```
        1 2 3 4 5 6
5' d-   T G A T C A  3'
3'      A C T A G T  5'
```

Figs. 5.1 (a-d) show the expansions of one-dimensional NMR spectrum of the hexamer in D_2O at 295 K. The 1D NMR spectrum recorded at 325 and 305 K are shown in Figs. 5.2 (a-d) and Figs. 5.3(a,b), respectively. Fig. 5.3(c) shows the stack plot of 1D NMR spectra recorded at various temperatures. The region between 7.2 - 8.4 ppm (Fig. 5.1(a)) shows the resonances due to the

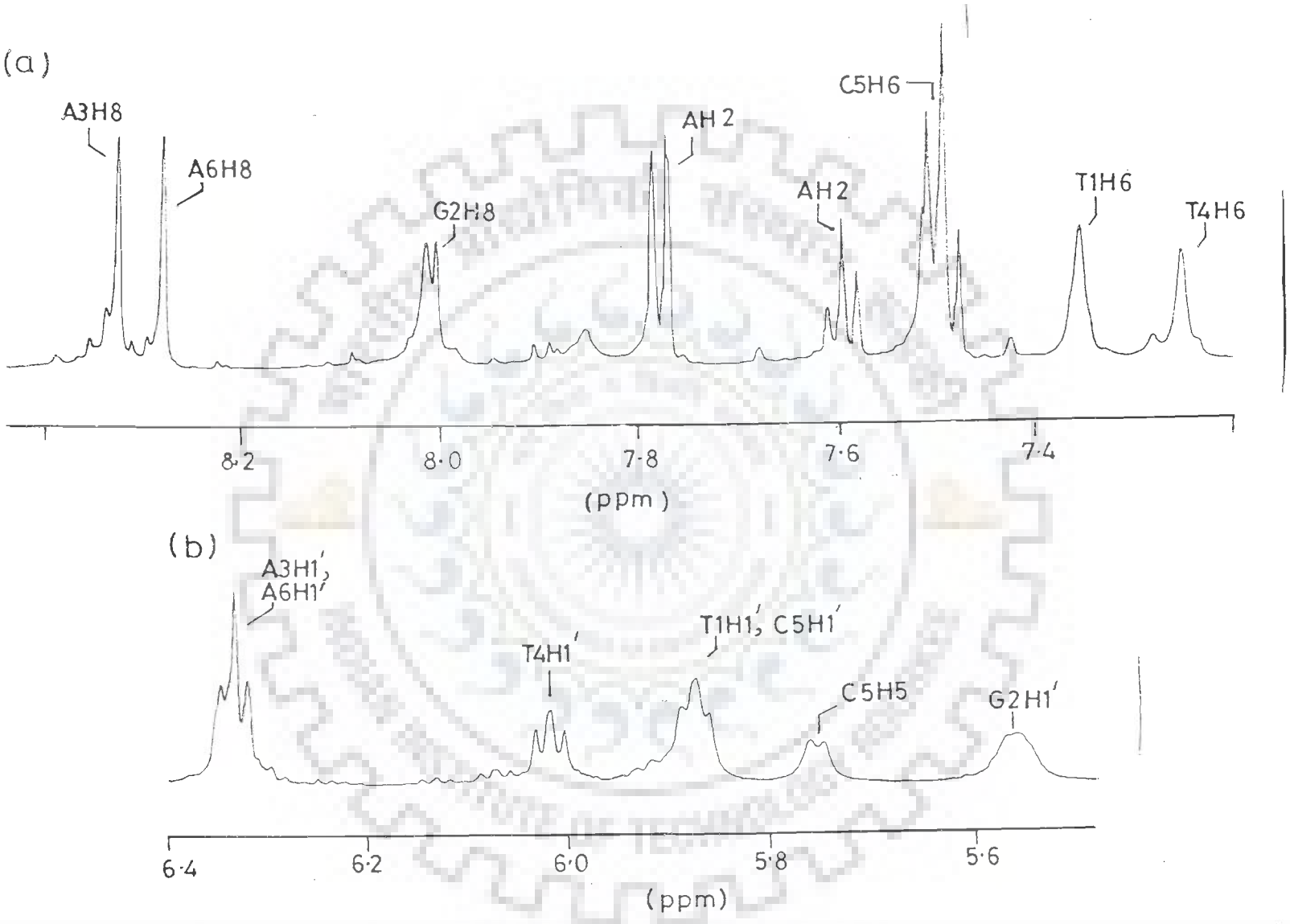

Fig. 5.1(a, b) : 1D proton NMR spectra of d-$(TGATCA)_2$ in D_2O at 295 K. (a) Base protons of all residues (b) H1′ of all residues along with C5H5.

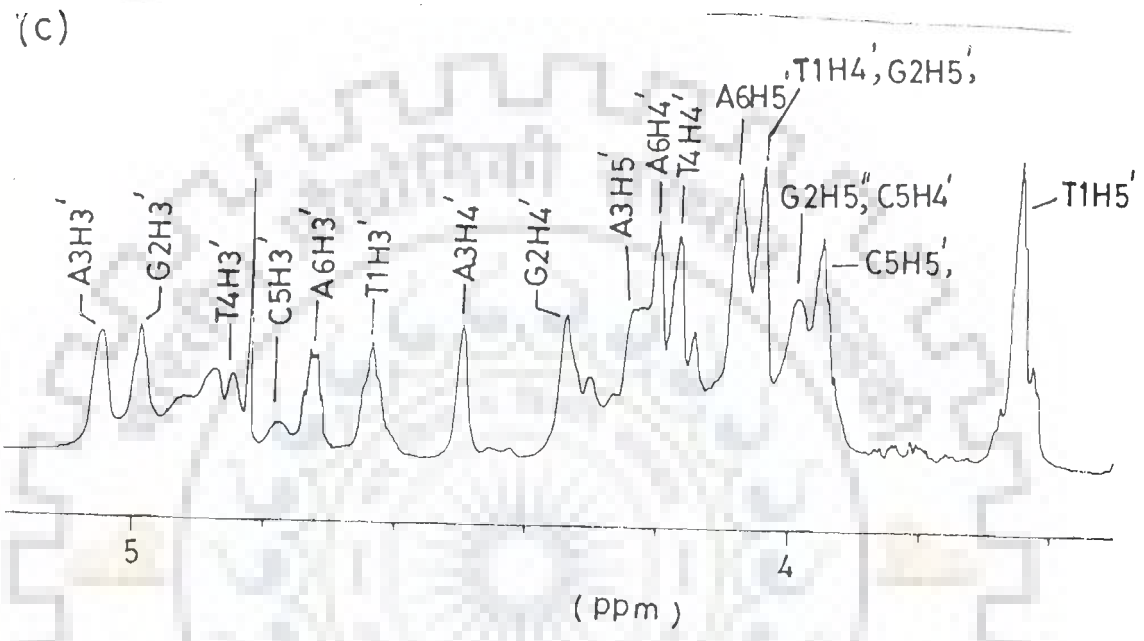

Fig. 5.1(c) : Expanded portion of 1D proton NMR spectra of d-$(TGATCA)_2$ showing H3', H4', H5' and H5" resonances at 295 K in D_2O.

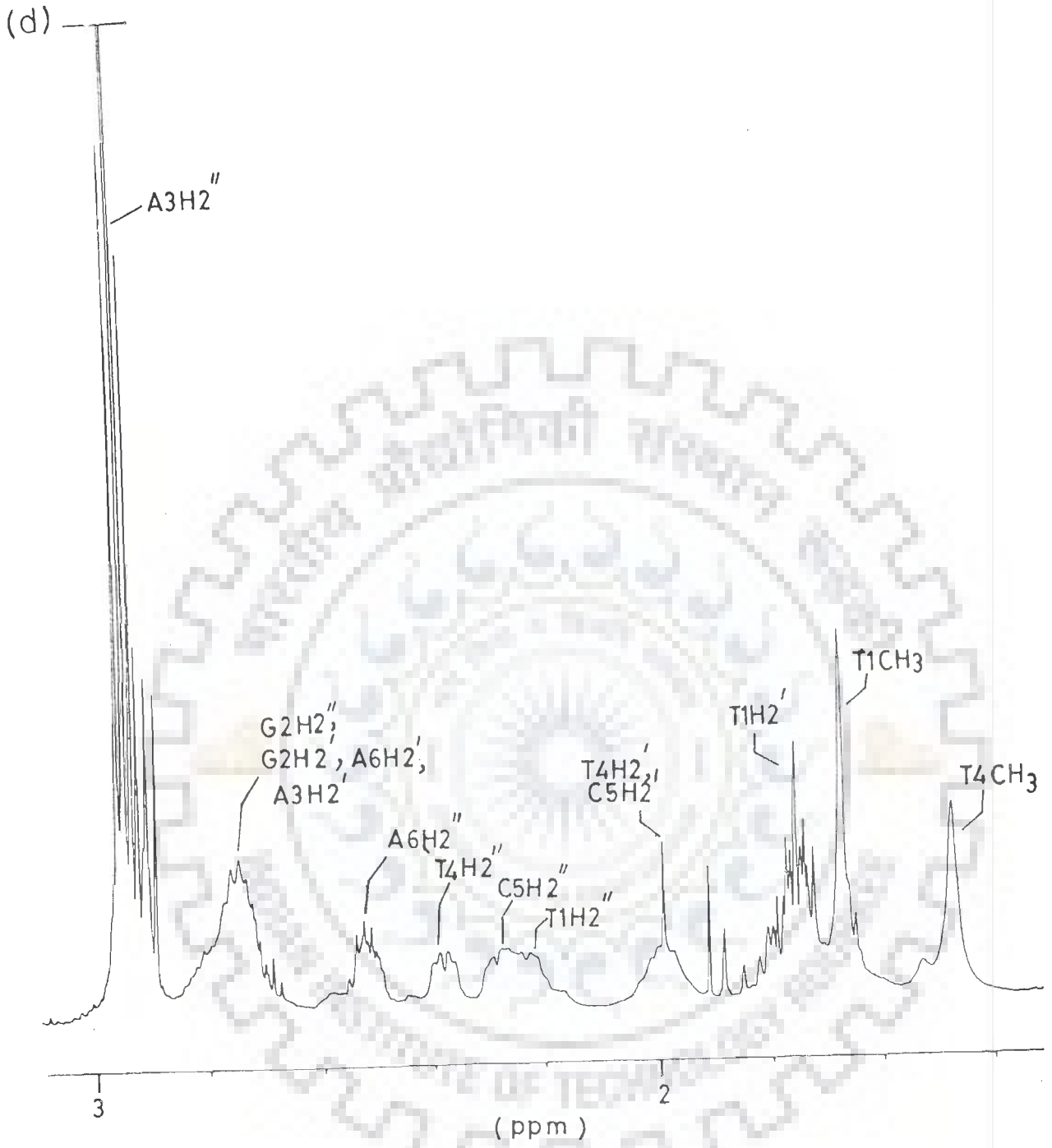

Fig.5.1(d) : Expanded portion of 1D proton NMR spectra showing H2', H2" and CH_3 protons of d-$(TGATCA)_2$ at 295 K in D_2O.

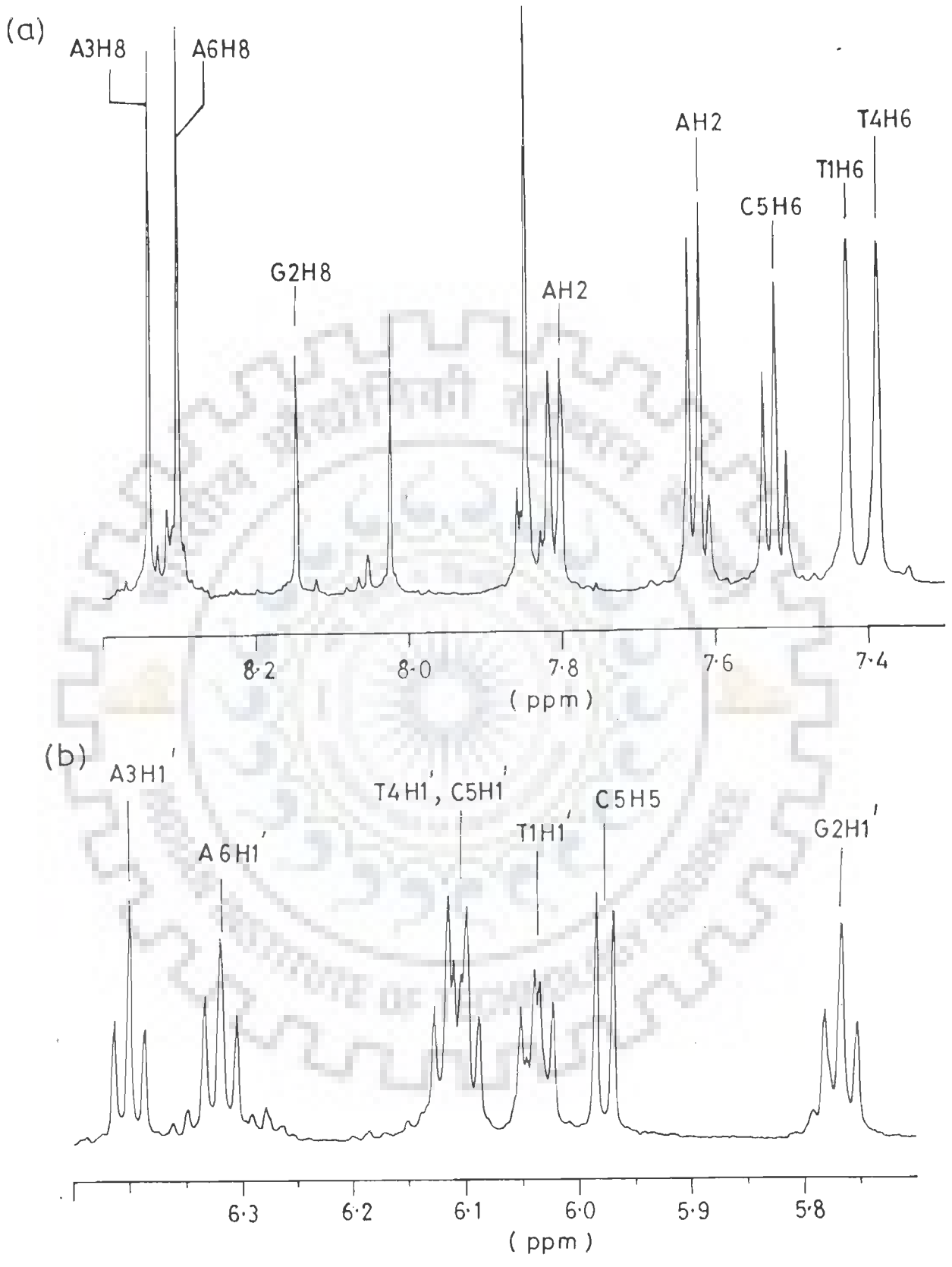

Fig. 5.2(a, b) : 1D proton NMR spectra of d-$(TGATCA)_2$ in D_2O at 325 K. (a) Base protons of all residues. (b) H1' of all residues along with C5H5.

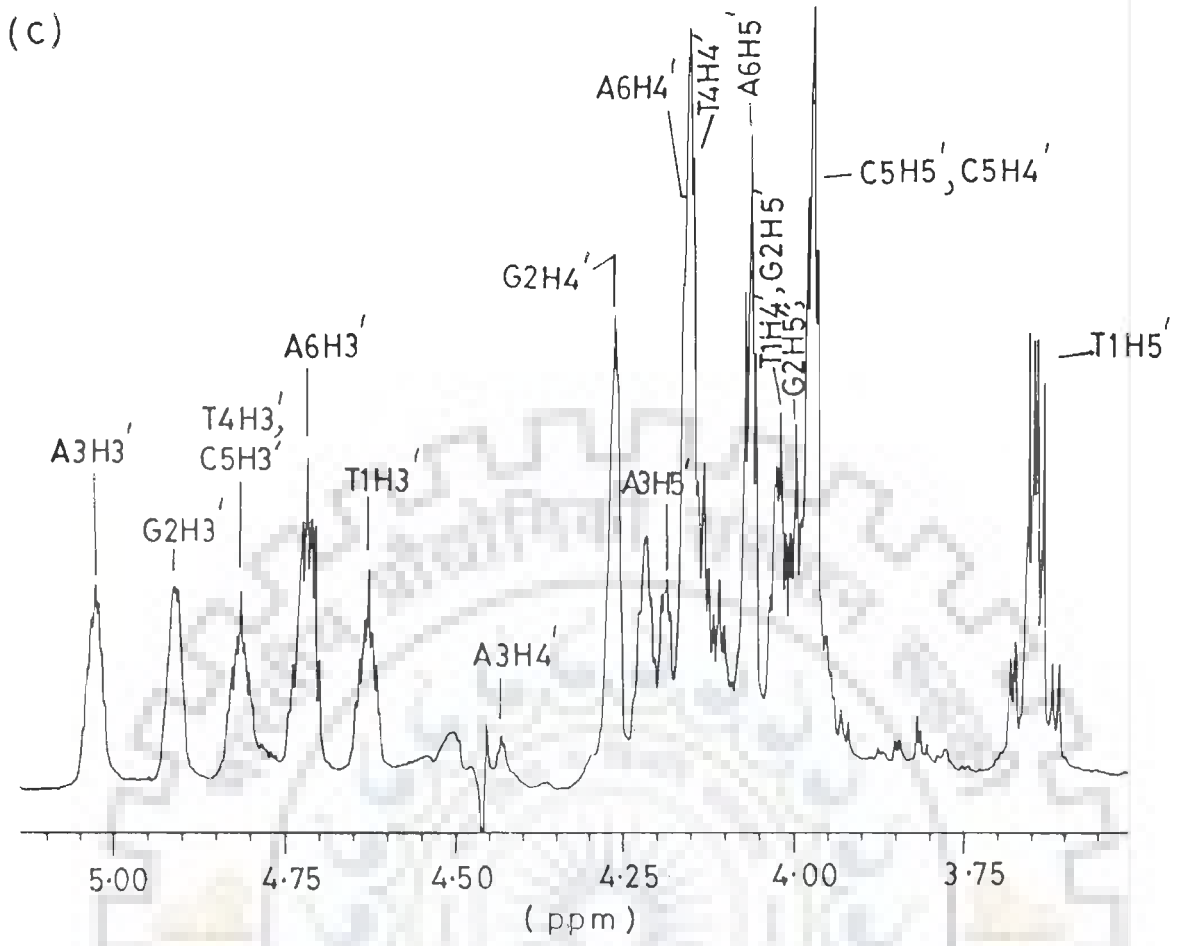

Fig. 5.2(c) : Expanded portion of 1D proton NMR spectra showing H3', H4', H5', H5" resonances of d-(TGATCA)$_2$ at 325 K in D_2O.

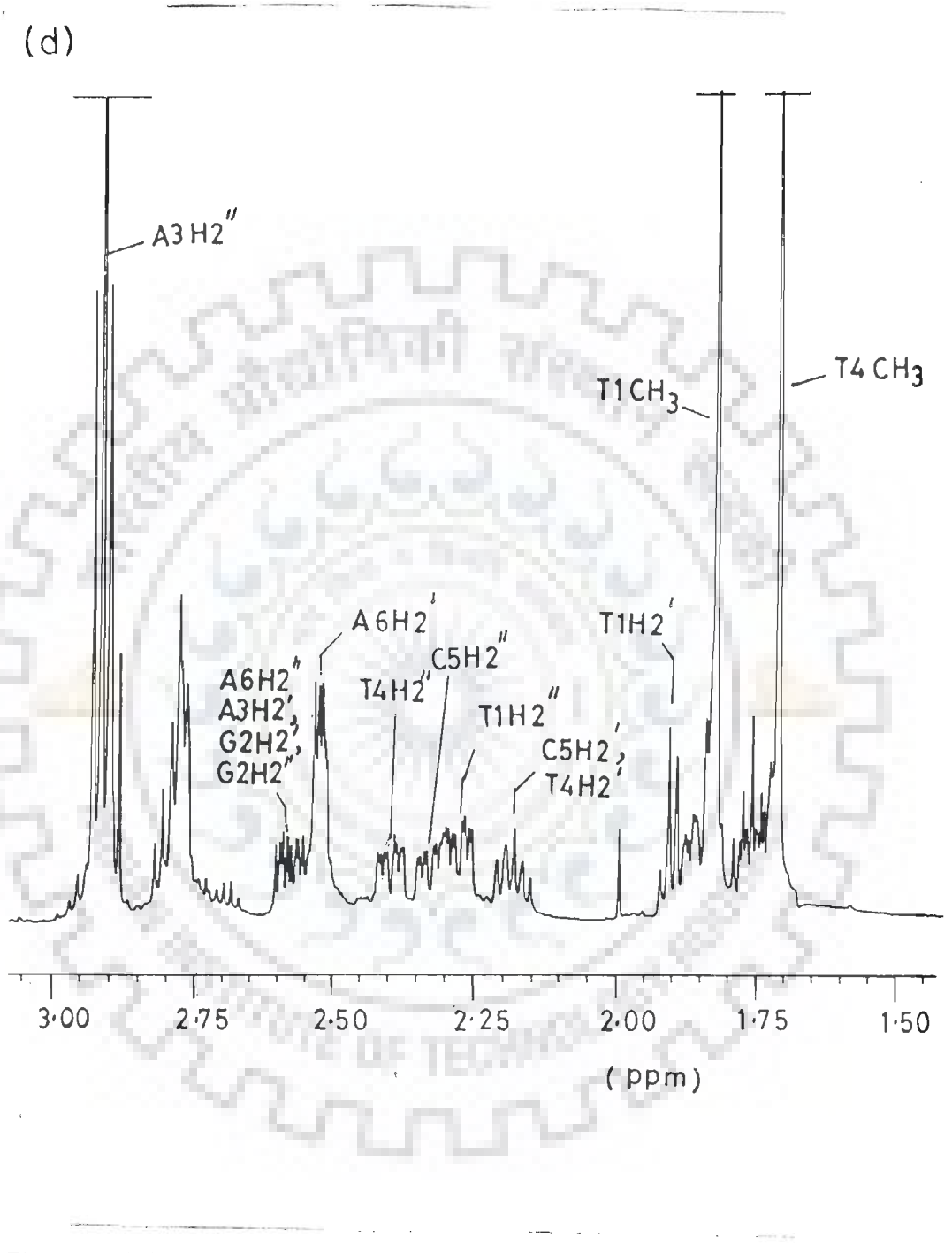

Fig. 5.2(d) : Expanded portion of proton NMR spectra showing H2', H2" and CH_3 protons of d-$(TGATCA)_2$ at 325 K in D_2O.

(a)

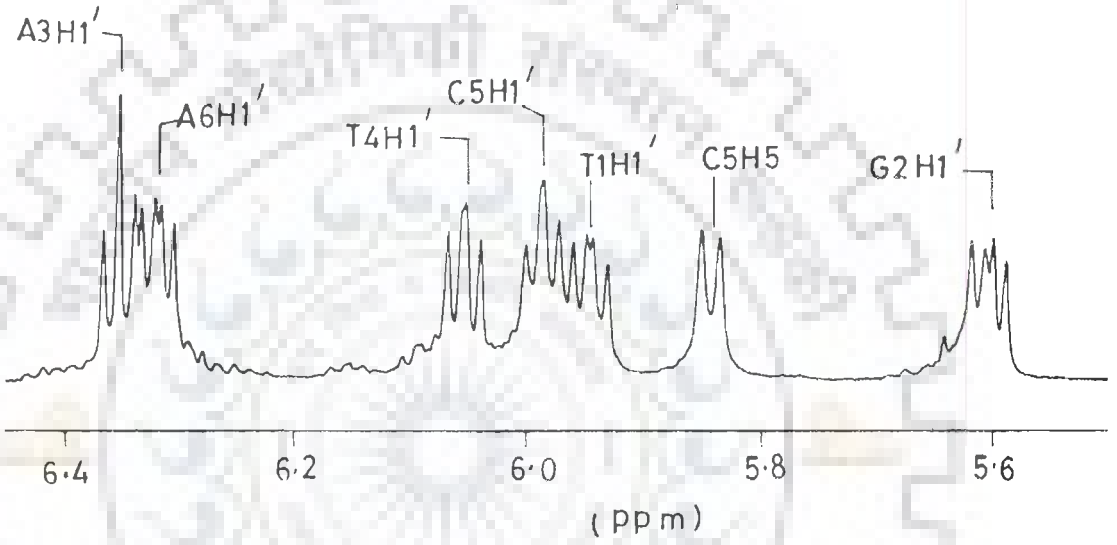

Fig. 5.3(a, b) : Expanded portion of proton NMR spectra showing H1′, H2′, H2" protons of d-(TGATCA) at 305 K in D_2O.

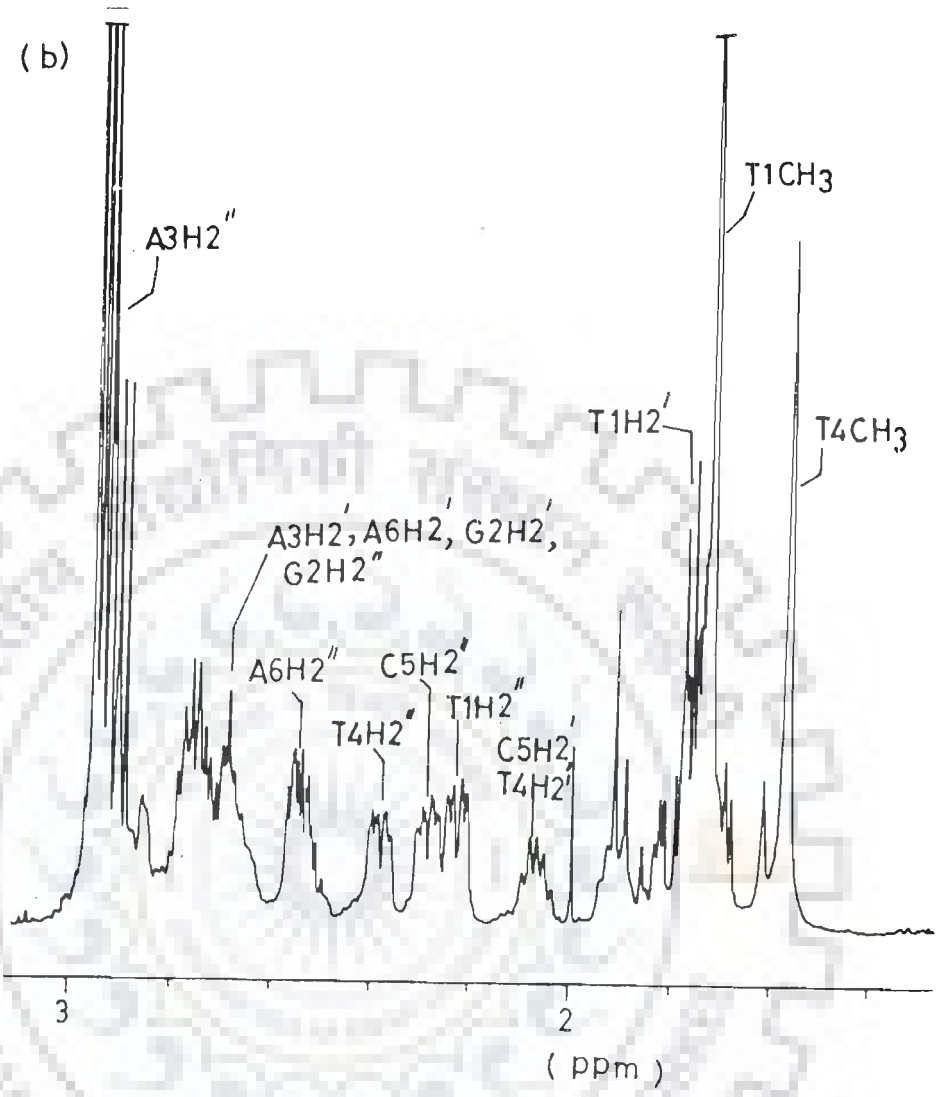
(b)
A3H2''
T1CH3
T1H2'
T4CH3
A3H2', A6H2', G2H2',
G2H2''
A6H2''
C5H2'
T1H2''
T4H2''
C5H2',
T4H2'
3
2
(ppm)

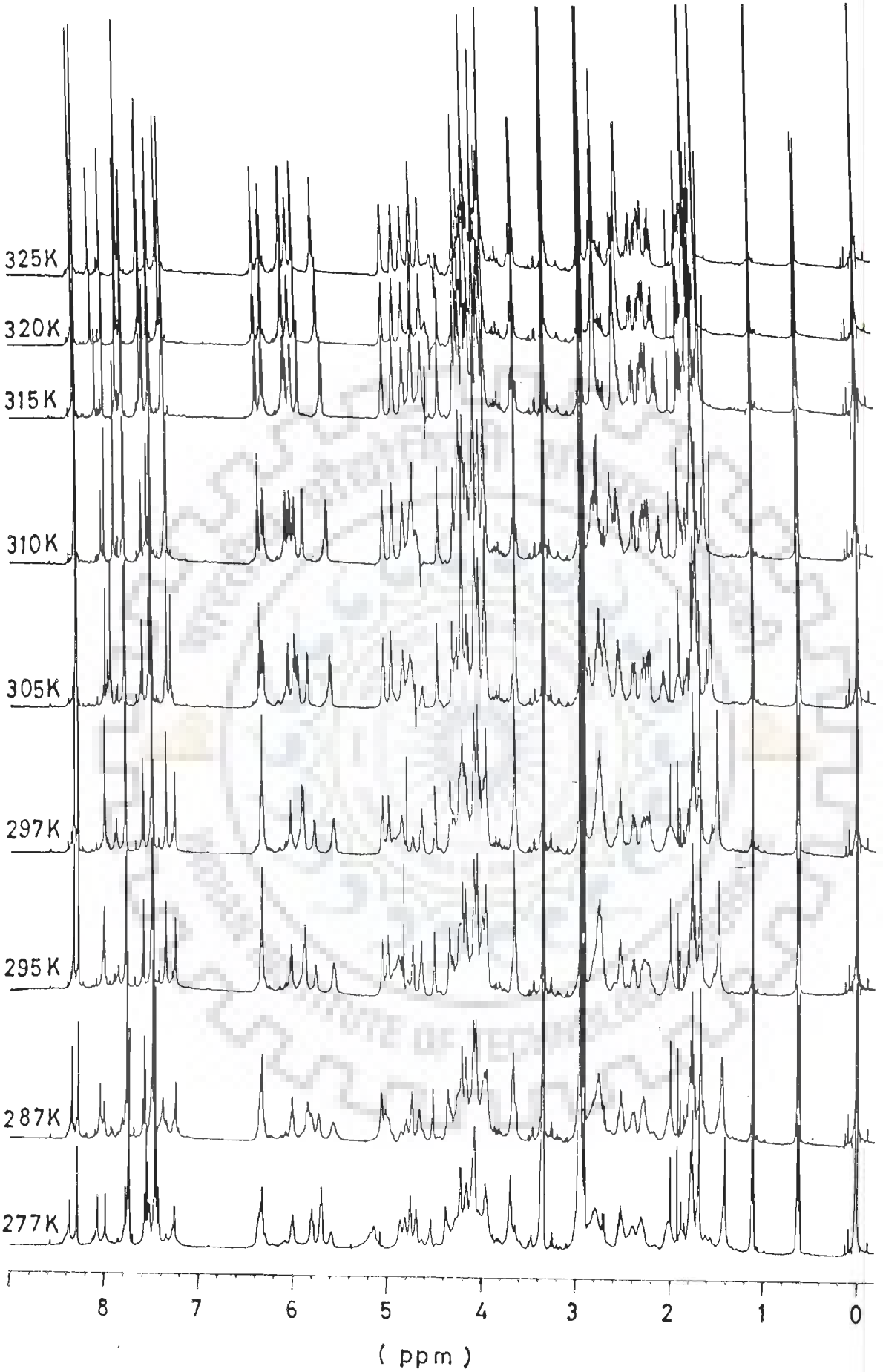

Fig. 5.3(c) : Stack plot of 1D proton NMR spectra of d-$(TGATCA)_2$ recorded with varying temperatures in the range 277-325 K.

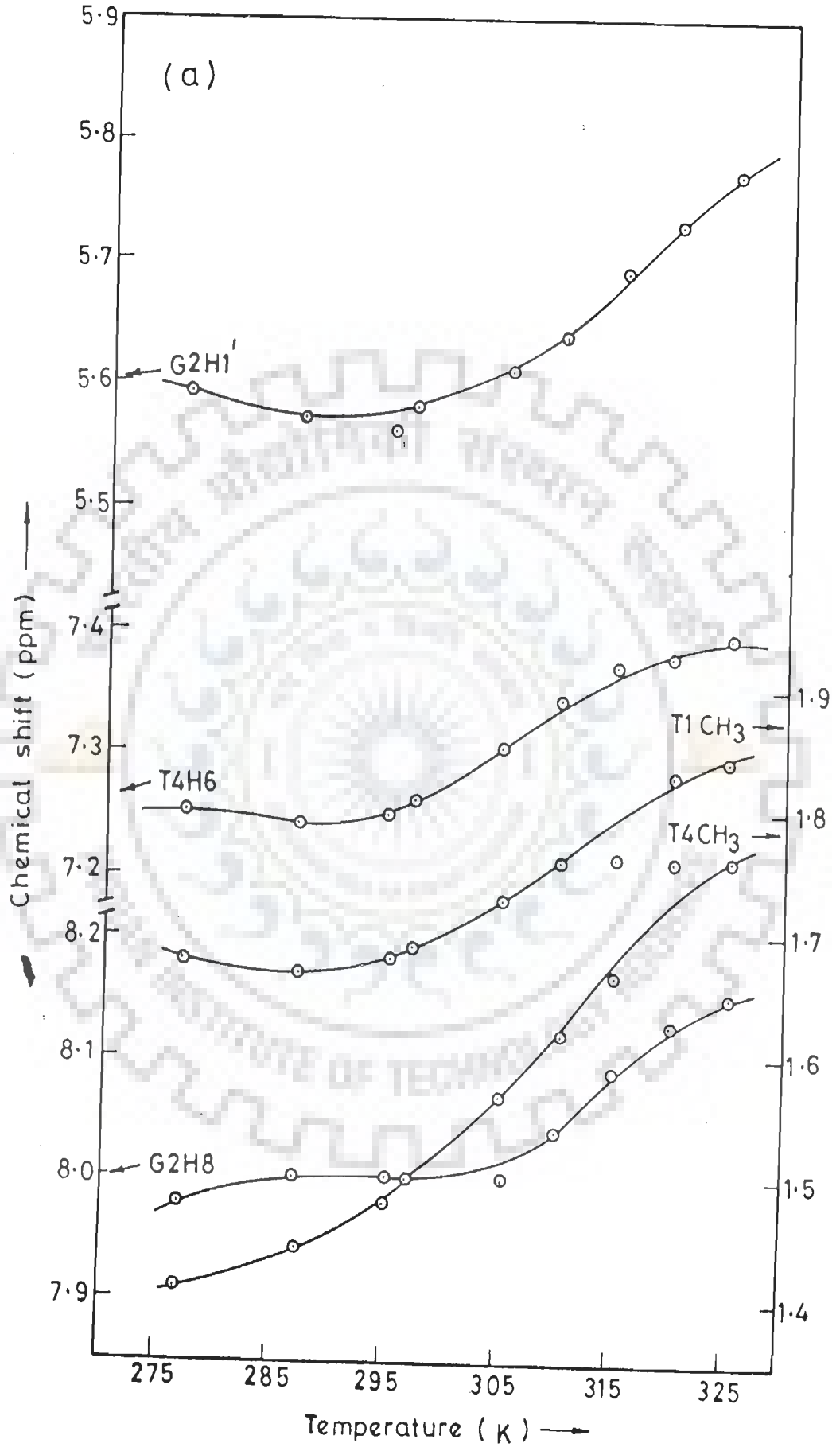

Fig. 5.4(a, b) : Chemical shift of various protons of d-$(TGATCA)_2$ as a function of temperature in the range 277-325 K.

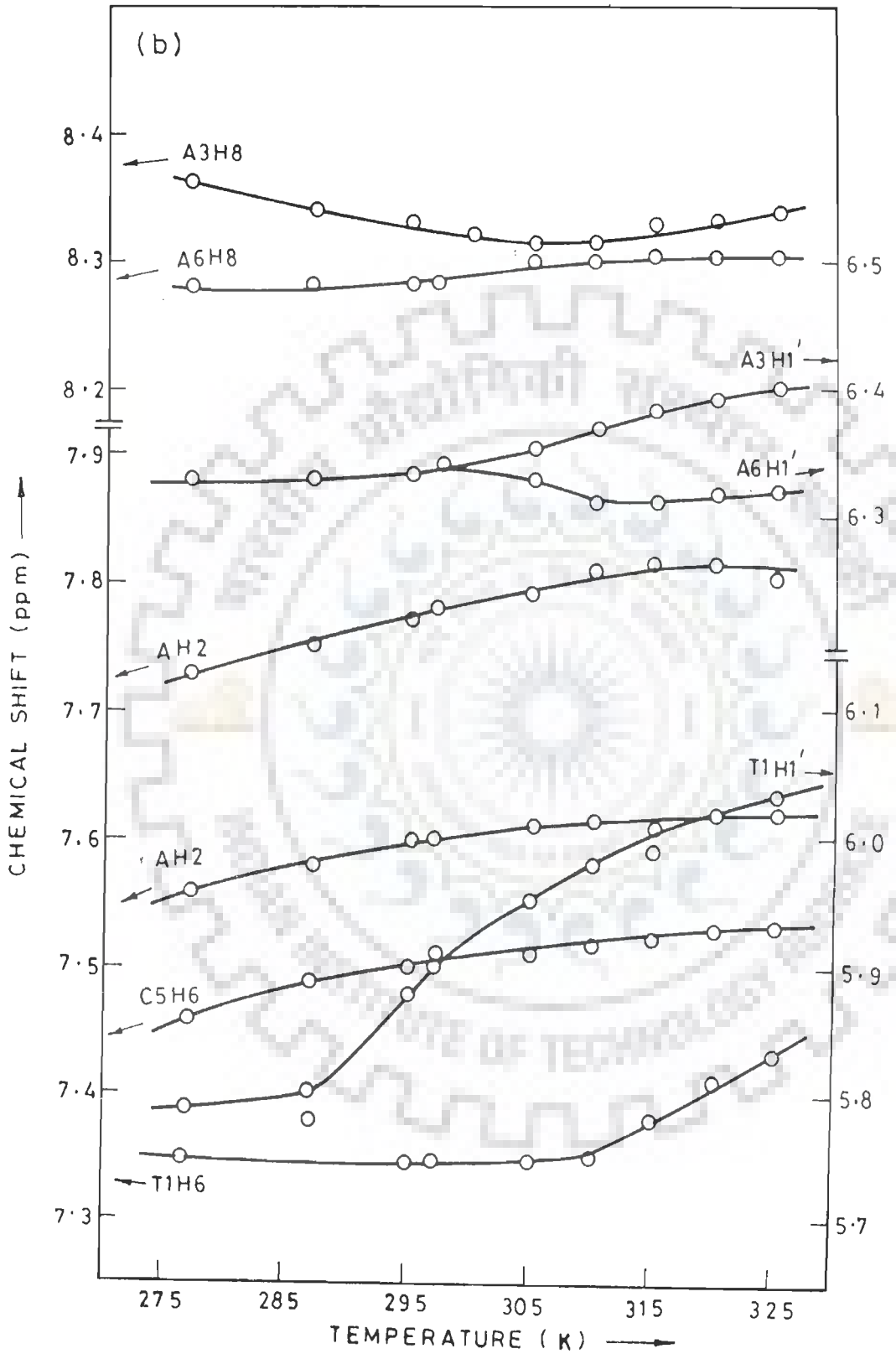
(b)
A3H8
A6H8
A3H1'
A6H1'
AH2
AH2
T1H1'
C5H6
T1H6
8·4
8·3
8·2
7·9
7·8
7·7
7·6
7·5
7·4
7·3
6·5
6·4
6·3
6·1
6·0
5·9
5·8
5·7
CHEMICAL SHIFT (ppm)
275
285
295
305
315
325
TEMPERATURE (K)

aromatic protons, that is, the AH8, AH2, GH8, CH6 and TH6. The resonance CH6 appear as doublets, AH8, AH2, GH8 as singlets. The region between 5.5 - 6.4 ppm consists of resonances due to six deoxyribose sugar H1′ protons and one CH5 proton (Fig. 5.1(b)). The resonances in the range 1.7 - 3.0 ppm are due to H2′, H2" protons (Fig. 5.1(d)). Sugar H3′ protons are observed in the range of 4.6 - 5.1 ppm (Fig. 5.1(c)), sugar H4′ protons resonate in the range 4.0 - 4.5 ppm (Fig. 5.1(c)) and the sugar H5′, H5" protons are observed in the range 3.6-4.3 ppm (Fig. 5.1(c)). The methyl resonances of thymine resonate between 1.4 - 1.8 ppm (Fig. 5.1(d)). The specific assignments to various base residues is made by two-dimensional NMR experiments. The phase-sensitive 2D DQF COSY and NOESY spectra recorded at τ_m = 250, 150 and 75 ms are shown in Figs. 5.5(a-j) and Figs. 5.6(a-k) along with expansions of certain regions to highlight specific connectivities. The chemical shifts, δ (in ppm), for various protons at 295 K are listed in Table 5.1. Table 5.2 shows the list of chemical shifts of protons at different temperatures.

In Figs. 5.5 (a-g), the sets of sugar proton resonances are easily recognisable. Five intense cross peaks of pairs of protons the H2′-H2" are seen in Fig. 5.5 (b) for the sugar residues however one pair of H2′-H2" connectivity is not distinct. Each of the H2′ and H2" pair of coupled proton shows intense cross peak with only one H1′ proton in region 5.55-6.35 ppm and one H3′ proton in region 4.60-5.10 ppm (Figs. 5.5(c-e)) which are assigned to its corresponding H1′ and H3′ protons. The H1′ and

Table 5.1 : **Chemical shift (in ppm) of protons of d-$(TGATCA)_2$ at 295 K in D_2O.**

Protons	T1	G2	A3	T4	C5	A6
H8/H6	7.35	8.02	8.33	7.26	7.52	8.28
H1′	5.90	5.57	6.34	6.04	5.90	6.34
H2′	1.76	2.79	2.76	2.02	1.99	2.76
H2"	2.25	2.79	2.96	2.39	2.30	2.53
H3′	4.65	5.00	5.06	4.86	4.80	4.74
H4′	4.07	4.35	4.52	4.20	4.02	4.23
H5′	3.65	4.07	4.25	0	3.97	4.10
H5"	-	3.98	0	0	0	0
H5/H2/CH_3	1.73	-	-	1.49	5.80	-

0-overlap

Table 5.2 : Chemical shift (in ppm) of protons of d-$(TGATCA)_2$ at different temperature in D_2O.

Temp. (K)	T1H6	$T1CH_3$	G2H8	A3H8	AH2	T4H6	$T4CH_3$
277	7.35	1.68	7.98	8.36	7.73	7.25	1.41
287	7.38	1.67	8.00	8.34	7.75	7.24	1.44
295	7.35	1.68	8.00	8.33	7.77	7.25	1.48
297	7.35	1.69	8.00	8.32	7.78	7.26	1.50
305	7.35	1.73	8.00	8.31	7.79	7.30	1.57
310	7.35	1.76	8.04	8.31	7.81	7.34	1.62
315	7.38	1.76	8.09	8.33	7.81	7.37	1.67
320	7.41	1.83	8.13	8.33	7.81	7.38	1.71
325	7.43	1.84	8.15	8.34	7.80	7.39	1.73

Temp. (K)	C5H6	C5H5	A6H8	AH2	T1H1'	G2H1'	A3H1'
277	7.46	5.69	8.28	7.56	5.79	5.59	6.33
287	7.49	5.73	8.28	7.58	5.80	5.57	6.33
295	7.50	5.76	8.28	7.60	5.88	5.56	6.33
297	7.50	5.77	8.28	7.60	5.91	5.58	6.34
305	7.51	5.85	8.30	7.61	5.95	5.61	6.35
310	7.52	5.89	8.30	7.61	5.98	5.64	6.37
315	7.52	5.94	8.30	7.59	6.01	5.69	6.38
320	7.53	5.96	8.30	7.62	6.02	5.73	6.39
325	7.53	5.98	8.30	7.62	6.03	5.77	6.40

Temp. (K)	T4H1′	C5H1′	A6H1′	T1H2′	G2H2′	A3H2′	T4H2′
277	6.00	5.79	6.33	1.76	2.78	2.78	1.99
287	6.00	5.85	6.33	1.76	2.76	2.76	1.99
295	6.02	5.88	6.33	1.76	2.76	2.76	2.00
297	6.03	5.91	6.34	1.76	2.74	2.74	2.00
305	6.05	5.99	6.33	1.76	2.70	2.70	2.08
310	6.08	6.05	6.31	1.89	2.63	2.63	2.19
315	6.10	6.07	6.31	1.91	2.57	2.57	2.15
320	6.10	6.10	6.32	1.90	2.59	2.59	2.17
325	6.12	6.12	6.32	1.91	2.59	2.59	2.19

Temp. (K)	C5H2′	A6H2′	T1H2″	G2H2″	A3H2″	T4H2″	C5H2″
277	1.99	2.78	2.29	2.78	2.93	2.38	2.29
287	1.99	2.76	2.28	2.76	2.93	2.40	2.28
295	2.00	2.76	2.24	2.76	2.95	2.39	2.29
297	2.00	2.74	2.21	2.74	2.93	2.38	2.27
305	2.08	2.70	2.23	2.70	2.93	2.38	2.28
310	2.19	2.63	2.23	2.63	2.92	2.38	2.29
315	2.15	2.57	2.24	2.57	2.93	2.40	2.29
320	2.17	2.54	2.25	2.59	2.92	2.40	2.30
325	2.19	2.54	2.27	2.59	2.92	2.40	2.32

Temp. (K)	A6H2"	T1H3'	G2H3'	A3H3'	T4H3'	C5H3'	A6H3'
277	2.51	4.68	5.07	5.13	4.85	4.80	4.74
287	2.52	4.69	5.02	5.06	4.84	4.80	4.74
295	2.53	4.64	4.99	5.05	4.84	4.82	4.74
297	2.53	4.64	4.99	5.05	4.82	4.82	4.71
305	2.56	4.62	4.96	5.04	4.83	4.83	4.76
310	2.56	-	4.94	5.04	4.82	4.82	4.73
315	2.57	4.63	4.93	5.04	4.83	4.83	4.73
320	2.59	4.63	4.92	5.03	4.82	4.82	4.72
325	2.59	4.63	4.91	5.03	4.82	4.82	4.72

Temp. (K)	T1H4'	G2H4'	A3H4'	T4H4'	C5H4'	A6H4'	T1H5'
277	4.07	4.35	4.53	4.15	3.96	4.22	3.69
287	4.06	4.36	4.51	4.17	3.97	4.21	3.67
295	4.05	4.34	4.50	4.17	3.99	4.21	3.66
297	4.05	4.34	4.49	4.18	3.98	4.21	3.65
305	4.03	4.31	4.47	4.16	3.97	4.21	3.64
310	4.03	4.29	4.46	4.15	3.96	4.19	3.64
315	4.02	4.28	4.45	4.15	3.97	4.18	3.64
320	4.02	4.27	4.44	4.14	3.97	4.17	3.64
325	4.02	4.27	4.44	4.16	3.98	4.16	3.65

Temp. (K)	G2H5′	A3H5′	T4H5′	C5H5′	A6H5′	G2H5″
277	4.07	4.26	4.07	3.96	4.07	3.96
287	4.06	4.23	4.06	3.95	4.09	3.97
295	4.05	4.24	4.05	3.96	4.09	3.99
297	4.05	4.24	4.05	3.96	4.08	3.98
305	4.03	4.27	4.03	3.97	4.08	3.97
310	4.03	4.23	4.03	3.96	4.08	3.96
315	4.02	4.22	4.02	3.97	4.07	3.97
320	4.02	4.21	4.02	3.97	4.07	3.97
325	4.02	4.21	4.02	3.98	4.07	3.98

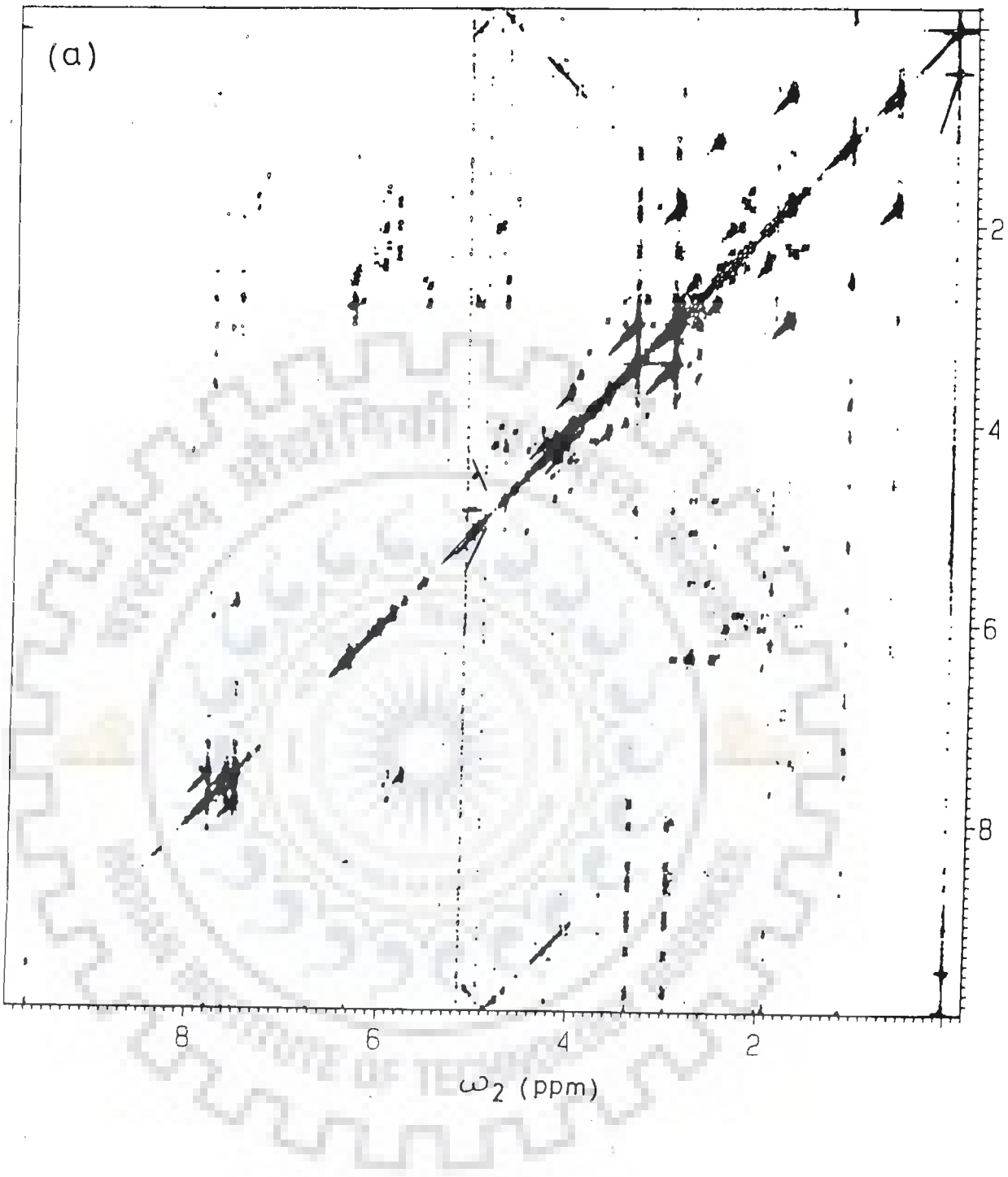

Fig. 5.5(a) : Phase-sensitive double quantum filter COSY spectrum of d-$(TGATCA)_2$ at 295 K in D_2O.

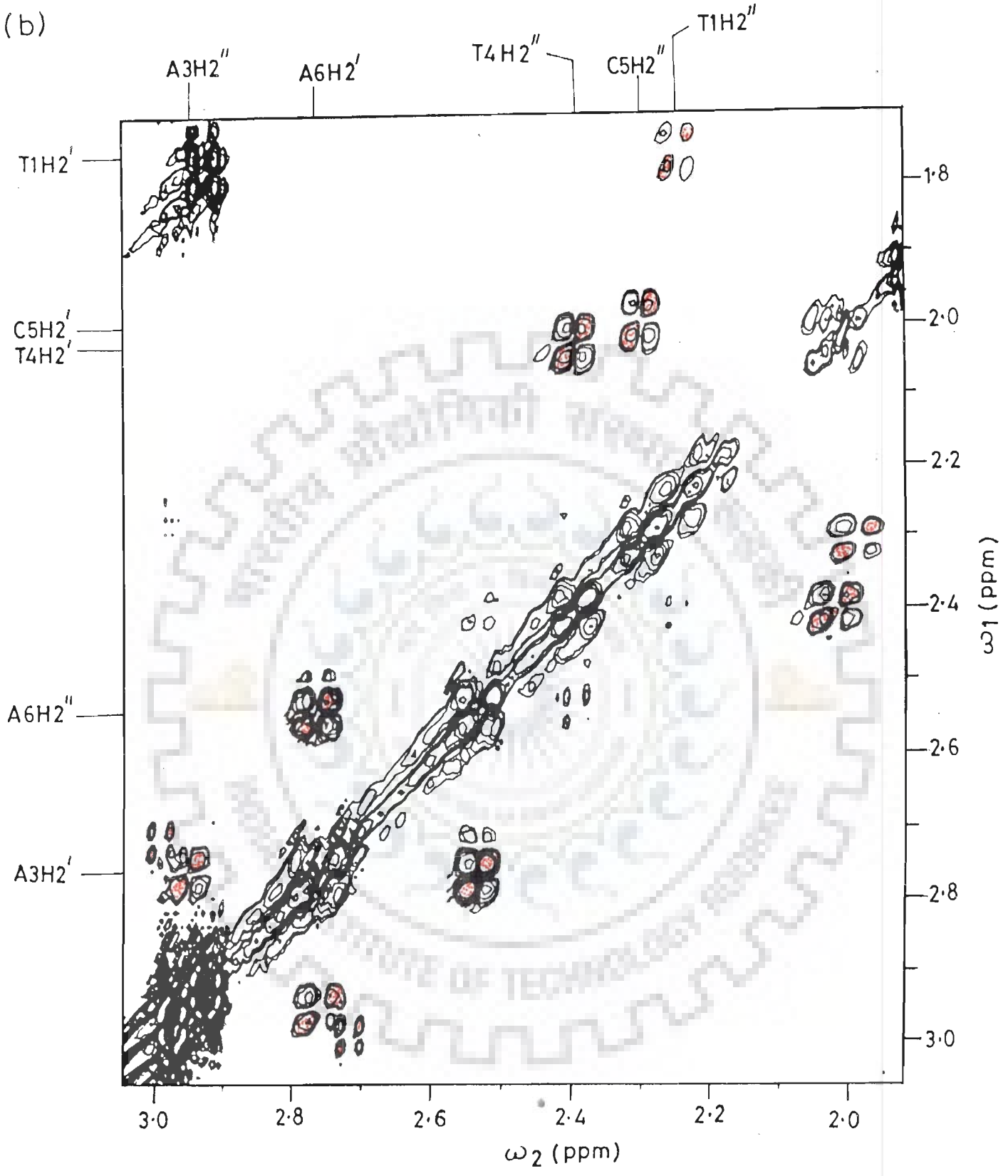

Fig. 5.5(b) : Expanded portion of phase-sensitive double quantum filter COSY spectrum of d-$(TGATCA)_2$ showing H2'-H2" connectivities.

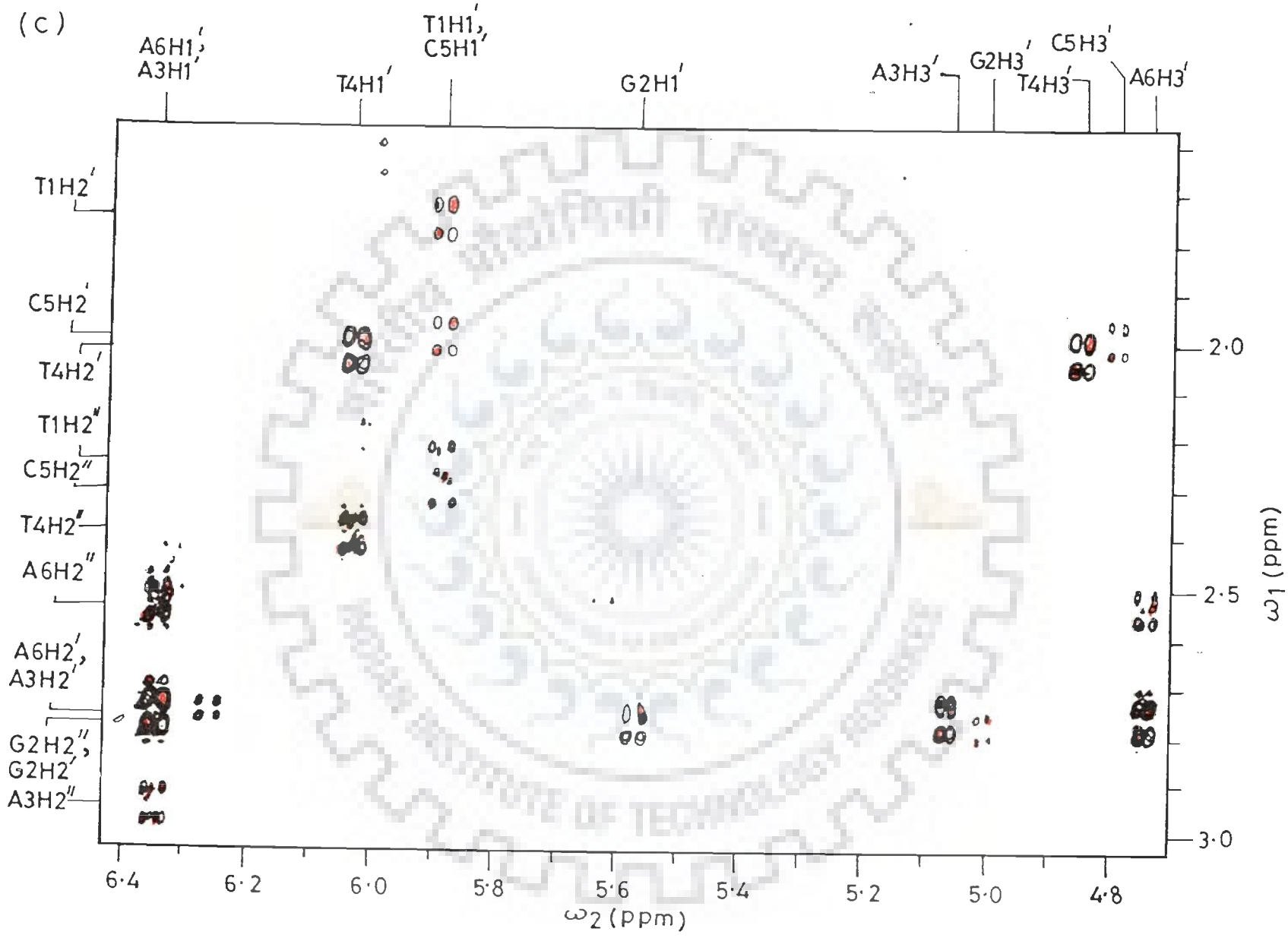

Fig. 5.5(c) : Expanded portion of phase-sensitive double quantum filter COSY spectrum of d-$(TGATCA)_2$ showing H1′-H2′, H2"; H3′-H2′, H2" connectivities.

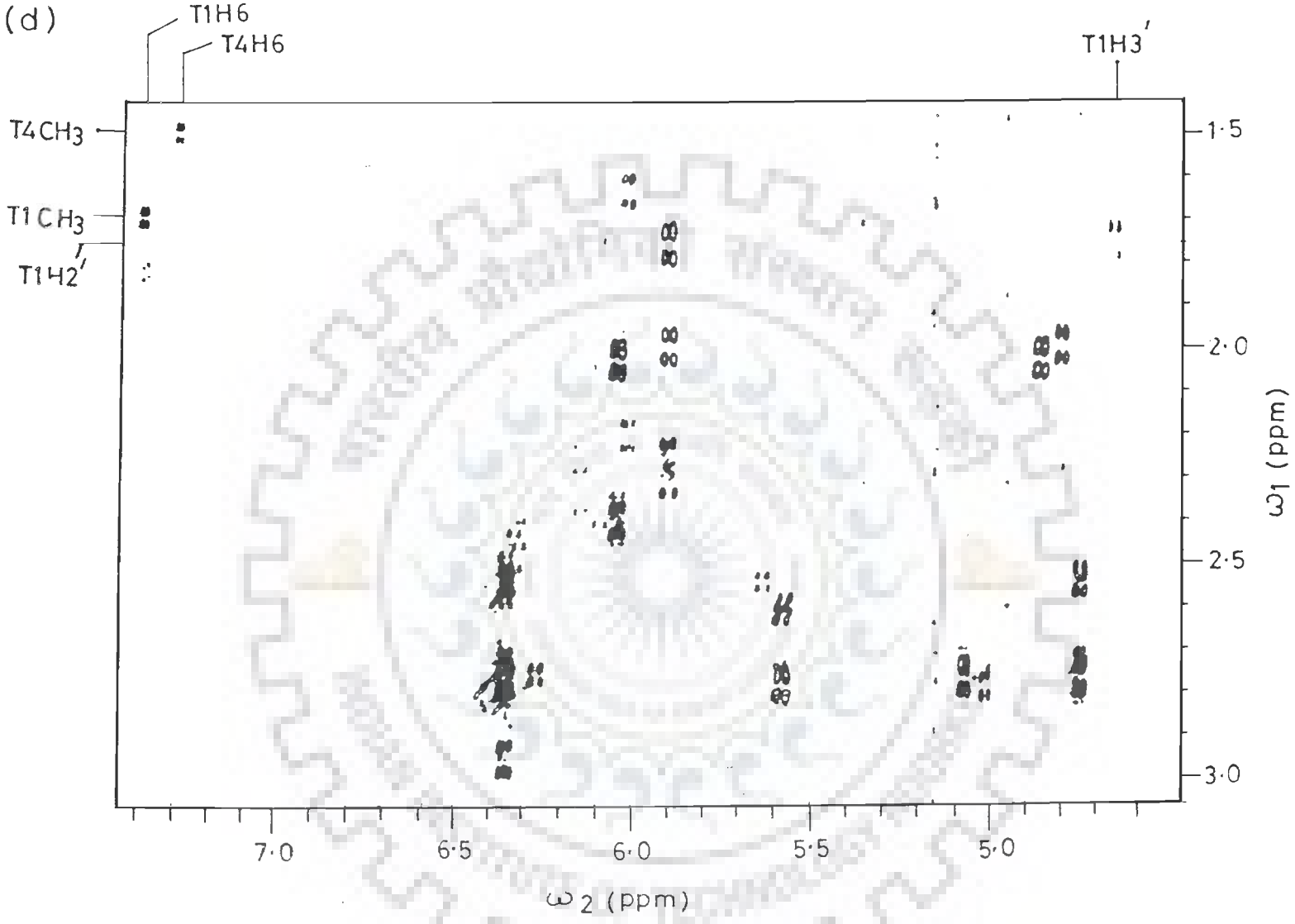

Fig. 5.5(d) : Expanded portion of phase-sensitive double quantum filter COSY spectrum of d-$(TGATCA)_2$ showing base-base, T1H2′-T1H3′ connectivities.

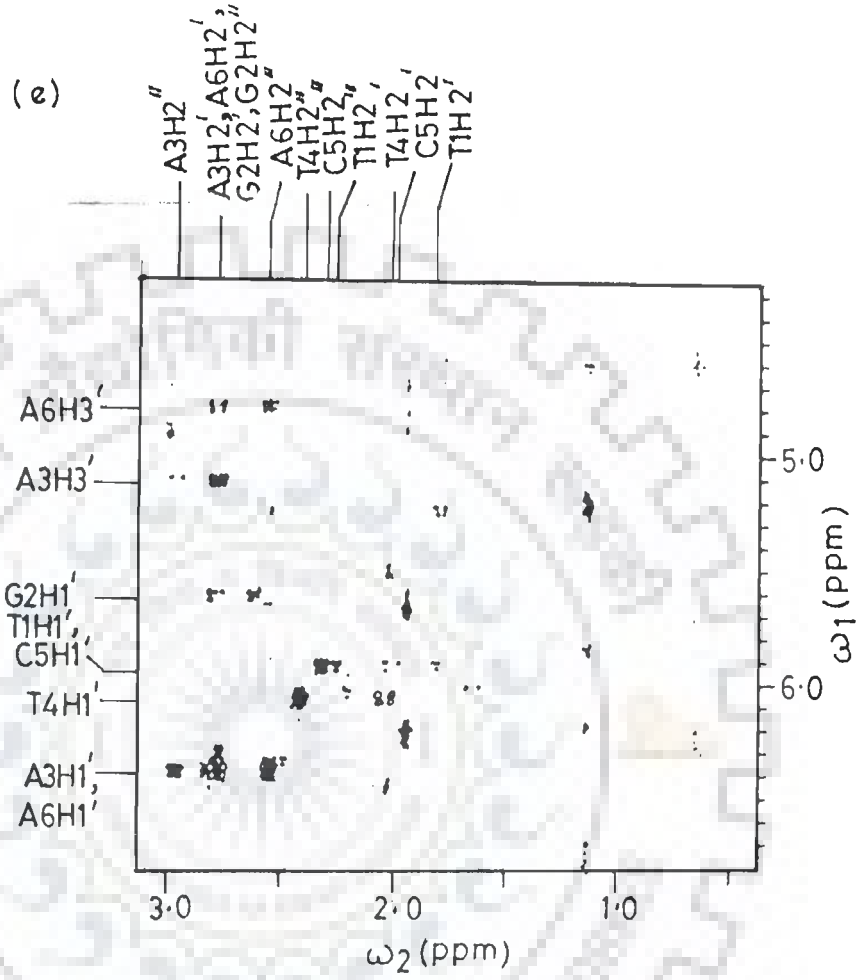

Fig. 5.5(e) : Expanded portion of phase-sensitive double quantum filter COSY spectrum of d-$(TGATCA)_2$ showing H1'-H2', H2" and H3'-H2', H2" connectivities.

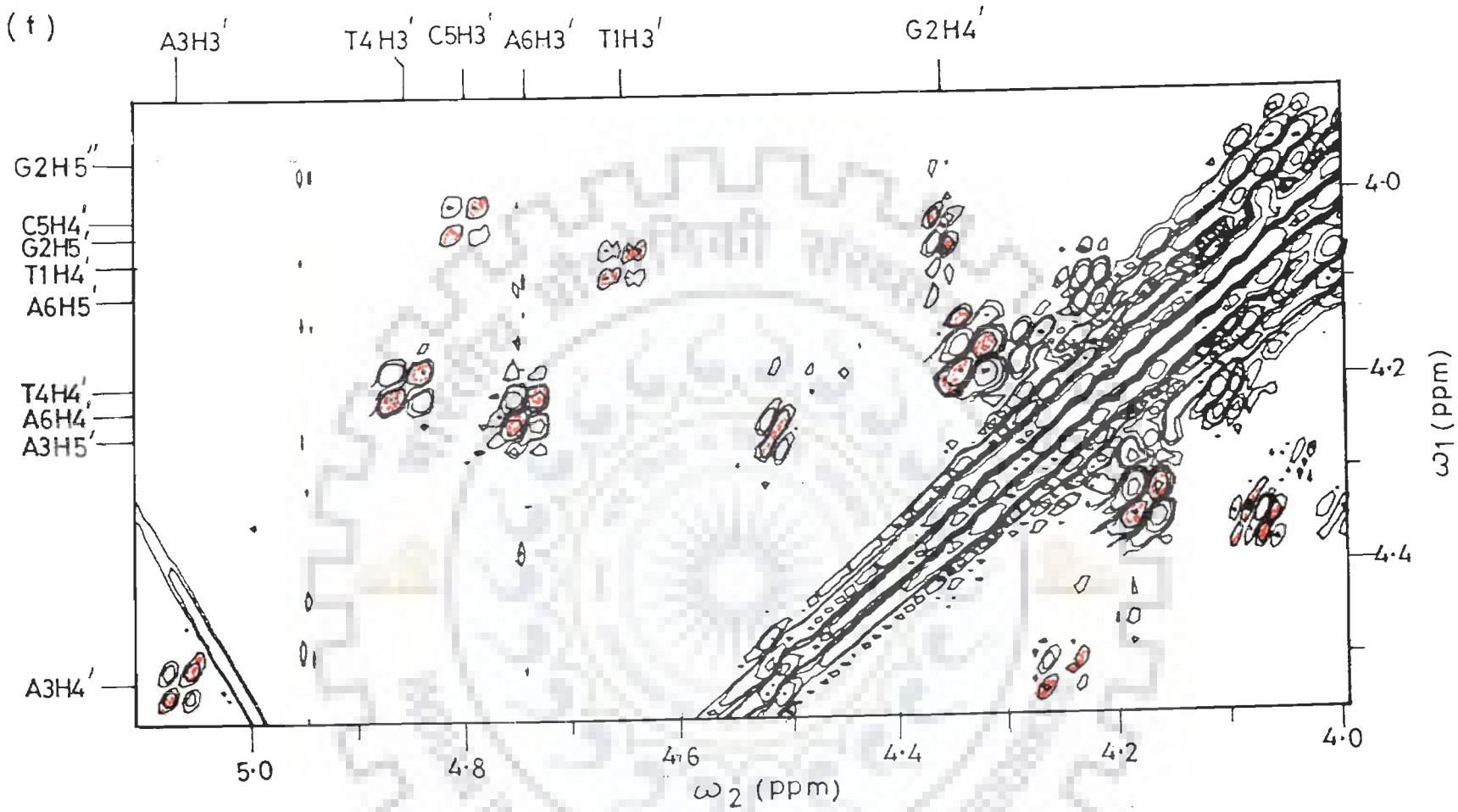

Fig. 5.5(f) : Expanded portion of phase-sensitive double quantum filter COSY spectrum of d-$(TGATCA)_2$ showing H3'-H4', H4'-H5', H5'-H5" connectivities.

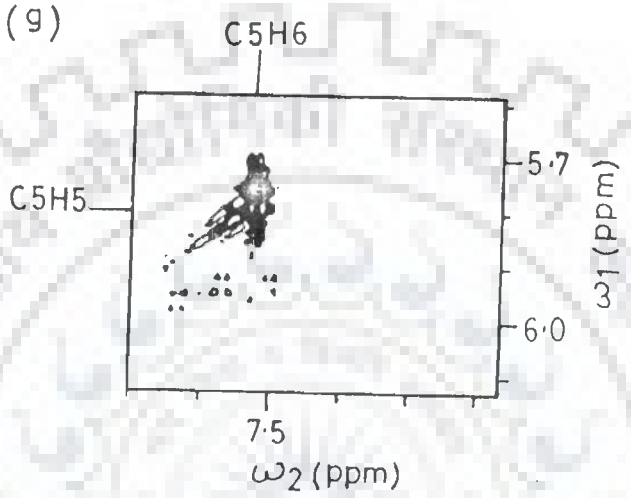

Fig. 5.5(g) : Expanded portion of phase-sensitive double quantum filter COSY spectrum of d-$(TGATCA)_2$ showing C5H5-C5H6 connectivity.

H3′ resonances at 5.57 and 5.00 ppm, respectively give only one COSY connectivity with their corresponding H2′/H2" protons resonating at 2.79 ppm. (Fig. 5.5(c)). Thus it is evident that chemical shift position of H2′ and H2" protons of this residue is not very different, due to which H2′-H2" COSY connectivity is not clearly seen in Fig. 5.5(b). Fig 5.5 (f) show that each H3′ is coupled to H4′ and further each H4′ is coupled to H5′ and H5" proton. Thus each set of sugar protons of a residue is assigned , the positions of which match with the corresponding position in 1D NMR spectra (Figs. 5.1(a-d)). The cytosine and two thymine H6 protons are distinguishable in Fig 5.5 (g) and 5.5 (d) since they are coupled to their corresponding H5 and CH_3 protons. The assignment of the sugar protons to a specific nucleotide residue has been made using the strategies available in literature [44,50,65,75,114] for sequential assignment in right-handed B-DNA with sugar in C2′-endo/ C3′-endo/ O1′-endo conformations and glycosidic angle in anti domain (discussed in chapter III). The three AH8 and GH8 protons resonating in the range 8.0-8.4 ppm give NOE cross peak with their corresponding H2′ and H2" protons (Fig. 5.6(c)). It is noted that five of the H8/H6 protons give NOE cross peak with two (H2′-H2") pair of protons. One of the TH6 gives only 2 NOE cross peaks and is assigned as the terminal one at 5′-end. As expected each of the base proton gives NOE cross peak with one pair of H2′-H2" which is the sugar belonging to the base itself and one with sugar of the base preceeding it in the sequence 5′-3′ (Fig. 5.6(c)). Two NOE cross peaks are observed between base proton A3H8 and T4H6, $T4CH_3$ protons (Fig. 5.6(c,j))

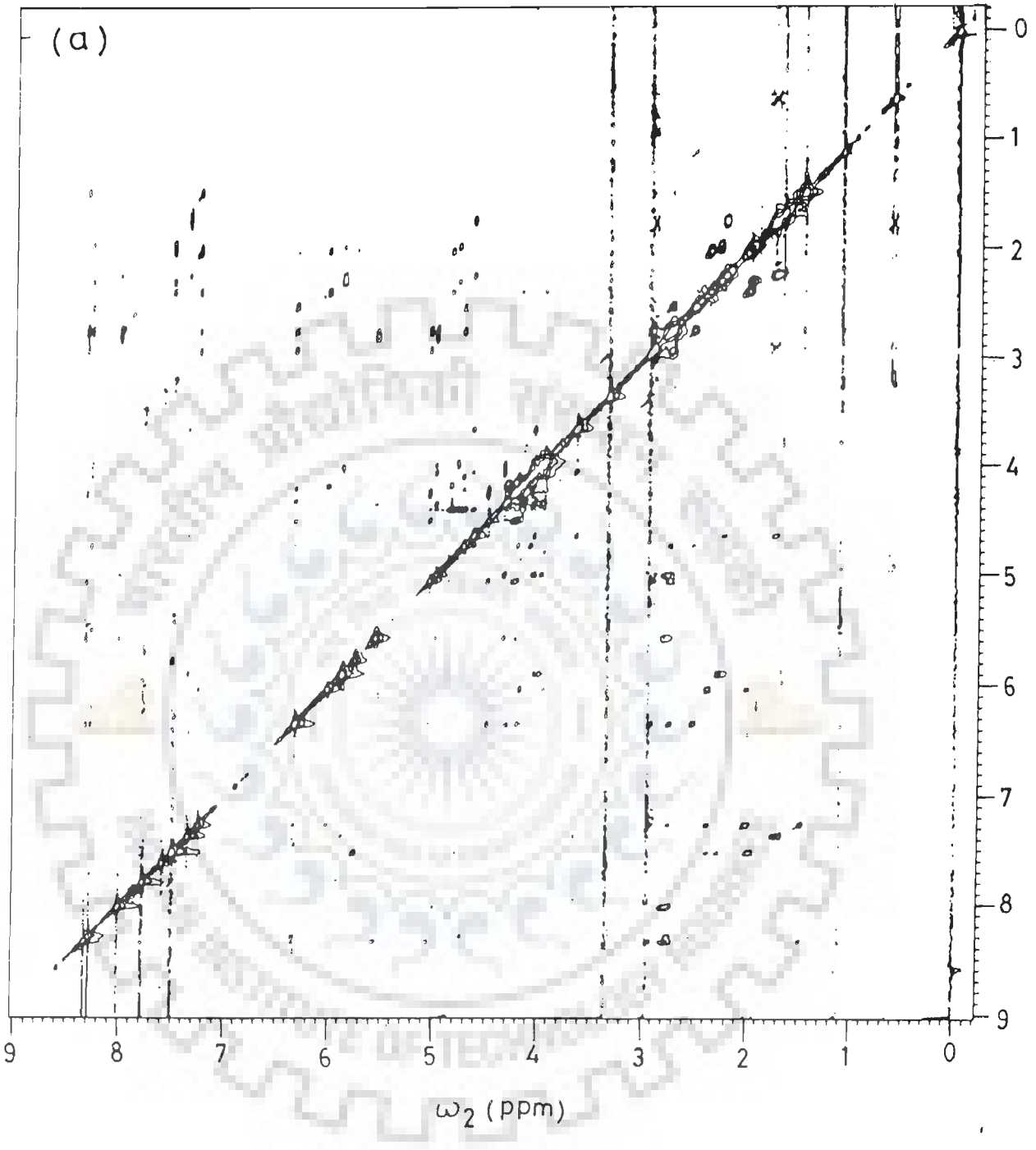

Fig. 5.6(a) : Phase-sensitive NOESY spectrum (at τ_m 250 ms) of d-$(TGATCA)_2$ at 295 K in D_2O.

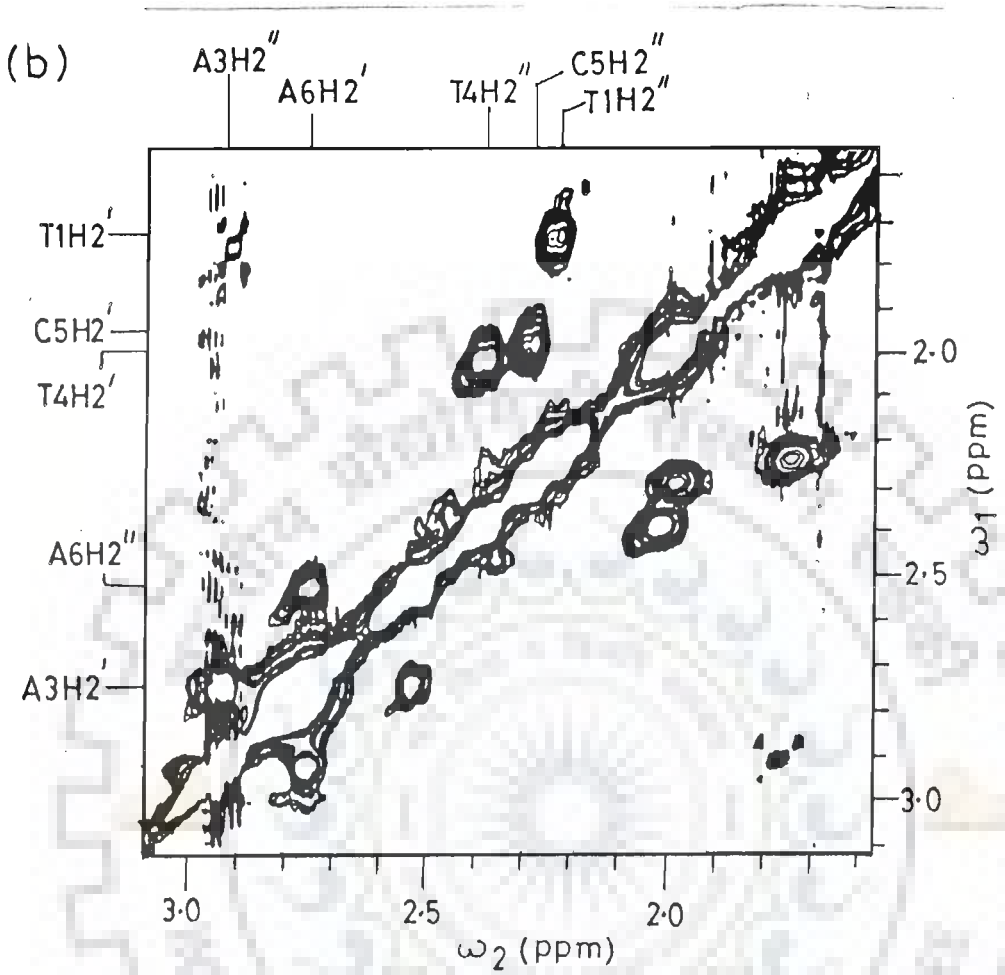

Fig. 5.6(b) : Expanded portion of phase-sensitive NOESY spectrum (at τ_m 250 ms) of d-$(TGATCA)_2$ showing H2'-H2" connectivities.

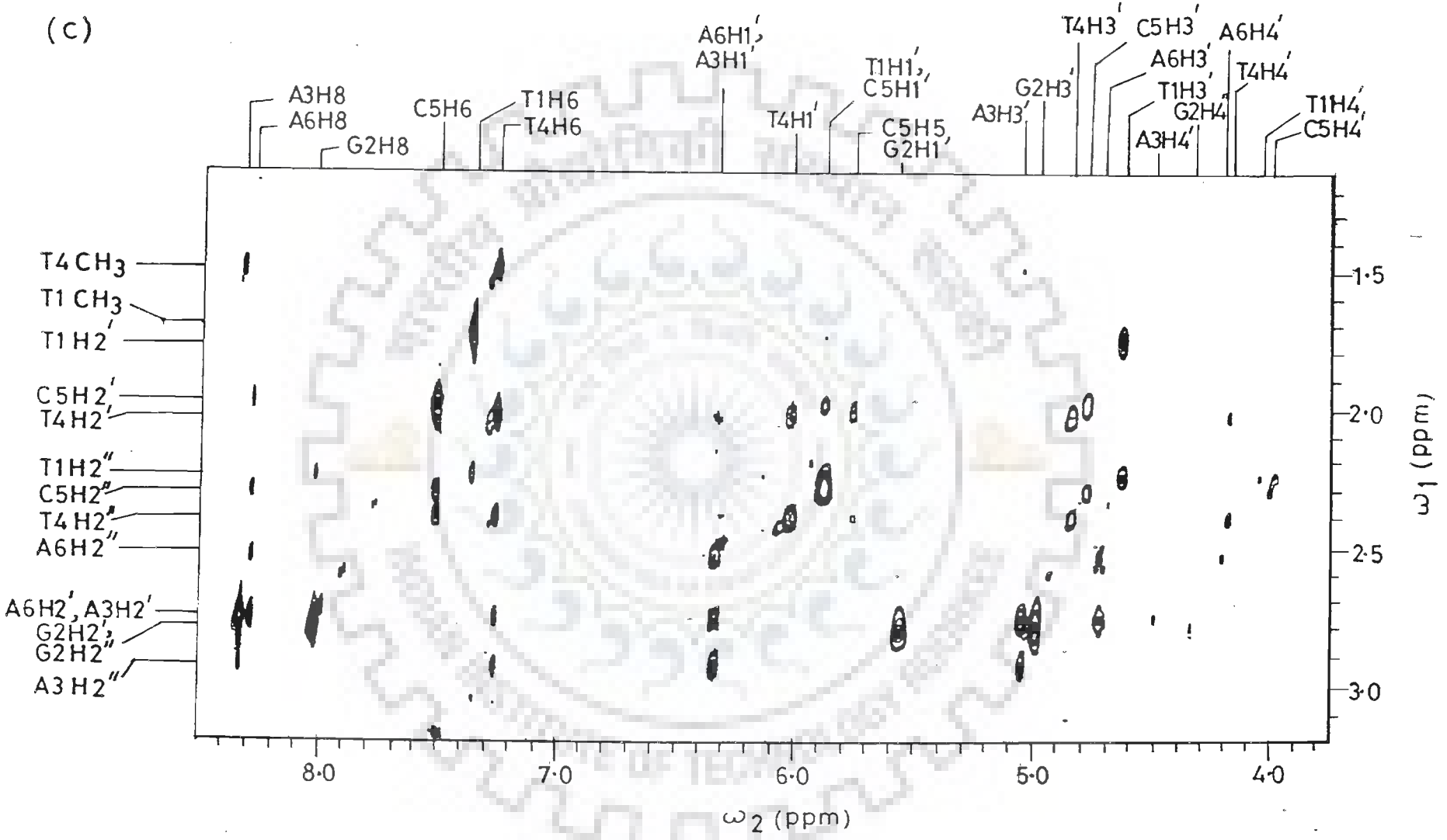

Fig. 5.6(c) : Expanded portion of phase-sensitive NOESY spectrum (at τ_m 250 ms) of d-$(TGATCA)_2$ showing H1′-H2′, H2"; H3′-H2′, H2", H4′-H2′; intra and inter-residue connectivities.

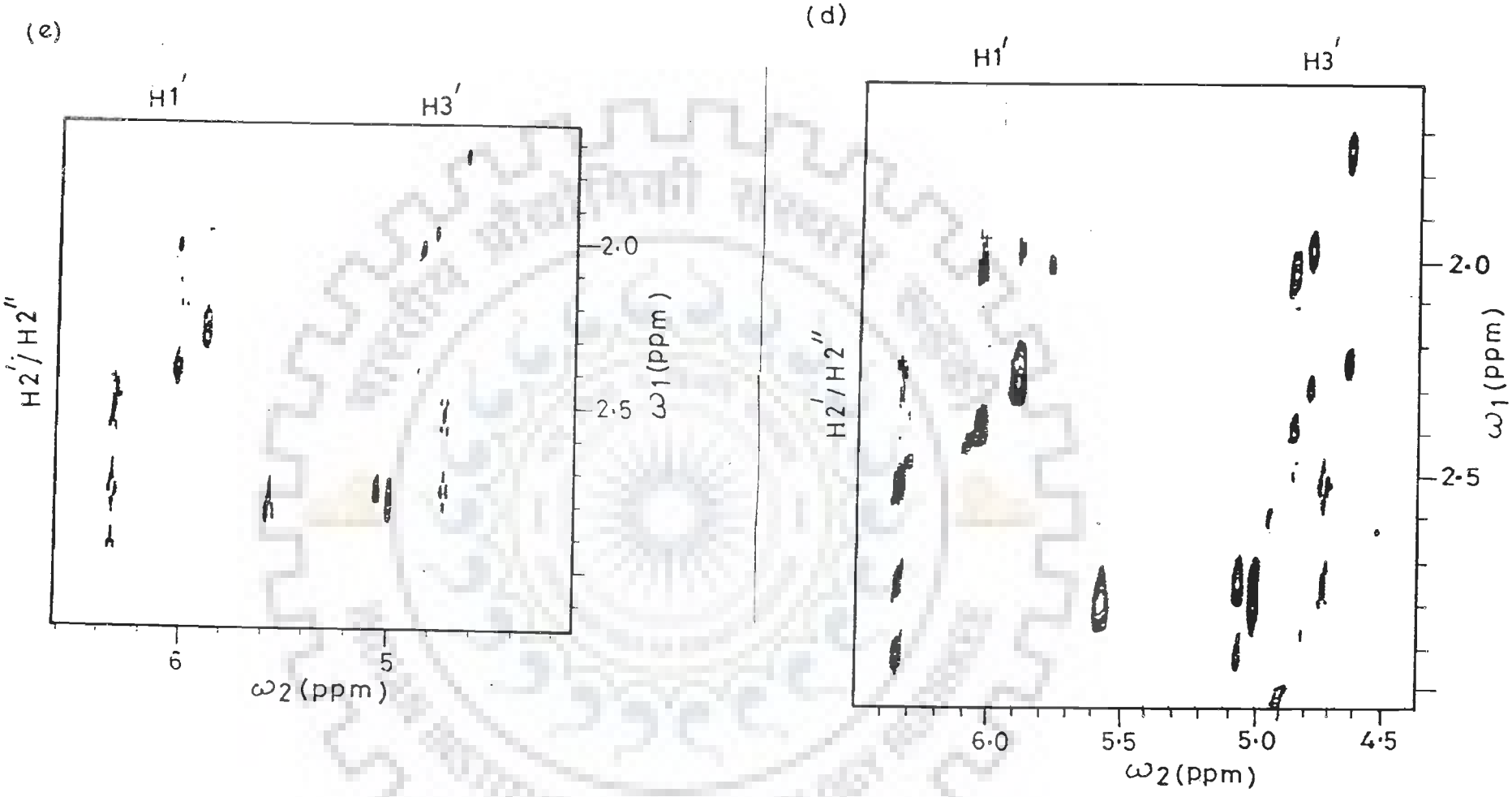

Fig. 5.6(d, e) : Expanded portion of phase-sensitive NOESY spectrum (at τ_m 150 and 75 ms, respectively) of d-$(TGATCA)_2$ showing H1′-H2′, H2"; H3′-H2′, H2" connectivities.

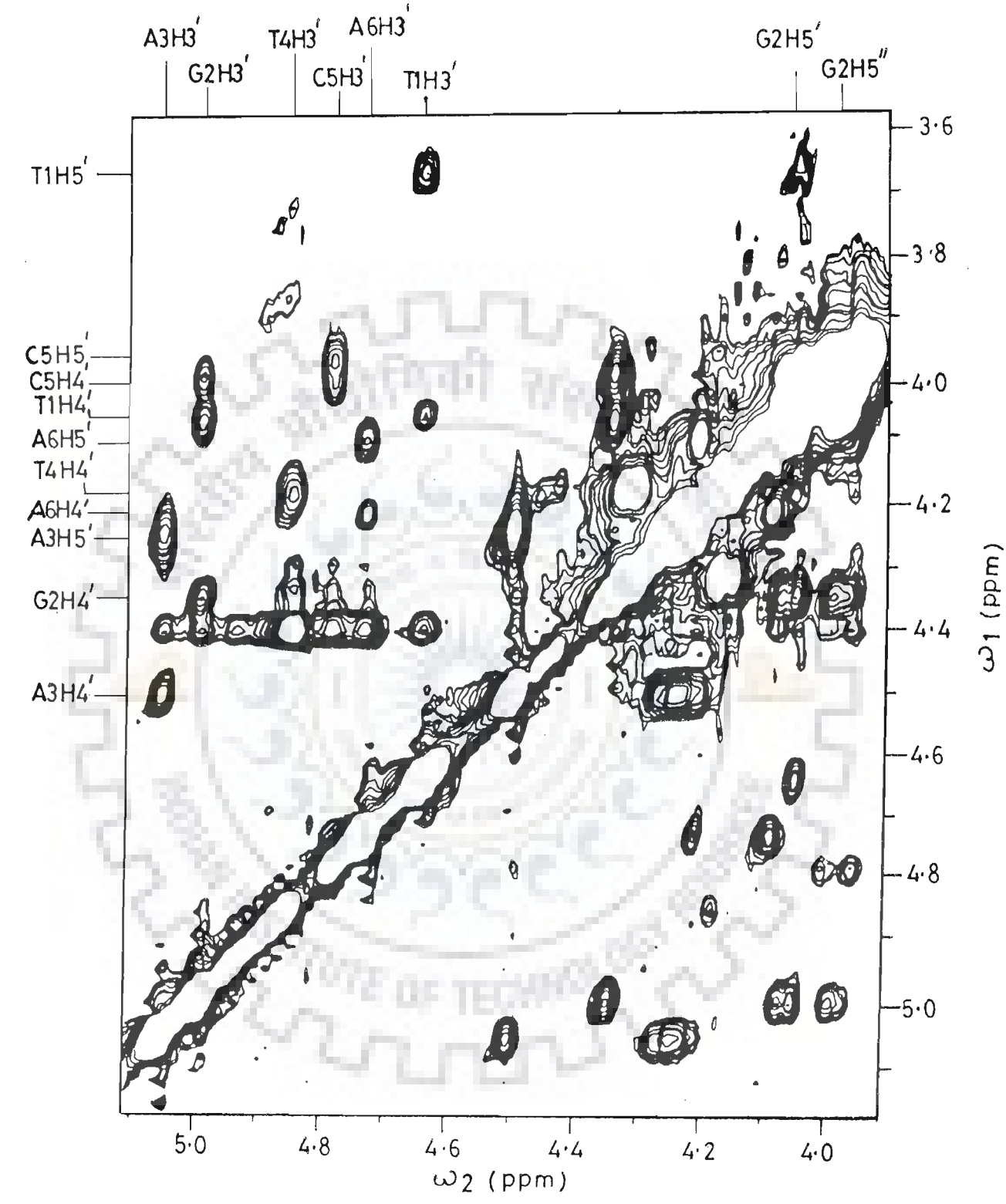

Fig. 5.6(f) : Expanded portion of phase-sensitive NOESY spectrum (at τ_m 250 ms) of d-$(TGATCA)_2$ showing H3'-H4', H4'-H5', H5'-H5" connectivities.

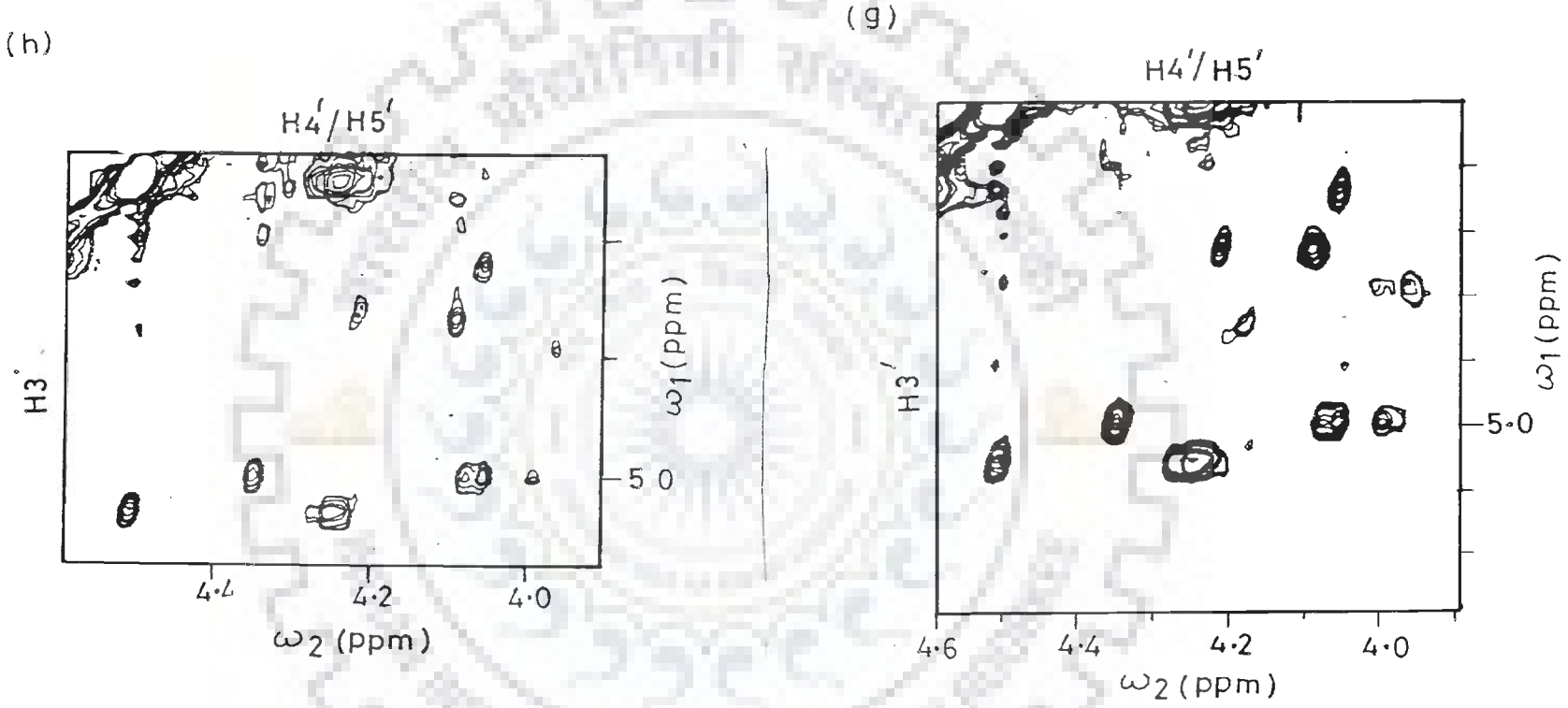

Fig. 5.6(g, h) : Expanded portion of phase-sensitive NOESY spectrum (at τ_m 150 and 75 ms respectively) of d-$(TGATCA)_2$ showing H3′-H4′, H3′-H5′ connectivities.

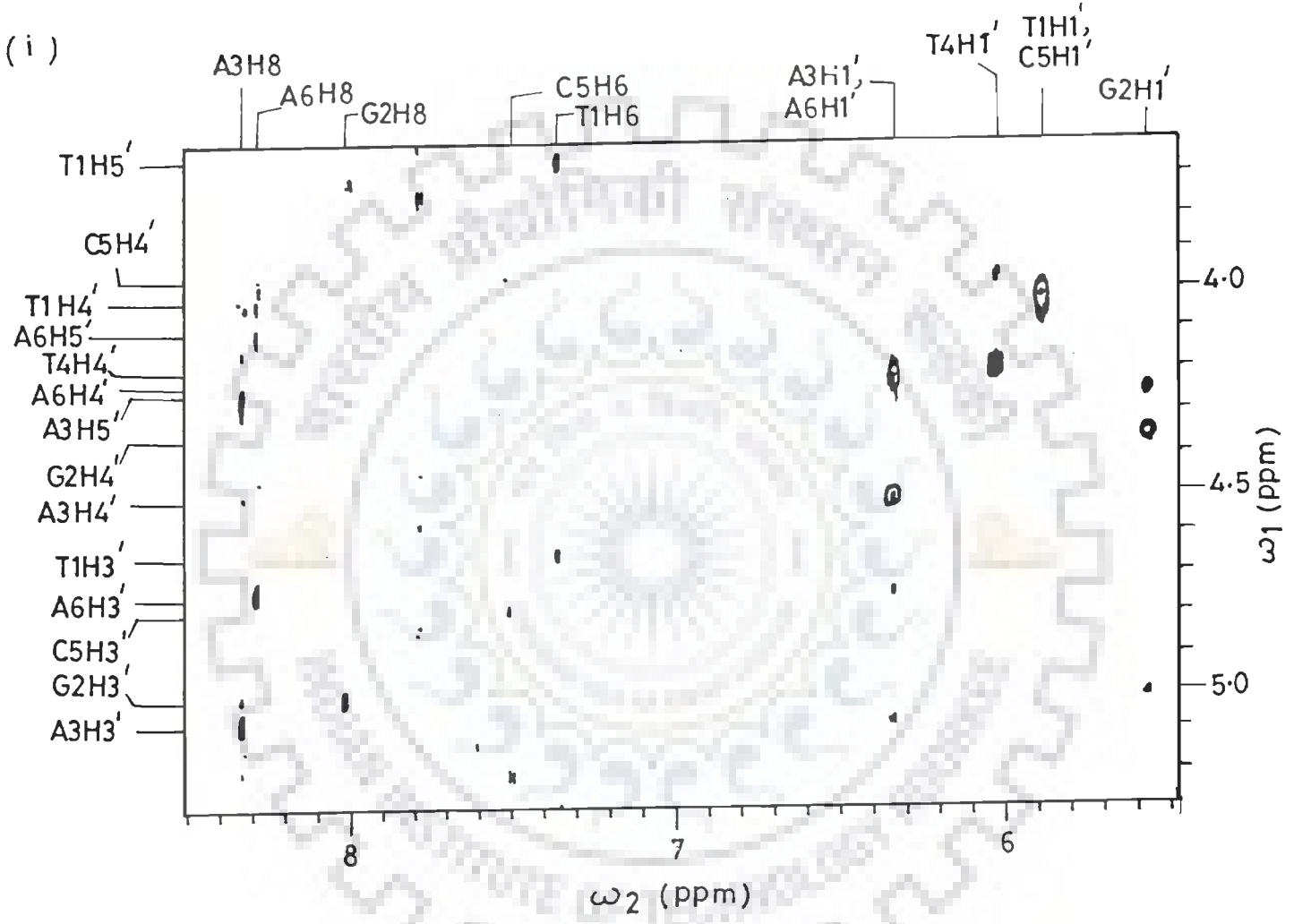

Fig. 5.6(i) : Expanded portion of phase-sensitive NOESY spectrum (at τ_m 250 ms) of d-$(TGATCA)_2$ showing H1′-H3′, H1′-H4′, base-H3′, base-H5′ connectivities.

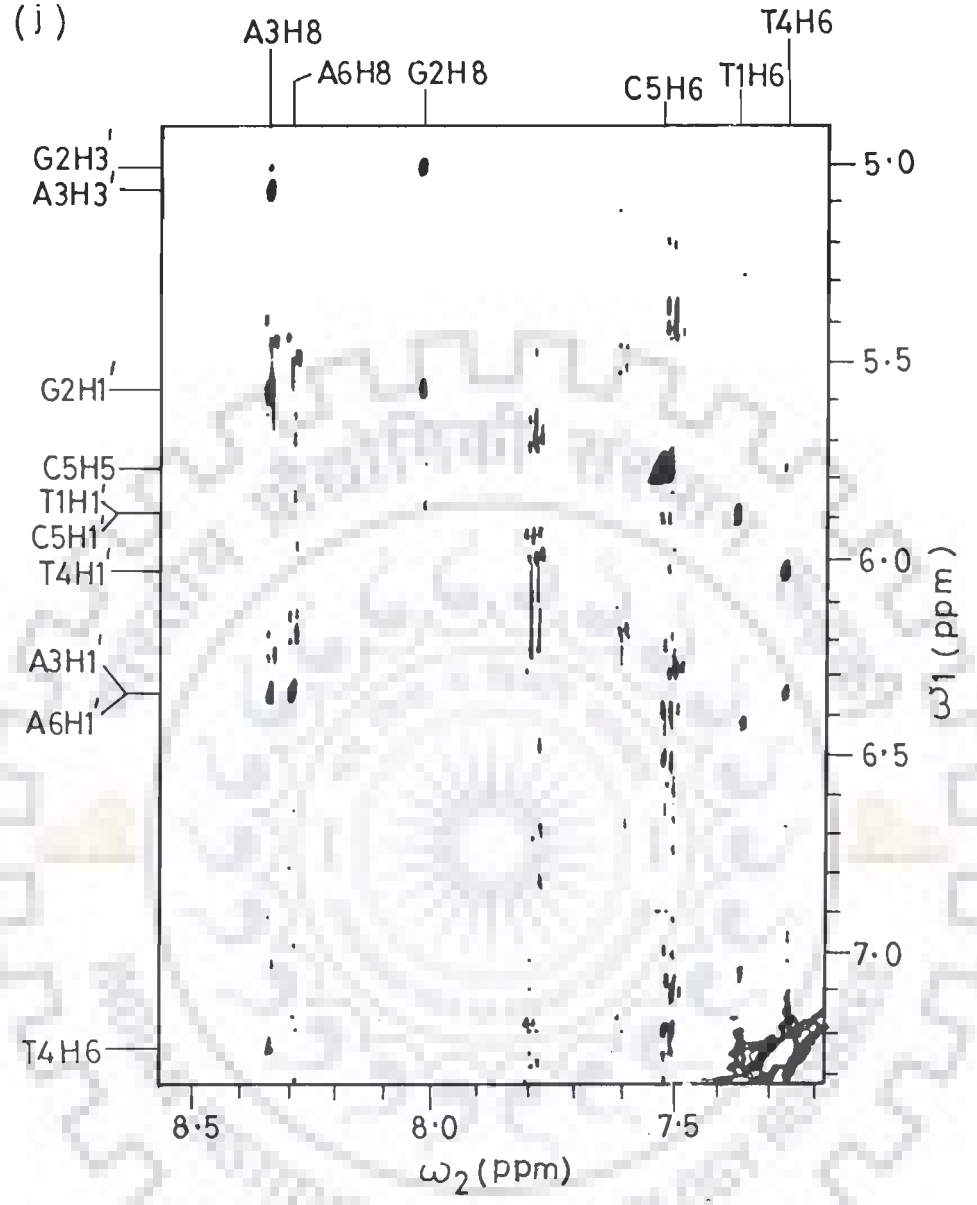

Fig. 5.6(j) : Expanded portion of phase-sensitive NOESY spectrum (at τ_m 250 ms) of d-$(TGATCA)_2$ showing intra and inter-residue base-H1', base-base connectivities.

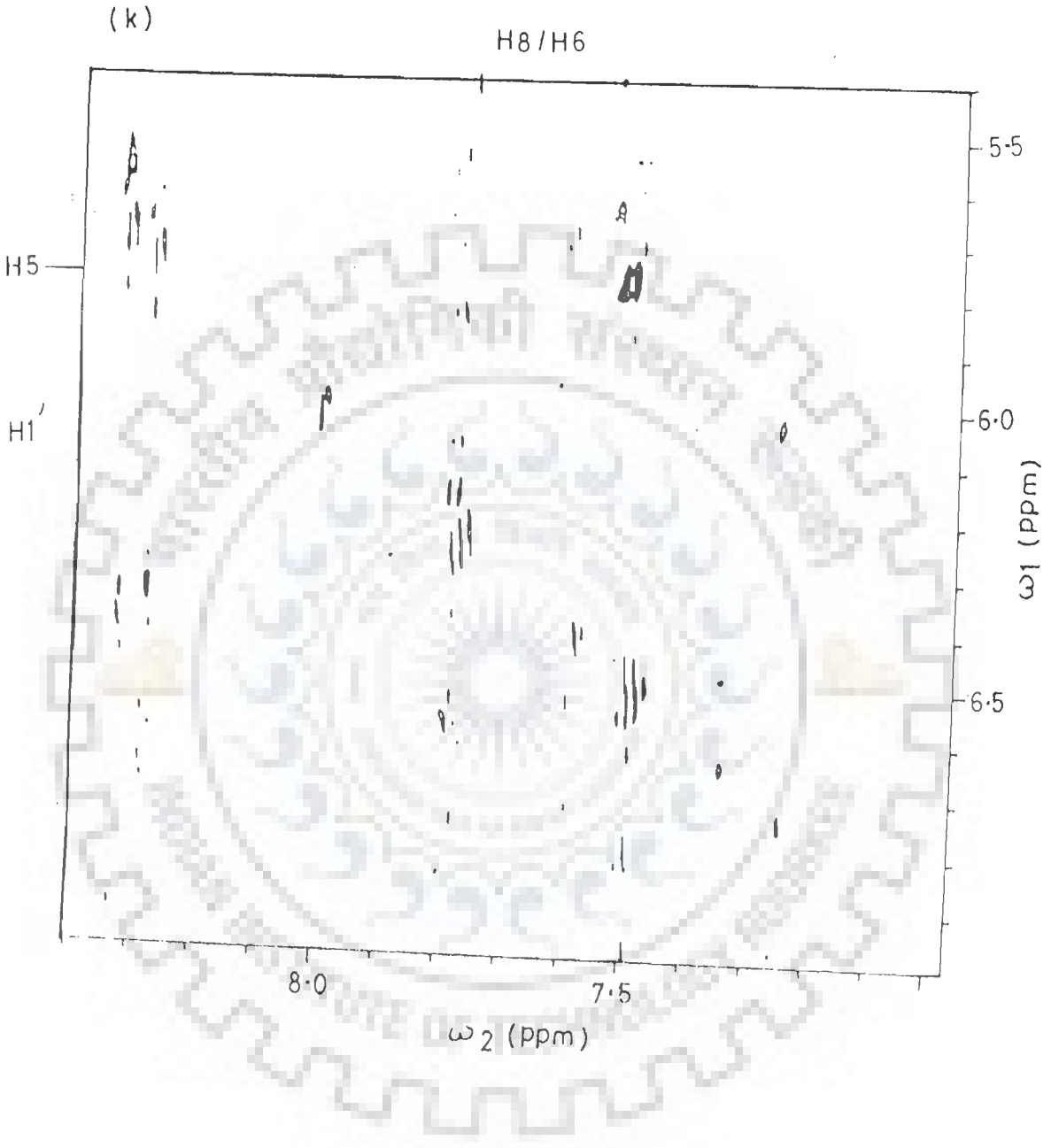

Fig. 5.6(k) : Expanded portion of phase-sensitive NOESY spectrum (at τ_m 150 ms) of d-$(TGATCA)_2$ showing intra and inter-residue: base-H1', base-base connectivities.

showing their proximity and which are expected to be at a distance ≃ 3.8-3.9 A°. Further A3H8 and T4H6 base proton give NOE cross peaks with H1′ of the base preceeding to it (Fig. 5.6(j)). Table 5.3(a-c) gives the list of connectivities observed in DQF-COSY and NOESY spectra.

Thus each of the set of sugar resonances gets assigned to a particular base in the sequence d-$(TGATCA)_2$ and unambiguous spectral assignment is made. Several additional NOE connectivities are observed in the Figs. 5.6 (c-k), Table 5.3(b). These include intra sugar NOE cross peaks H3′-H5′/H5", H1′-H3′, H2′-H4′, H2"-H4′, base - H1′/H2′/H2"/H3′/H4′/H5′ protons which are used for conformational analysis and are discussed later.

DUPLEX TO SINGLE STRAND TRANSITION

The one-dimensional NMR spectra are recorded in the temperature range 277 - 325 K in order to monitor the duplex to single strand transition (Fig. 5.3(c)). Change in chemical shift with temperature for some of the protons are shown in Figs. 5.4 (a, b) and the positions of resonances at different temperature are given in Table 5.2. It is observed that practically all the non-exchangeable protons and sugar H1′ proton (which being close to the base aromatic ring experience upfield shift in oligonucleotides) shift downfield with temperature up to a value of ≃ 0.35 ppm. The temperature at which half the change in chemical shift occur is 308, 309, 310, 311, 314 K for T4H6, A3H1′, G2H1′, $T1CH_3$ and G2H8 protons,respectively and more than 95% of

Table 5.3(a): **Presence (marked as +) and absence (marked as -) of intra-residue cross peak as observed in phase-sensitive double quantum filter COSY spectra of d-$(TGATCA)_2$ at 295 K in D_2O.**

Connectivities	T1	G2	A3	T4	C5	A6
H2′-H2"	+	O	+	+	+	+
H1′-H2′	+	O	+	+	+	+
H1′-H2"	+	O	+	+	+	+
H2′-H3′	+	O	+	+	+	+
H2"-H3′	-	-	+	-	-	+
H3′-H4′	+	-	+	+	+	+
H4′-H5′	-	+	+	O	O	+
H5′-H5"	-	+	O	O	O	O
B-B	+	-	-	+	+	-

O - overlap. B - Base proton.

Table 5.3(b) : Presence (marked as +) and absence (marked as -) of intra-residue cross peaks as observed in phase-sensitive NOESY spectra (at τ_m 75, 150, 200 and 250 ms) of d-$(TGATCA)_2$ at 295 K in D_2O.

Connectivities	T1	G2	A3	T4	C5	A6
H2′-H2"	+	O	+	+	+	+
H1′-H2′	+	O	+	+	+	+
H1′-H2"	+	O	+	+	+	+
H2′-H3′	+	O	+	+	+	+
H2"-H3′	+	O	+	+	+	+
H3′-H4′	+	+	+	+	+	+
H3′-H5′	+	+	+	-	+	+
H3′-H5"	-	+	-	-	-	-
H4′-H5′	+	+	+	O	O	+
H4′-H5"	-	+	-	-	-	-
H5′-H5"	-	+	O	O	O	O
H1′-H3′	-	+	+	-	-	+
H1′H4′	+	+	+	+	+	+
H2′-H4′	-	O	+	+	-	-
H2"-H4′	+	O	-	+	+	+
B-B	+	-	-	+	+	-
B-H1′	+	+	+	+	+	+
B-H2′	+	+	+	+	+	+

B-H2"	+	+	+	+	+	+
B-H3′	+	+	+	-	+	+
B-H4′	-	-	+	-	-	-
B-H5′	+	-	+	-	-	+

B - Base proton, O - Overlap.

Table 5.3(c) : Inter-nucleotide NOE connectivities as observed in phase-sensitive NOESY spectra (at τ_m 75, 150, 200 and 250 ms) of d-$(TGATCA)_2$ at 295 K in D_2O.

A6H8 - C5H2′
A6H8 - C5H2"
C5H6 - T4H2′
C5H6 - T4H2"
T4H6 - A3H2′
T4H6 - A3H2"
A3H8 - G2H2′
A3H8 - G2H2"
G2H8 - T1H2"
T4H6 - A3H1′
A3H8 - G2H1′
C5H5 - T4H2′
C5H5 - T4H2"
A3H8 - $T4CH_3$
T4H6 - A3H8

the hexanucleotide exists in duplex state at 295 K at which the two-dimensional experiments are carried out.

SUGAR GEOMETRY OF d-(TGATCA)$_2$

There are two ways of determining sugar geometries as from the NMR parameters : (a) from the knowledge of three bond ^1H - ^1H coupling constants determined from correlation spectroscopy and splitting patterns in 1D NMR spectra and (b) from the knowledge of interproton distances in the sugar ring determined from NOESY spectra. Both the methods can be used in a complimentary fashion. It is recognized [13,115,123] that the very nature of pseudorotation phenomena in combination with conformational heterogeneity, virtually precludes an unambiguous and precise determination of sugar geometry from these distances. The dependence of distance constraints on glycosyl torsional angle (χ), the pseudorotation (P), pucker amplitude (ϕ_m) and mole fraction of S-conformer in case of a dynamic S to N interconversion show that the NOE data needs to be supplemented by other experimental factors before a reliable picture of the behaviour of an individual deoxyribose ring in a DNA duplex can be obtained. We have followed the strategy of determining the sugar geometry from analysis of J values and then supplementing it with distance data to arrive at specific conclusion.

Determination of deoxyribose pucker in d-(TGATCA)$_2$ by coupling constant analysis

The proton-proton coupling constants of interest in oligonucleotides are J(H1'-H2'), J(H1'-H2"), J(H2'-H3'),

J(H2"-H3'), J(H3'-H4') and J(H2'-H2"). Among these the five, three bond coupling constants define the sugar geometry. Of these, the J(H2'-H3') and J(H1'-H2") vary in a narrow range and are insensitive to sugar geometry. The other three coupling constants vary significantly between 0-10 Hz depending on sugar geometry [50,107,123], and thus their estimation from experimental spectra provides an effective tool for fixing the sugar geometries in oligonucleotides.

The coupling constants can be determined by analysing the patterns of cross peak components in COSY spectra. However since the patterns depend on the magnitudes of J, which in turn depend on sugar geometry, it is necessary to have a dictionary of expected patterns for various sugar geometries. The experimentally observed patterns are then matched with calculated patterns to derive the coupling constant information. The procedure used by us is described below.

The five coupling constants J(H1'-H2'), J(H1'-H2"), J(H2'-H3'), J(H2"-H3') and J(H3'-H4') are calculated as a function of the sugar geometry using the Karplus type relationship [55,56]. For the flip angle ϕ of the read pulse (Fig. 3.2) as $\pi/2$, the multiplet structure is simply calculated by combining the + and - along the ω_1 axis with those along the ω_2 axis. This is illustrated in Fig. 5.7(a-c) for four cross peaks H1'-H2', H1'-H2", H2'-H3', H2"-H3', for three standard sugar geometries , that is, C2'-endo, O1'-endo and C3'-endo. For example, it may be noted that in case of H1'-H2" that is, H2" along ω_1 axis and H1'

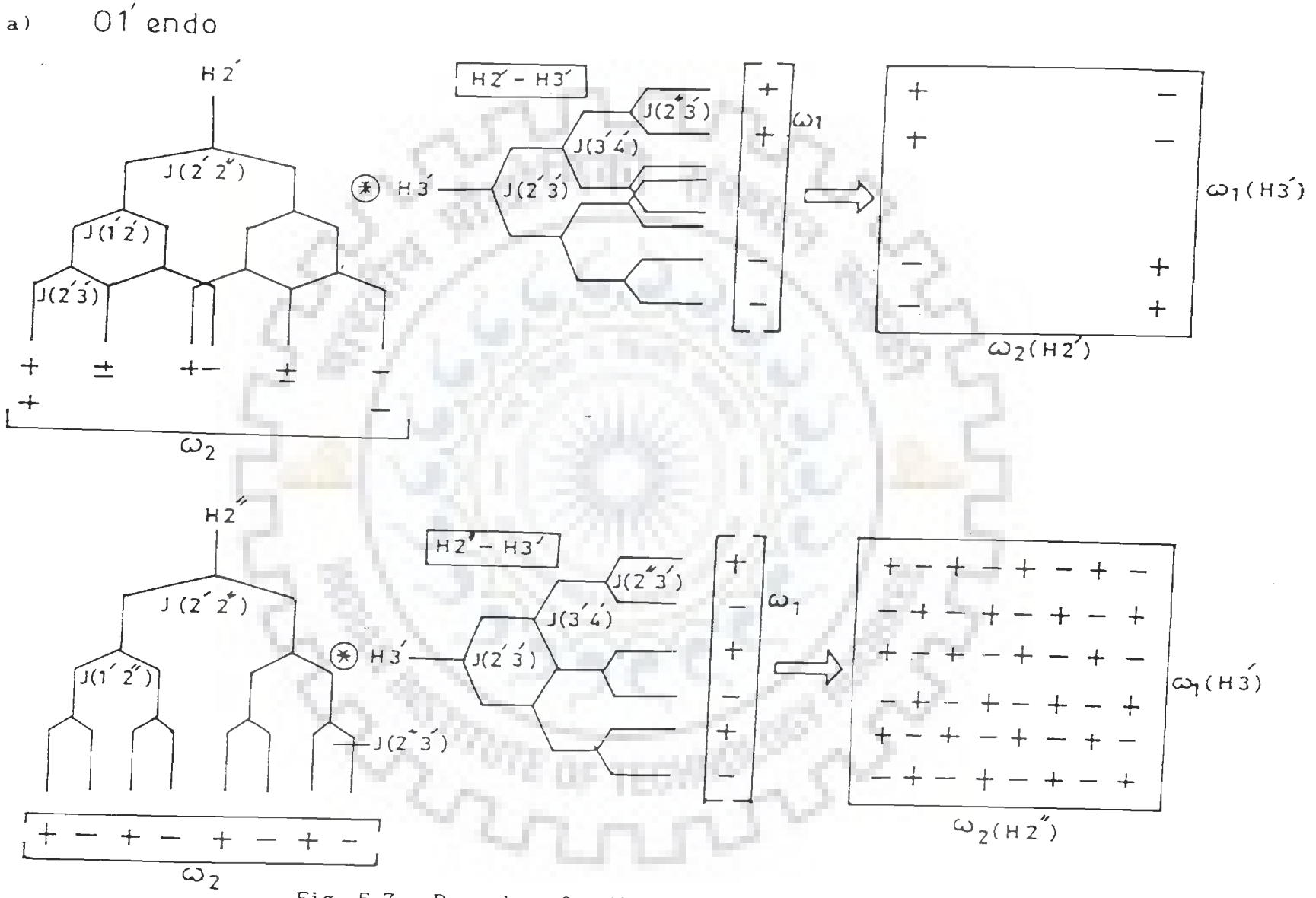

Fig. 5.7 : Procedure for the calculation of cross peak patterns in COSY spectra, illustrated for (a) O1′-endo (b) C2′-endo and (c) C3′-endo for (i) H1′-H2′ (ii) H1′-H2" (iii) H2′-H3′ and (iv) H2"-H3′.

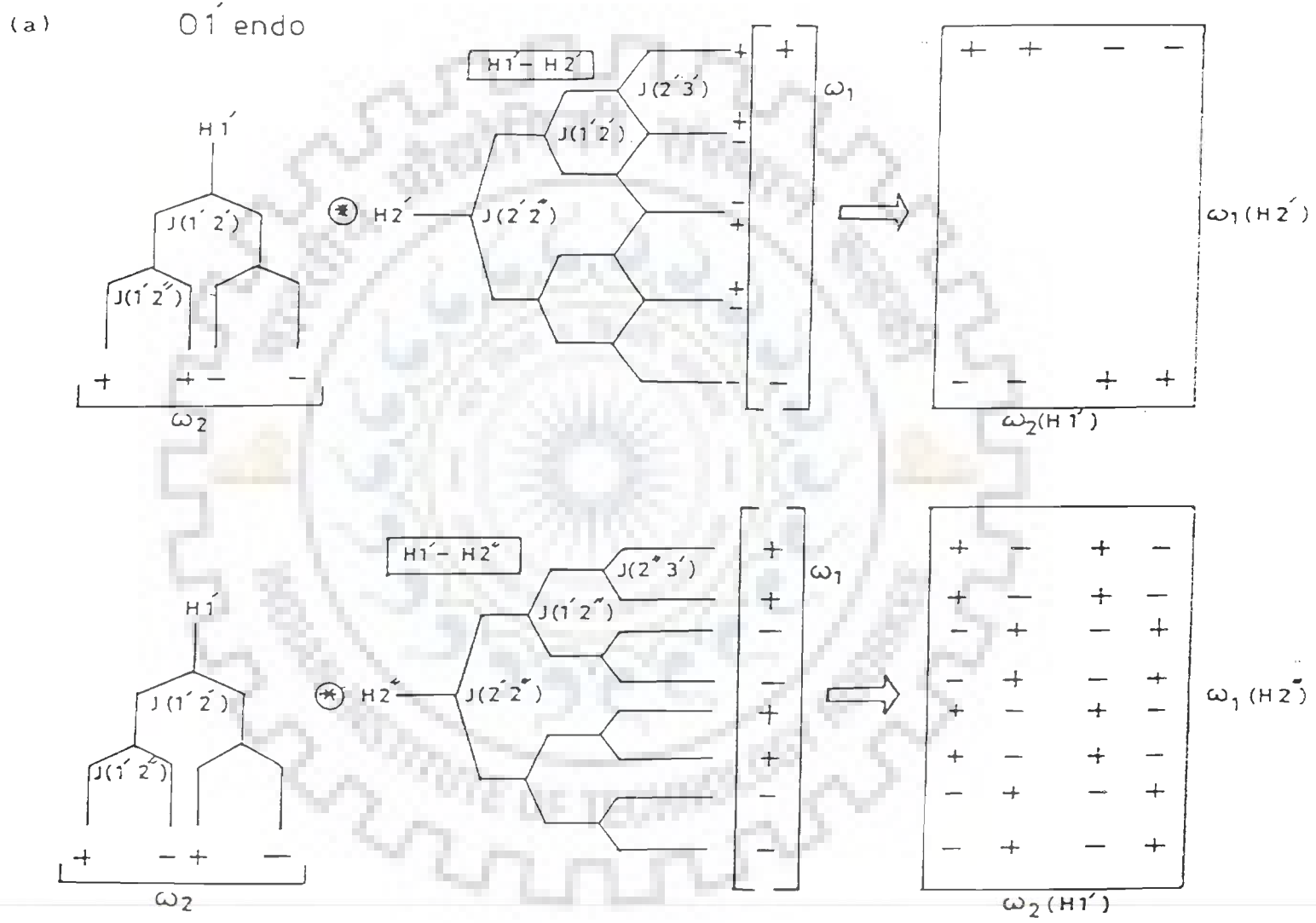
(a)
01´ endo
H1´
J(1´2´)
J(1´2´´)
+ + − −
ω2
H1´− H2´
J(2´3´)
J(1´2´)
J(2´2´´)
H2´
ω1
ω1(H2´)
ω2(H1´)
H1´
J(1´2´)
J(1´2´´)
+ − + −
ω2
H1´− H2´´
J(2´´3´)
J(1´2´´)
J(2´2´´)
H2´´
ω1
ω1(H2´´)
ω2(H1´)

(b) C 2′ endo

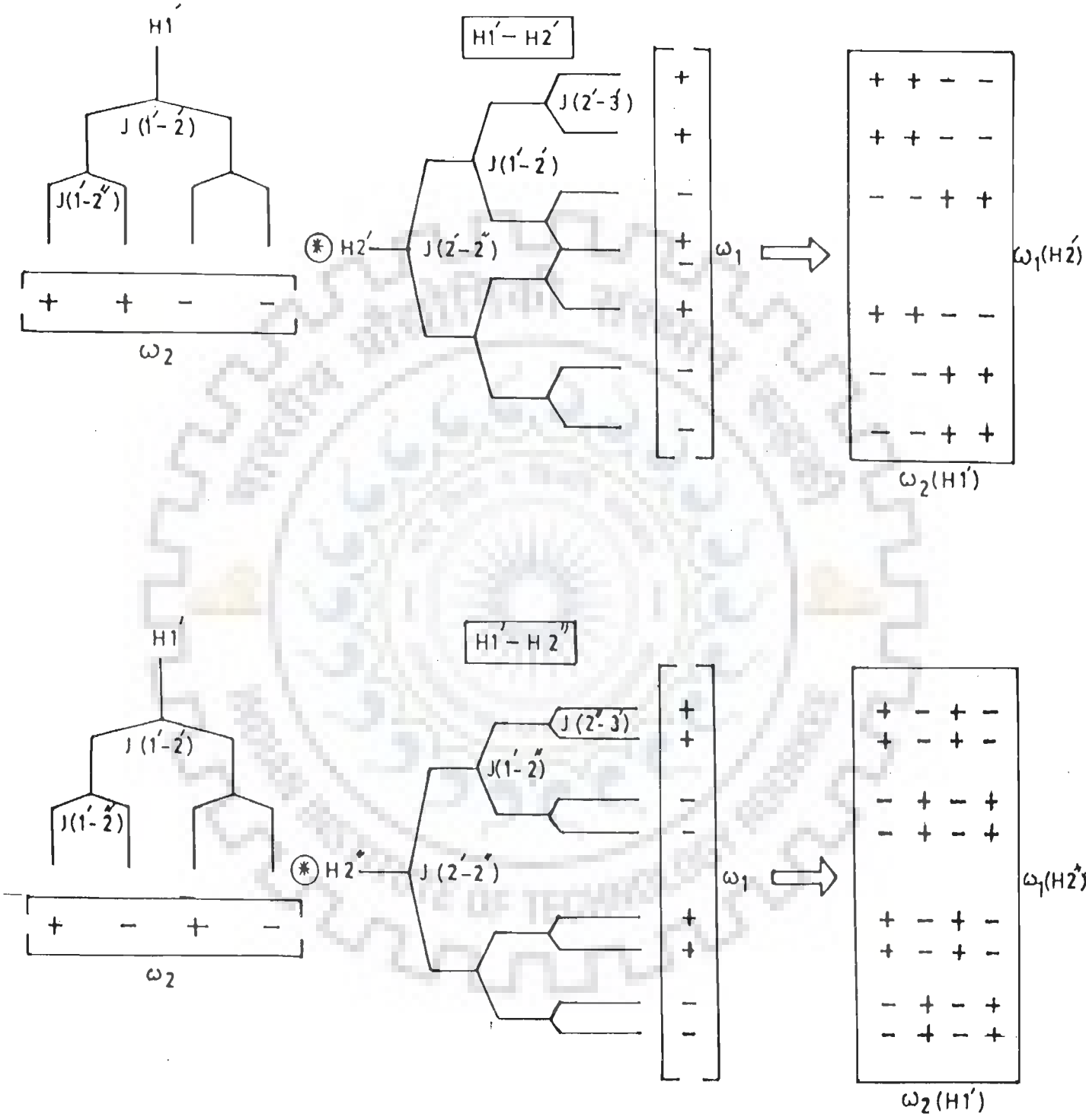
H1′
J (1′- 2′)
J(1′-2″)
+ + − −
ω2
H1′ − H2′
H2′
J(2′-3′)
J(1′-2′)
J(2′-2″)
ω1
+ + − −
+ + − −
− − + +
+ + − −
− − + +
− − + +
ω1(H2′)
ω2(H1′)
H1′
J (1′-2′)
J(1′-2″)
+ − + −
ω2
H1′ − H2″
H2″
J(2′-3′)
J(1′-2″)
J(2′-2″)
ω1
+ − + −
+ − + −
− + − +
− + − +
+ − + −
+ − + −
− + − +
− + − +
ω1(H2″)
ω2(H1′)

(b) C2′endo

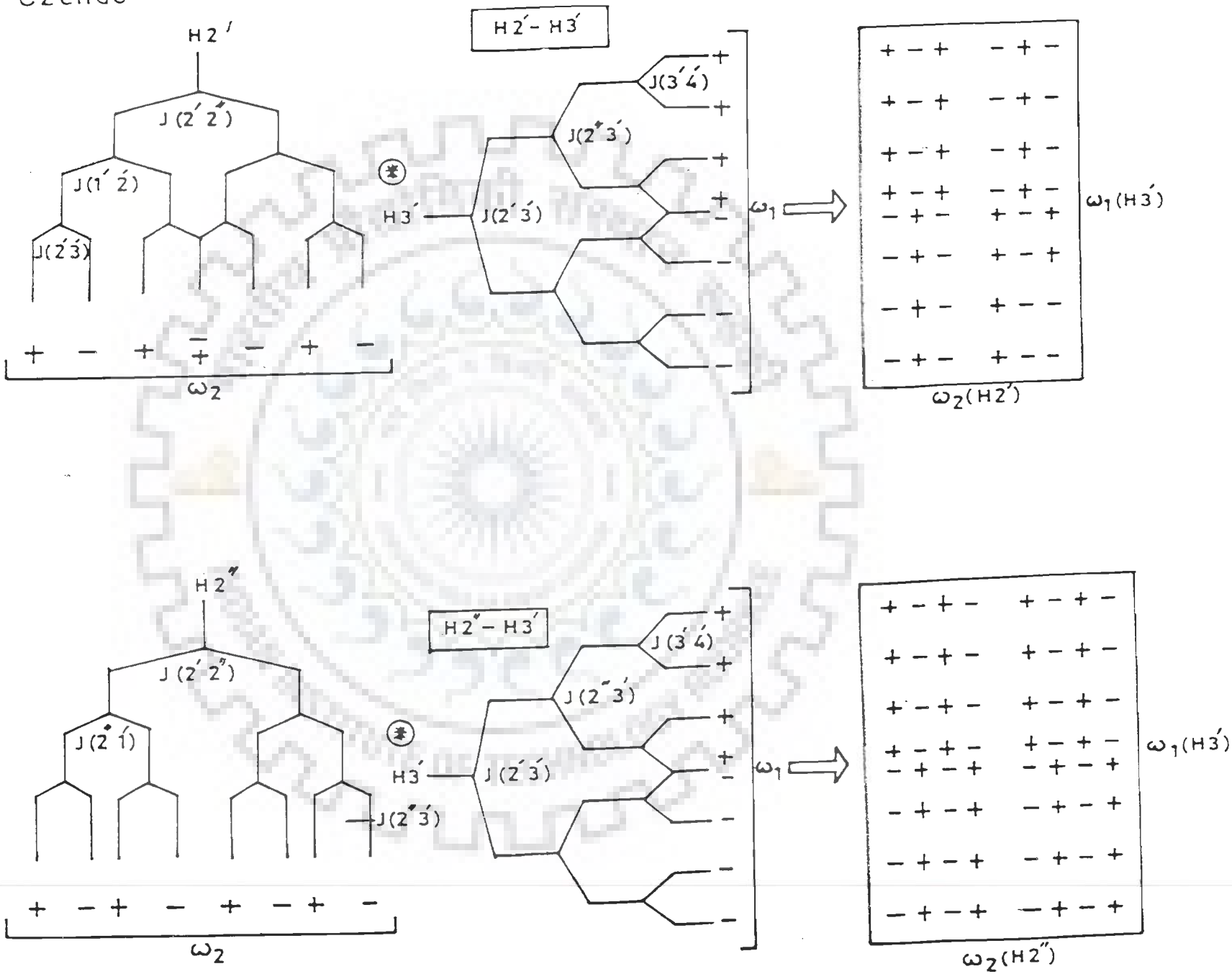
H2′
J(2′2″)
J(1′2′)
J(2′3′)
+ − + − + − + −
ω2
H2′- H3′
H3′
J(2″3′)
J(3′4′)
J(2′3′)
ω1
+ − + − + − +
− + − + − + −
ω1(H3′)
ω2(H2′)
H2″
J(2′2″)
J(2″1′)
J(2″3′)
H2″- H3′
ω2(H2″)

(c) C3′ endo

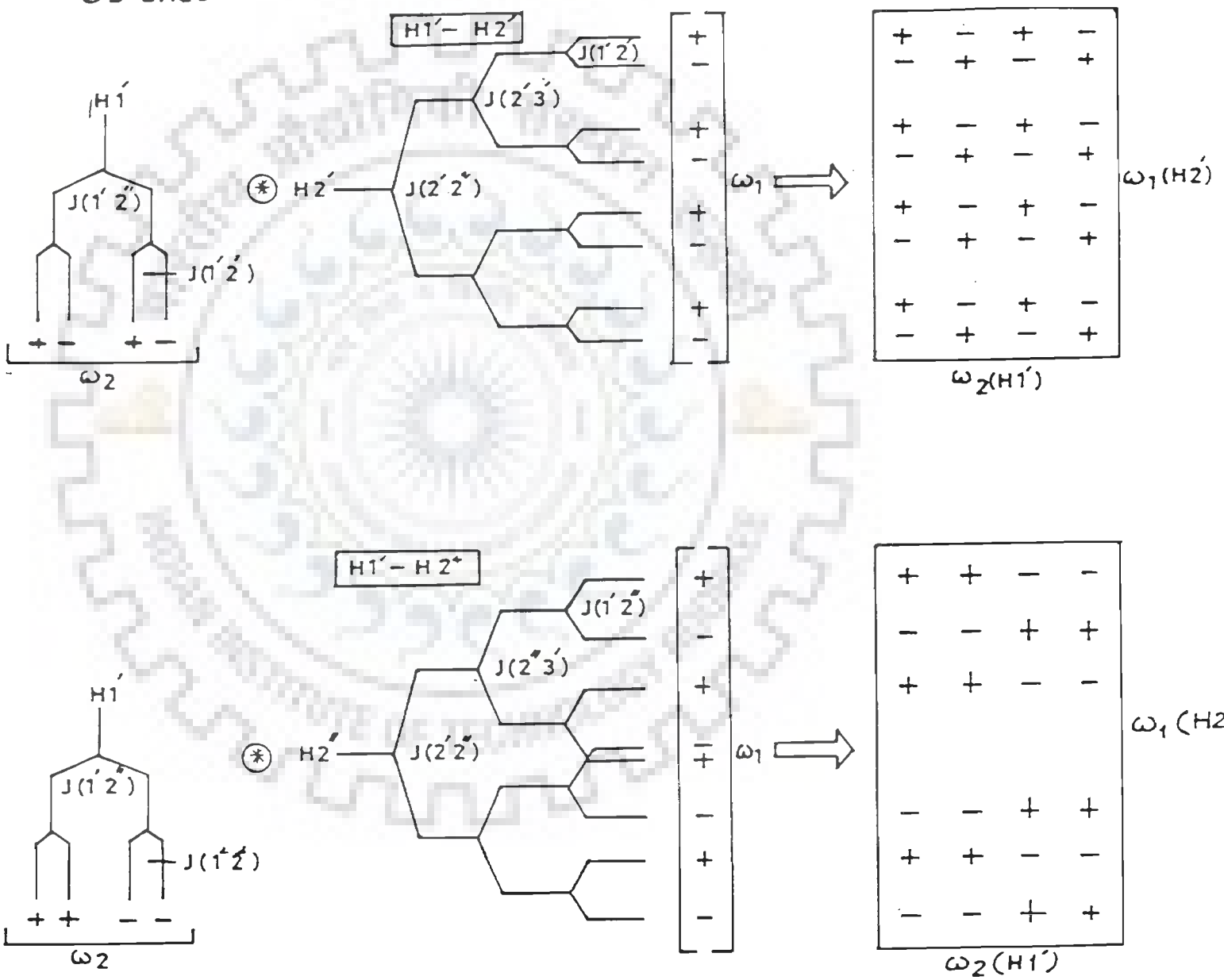
H1′
J(1′2″)
J(1′2′)
+ − + −
ω2
H1′− H2′
J(1′2′)
J(2′3′)
H2′
J(2′2″)
ω1
ω1(H2′)
ω2(H1′)
H1′− H2″
J(1′2″)
J(2″3′)
H2″
J(2″2′)
ω1
ω1(H2″)
ω2(H1′)

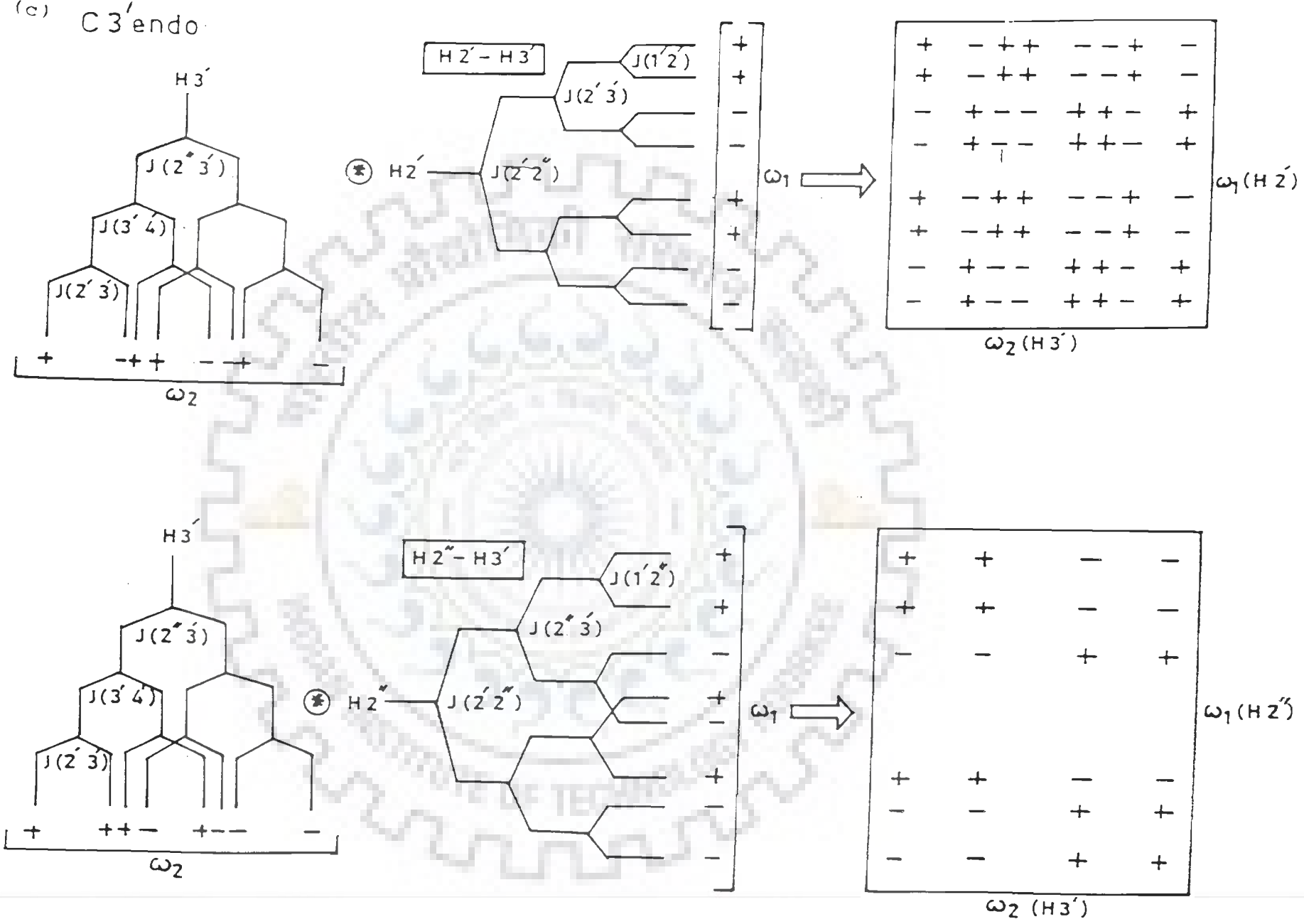
(c) C3′endo
H3′
J(2′3′)
J(3′4′)
J(2′3′)
+ −+ + − − −
ω2
H2′ − H3′
J(1′2′)
J(2′3′)
H2′
J(2′2″)
ω1
ω1(H2′)
ω2(H3′)
H3′
J(2″3′)
J(3′4′)
J(2′3′)
+ ++ − +−− −
ω2
H2″ − H3′
J(1′2″)
J(2″3′)
H2″
J(2′2‴)
ω1
ω1(H2″)
ω2 (H3′)

along ω_2 axis cross peak of C2'-endo sugar pucker, the fine structure along the ω_1 axis arises from the H1'-H2", H2"-H3' and H2'-H2" coupling constants while that along the ω_2 axis arises from the H1'-H2' and H1'-H2" coupling constants. Only the active coupling H1'-H2" leads to antiphase components along both the axis. Similarly, for the H1'-H2' cross peaks, only the H1'-H2' coupling leads to antiphase components. This feature helps in identifying the coupling constants as indicated in Fig. 5.7 (a-c).

Fig. 5.8 shows several patterns generated for H1'-H2" and H1'-H2' cross peaks for flip angle of read pulse, ϕ, as $\pi/2$ for three different sugar geometries. For C3'-endo geometry, the H1'-H2" cross peak looks more elongated along the ω_1 axis and is compressed along the ω_2 axis . For C2'-endo pucker, the H1'-H2"-ω_1 cross peak pattern gives rise to four components along each ω_2 as well as ω_1 axis and hence a total of sixteen components. The H1'-H2" - ω_1 cross peak pattern, on the other hand, gives rise to four major components due to overlap of inphase components and cancellation of antiphase components in the middle of the pattern. The peak separations (indicated in Fig. 5.8) are directly read from the scale along ω_2 axis. The active coupling is always the separation between the antiphase components, irrespective of sugar geometry. The success in the estimation of coupling constants is crucially connected with the resolution of the multiplet components. If the required resolution is not achieved then the separation can be simulated by taking into consideration line widths and the line shapes along both the frequency axis. A low

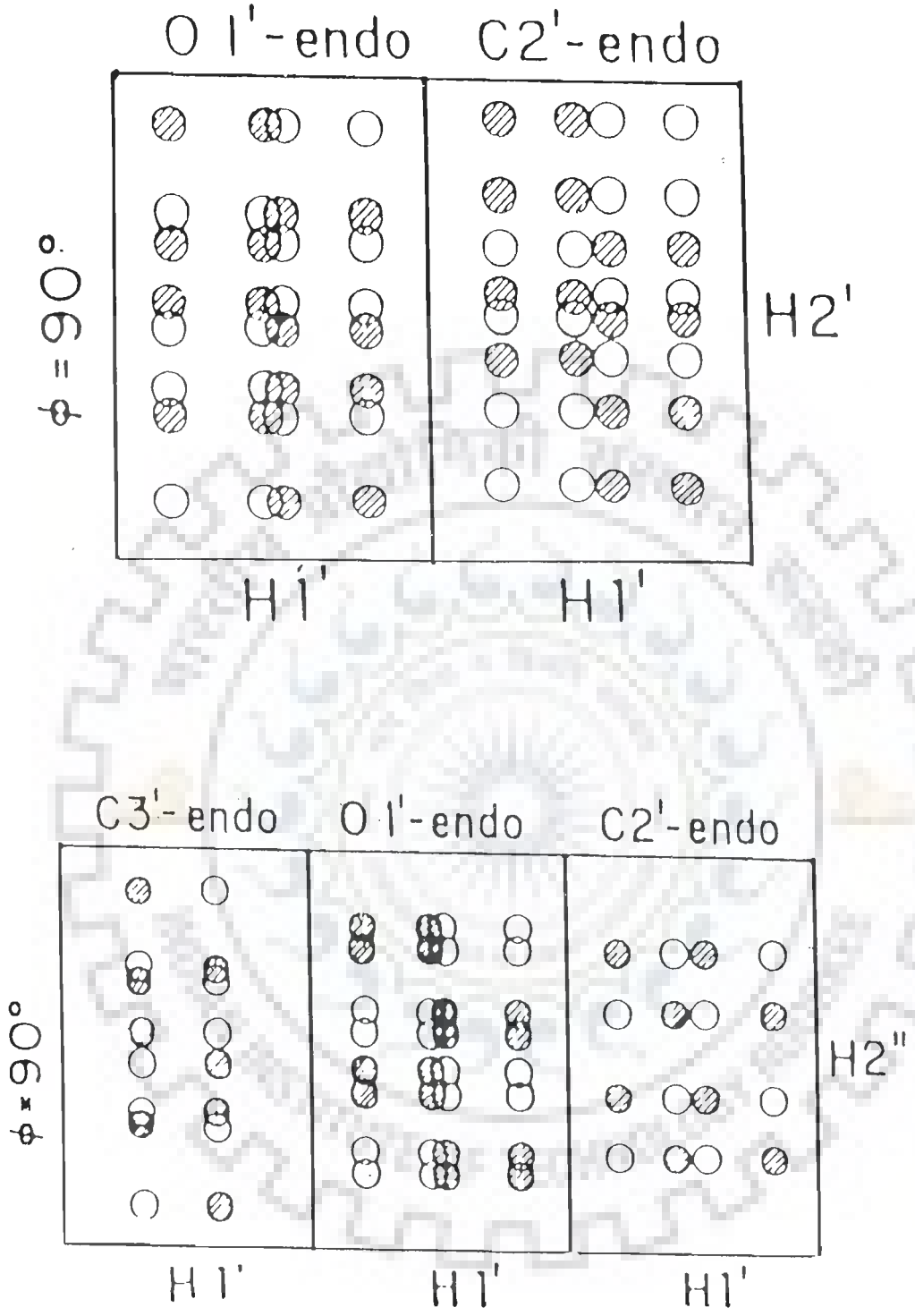

Fig. 5.8 : Calculated H1′-H2′ and H1′-H2" cross peak patterns for flip angle $\phi = \pi/2$ for C2′-endo, O1′-endo and C3′-endo sugar geometries [50].

resolution COSY technique assesses the cross peak intensities to evaluate the relative size of the coupling constants [13(a,b),50], assuming that active coupling is the prevailing factor determining intensities. The success of this method is highly dependent on the actual line widths of the pertinent peaks. We have not carried out spectral simulation as the relevant programs were not available. Instead we have tried to match the observed patterns with those available in literature [13,74,74(a), 115,115(a),129,129(a)] particularly the DQF - cross peaks simulated by Schmitz et al. [115] using SPHINX and LINSHA programs [129,129(a)] which are reproduced here in Fig. 5.9. The extraction of coupling constant value is complicated due to peak overlap and increase in line widths. The limitation of 2D NMR technique the digital resolution of about 2.3 Hz/point (in our case) in the better resolved dimension ω_2 axis allows an estimate of the range of J (H1'-H2'), J(H1'-H2") etc. values assuming that the line width does not vary even within the residue [115].

Initially we have tried to match the observed patterns with those obtained (Fig. 5.9) for different rigid sugar puckers, defined by pseudorotation phase angle P and the pucker amplitude $\phi_m = 35^\circ$ [2]. Values of J (H2'-H2") = 14 Hz and J (H3'-^{31}P) = 5.8 Hz and a line width of 9 Hz has been employed here. We find that there are lot of difficulties in interpreting the data. Table 5.3(a) gives the presence/absence of intra residue cross peak patterns as observed in DQF COSY spectra of d-$(TGATCA)_2$ at 295 K in D_2O. For four of the residues viz. T1, G2, T4 and C5 (that is

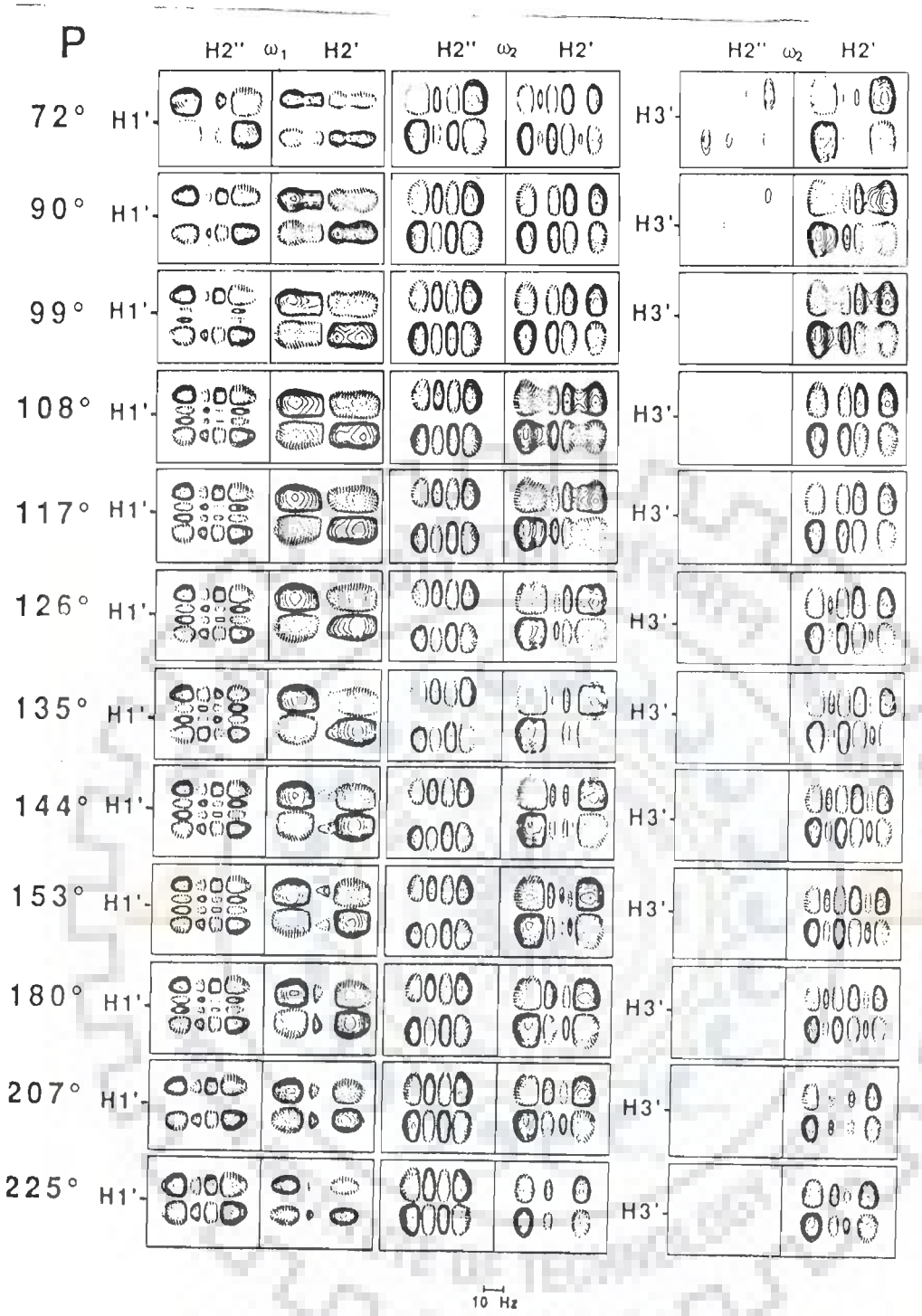

Fig. 5.9 : Simulated DQF-COSY cross peaks for different rigid deoxyribose conformations, described by a pseudorotation phase angle, P an amplitude $\phi_m = 35^\circ$: H1′ H2" - ω_1, H1′ H2′-ω_1, H1′ H2"-ω_2, H1′ H2′-ω_2, H3′ H2"-ω_2 and H3′ H2′-ω_2 from left to right. Negative peaks are indicated by dashed lines. An empty box indicates that the corresponding cross peak is of negligible intensity [115].

all except A3 and A6 residue) we did not observe the H2"-H3′ cross peak indicating that active coupling constant involved is < 2.3 Hz and the pseudorotation phase angle lies in the range 90° to 225° (Fig. 5.9). The H3′-H4′ cross peak pattern is however observed for all residues except G2 residue indicating that P lies in the range 9°-108° or ≃ 324° [74(a)]. Therefore the non occurrence of H2"-H3′ and occurrence of H3′-H4′ cross peak would restrict the P value to a range of 90° - 108° i.e. close to O1′ endo sugar pucker for most of the residues. However the observed H1′-H2", H1′-H2′ and H2′-H3′ cross peak patterns (Fig. 5.5 (c-e)) do not qualitatively agree with the corresponding simulated patterns for P = 90° to 108° (Fig. 5.9).

We then looked into possibility of existence of rapid interconversion on the NMR time scale between two sugar conformations observed in several studies on deoxyoligonucleotide [6,13,50,74(a),107,115,115(a),123] instead of rigid structure with P angle restricted to a small domain. A dynamic two state model commonly employed [107,123] with DNA uses one conformer from the S region and one from the N region of the pseudorotation cycle. In this model, the two conformation states are defined : (a) a minor conformer (N) with pseudorotation phase angle, P_N, and pucker amplitude, ϕ_N, essentially same as those of C3′-endo geometry i.e. $P_N = 18°$, $\phi_m = 36°$ [123] or that observed for A-DNA structures i.e. $P_N = 9°$, $\phi_m = 36°$ [111,115] and (b) a dominant S conformer with a pucker amplitude range $\phi_S = 28°$-$44°$ and a pseudorotation phase angle P_S corresponding to approximately the C2′-endo range

of puckers but subject to some variation [123] in the range 108° to 162°. The resulting observed coupling constant J between two protons is calculated as :

$$J = \chi_S J_S + \chi_N J_N$$

where χ_S and χ_N are the fractional populations of S and N conformers ($\chi_S + \chi_N = 1$), respectively and J_N and J_S are the ^1H-^1H vicinal coupling constants for N and S conformers respectively. The sums of coupling constants usually measured to a fairly good accuracy than the individual couplings are defined as follows :

$$\Sigma\ H1' = J\ (H1'\text{-}H2') + J\ (H1'\text{-}H2")$$

$$\Sigma\ H2' = J\ (H1'\text{-}H2') + J\ (H2'\text{-}H3') + J\ (H2'\text{-}H2")$$

$$\Sigma\ H2" = J\ (H1'\text{-}H2") + J\ (H2"\text{-}H3') + J\ (H2'\text{-}H2")$$

$$\Sigma\ H3' = J\ (H2'\text{-}H3') + J\ (H2"\text{-}H3') + J\ (H3'\text{-}H4') + J\ (H3'\text{-}^{31}P)$$

These summations include the absolute value of the geminal coupling J(H2'-H2"), which is not related to the deoxyribose conformation. It is expected to be close to ~ 14.0 Hz [29(a)] and this value has been used in analysis wherever required. The sums correspond to the distance in Hertz measured between the outer peaks of the H1', H2', H2" and H3' resonance patterns. For ΣH2' and ΣH2" the above statement is only strictly true when first order conditions apply [107,123]. In the present case, the Δδ (H2'-H2") = δ(H2') - δ(H2") exceeds 40 Hz (except for G2 residue) so that the nearest lines of the H2' and H2" resonance multiplets are separated from each other by at least 15 Hz and hence ΣH2' and ΣH2" can be trusted. The sums ΣH1' and ΣH3' are independent of Δδ

(H2′-H2") although deceptively simple pattern are seen, when Δδ (H2′-H2") < 4 Hz a triplet for the H1′ resonance and a quartet for H2′/H2" [107,123]. The summation ΣH3′ includes J (H3′-^{31}P) which affects the H3′-H2′, H3′-H2" and H3′-H4′ cross peak patterns. It does not directly pertain to the deoxyribose conformation and a fixed value of 5.8 Hz has been used [115] wherever required. For our analysis we have used spin-spin coupling values given by Van Wijk et al. [123] which are reproduced here in Table 5.4 (a-c) and Fig. 5.10. Structures with the motions of the sugar ring restricted to a small region of the P angle, the following observations about J values are made from the data of Table 5.4 (a) [123], when P value is gradually changed from 162° to 9° :

(a) J(H1′-H2′) decreases significantly by ~ 9 Hz from a value of 10.5 Hz to 1.1 Hz.

(b) J(H1′-H2") increases to a lesser extent by ~ 2.5 Hz from a value of 5.2 Hz to 7.7 Hz.

(c) J(H2′-H3′) first increases from 5.3 Hz to 8.5 Hz then decreases to 6.6 Hz so that the net change is rather small ~ 1.3 Hz.

(d) J(H2"-H3′) first increases slowly then rapidly to a significant extent from 0.8 Hz to 9.9 Hz.

(e) J(H3′-H4′) increases at a uniform rate but significantly from 0.8 Hz to 8.3 Hz.

Hence the change in sugar conformation gets reflected in J (H1′-H2′), J(H2"-H3′) and J(H3′-H4′).

Table 5.4(a)

CALCULATED COUPLING CONSTANTS FOR RANGE OF SUGAR GEOMETRIES OF DEOXYRIBOSE RING IN NUCLEOSIDES AND NUCLEOTIDES, ENCOUNTERED ALONG PSEUDOROTATION ITINERARY

	$J_{1'2'}$ for Φ_m			$J_{1'2'}$ for Φ_m			$J_{2'3'}$ for Φ_m			$J_{2'3'}$ for Φ_m			$J_{3'4'}$ for Φ_m		
$P(^\circ)$	28°	36°	44°	28°	36°	44°	28°	36°	44°	28°	36°	44°	28°	36°	44°
0	1.3	0.8	0.7	7.9	7.5	6.8	7.5	6.6	5.5	8.6	10.0	11.0	7.0	8.0	8.7
9	1.5	1.1	0.8	8.1	7.7	7.3	7.5	6.6	5.6	8.5	9.9	10.9	7.4	8.3	9.0
18	1.9	1.4	1.0	8.2	8.0	7.7	7.6	6.8	5.8	8.3	9.7	10.8	7.6	8.6	9.2
27	2.4	1.9	1.5	8.3	8.2	8.1	7.7	7.1	6.2	8.0	9.3	10.4	7.8	8.7	9.3
36	3.0	2.6	2.2	8.4	8.3	8.3	7.9	7.4	6.6	7.5	8.8	9.9	7.8	8.8	9.3
45	3.7	3.4	3.2	8.3	8.3	8.3	8.1	7.7	7.2	6.9	8.1	9.2	7.8	8.7	9.3
54	4.4	4.4	4.4	8.2	8.2	8.2	8.3	8.0	7.7	6.2	7.2	8.2	7.6	8.6	9.2
63	5.3	5.5	5.7	8.0	8.0	7.9	8.4	8.3	8.1	5.4	6.2	7.0	7.4	8.3	9.0
72	6.1	6.6	7.1	7.8	7.6	7.4	8.5	8.5	8.4	4.6	5.1	5.6	7.0	8.0	8.7
81	6.9	7.6	8.3	7.5	7.2	6.8	8.5	8.5	8.5	3.8	4.0	4.2	6.5	7.4	8.2
90	7.6	8.5	9.3	7.2	6.7	6.2	8.4	8.4	8.4	3.0	3.0	3.0	6.0	6.8	7.5
99	8.2	9.2	10.1	6.9	6.3	5.6	8.2	8.2	8.1	2.3	2.1	1.9	5.3	6.0	6.6
108	8.7	9.8	10.6	6.6	5.8	5.0	8.0	7.8	7.6	1.7	1.4	1.2	4.6	5.0	5.5
117	9.1	10.2	11.0	6.3	5.5	4.6	7.7	7.4	7.0	1.3	1.0	0.8	3.9	4.1	4.3
126	9.4	10.5	11.2	6.1	5.2	4.2	7.4	6.9	6.4	1.0	0.7	0.6	3.2	3.2	3.2
135	9.6	10.6	11.3	6.0	5.1	4.0	7.0	6.4	5.7	0.8	0.6	0.7	2.5	2.3	2.2
144	9.6	10.7	11.3	6.0	5.0	4.0	6.7	6.0	5.1	0.7	0.6	0.9	1.9	1.6	1.4
153	9.6	10.6	11.3	6.0	5.1	4.0	6.5	5.6	4.6	0.6	0.7	1.1	1.5	1.1	0.9
162	9.4	10.5	11.2	6.1	5.2	4.2	6.3	5.3	4.3	0.6	0.8	1.4	1.1	0.8	0.6
171	9.1	10.2	11.0	6.3	5.5	4.6	6.1	5.1	4.1	0.6	0.9	1.5	0.9	0.6	0.5
180	8.7	9.8	10.6	6.6	5.8	5.0	6.1	5.1	4.0	0.6	0.9	1.6	0.7	0.5	0.6
189	8.2	9.2	10.1	6.9	6.3	5.6	6.1	5.1	4.1	0.6	0.9	1.5	0.6	0.5	0.7
198	7.6	8.5	9.3	7.2	6.7	6.2	6.3	5.3	4.3	0.6	0.8	1.4	0.6	0.5	0.8
207	6.9	7.6	8.3	7.5	7.2	6.8	6.5	5.6	4.6	0.6	0.7	1.1	0.6	0.6	0.9
216	6.1	6.6	7.1	7.8	7.6	7.4	6.7	6.0	5.1	0.7	0.6	0.9	0.5	0.6	0.9
225	5.3	5.5	5.7	8.0	8.0	7.9	7.0	6.4	5.7	0.8	0.6	0.7	0.6	0.6	0.9
234	4.4	4.4	4.4	8.2	8.2	8.2	7.4	6.9	6.4	1.0	0.7	0.6	0.6	0.5	0.8
243	3.7	3.4	3.2	8.3	8.3	8.3	7.7	7.4	7.0	1.3	1.0	0.8	0.6	0.5	0.7
252	3.0	2.6	2.2	8.4	8.3	8.3	8.0	7.8	7.6	1.7	1.4	1.2	0.7	0.5	0.6
261	2.4	1.9	1.5	8.3	8.2	8.1	8.2	8.2	8.1	2.3	2.1	1.9	0.8	0.6	0.5
270	1.9	1.4	1.0	8.2	8.0	7.7	8.4	8.4	8.4	3.0	3.0	3.0	1.0	0.8	0.6
279	1.5	1.1	0.8	8.1	7.7	7.3	8.5	8.5	8.5	3.8	4.0	4.2	1.5	1.1	0.9
288	1.3	0.8	0.7	7.9	7.5	6.8	8.5	8.5	8.4	4.6	5.1	5.6	1.9	1.6	1.4
297	1.1	0.7	0.7	7.8	7.2	6.4	8.4	8.3	8.1	5.4	6.2	7.0	2.5	2.3	2.2
306	1.0	0.7	0.7	7.6	7.0	6.1	8.3	8.0	7.7	6.2	7.2	8.2	3.2	3.2	3.2
315	0.9	0.7	0.8	7.6	6.8	5.9	8.1	7.7	7.2	6.9	8.1	9.2	3.9	4.1	4.3
324	0.9	0.7	0.8	7.5	6.8	5.8	7.9	7.4	6.6	7.5	8.8	9.9	4.6	5.0	5.5
333	0.9	0.7	0.8	7.6	6.8	5.9	7.7	7.1	6.2	8.0	9.3	10.4	5.3	6.0	6.6
342	1.0	0.7	0.7	7.6	7.0	6.1	7.6	6.8	5.8	8.3	9.7	10.8	6.0	6.8	7.5
351	1.1	0.7	0.7	7.8	7.2	6.4	7.5	6.6	5.6	8.5	9.9	10.9	6.5	7.4	8.2

Reproduced from ref. [123]

Table 5.4(b)

CALCULATED SUMS OF COUPLING CONSTANTS FOR RANGE OF SUGAR GEOMETRIES OF DEOXYRIBOSE RING IN NUCLEOSIDES AND NUCLEOTIDES, ENCOUNTERED ALONG PSEUDOROTATION ITINERARY

	Σ 1′ for Φ_m			Σ 2′ for Φ_m			Σ 2″ for Φ_m			Σ 3′ for Φ_m		
P(°)	28°	36°	44°	28°	36°	44°	28°	36°	44°	28°	36°	44°
0	9.2	8.3	7.5	22.7	21.4	20.2	30.5	31.4	31.8	23.1	24.5	25.3
9	9.6	8.8	8.0	23.0	21.7	20.4	30.6	31.6	32.2	23.4	24.9	25.6
18	10.1	9.4	8.7	23.5	22.2	20.9	30.5	31.7	32.5	23.5	25.1	25.8
27	10.7	10.1	9.6	24.1	23.0	21.7	30.3	31.5	32.5	23.5	25.1	25.9
36	11.3	10.9	10.5	24.9	24.0	22.9	29.9	31.1	32.2	23.3	24.9	25.9
45	12.0	11.8	11.6	25.8	25.1	24.4	29.2	30.4	31.5	22.8	24.5	25.6
54	12.7	12.7	12.7	26.7	26.5	26.1	28.4	29.4	30.4	22.1	23.8	25.1
63	13.3	13.5	13.6	27.7	27.8	27.8	27.5	28.2	28.9	21.2	22.8	24.1
72	13.9	14.2	14.5	28.6	29.0	29.5	26.4	26.7	27.0	20.1	21.5	22.7
81	14.4	14.8	15.1	29.4	30.1	30.8	25.3	25.2	25.1	18.8	19.9	21.0
90	14.8	15.2	15.5	30.0	30.9	31.7	24.2	23.7	23.2	17.4	18.1	18.9
99	15.1	15.5	15.7	30.5	31.4	32.2	23.1	22.4	21.5	15.8	16.2	16.6
108	15.3	15.6	15.7	30.7	31.6	32.2	22.3	21.3	20.2	14.3	14.3	14.3
117	15.5	15.7	15.6	30.8	31.6	32.0	21.6	20.5	19.3	12.8	12.4	12.1
126	15.5	15.7	15.4	30.8	31.4	31.5	21.1	19.9	18.9	11.5	10.8	10.1
135	15.6	15.7	15.3	30.6	31.0	31.0	20.8	19.7	18.7	10.3	9.4	8.6
144	15.6	15.7	15.3	30.4	30.6	30.4	20.6	19.6	18.9	9.3	8.3	7.4
153	15.6	15.7	15.3	30.0	30.2	29.9	20.6	19.8	19.2	8.6	7.4	6.7
162	15.5	15.7	15.4	29.7	29.8	29.5	20.8	20.0	19.6	8.0	6.9	6.2
171	15.5	15.7	15.6	29.3	29.3	29.0	20.9	20.4	20.1	7.6	6.6	6.1
180	15.3	15.6	15.7	28.8	28.9	28.6	21.2	20.8	20.6	7.5	6.5	6.1
189	15.1	15.5	15.7	28.4	28.3	28.1	21.5	21.2	21.1	7.4	6.5	6.3
198	14.8	15.2	15.5	27.9	27.8	27.6	21.8	21.5	21.6	7.5	6.7	6.4
207	14.4	14.8	15.1	27.4	27.2	26.9	22.1	21.9	22.0	7.6	6.9	6.7
216	13.9	14.2	14.5	26.8	26.5	26.2	22.5	22.3	22.3	7.9	7.2	6.9
225	13.3	13.5	13.6	26.3	25.9	25.5	22.8	22.6	22.6	8.4	7.6	7.3
234	12.7	12.7	12.7	25.8	25.3	24.8	23.2	22.9	22.8	8.9	8.1	7.8
243	12.0	11.8	11.6	25.3	24.8	24.3	23.6	23.3	23.1	9.6	8.9	8.4
252	11.3	10.9	10.5	24.9	24.4	23.9	24.1	23.8	23.5	10.4	9.8	9.4
261	10.7	10.1	9.6	24.6	24.1	23.6	24.6	24.3	24.0	11.4	10.9	10.5
270	10.1	9.4	8.7	24.3	23.8	23.4	25.2	25.0	24.7	12.5	12.2	12.0
279	9.6	8.8	8.0	24.0	23.6	23.3	25.8	25.7	25.5	13.7	13.6	13.6
288	9.2	8.3	7.5	23.8	23.3	23.1	26.5	26.5	26.4	15.0	15.2	15.4
297	8.9	7.9	7.1	23.5	23.0	22.8	27.2	27.4	27.4	16.4	16.8	17.2
306	8.6	7.7	6.8	23.3	22.7	22.4	27.9	28.2	28.3	17.7	18.4	19.0
315	8.5	7.5	6.7	23.0	22.4	21.9	28.5	28.9	29.1	18.9	19.9	20.6
324	8.4	7.4	6.6	22.8	22.0	21.4	29.1	29.6	29.8	20.0	21.2	22.0
333	8.5	7.5	6.7	22.7	21.7	20.9	29.6	30.2	30.3	21.0	22.3	23.2
342	8.6	7.7	6.8	22.6	21.5	20.5	30.0	30.7	30.9	21.9	23.3	24.1
351	8.9	7.9	7.1	22.6	21.4	20.3	30.3	31.1	31.4	22.6	24.0	24.8

Table 5.4(c)

CALCULATED SUMS OF COUPLINGS FOR VARIOUS CONFORMATIONAL EQUILIBRIUM COMPOSITIONS AND S-TYPE GEOMETRIES

	P_s 108°				P_s 153°				P_s 180°			
X_s	Σ 1′	Σ 2′	Σ 2″	Σ 3′	Σ 1′	Σ 2′	Σ 2″	Σ 3′	Σ 1′	Σ 2′	Σ 2″	Σ 3′
0	9.4	22.2	31.7	25.1	9.4	22.2	31.7	25.1	9.4	22.2	31.7	25.1
5	9.7	22.7	31.2	24.6	9.7	22.6	31.1	24.2	9.7	22.5	31.1	24.2
10	10.0	23.1	30.7	24.0	10.0	23.0	30.5	23.3	10.0	22.9	30.6	23.2
15	10.3	23.6	30.1	23.5	10.3	23.4	29.9	22.4	10.3	23.2	30.1	22.3
20	10.6	24.1	29.6	22.9	10.7	23.8	29.3	21.6	10.6	23.5	29.5	21.4
25	11.0	24.6	29.1	22.4	11.0	24.2	28.7	20.7	11.0	23.9	29.0	20.4
30	11.3	25.0	28.6	21.8	11.3	24.6	28.1	19.8	11.3	24.2	28.4	19.5
35	11.6	25.5	28.0	21.3	11.6	25.0	27.5	18.9	11.6	24.5	27.9	18.6
40	11.9	26.0	27.5	20.8	11.9	25.4	26.9	18.0	11.9	24.9	27.3	17.7
45	12.2	26.4	27.0	20.2	12.2	25.8	26.3	17.2	12.2	25.2	26.8	16.7
50	12.5	26.9	26.5	19.7	12.5	26.2	25.7	16.3	12.5	25.5	26.2	15.8
55	12.8	27.4	26.0	19.1	12.9	26.6	25.1	15.4	12.8	25.9	25.7	14.9
60	13.1	27.8	25.4	18.6	13.2	27.0	24.5	14.5	13.1	26.2	25.1	13.9
65	13.5	28.3	24.9	18.1	13.5	27.4	23.9	13.6	13.5	26.5	24.6	13.0
70	13.8	28.8	24.4	17.5	13.8	27.8	23.4	12.7	13.8	26.9	24.0	12.1
75	14.1	29.3	23.9	17.0	14.1	28.2	22.8	11.9	14.1	27.2	23.5	11.2
80	14.4	29.7	23.4	16.4	14.4	28.6	22.2	11.0	14.4	27.5	22.9	10.2
85	14.7	30.2	22.8	15.9	14.7	29.0	21.6	10.1	14.7	27.9	22.4	9.3
90	15.0	30.7	22.3	15.4	15.0	29.4	21.0	9.2	15.0	28.2	21.9	8.4
95	15.3	31.1	21.8	14.8	15.4	29.8	20.4	8.3	15.3	28.5	21.3	7.4
100	15.6	31.6	21.3	14.3	15.7	30.2	19.8	7.4	15.6	28.9	20.8	6.5

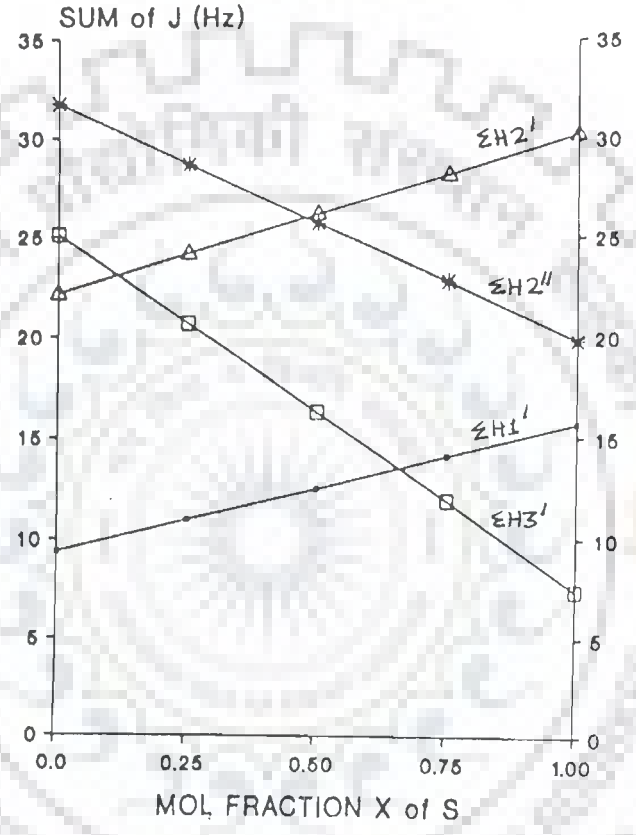

Fig. 5.10 : Predicted sums of coupling constants plotted versus mole fraction of S-type conformer for deoxyribofuranose rings in nucleosides and nucleotides that occur in a fast conformational equilibrium between an N-type conformer (P_N 18°, ϕ_N 36°) and an S-type conformer (P_S 153°, ϕ_S 36°) [123].

From Table 5.4(b) [123], it is seen that when P value is gradually changed from 162° to 9°, the

(f) ΣH1′ decreases from 15.7 Hz to 8.8 Hz.

(g) ΣH2′ increases from 29.8 to 31.6 Hz and then decreases ultimately to 21.7 Hz.

(h) ΣH2" increases from 20.0 Hz to 31.6 Hz.

(i) ΣH3′ increases most dramatically from 6.9 Hz to 24.9 Hz and hence is very sensitive to the pseudorotation angle.

These observations are very useful in ascertaining the presence of C3′-endo ⇋ C2′-endo equilibrium in solutions. Starting from the pure S conformer with P = 162°, as the fraction population of N conformer is increased from 0 to 1, the following will result [50] :

(j) J(H1′-H2′) decreases significantly from 10.5 to 1.1 Hz.

(k) J(H1′-H2") increases to a lesser extent from 5.2 to 7.7 Hz.

(l) J(H2′-H3′) does not show any variation and hence is independent of the proportion of S and N conformer (due to (g) stated above). Its value is ~ 6 Hz [50].

(m) J(H2"-H3′) increases significantly from 0.8 Hz to 9.9 Hz.

(n) J(H3′-H4′) increases significantly from 0.8 to 8.3 Hz in a manner similar to J(H2"-H3′).

The last observation, that is, (n) is particularly crucial since this allows the identification of the presence of a C3′-endo ⇆ C2′-endo (N ⇆ S) equilibrium even without actually measuring the magnitudes of the coupling constants and by simply monitoring the relative intensities of the cross peaks in a low resolution COSY spectrum [50]. In a low resolution COSY spectrum, the intensity of a cross peak is largely determined by the magnitude of the active coupling constant. Thus the intensities of the H2"-H3′ and H3′-H4′ cross peaks are largely determined by the respective coupling constants, the multiplicities in both these cross peaks are similar. Thus in a given COSY spectrum, if these two types of cross peaks have dissimilar intensities, it would imply that the sugar geometry is different to C3′-endo [J (H2"-H3′) ≃ J(H3′-H4′) ~ 9 Hz] or C2′-endo [J(H2"-H3′) = J (H3′-H4′) = 0.8 Hz] or there is no C3′-endo = C2′-endo equilibrium. [J(H2"-H3′) = J(H3′-H4′) ≃ 0.9 Hz for χ_s = 0.90; J(H2"-H3′) = J(H3′-H4′) ≃ 1.8 Hz for χ_s = 0.80; and so on]. In the present investigations, which are not exactly a low resolution COSY experiment, the cross peak pattern of H2"-H3′ as well as H3′ - H4′ are observed for A3 residue as well as A6 residue (Fig. 5.5 (c-f)). A quick approximate inference may be drawn that these are likely to be in a dynamic C3′-endo ⇆ C2′-endo conformers equilibrium [Table 5.3(a)]. Further for G2 residue, both the cross peak patterns, i.e. H2"-H3′ and H3′-H4′ are not observed (Fig. 5.5 (c,f)) which may also be either a pure C2′-endo conformer or a dynamic C3′-endo ⇆ C2′-endo conformers with relatively very low fractional population of C3′-endo conformer.

For T1, T4 and C5 residues, the H2"-H3' cross peak patterns are not seen (may be very weak) but relatively intense H3'-H4' cross peak patterns are found to exist. It is possible that these have a dynamic N ⇆ S conformer equilibrium with P_S value quite different from that of C2' endo i.e. 162° or else a single conformer other than that for P = 162° or else a more complex deoxyribose conformation. However a more systematic analysis is carried out by following strategies discussed below.

Van Wijk et al. [123] have shown the importance of sums of couplings and have predicted those for different mole fractions of S conformer for sugars existing in a fast conformational equilibrium between an N type conformer (P_N = 18°, ϕ_m = 36°) and an S-type conformer (P_S = 153°, ϕ_m = 36°) which are reproduced in Table 5.4(c) and Fig. 5.10. The following observations useful in ascertaining the presence of N ⇆ S equilibrium are made for an increase in mole fraction of N-conformer from 0 to 1 :

(o) ΣH1' decreases from 15.7 Hz to 8.8 Hz.

(p) ΣH2' decreases from 30 Hz to 22 Hz.

(q) ΣH2" increases from 20 Hz to 31.6 Hz.

(r) ΣH3' increases dramatically from 6.9 to 24.9 Hz.

For most oligonucleotides, χ_S is found to lie in the range 0.65 to 1.0 [6,74,115,115(a),123]. Fig. 5.10 shows that the difference between ΣH2' and ΣH2" is least for χ_S = 0.50; it being ~ 0.5 Hz. The difference increases to 2.5, 6.4 and 10.4 Hz for χ_S = 0.6, 0.8 and 1.0, respectively. It is notable since inspite of

poor resolution in 2D DQF-COSY spectra, the ΣH2′ and ΣH2" values along the better resolved ω_2 axis can still be differentiated. A smaller difference in ΣH2′ and ΣH2" will correspond to a greater fraction of N conformer to be present in solution. This observation is however to be used more cautiously since it has been observed [115] that the line width for H2′ proton are generally 2-3 Hz larger than that for H2" protons due to different environment and molecular motions. Further the smallest line width are found for terminal residues (6-9 Hz) while the non terminal ones exhibit larger variations (7-12 Hz).

In order to analyse the deoxyribose sugar conformation we have first attempted to match the cross peak patterns obtained in DQF COSY spectra with Fig. 5.9. As a second step, we followed the strategy of Van Wijk et al. [123] in which the first marker used is ΣH1′. It was possible to measure these from the peak print outs of the 1D NMR spectra to an accuracy of 0.5 Hz (resolution in 1D NMR spectra) particularly at 305, 310, 315, 320 and 325 K. In few cases, ΣH1′ was obtained at 295 and 297 K also. We did not observe a value of 15.7 Hz (or 15.2 Hz as accuracy is ± 0.5 Hz) for any residue at any temperature. The observed values are found in the range 13.3-14.9 Hz. It has been shown [123] that a value in excess of 13.2 Hz indicates a predominance of the S-type conformer ($\chi_S \geq 65 \pm 5\%$). If that is the case a relatively safe conclusion follows: of the two H2′/H2" multiplets the one with the largest separation between the outer lines (typically 26-32 Hz) can be identified with H2′; the signal with the smaller separation

(typically 19-25 Hz) is then assigned to H2". In the majority of cases an S/N conformer ratio no less than 65/35 also implies that the larger of the two couplings present in the H1′ multiplet belongs to J(H1′-H2′). The value of ΣH1′ is not very sensitive (Table 5.4 (c) and Fig. 5.10) to variations in P_S and ϕ_S and is used to determine the approximate fraction for S-type conformer ($\chi_S \pm 0.05$) whenever the S form predominates :

$$\chi_S = (\Sigma H1' - 9.4) / (15.7 - 9.4) \qquad ...(5.1)$$

We have also looked into the fine splitting of H1′ resonance which allows a good insight into the population ratio of the sugar ring χ_S / χ_N [107]. It has been shown that the H1′ resonance appears as a quartet (Fig. 5.11), the distance between the outer peaks exceeds 14.5 Hz; the larger the distance between the inner two peaks of the quartet the higher the conformational purity. In contrast, the observation of a H1′ resonance of a given residue which occurs as a triplet and for which the corresponding H2′ and H2" resonances are not (near) isochronous, indicates that the sugar ring of this residue displays a relatively high conformational flexibility, $0.40 \leq \chi_S \leq 0.70$. We observed a quartet with maximum separation between inner two peaks for G2 residue (Fig. 5.3 (a)) between 305-315 K. The A3 residue on the other hand is a triplet (Fig. 5.1 (b) and 5.2 (b)) while all other residues show a pattern in between the two extremes.

Once χ_S is known to a first approximation the next step (third step) is to use the simulated DQF-COSY cross peaks for different mixtures using a dynamic two state model for deoxyribose

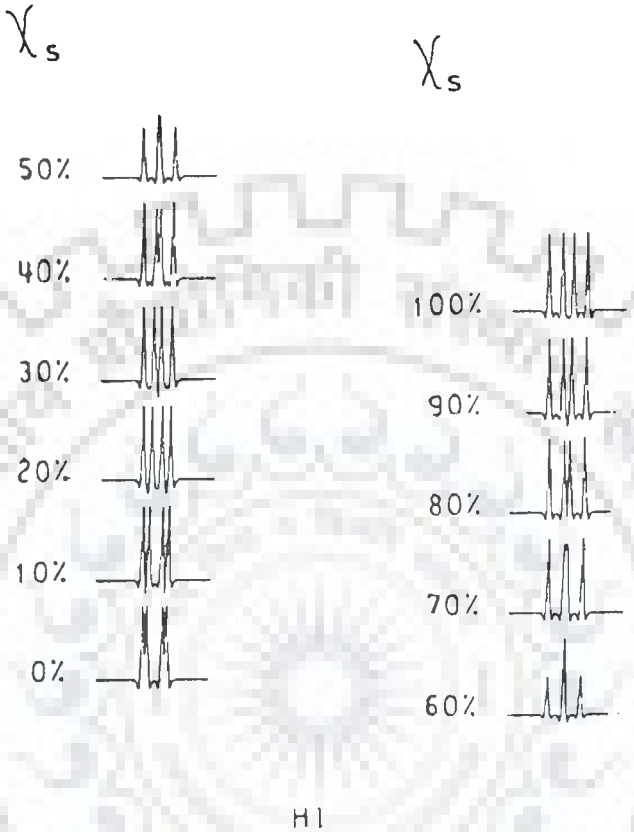

Fig. 5.11 : Predicted splitting patterns of the H1′ resonance for different values of the fraction S-type conformer [107].

with P_S = 162° and P_N = 9° for the interconverting conformers available in literature [13,74,74(a),115,115(a),129,129(a)]. We have used those obtained by Schmitz et al. [115] more frequently which are reproduced here as Fig. 5.12. We made an attempt to match the observed patterns with Fig. 5.12 and arrived at a value of χ_S. In most cases, the value obtained matched with that obtained from ΣH1′ using 1D NMR spectra and equation (5.1) within ± 10%. In a particular case, where in the observed cross peak pattern did not match with Fig. 5.12, an alternate such as presence of three conformation in equilibrium was looked into.

The fourth step is to use the sum of couplings for P_N = 18°, ϕ_N = 36° or P_N = 9°, ϕ_N = 36° (Table 5.4 (a,b)) and the same for unknown S-type form at hand for P_S = 108°, 153° and 180°, ϕ_S = 36° (Table 5.4(c) and Fig. 5.10). The corresponding observed values from 1D NMR (to an accuracy of ± 0.5 Hz) are fitted in three sets of predicted lines at χ_S = ± 0.05 simultaneously (Table 5.4(c)). With some experience we are able to narrow the possible P_S range of solutions. As a final step, we calculated J values and sums of couplings by adjusting P_S untill all the observed results are in agreement with the calculated values. The analysis of each residue following this procedure is illustrated below :

G2

The observed values of couplings, sum of couplings from 1D NMR spectra at different temperature are given in Table 5.5 (a,b). For G2 residue, the χ_S evaluated from equation 5.1 using ΣH1′ of 14.9 Hz, is 0.88.

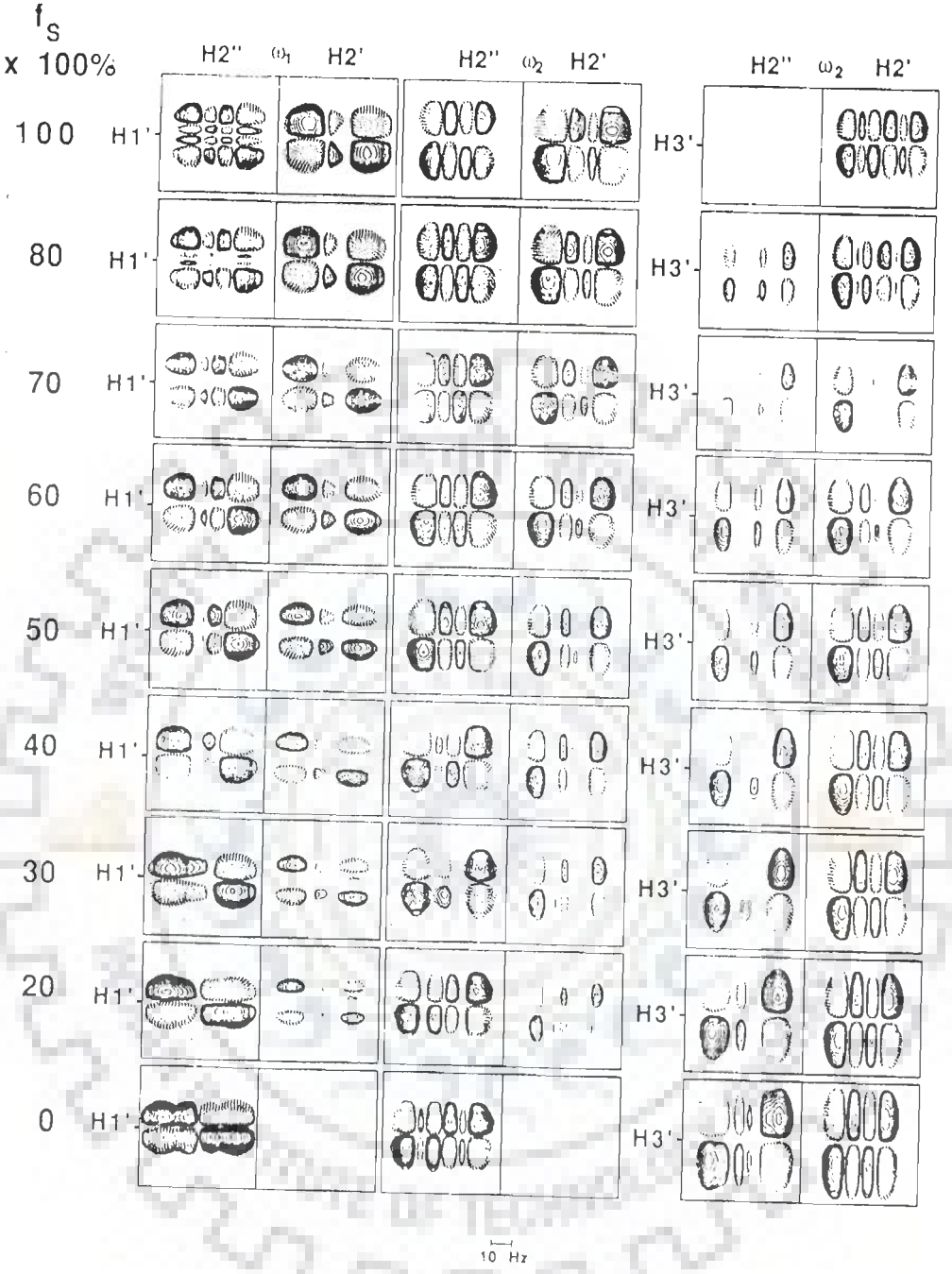

Fig. 5.12 : Simulated DQF-COSY cross peaks for different mixtures using a dynamic two-state model for deoxyribose, with $P_S = 162^\circ$ and $P_N = 9^\circ$ for the interconverting conformers ($\phi_m = 35^\circ$: H1′ H2" - ω_1, H1′ H2′-ω_1, H1′ H2"-ω_2, H1′ H2′-ω_2, H3′ H2"-ω_2 and H3′ H2′-ω_2 from left to right [115]. Vicinal coupling constants for the conformers are taken from Rinkel and Altona [107].

Table 5.5(a) : The observed value of coupling constants (in Hertz) and sum of couplings (in Hertz) from 1D NMR spectra of d-$(TGATCA)_2$ at different temperatues.

Temp. (K)	T1	G2	A3	T4	C5	A6
J(H1'-H2')						
305	8.6	9.2	6.9	7.8	7.3	8.7
310	8.5	8.7	6.7	8.3	7.6	8.6
315	8.4	8.1	6.8	8.1	7.0	7.7
320	8.3	7.6	6.7	8.2	7.8	7.3
325	8.2	7.4	6.7	8.2^{o}	8.0^{o}	7.5
J(H1'-H2")						
305	6.0	5.7	6.7	6.7	6.8	5.9
310	6.0	6.1	6.7	6.3	6.5^{o}	5.8
315	6.1	6.9	6.6	6.0	6.4	6.6
320	6.2	7.1	6.6	6.1	6.1	7.2
325	6.0	7.1	6.6	5.7^{o}	5.7^{o}	6.8
ΣH1'						
305	14.6	14.9	13.6	14.5	14.1	14.5
310	14.5	14.8	13.4	14.5	14.1	14.4
315	14.4	14.9	13.4	14.1	14.4	14.3
320	14.4	14.7	13.4	14.3	14.0	14.4
325	14.2	14.5	13.3	13.9^{o}	13.7^{o}	14.3

ΣH2'						
297	-	-	-	-	-	24.0
305	-	-	26.1	-	-	24.8
325	29.5	-	-	29.3	29.3	-
ΣH2"						
297	19.6	o	o	20.4	19.7	-
305	18.5	o	o	20.6	20.0	29.5
315	o	o	o	22.2	o	-
320	o	o	o	22.4	o	-
325	22.3	-	-	22.2	22.6	-

o - overlap.

All values are within accuracy of ± 0.5 Hz.

Table 5.5(b) : Observed average values of J (in Hertz) and sum of couplings (in Hertz) from 1D NMR spectra (Fig. 5.1(b-d), 5.2(b-d), 5.3(a,b) to an accuracy of ± 0.5 Hz. The average value at 305 K extrapolated and used for analysis is shown below.

	T1	G2	A3	T4	C5	A6
J(H1'-H2')	8.4	9.2	6.9	8.2	7.9	8.6
J(H1'-H2")	6.0	5.7	6.7	6.0	6.2	5.9
ΣH1'	14.5	14.9	13.6	14.2	14.1	14.5
ΣH2'	29.4	o	26.1	29.3	29.3	29.5
ΣH2"	22.3	o	o	22.3	21.1	24.0
ΣH3'	11.5	9.8	12.4	12.5	13.1	15.9

o - overlap.

A value of $J(H-^{31}P)$ coupling of 5.8 Hz is substracted from ΣH3' measured from 1D NMR spectra at 325 K.

Since ΣH1′ is accurate to a value of ± 0.5 Hz the χ_S may essentially range between 0.78 and 0.94. The H1′ peak is found to be quartet at 305 - 315 K and a triplet at 320 - 325 K (Fig. 5.3(a), 5.2(b)). It is noted that of all the residues G2 residue has maximum value of ΣH1′ as well as maximum separation between inner two peaks of H1′ quartet [107] at 305 K (Fig. 5.3(a)) and therefore has least mixing of N conformer. Since S/N conformer ratio is rather high, it also implies [123] that the larger of the two couplings is J(H1′-H2′) in the H1′ quartet. Due to overlapping ΣH2′, ΣH2", etc are not available from 1D or 2D spectra. The cross peaks of H2" - H3′ as well as H3′ - H4′ are not observed (Table 5.3(a)) in DQF-COSY spectra so that active couplings involved are low and < 2.3 Hz that is, below the digital resolution of 2.3 Hz/point used along ω_2 axis. In fact, it is only G2 residue which does not show H3′-H4′ peak (Table 5.3(a)) which is in confirmity with the fact that it has the maximum content of S - conformer (highest χ_S = 0.88). Further since both H2"-H3′ and H3′-H4′ couplings are low the ΣH3′ is lowest for this residue and the multiplet of H3′ is least wide being about 10 Hz (Fig. 5.2 (c)). Observed patterns of H1′- H2′/H2" are matched with simulated patterns shown in Fig. 5.9 [115] for a rigid sugar conformer. For patterns above the diagonal (Fig. 5.5(c)) :

(a) H1′ - H2′/H2" pattern indicates (Fig. 5.9) P = 153°-180°, 207°, 225°

(b) Absence of H3′- H4′ pattern indicates [74(a)] P = 144° - 280°.

For patterns below the diagonal (Fig. 5.5(e)) :

(c) H1′ - H2′/H2" pattern indicates (Fig. 5.9) P = 153 - 225°.

Combining (a-c), it is seen that P = 162° - 216° fits into the observed DQF patterns. Comparing the observed patterns with those for a dynamic two state model [115] it is found (Fig. 5.12) that the observed pattern match with that expected between those for 100% S and 80% S conformer and are more close to that for 100% χ_S, so that the observed χ_S = 0.88 is in accord with DQF cross peak pattern. As a last step, we calculated the various couplings and sums of couplings by considering P_N = 9°, 18° and P_S = 144°, 153°, 162°, 180° for χ_S = 0.88 and χ_N = 0.12 and attempted to match particularly the observed value of J(H1′ - H2′), J(H1′-H2"), ΣH1′ and ΣH3′ i.e. 9.2, 5.7, 14.9 and 9.8 Hz, respectively with the constraint that H2" - H3′ and H3′ - H4′ be < 2.3 Hz (Table 5.6). Table 5.6 shows results of such calculations and it is easily seen that P_S = 153°, χ_S = 0.88 and P_N = 9/18°, χ_N = 0.12 fits into all the observed results.

A6

Considering A6 residue, since ΣH1′ = 14.5 Hz, the S conformer is the predominant one and χ_S = 0.79 with exact value possibly in the range 0.71 - 0.88 by taking the maximum error in ΣH1′ to be ± 0.5 Hz. This is the only residue for which H2" - H3′ cross peak pattern is seen above the diagonal (Fig. 5.5(c)). Below the diagonal H2"-H3′ is seen for two of the residues, that is, A3 and A6 (Fig. 5.5(e)). The observed DQF-COSY cross peak

Table 5.6 : Calculated value of J (in Hertz) and sum of coupling (in Hertz) for a mixture deoxyribose sugar at various P_S and P_N values and those observed experimentally for all residues.

	1'-2'	1'- 2"	2'- 3'	2"-3'	3'-4'	Σ1'	Σ2'	Σ2"	Σ3'
G2									
$p_N = 9^\circ$, $\chi_N = 0.12$, P_S 162°, $\chi_S = 0.88$									
	9.4	5.5	5.5	1.9	1.6	14.9	28.8	21.4	9.1
$p_N = 18^\circ$, $\chi_N = 0.12$, $P_S = 162^\circ$, $\chi_S = 0.88$									
	9.4	5.5	5.5	1.9	1.7	14.9	28.9	21.4	9.1
$p_N 18^\circ$, $\chi_N = 0.12$, P_S 144°, $\chi_S = 0.88$									
	9.6	5.4	6.1	1.7	2.4	14.9	29.7	21.1	10.2
$p_N = 9^\circ$, $\chi_N = 0.12$, $P_S = 144^\circ$, $\chi_S = 0.88$									
	9.5	5.3	6.1	1.7	2.4	14.9	29.5	21.0	10.3
$P_N = 9^\circ$, $\chi_N = 0.12$, $P_S = 153^\circ$, $\chi_S = 0.88$									
	9.4	5.4	5.7	1.8	2.0	14.9	29.2	21.2	9.5
Observed									
	9.2	5.7	>2.3	<2.3	<2.3	14.9	-	-	9.8
A6									
$p_N = 18^\circ$, $\chi_N = 0.20$, $P_S = 153^\circ$, $\chi_S = 0.80$									
	8.7	5.6	5.8	2.5	2.6	14.4	28.6	22.2	11.0
$p_N = 18^\circ$, $\chi_N = 0.20$, $P_S = 135^\circ$, $\chi_S = 0.80$									
	8.7	5.6	6.4	2.4	3.5	14.3	29.1	22.1	12.5
$p_N = 18^\circ$, $\chi_N = 0.20$, $P_S = 108^\circ$, $\chi_S = 0.80$									
	8.1	6.2	7.6	3.1	5.7	14.2	29.7	23.4	16.4

	1′-2′	1′- 2"	2′- 3′	2"-3′	3′-4′	Σ1′	Σ2′	Σ2"	Σ3′
$p_N = 18^\circ$, $\chi_N = 0.20$, $P_S = 117^\circ$ $\chi_S = 0.80$									
	8.4	6.0	7.3	2.7	5.0	14.4	9.7	23.4	15.0
$p_N = 9^\circ$, $\chi_N = 0.20$, $P_S = 117^\circ$, $\chi_S = 0.80$									
	8.4	5.9	7.2	2.8	4.9	14.3	29.6	23.4	14.9
Observed									
	8.6	5.9	>2.3	>2.3	>2.3	14.5	29.5	~21	15.8
T4									
$p_N = 18^\circ$, $\chi_N = 0.25$, $P_S = 153^\circ$, $\chi_S = 0.75$									
	8.3	5.8	5.9	3.0	3.0	14.1	28.2	22.8	11.8
$p_N = 18^\circ$, $\chi_N = 0.25$, $P_S = 135^\circ$, $\chi_S = 0.75$									
	8.3	5.8	6.5	2.9	3.9	14.1	28.8	22.7	13.3
$p_N = 9^\circ$, $\chi_N = 0.25$, $P_S = 144^\circ$, χ_S 0.75									
	8.3	5.7	6.1	2.9	3.3	14.0	28.4	22.6	12.5
$p_N = 9^\circ$, $\chi_N = 0.25$, $P_S = 135^\circ$, $\chi_S = 0.75$									
	8.2	5.7	6.5	2.9	3.8	14.0	28.7	22.7	13.3
$p_N = 9^\circ$, $\chi_N = 0.23$, $P_S = 135^\circ$, $\chi_S = 0.77$									
	8.4	5.7	6.5	2.7	3.5	14.1	28.9	22.4	13.0
$p_N = 9^\circ$, $\chi_N = 0.23$, $P_S = 144^\circ$, $\chi_S = 0.77$									
	8.5	5.6	6.1	2.7	2.9	14.1	28.6	22.4	12.1
Observed									
	8.2	6.0	>2.3	<2.3	>2.3	14.2	29.3	22.3	12.5

	1′-2′	1′- 2"	2′- 3′	2"-3′	3′-4′	Σ1′	Σ2′	Σ2"	Σ3′
A3									
$P_N = 9^\circ$, $\chi_N = 0.35$, $P_S = 162^\circ$, $\chi_S = 0.65$	7.2	6.1	5.8	4.0	3.4	13.3	26.9	24.1	13.2
$P_N = 9^\circ$, $\chi_N = 0.35$, $P_S = 135^\circ$, $\chi_S = 0.65$	7.4	6.1	6.5	3.9	4.4	13.5	27.7	23.9	14.9
$P_N = 18^\circ$, $\chi_N = 0.35$, $P_S = 135^\circ$, $\chi_S = 0.65$	7.4	6.1	6.5	3.8	4.5	13.5	27.9	23.9	14.9
$P_N = 9^\circ$, $\chi_N = 0.35$, $P_S = 108^\circ$, $\chi_S = 0.65$	6.8	6.5	7.4	4.4	6.2	13.3	28.1	24.9	18.0
$P_S = 18^\circ$, $\chi_N = 0.35$, $P_S = 108^\circ$, $\chi_N = 0.65$	6.9	6.6	7.5	4.3	6.3	13.5	28.3	24.9	18.1
$P_N = 9^\circ$, $\chi_N = 0.35$, $P_S = 180^\circ$, $\chi_S = 0.65$	6.8	6.5	5.6	4.1	3.2	13.2	26.4	24.6	12.9
$P_N = 9^\circ$, $\chi_N = 0.35$, $P_S = 180^\circ$, $\chi_S = 0.65$	6.9	6.6	5.7	4.0	3.2	13.4	26.5	24.6	13.0
Observed									
	6.9	6.7	>2.3	>2.3	>2.3	13.6	26.1	-	12.4
T1									
$P_N = 18^\circ$, $\chi_N = 0.20$, $P_S = 144^\circ$, $\chi_S = 0.80$	8.7	5.6	6.2	2.4	3.0	14.4	28.9	22.0	11.7
$P_N = 18^\circ$, $\chi_N = 0.20$, $P_S = 135^\circ$, $\chi_S = 0.80$	8.7	5.6	6.4	2.4	3.5	14.3	29.1	22.1	12.5

	1′-2′	1′- 2"	2′- 3′	2"-3′	3′-4′	Σ1′	Σ2′	Σ2"	Σ3′
$P_N = 18^\circ$, $\chi_N = 0.20$, $P_S = 117^\circ$, $\chi_S = 0.80$									
	8.7	6.0	7.3	2.7	5.0	14.4	29.7	23.4	15.0
$P_N = 9^\circ$, $\chi_N = 0.22$, $P_S = 126^\circ$, $\chi_S = 0.20$, $P_S = 162^\circ$, $\chi_S = 0.58$									
	8.4	5.8	5.9	2.6	2.9	14.2	28.3	22.5	11.6
Observed									
	8.4	6.0	>2.3	<2.3	>2.3	14.4	29.4	22.3	11.5
C5									
$P_N = 9^\circ$, $\chi_N = 0.29$, $P_S = 153^\circ$, $\chi_S = 0.71$									
	7.8	5.2	5.9	3.4	3.2	13.7	27.7	23.2	12.5
$P_N = 18^\circ$, $\chi_N = 0.22$, $P_S = 126^\circ$, $\chi_S = 0.58$, $P_S = 162^\circ$, $\chi_S = 0.20$									
	8.5	5.8	6.6	2.7	3.9	14.3	29.1	22.5	13.2
Observed									
	7.9	6.2	>2.3	>2.3	>2.3	14.1	29.3	21.1	13.1

All observed values are in ± 0.5 Hz accuracy.

χ_S, χ_N are mole fraction of south and north conformers respectively.

A value of 5.8 Hz (H3′-P) coupling is substracted from ΣH3′.

pattern of H1′ - H2′, H1′ - H2", H2′ - H3′ and H3′ - H4′ are matched with Fig. 5.9 i.e. for a rigid sugar conformer. The comparison shows that for peaks above diagonal (Fig. 5.5(c,f)):

(a) H1′ - H2′ pattern indicates (Fig. 5.9) P = 99°, 144°.

(b) H1′ - H2" pattern indicates (Fig. 5.9) P = 99°-180°.

(c) H2′ - H3′ pattern indicates [74(a)] P = 144°, 162°.

(d) H2" - H3′ pattern indicates [74(a)] P = 36°, 72°, 288°.

(e) H3′ - H4′ pattern indicates [74(a)] P = 9°-108°.

For patterns below the diagonal (Fig. 5.5(e)), it is found that :

(f) H1′ - H2′ pattern indicates (Fig. 5.9) P = 126°- 207°.

(g) H1′ - H2" pattern indicates (Fig. 5.9) P = 90°- 207°.

(h) H2′ - H3′ pattern indicates [115] (Fig. 5.9) P = 72 - 108°, 207 - 225°.

(i) H2" - H3′ pattern indicates [74(a)] P = 9°, 36°, 324°.

(j) H3′ - H4′ pattern indicates (below diagonal pattern not shown) [74(a)] P = 9°- 108°.

From (a-c) it may be inferred that P could lie in the range 99° - 180° and perhaps more close to 144°, 162°. But from (d), (e) we find that P could be 36° or 72°, which is in contradiction to the inference drawn from (a-c). Same is true for the patterns observed below diagonal as shown in (f) to (j). Clearly a single rigid sugar conformation does not explain the observed DQF cross

peak patterns. Since ΣH1' is certainly less than 15.7 Hz (Table 5.5(b)) within the experimental errors and χ_S = 0.79, we looked into possibility of a two state model. We compare the observed cross peak patterns with those simulated for two interconverting conformers $P_N = 9^\circ$ and $P_S = 162^\circ$ (Fig. 5.12) and find that the above diagonal (Fig. 5.5(c)) :

(k) H1' - H2' pattern indicates [115] χ_S = 0.8, 1.0.

(l) H1' - H2" pattern indicates [115] χ_S = 0.8, 1.0.

(m) H2' - H3' pattern indicates [74(a) deduced from COSY - 45 pattern] χ_S = 0.7, 0.8.

(n) H2" - H3' pattern indicates [74(a) deduced from COSY - 45 pattern] χ_S = 0.6, 0.5, 0.4.

For patterns below the diagonal (Fig. 5.5(e)), comparison with Fig. 5.12 [115] gives the following :

(o) H1' - H2' pattern indicates χ_S = 0.8, 1.0.

(p) H1' - H2" pattern indicates χ_S = 0.6 - 1.0 (wide range).

(q) H2' - H3' pattern indicates χ_S = 0.8, 0.7.

(r) H2" - H3' pattern indicates χ_S = 0.8.

Although χ_S = 0.8 generally satisfies the experimental results but deviation in H2' - H3' and H2" - H3' patterns (m, n, q) are notable. It may be inferred that although $\chi_S \simeq 0.80$, P_S value is not close to 162° and therefore the observed DQF patterns do not match satisfactorily with Fig. 5.12. The sums of couplings

ΣH1′ and ΣH3′ are measured to an accuracy of ± 0.50 Hz from Fig. 5.2 (b,c) as 14.3 and 15.8 Hz at 325 K and as 14.4 and 16.0 Hz at 320 K (Table 5.5(a,b)). We compared these values with those predicted [123] for a fast conformational equilibrium between N conformer $P_N = 18^\circ$, $\phi_N = 36^\circ$ and S conformer $P_S = 153^\circ$, $\phi_S = 36^\circ$ (Table 5.4 (c)). We find that predicted values are ΣH1′ = 14.4 and ΣH3′ = 11.0 Hz. Therefore in the present case P_S is not close to 162° or 153° and may be close to 108° (Table 5.4(c)). As a next step, we calculated the J values for $P_N = 18^\circ/9^\circ$, $\phi_N = 36^\circ$ and $P_S = 90^\circ - 144^\circ$ using Tables 5.4 (a-c). Some of these values along with the observed values are shown in Table 5.6. It is clear that the observed results fit in to $P_S = 117^\circ$ and $P_N = 9^\circ/18^\circ$ with $\chi_S = 0.80$. The individual coupling J(H1′ - H2′) and J(H1′ - H2") measured easily in 1D NMR spectra (Table 5.5(a,b)) as 8.6 and 5.9 Hz (± 0.5 Hz) as well as approximate values of ΣH2′ and ΣH2" fit into these predicted for $P_S = 117^\circ$ and $P_N = 9^\circ$. It has been shown in literature that lot of conformational flexibility may be expected for the residues at 3′ end [107,115,123] of a deoxyoligonucleotide. Out of the six residues in d- TGATCA, it is only A6 residue which gives most intense H2" - H3′ cross peaks and has maximum observed value of ΣH3′. Since $\chi_S \simeq 0.80$ only a low value of P_S can explain these results (particularly large ΣH3′) as well as the DQF cross peak patterns.

T4

Considering T4 residue, since ΣH1′ = 14.2 Hz the S conformer is the predominant one with $\chi_S = 0.75$ with exact values possibly

in the range 0.68 to 0.86 by taking the maximum error in ΣH1′ to be ± 0.50 Hz. The cross peak pattern for H2" - H3′ connectivity is not seen in DQF COSY indicating that J (H2" - H3′) < 2.3 Hz. Comparing the observed DQF COSY cross peak patterns of H1′ - H2′, H1′ - H2", H2′- H3′ and H3′- H4′ with those obtained by simulation for a rigid sugar conformer for different P values (Fig. 5.9), for peaks above diagonal (Fig. 5.5(c)) we find that -

(a) H1′ - H2′ pattern indicates [Fig. 5.9] P = 117° - 144°

(b) H1′ - H2" pattern indicates [Fig. 5.9] P = 108° - 180°

(c) H2′ - H3′ pattern indicates [74(a)] P = 144°, 162°.

(d) Absence of H2" - H3′ indicates [115,74(a)] P = 90° - 252°.

(e) H3′ - H4′ pattern indicates [74(a)] P = 9° - 108°, 324°.

For pattern below the diagonal [Fig. 5.5(e)], it is found that :

(f) H1′ - H2′ pattern indicates [Fig. 5.9] P = 126° - 153°

(g) H1′ - H2" pattern indicates [Fig. 5.9] P = 90° - 207°

(h) H3′ - H4′ pattern indicates (below diagonal pattern not shown) [74(a)] P = 9° - 108°, 324°.

From (a-d), it may be inferred that P = 144° fits, into experimental results. However the presence of H3′ - H4′ cross peak pattern (e) is in contradiction to P = 144°. Therefore clearly a single rigid conformer does not exist for T4 residue. Since observed χ_S ~ 0.75, we made an attempt to match the observed patterns with those obtained by simulation for two interconverting

conformers with $P_N = 9^\circ$ and $P_S = 162^\circ$ (Fig. 5.12). For cross peaks above the diagonal (Fig. 5.5 (c)), we find that :

(i) H1′ - H2′ pattern indicates [Fig. 5.12] $\chi_S = 0.6 - 0.8$.

(j) H1′ - H2" pattern indicates [Fig. 5.12] $\chi_S = 0.6 - 0.8$.

(k) H2′ - H3′ pattern indicates [74(a) deduced from COSY - 45 pattern] $\chi_S = 0.7 - 0.8$.

(l) Absence of H2" - H3′ pattern indicates [115,74(a)], $\chi_S = 0.7-0.8$.

For pattern below the diagonal (Fig. 5.5 (e)) comparison with Fig. 5.12 gives the following :

(m) H1′ - H2′ pattern indicates $\chi_S = 0.6 - 1.0$

(n) H1′ - H2" pattern indicates $\chi_S = 0.6 - 1.0$

Combining (i-n), we find that $\chi_S = 0.7 - 0.8$ satisfies all the observed results.

In order to limit our χ_S in the range 0.7 to 0.8 as well as define P_S more precisely, the next step is to match the various observed couplings and sums of couplings with those predicted for different mixing ratios and P_S values using Table 5.4 (a-c) and Fig. 5.10. At this stage, the observed values of J(H1′ - H2′), J(H1′ - H2"), ΣH1′, ΣH2′, ΣH2" and ΣH3′ as 8.2, 6.0, 14.2, 29.3, 22.3 and 12.5 Hz, respectively measured with confidence to an accuracy of ± 0.50 Hz (particularly as some of these peaks

including H2′, H2" did not show any overlap with other peaks, please refer to Fig. 5.3 (b) which serves as a guide line). A close look at Table 5.4(c) revealed that χ_S in the range 0.75 to 0.80 can explain all the results. Starting with χ_S = 0.80, it is seen that a difference between P_N = 9° and P_N = 18° does not show any significant difference in J values (see Table 5.6). By fixing P_N = 18°, χ_S = 0.80 a variation in P_S is now made in the range 108 - 153° and values of J and sums of couplings are calculated (Table 5.6). The lowest P_S = 108° fits into several observed results except that they yield high ΣH3′ ~ 16.4 in comparison to that observed i.e. ΣH3′ 12.5 Hz. The higher P_S = 135° fit into all the observed results except that predicted J (H1′ - H2′) = 8.7 Hz, is some what higher than observed value of 8.2 Hz (considering the fact that actual value of J (H1′ - H2′) at different temperatures are 7.8, 8.1, 8.2 and 8.3 Hz, Table 5.5(a)). Therefore it appears that a lower χ_S will probably provide a better fit and therefore χ_S = 0.75 is attempted. From Table 5.6 it is seen that P_N = 9°/18° and P_S = 135°-153° are fairly alright except that J (H2" - H3′) = 2.9 Hz is some what higher as this peak is not observed at all in DQF COSY spectra. A better fit ultimately emerges by using χ_S in between 0.75 and 0.80, that is χ_S = 0.77. It can be seen (Table 5.6) that P_N = 9° and P_S = 135°/144° with χ_S = 0.77 explains all the observed results satisfactorily. J (H2" - H3′) = 2.7 Hz is close to the resolution used and therefore its cross peak is not seen.

A3

Considering A3 residue, it is observed that this is the only residue whose H1′ does not show quartet as the splitting pattern in 1D NMR spectra at any temperature (Fig. 5.2(b), 5.3(a)) and has minimum ΣH1′ ~ 13.6 ± 0.5 Hz (Table 5.5(a,b)). Therefore A3 sugar apparently has maximum population of N-conformer. The $\chi_S \simeq 0.65$ and lies within the range 0.57 to 0.73. Although single rigid sugar conformer is not expected, we attempted to match the observed DQF cross peak patterns with Fig. 5.9, i.e. those obtained for different P values for a rigid conformer [115] in order to check the results. Comparison of cross peak patterns above the diagonal (Fig. 5.5 (c)) We find that :

(a) H1′ - H2′ pattern indicates (Fig. 5.9) P = 108° - 144°.

(b) H1′ - H2" pattern indicates (Fig. 5.9) P = 117°- 180°.

(c) H2′ - H3′ pattern indicates [74(a)] P = 144°, 162°.

(d) Absence of H2"-H3′ pattern indicates [115,74(a)] P = 90° - 252°.

(e) H3′ - H4′ pattern indicates [74(a)] P = 9°-108°, 324°.

For cross peak patterns below the diagonal (Fig. 5.5(e))comparison with Fig. 5.9 gives the following results :

(f) H1′ - H2′ pattern indicates P = 117°- 207°.

(g) H1′ - H2" pattern indicates P = 99°- 225°.

(h) H2′ - H3′ pattern indicates P = 108°- 180°.

(i) H2" - H3′ pattern indicates P = 72°- 90°.

Obviously, from (a-i), it is clear that single rigid conformer does not provide a fit to observed results.

Since $\chi_S \simeq 0.65$, an attempt is made to match the patterns with those obtained for two interconverting conformers with $P_N = 9^\circ$ and $P_S = 162^\circ$ (Fig. 5.12). For cross peaks above the diagonal (Fig. 5.5 (c)) we find that :

(j) H1′ - H2′ pattern indicates (Fig. 5.12) $\chi_S = 0.5 - 0.8$.

(k) H1′ - H2" pattern indicates (Fig. 5.12) $\chi_S \simeq 0.8$.

(l) H2′ - H3′ pattern indicates [74(a) deduced from COSY 45] $\chi_S \simeq 0.6 - 0.8$.

For below the diagonal (Fig. 5.5 (e)) we find that comparison with Fig. 5.12 gives the following results :

(m) H1′ - H2′ pattern indicates $\chi_S = 0.6 - 0.7$.

(n) H1′ - H2" pattern indicates $\chi_S = 0.5 - 1.0$ (wide range).

(o) H2′ -H3′ pattern indicates $\chi_S = 0.5 - 0.8$.

(p) H2" -H3′ pattern indicates $\chi_S = 0.5 - 0.6$.

Combining (j-p), we find that $\chi_S = 0.65$ satisfies all the observed results except perhaps (k).

In order to narrow down the range of P_S as well as explain the observed results of J(H1′ -H2′) , J(H1′ -H2"), ΣH1′ , ΣH2′ and ΣH3′ as 6.9, 6.7, 13.6, 26.1, 12.4 (± 0.5 Hz) (Table 5.5 (b)). The next step is to match these values with those predicted for different P_S for $\chi_S = 0.65$ using Table 5.4 (a-c) and Fig. 5.10 .

The calculated values are given in Table 5.6. For $P_N = 9^\circ$ and $P_S = 162^\circ$ the J (H1′ - H2′) and J(H1′ - H2") are 7.2 and 6.1 Hz, respectively . In order to bring these two values close to each other which will result in a triplet pattern of H1′ at all temperatures as observed, the P_S value is decreased from 162° to 135° and then to 108° (Table 5.6) . It is noted that $P_N = 9^\circ$ or $P_N = 18^\circ$ do not give significantly different results. Choosing $P_S = 108^\circ$ brings calculated values close to the observed values. However, ΣH3′ becomes ≃ 18 Hz and is much larger than the observed value of ≃ 12.4 Hz . It is clear from Fig. 5.2(c) that ΣH3′ is certainly much lesser than 18 Hz. Therefore an increase in P_S is tried. It is evident from Table 5.6 that $P_S = 180^\circ$ fits into all the observed experimental results satisfactorily for $\chi_S = 0.65$.

T1

Considering T1 residue, since ΣH1′ = 14.5 Hz, the S conformer is the predominant one with $\chi_S \simeq 0.79$ and lies, within the experimental errors, in the range 0.71 - 0.88. The DQF COSY cross peak patterns are observed for H1′ - H2′, H1′ - H2", H2′ - H3′ and H3′ - H4′. A close look at Fig. 5.5(c, d) shows that H1′ - H2′ and H1′ - H2" patterns of T1 and C5 residues are rather peculiar and different from all other residues. Further the H2′ - H3′ of T1 and C5 residues are alike and different from others. Comparing these with that for a rigid sugar conformer [115], for peaks above diagonal, (Fig. 5.5(d)) the following is obtained :

(a) H1′ - H2′ pattern indicates (Fig. 5.9) P = 207°, 225°.

(b) H1′ - H2" pattern indicates (Fig. 5.9) P = 90°-207°.

(c) H2′ - H3′ pattern indicates [74(a)] P = 90°-108°, 180° - 216°.

(d) Absence of H2" - H3′ cross peak indicates [74(a)] P = 90°- 225°.

(e) H3′ - H4′ pattern indicates [74(a)] P = 90°, 108°.

For patterns below the diagonal (Fig. 5.5(e)) it is found that :

(f) H1′ - H2′ pattern indicates (Fig. 5.9) P = 207°, 225°.

(g) H1′ - H2" pattern indicates (Fig. 5.9) P = 72°- 225°.

From (a-g) it is clear that a single rigid sugar conformer does not exist in the present case. Since ΣH1′ < 15.7 Hz and $\chi_S \simeq$ 0.79, the possibility of two state model is explored and the observed patterns are compared with Fig. 5.12. For cross peaks above the diagonal (Fig. 5.5(c, d)) we find :

(h) H1′ - H2′ pattern indicates (Fig. 5.12) χ_S = 0.4 - 0.7 and perhaps more close to χ_S = 0.6/0.7.

(i) H1′ - H2" pattern indicates (Fig. 5.12) χ_S = 0.7 (perhaps 0.8).

(j) H2′ - H3′ pattern indicates [74(a) derived from COSY-45 peaks], χ_S = 0.7, 0.8.

(k) Absence of H2" - H3′ cross peak indicates (Fig. 5.12) χ_S = 0.7 to 1.0.

For cross peaks below the diagonal (Fig. 5.5(e)) we find that

(l) H1′ - H2′ pattern indicates (Fig. 5.12) χ_S = 0.6 - 0.8.

(m) H1′ - H2" pattern indicates (Fig. 5.12) χ_S = 0.5 - 1.0 (large range).

It is clear from (h-m) that χ_S = 0.7 generally satisfies all the experimental results although the fit of H1′ - H2′ and H1′ - H2" pattern is still not satisfactory. The observed patterns give four components with wide separation along both ω_1 and ω_2 axis. Besides the value of χ_S obtained from H1′ independently is certainly close to 0.80. The deviations may be attributed to a P_S value different from $P_S = 162^\circ$. As a next step we calculated J values for conformational equilibrium of two conformers of $P_N = 9^\circ/18^\circ$ and $P_S >$ as well as $< 162^\circ$, for χ_S = 0.8 using Table 5.4(a-c). Some of these calculated values and observed values are shown in Table 5.6. It is seen that the observed results of J(H1′ - H2′), J(H1′ - H2"), ΣH2′, ΣH2" and ΣH3′ as 8.4, 6.0, 29.4, 22.3 and 11.5 Hz fits into those predicted for $P_S = 144^\circ$ and $P_N = 18^\circ$.

It has been shown in literature that it is possible to have a two state model and a three state model providing essentially the same simulated spectra. For example, for T2 residue in [d-$(GTATATAC)_2$] a fit was obtained for 85 % S mixture with $P_S = 144^\circ$ as well as by employing two different conformers in the S range of pseudorotation, with 52 % of S, $P_S = 162^\circ$ and 33% of S, $P_S = 126^\circ$, the minor conformer being 9° [115]. Since there are more parameters available in a three state model, the results fit more readily. Low conformational barriers could mean that a three state model is more realistic. At this stage, the influence of line widths [74(a),115] on the simulations and the results derived

there from is also looked into. Schmitz et al. [115] have shown that line width of 13 Hz yield H1′ - H2" cross peak patterns in DQF - COSY spectra which have four main components with each component placed far apart both along ω_1 as well as ω_2 axis. In the present case of T1 residue, it is found that line widths of various peaks are 6-9 Hz, like all other residues. The line widths of H2′ peak is ≃ 8-9 Hz whereas that for H2" peak is generally about 6-7 Hz. The 1D NMR spectra (Fig. 5.2(d), 5.3(b)) also shows that line widths for T1 residues are similar, and infact some what smaller, than that for other residues. Eventually by calculating the J values, we find that observed results fit typically into a three state model having 22 % of N conformer with $P_N = 9^\circ$, 20 % of S-conformer with $P_S = 126^\circ$ and 58 % of S conformer with $P_S = 162^\circ$. Several others with about 2 % difference in percentage of N conformer and upto 10 % variation in percentage of S conformer and P_S values also fit in.

C5

Considering C5 residue, an average value of ΣH1′ = 14.1 Hz gives $\chi_S \simeq 0.75 \pm 0.06$. We compare the observed cross peak patterns with the simulated ones for single rigid conformer.

For cross peaks above the diagonal (Fig. 5.5(c)) we get :

(a) H1′ - H2′ pattern indicates (Fig. 5.9) P = 207°, 225°.

(b) H1′ - H2" pattern indicates (Fig. 5.9) P = 90°- 207°.

(c) H2′ - H3′ pattern indicates [74(a)] P = 180°, 216°.

(d) Absence of H2" - H3′ pattern indicates [74(a), 115] P = 90°-225°

(e) H3′ - H4′ pattern indicates [74(a)] P = 9° - 108°, 324°

Below the diagonal (Fig. 5.5(e)) we find that :

(f) H1′ - H2′ pattern indicates (Fig. 5.9) P = 72° - 99°, 135°, 144°

(g) H1′ - H2" pattern indicates (Fig. 5.9) P = 99° - 225°

Clearly single conformer does not provide a fit to the observed results. Comparing observed patterns with those in Fig. 5.12 for a two state model we find that for peak above diagonal :

(h) H1′ - H2′ pattern indicates χ_S = 0.6, 0.7.

(i) H1′ - H2" pattern indicates χ_S = 0.7.

(j) H2′ - H3′ pattern indicates [74(a)] χ_S = 0.7, 0.8.

(k) Absence of H2" - H3′ cross peak indicates χ_S = 0.7 - 1.0.

For peaks below the diagonal (Fig. 5.5(e)) :

(l) H1′ - H2′ pattern indicates χ_S = 0.6 - 0.8.

(m) H1′ - H2" pattern indicates large range of χ_S = 0.5 - 1.0.

Thus generally (h-m) show that χ_S = 0.7 fits the best in all experimental results. Next, we calculated J values for a two state and three state model. We find that observed values of J(H1′ - H2′) = 7.9 Hz, J(H1′ - H2") = 6.2 Hz, ΣH2′ ≃ 29.3 Hz, ΣH2" ≃ 21.1 Hz and ΣH3′ ≃ 13 Hz fit into two state model of P_N = 9°, χ_N = 0.29 and P_S = 153°, χ_S = 0.71. Alternately as observed in case

of T1 residue, it fits into a three state model having $P_N = 18^\circ$, $\chi_N = 0.22$, $P_S = 126^\circ$, $\chi_S = 0.58$, $P_S = 162^\circ$, $\chi_S = 0.20$.

Table 5.7 summarizes, the results obtained for all residues. It is observed that in all residues single rigid conformation of sugar with P_S localized in a small domain does not exist and there is generally a conformational equilibrium between N and S states. A three state model with two different P_S value, permits more parameters and an easier fit into experimental results. The residue at 3′ terminus i.e. A6 has a greater conformational flexibility, as expected [13,74,115,115(a)] and has P_S as low as 117°.

CONFORMATION OF DEOXYRIBOSE SUGARS IN d-(TGATCA)$_2$ FROM RELATIVE INTENSITIES OF NOE

In recent years, much use has been made of cross-relaxation rates measured by one-dimensional or two-dimensional NOE. These are translated into proton - proton distances. However there are difficulties in obtaining sugar conformation from these distances alone due to the very nature of pseudorotation phenomena and the conformational heterogeneity. It has since been shown [123,123(a)] that unambiguous and precise determination of conformation of deoxyribose sugars in oligonucleotides is further complicated due to presence of S to N equilibrium with $\chi_S \simeq 0.65$ to 1.0 and P_S lying in the range 90°-180°. The NOE data therefore needs to be supplemented by other data, to arrive at a conclusion. We have therefore followed the strategy of using results obtained by coupling constant analysis and check if these are in confirmity

Table 5.7 : Average P_S, P_N (in degrees) χ_S, χ_N values for mixture of deoxyribose sugars for all residues which fits best to the observed J (in Hertz) and sum of couplings (in Hertz).

	T1	G2	A3	T4	C5	A6
p_N	9	18	9	9	18	18
p_S	126	153	180	135	126	117
p_S	162	-	-	-	162	-
χ_S	0.20	0.88	0.65	0.77	0.58	0.80
χ_S	0.58	-	-	-	0.20	-
χ_N	0.22	0.12	0.35	0.23	0.22	0.20

χ_S, χ_N are mole fraction of south and north conformers respectively.

P_N may vary $\pm 9^\circ$ and χ_S may vary $\pm$ 0.05.

with the observed intensities of cross peaks in NOESY spectra. The intra sugar proton-proton distances vary over a large range with pseudorotation as shown in Fig. 5.13. From the table of distances (Table 5.8) obtained for different standard sugar geometries in the pseudorotation cycle we find that all but two of the intra sugar ^{1}H - ^{1}H distances vary less than 0.25 A° relative to their average in going from N to S region of sugar conformational space and thus are not useful. The H1′ - H4′ distance varies by more than 1 A° but the minimum distance lies in the O1′-endo (P = 90°) region, thus this distance can not discriminate between N and S conformers or their relative populations. The H2" - H4′ distance serves as a marker as it changes from approximate 2.3 A° in the N region to about 3.6 to 4.0 A° in S conformational space.

Table 5.3(b) gives a list of various intra sugar connectivities in NOESY spectra (Fig. 5.6 (a-k)) obtained for τ_m = 75, 150, 200 and 250 ms. The integrals could not be obtained quantitatively for NOESY spectra recorded at these τ_m values. We therefore attempted to analyse the data in the semiquantitative way by making use of standard distances. Table 5.9 gives the intensities of all observed peaks graded into small ranges designated as w (weakly intense), ws (fairly intense), s (intense), ss (very intense) in order of increasing intensity by visual inspection at different τ_m values using data in Fig. 5.6 (a-k). We have carried out independent studies on d-$(CGATCG)_2$ (unpublished) and obtained distances as well as NOE build up

Table 5.8 : Calculated intranucleotide distances (A°) between different hydrogen atoms in deoxyribose ring as a function of P [131].

P	1'-2'	1-2"	1'-3'	1'-4'	2'-3'	2"-3'	2'-4'	2"-4'	3'-4'
9°	2.52	2.18	3.64	3.15	2.29	2.91	3.54	2.31	2.84
18°	2.55	2.15	3.65	3.00	2.29	2.90	3.51	2.29	2.85
36°	2.65	2.11	3.69	2.73	2.25	2.91	3.48	2.36	2.84
90°	2.80	2.07	3.69	2.19	2.18	2.75	3.58	3.05	2.80
99°	2.83	2.11	3.65	2.20	2.18	2.71	3.58	3.19	2.77
108°	2.83	2.15	3.60	2.25	2.20	2.69	3.60	3.34	2.75
117°	2.84	2.18	3.60	2.36	2.20	2.64	3.60	3.48	2.73
126°	2.84	2.18	3.57	2.52	2.24	2.61	3.60	3.54	2.69
135°	2.84	2.20	3.54	2.58	2.25	2.58	3.58	3.66	2.64
144°	2.84	2.20	3.54	2.73	2.28	2.55	3.58	3.77	2.60
153°	2.84	2.20	3.54	2.84	2.30	2.55	3.57	3.79	2.55
162°	2.84	2.18	3.54	3.04	2.31	2.52	3.54	3.80	2.52
180°	2.84	2.16	3.58	3.28	2.33	2.52	3.51	3.90	2.45
189°	2.85	2.15	3.65	3.37	2.31	2.50	3.51	3.93	2.42
198°	2.83	2.11	3.69	3.48	2.30	2.50	3.51	3.93	2.42
207°	2.83	2.11	3.74	3.57	2.30	2.50	3.52	3.93	2.39
216°	2.80	2.07	3.82	3.65	2.29	2.80	3.57	3.93	2.39
225°	2.75	2.09	3.87	3.77	2.25	2.58	3.60	3.89	2.40

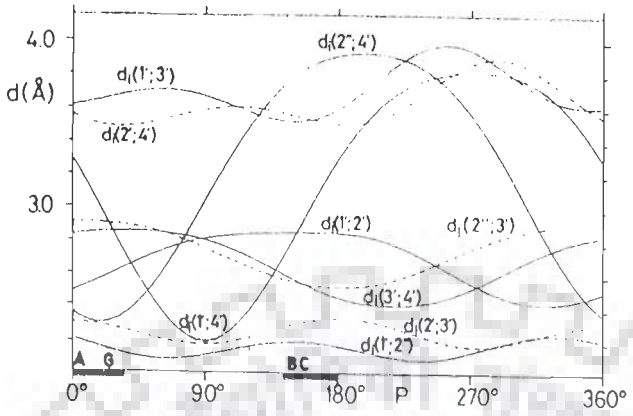

Fig. 5.13 Intranucleotide distances between different hydrogen atoms in the deoxyribose ring versus the pseudorotation phase angle P. The heavy lines below the P axis indicate the regions of the preferred ring puckers 3'C-*endo* near 20° and 2'C-*endo* near 160°. A, B, C, and G identify the P-values for A-DNA, B-DNA, and the nucleotides C and G in the Z form of $d(CGCGCG)_2$ [131].

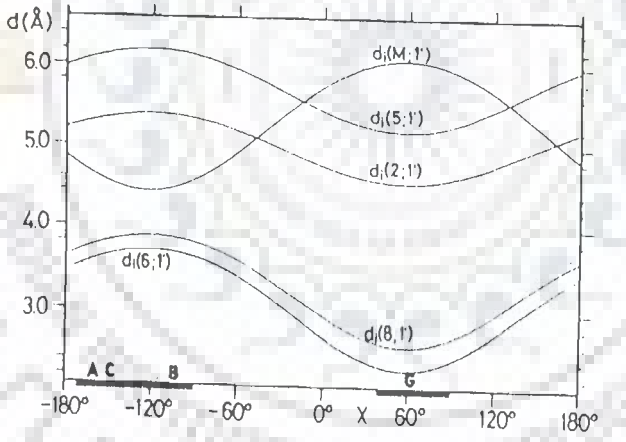

Fig. 5.14(a) Intranucleotide distances between base protons and 1'H versus the torsion angle χ. Preferred χ regions from −90 to −170° (anti) and 40 to 90° (syn) are indicated with heavy lines at the bottom. A, B, C, and G identify the χ-values for A-DNA, B-DNA, and the nucleotides C and G in the Z form of $d(CGCGCG)_2$ [131].

curves by integrating the cross peaks. Under conditions identical to that for the present study on d-$(TGATCA)_2$ it is found that spin diffusion takes place at 250 ms for practically all NOE connectivities whereas the integrals obtained are definitely in linear regime for τ_m = 75 as well as 150 ms and hence can be used safely for distance measurements. Since in present study although sequence used is different, it being a hexanucleotide we have assumed that the same is applicable for d-$(TGATCA)_2$.

The intensities of cross peaks obtained at 250 ms (Table 5.3(b, c)) have been used for assignment of resonances (described earlier) and at the most may be used to define a cut off value of distance beyond which the NOE cross peak is not observed at τ_m = 250 ms. Since H1′ - H3′ distance for all sugar conformations varies between 3.6 - 3.7 A° for P_S lying in the range 9° to 225° (Fig. 5.13 and Table 5.8). the observation that fairly intense peak (marked ws in Table 5.9) is seen (Fig. 5.6 (i)) for G2, A3 and A6 residues at τ_m = 250 ms while no corresponding peak is observed for T1, T4 and C5 residues shows that the cut off value of distance at τ_m = 250 ms is about 3.7 A°. The fairly intense peaks marked as ws correspond to a distance 3.6-3.7 A° (assuming that spin diffusion is similar in all residues). By similar arguments, since H2′ - H4′ distance varies in the range 3.5 - 3.6 A° (Fig. 5.13 and Table 5.8) for P_S lying in the range 0° to 225°, the cut off at 200 ms is close to 3.5 A° (Table 5.9). The H3′ - H4′ distance varies in the range 2.40 - 2.84 A° (Fig. 5.13 and

Table 5.9 : The observed relative intensities of various intra sugar NOE connectivities in NOESY spectra recorded at 75, 150, 200 and 250 ms of d-$(TGATCA)_2$ (Fig. 5.6(a-k)).

Connectivity	τ_m	T1	G2	A3	T4	C5	A6
H1'-H2'	250	w	ss	ss	ss	s	ss
	200	w	ss	ss	ss	s	ss
	150	-	ss	ss	ss	s	ss
	75	-	ss	ss	s	w	ss
H1'-H2"	250	ss	ss	ss	ss	ss	ss
	200	ss	ss	ss	ss	ss	ss
	150	ss	ss	ss	ss	ss	ss
	75	ss	ss	ss	ss	ss	ss
H2'-H3'	250	ss	ss	ss	ss	ss	ss
	200	ss	ss	ss	ss	ss	ss
	150	ss	ss	ss	ss	ss	ss
	75	ss	ss	ss	ss	ss	ss
H2"-H3'	250	ss	ss	ss	ss	ss	ss
	200	ss	ss	ss	ss	ss	ss
	150	s	s	s	s	s	s
	75	-	s	-	w	-	ss
H3'-H4'	250	ss	ss	ss	s	s	ss
	200	ss	ss	ss	s	s	ss
	150	ss	ss	ss	w	w	ss
	75	ss	ss	ss	-	-	ss

H1'-H4'	250	ss	ss	ss	ss	ss	ss
	200	ws	s	ss	ss	ss	s
	150	-	s	ss	ss	s	s
	75	-	-	ws	ws	-	-
H1'-H3'	250	-	ws	ws	-	-	ws
	200	-	-	-	-	-	-
	150	-	-	-	-	-	-
	75	-	-	-	-	-	-
H2'-H4'	250	-	-	ws	ws	-	-
	200	-	-	ws	w	-	-
	150	-	-	-	-	-	-
	75	-	-	-	-	-	-
H2"-H4'	250	ws	ws	-	s	ws	ws
	200	-	ws	-	s	ws	ws
	150	-	-	-	s	-	-
	75	-	-	-	-	-	-

(-) - absence of peak. w - weak intensity of peak.

ws - fairly intense. ss - very intense.

Table 5.8) for P_S lying in the range 9°-225°, the absence of peak at 75 ms for T4 and C5 residues (Fig. 5.6(h), Table 5.9) shows that at distance > 2.84 A° the cross peak will not be seen in NOESY spectra at τ_m = 75 ms. By similar arguments the absence of H1′ - H4′ peak for T1 residue (χ_S ~ 0.8, P_S ~ 126-162°, expected distance ~ 3.1 A°) (Table 5.9) at τ_m = 150 ms gives a rough estimate of cut off value as 3.1 - 3.2 A°. Thus the cut off values for absence of NOE cross peaks at τ_m = 75, 150, 200 and 250 ms are > 2.8, 3.1-3.2, ~ 3.5 and ~ 3.7 A° respectively. The intensities of peak at 75 ms and 150 ms may however be used to estimate distance since these are in linear regime of NOE build up curves. These values are however not used rigorously for arriving at any conclusion and serve only as rough guidelines.

In order to analyse the data in Table 5.9 we find that since H1′ - H2" and H2′- H3′ distances are low, being 2.1 - 2.3 A° and give very intense cross peaks for all residues, including that at τ_m = 75 ms (Table 5.9), they can not be of any use for discriminating various sugar conformations. The H2" - H3′ distance varies in the range 2.5 - 2.9 A° (Table 5.8 and Fig. 5.13). The observed data in Table 5.9 shows that H2" - H3′ distance for G2 residue is expected to be least since it has S conformer with maximum population i.e. χ_S = 0.88 with P_S = 144°. Other residues like T1, T4, C5 have either low χ_S value, 0.75 - 0.80 with average P_S ~ 144° (or a mixture of 126° and 162°) or have χ_S = 0.65 with P_S = 180°, like A3 residue, resulting in greater H2" - H3′ distance and hence the observed results (that

is, weakly intense peak for T4 residue and no cross peak for T1, A3 and C5 residue at τ_m 75 ms in Fig. 5.6(e)). Comparing the intensities of H3′ - H4′ cross peaks among all residues (Table 5.9 and Fig. 5.6(f-h)), the observed results suggest that the H3′ - H4′ distances of T4 and C5 residues are higher than those for other residues. We calculated these distances for the observed sugar geometry obtained by spin - spin coupling analysis and found that distances of these residues are indeed greater being about 2.7 A° whereas all others are < 2.6 A°. The H1′ - H4′ distance is not easily usable for sugar conformation analysis since we have a mixture of N ⇆ S equilibrium and it gives minimum value at $P_S = 90^{\circ}$ and increases on increasing or decreasing P_S value. The H2′ - H4′ distance varies in a small range 3.5 - 3.6 A° and these cross peaks are not observed at τ_m = 75 and 150 ms. The H2" - H4′ distance varies over a large range and could particularly be used to monitor N ⇆ S equilibrium as these distance are 2.3 and 3.8 A° for $P = 18^{\circ}$ and 162°, respectively. For G2 residue we calculated it for $\chi_S = 0.88$, $P_S = 144^{\circ}$ as ≃ 3.59 A°. The same for A3, T4 residues having higher N conformer population is calculated as ≃ 3.34 A°. Since in present case 3.34 A° distance is just about near the cut off value for the observation of NOE cross peak at τ_m = 150 ms, the fact that no cross peak is observed for G2 and corresponding peak is seen for T4 residue are in confirmity with the results of χ_S, P_S obtained. Among T1 and C5 residues, the H2"-H4′ distance is lower for C5 residue as compared to that in T1. This is expected (Table 5.6) since C5 residue has a greater percentage of $P_S = 126^{\circ}$ conformer

than that in T1 residue. Thus we find that the NOE results are generally in confirmity (except for A6 residue for which NOE data predicts P_S value lower than 180°) with that obtained for spin-spin coupling analysis. The disagreement in A6 residue may be attributed to a greater flexibility in its sugar conformation being the last residue at 3′ end.

GLYCOSIDIC BOND ROTATION (χ)

The glycosidic bond rotation defined as O4′ - C1′ - N9 - C8 in case of purines and O4′ - C1′ - N1 - C6 in case of pyrimidines may be estimated from the knowledge of intranucleotide distances between the base protons AH8/GH8/CH6/TH6 and their corresponding sugar protons H1′, H2′, H2", H3′ and H4′. Of these five distances, the base to H1′ distance depends only upon the value of χ (Fig. 5.14 (a)) while others (Fig. 5.14 (b, c)) depend upon both χ and pseudorotation angle P of the deoxyribose sugar. Fig. 5.14 (b, c) and Table 5.10(b, c) show these distances for some of the standard sugar geometries having $P_S = 90^\circ - 225^\circ$, with $\chi = -105^\circ$, -90°, -120°, -60°, $P_N = 18^\circ$, 9° with $\chi = -150^\circ$ that is close to both A and B-DNA [131]. The relative intensities of NOE cross peaks observed in NOESY spectra Fig. 5.6(c, j, k) at different τ_m values are given in Table 5.11. The data at 250 ms has earlier been used for spectral assignment and as argued earlier, our results for d-$(CGATCG)_2$ (unpublished) suggested that the relative intensities obtained in NOESY spectra at τ_m = 75 and 150 ms can be used for distance analysis.

(b)

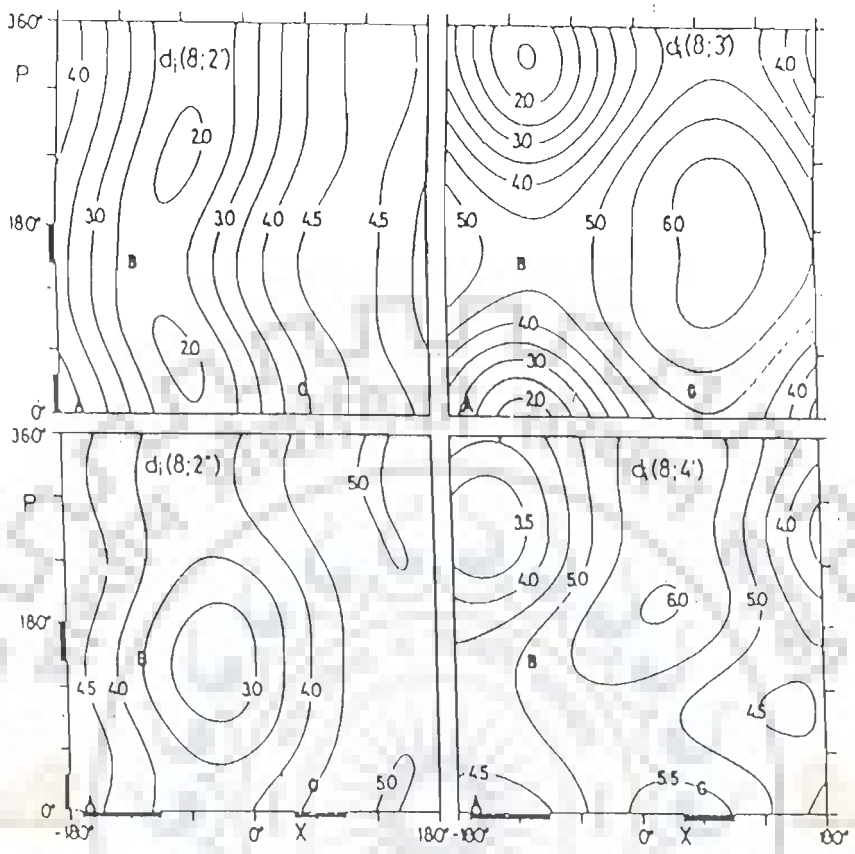

Fig. 5.14(b) : P-χ plane with contours indicating the H8 to (i) H2' (ii) H2" (iii) H3' and (iv) H4' distances. The preferred regions C3'-endo near 20° and C2'-endo near 160° for P and syn near 60° and anti near 130° for χ are indicated with heavy lines on the left and the bottom. A, B, and G identify the χ values for A DNA, B DNA and nucleotide G in the Z form of d-$(CGCGCG)_2$ [131].

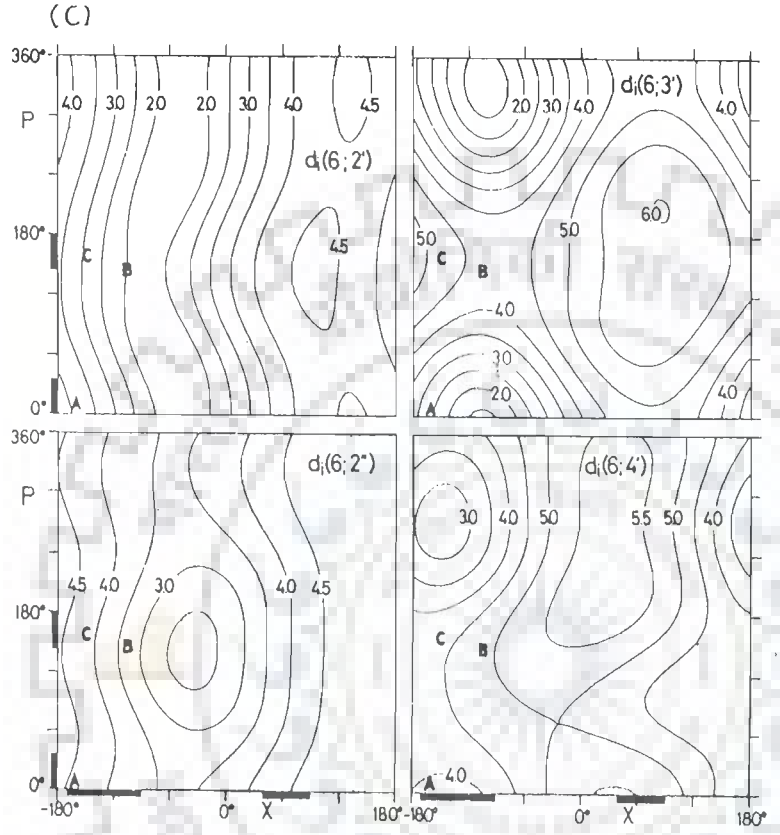

Fig. 5.14(c) : P-χ plane with contour lines indicating the H6 to (i) H2′ (ii) H2" (iii) H3′ and (iv) H4′ distances. The preferred regions C3′-endo near 20° and C2′-endo near 160° for P and syn near 60° and anti near 130° for χ are indicated with heavy lines on the left and the bottom. A, B and C identify the χ values for A DNA, B DNA and nucleotide C in the Z form of d-$(CGCGCG)_2$ [131].

Considering the base H8/H6 to H1′ distance, it is noted (Fig. 5.14(a), Table 5.10(a)) that it lies within a small range 3.72 - 3.88 A° for χ values - 150° and - 105°, which correspond to the χ values for standard A-DNA and B-DNA, respectively. Since the distance does not depend upon pseudorotation angle P, for G2 residue having χ_S = 0.88 we expect this distance to be (3.88 x 0.88 + 3.72 x 0.12) = 3.86 A° which is not expected to give NOE cross peak at τ_m = 75 or 150 ms, as observed (Table 5.11). However for A3 residue which has maximum population of N conformer, the distance H8 - H1′ is expected to be (3.88 x 0.65 + 3.72 x 0.35) = 3.82 A°. Thus for G2, A6 and A3 residues for which χ_S = 0.88, 0.80 and 0.65 respectively the base H8 - H1′ distance will be within a small range 3.82 to 3.86 A°. Since we observed (Fig. 5.6 (j-k) Table 5.11) intense cross peaks for A3 and A6 residues at 150 ms, it may be inferred that χ for the major sugar conformers in these residues is some what higher than -105° and shifted (Fig. 5.14 (a)) towards high anti conformation, i.e, χ = -90° to -60°. Considering the base H6-H1′ distances in pyrimidine residues T1, T4 and C5, (Table 5.10(a)) we observed the NOE cross peaks at τ_m = 150 ms for T4 and C5 residues and none for T1 (Fig. 5.6 (k) Table 5.11). The calculated distances for these residues (T4, C5) for χ_S in the range 0.75 - 0.80 lies between 3.688 and 3.692 A°. Thus for these three residues, irrespective of P_S value and χ_S value the distance expected is practically 3.7 A° if these are in confirmity with the χ values of standard A and B-DNA geometries. The observed results may be interpreted as an increase in χ from - 105° to say - 90° or values near about high

Table 5.10(a) : Intranucleotide distances (A°) between base protons H8, H6 and deoxyribose H1′ proton corresponding to different χ (in degrees) values [131].

χ	H8-H1′	H6-H1′
-150	3.72	3.50
-120	3.92	3.68
-105	3.88	3.66
-90	3.81	3.58
-60	3.58	3.33

Table 5.10(b) : Intranucleotide distances (A°) between base proton H8 and deoxyribose ring protons corresponding to different P and χ (in degrees) values [131].

P	χ=-105			χ= - 150			χ= - 90			χ= - 60		
	B-2′	B-2"	B-3′	B-2′	B-2"	B-3′	B-2′	B-2"	B-3′	B-2′	B-2"	B-3′
9	2.8	4.1	1.8	4.0	4.7	2.7	2.5	3.9	2.0	2.1	>3.5	2.5
18	4.0	4.1	3.0	2.7	4.7	3.0	2.5	3.9	2.3	2.0	>3.5	2.8
90	2.2	3.7	4.0	3.4	4.7	4.5	2.2	3.5	4.1	2.1	3.1	4.4
117	2.3	3.5	4.5	2.3	3.5	5.0	>2.0	3.4	4.5	>2.0	2.9	>4.5
126	>2.0	3.5	>4.5	3.4	4.5	>5.0	>2.0	3.4	>4.5	>2.0	<3.0	>4.5
135	2.3	3.5	>4.5	3.4	4.5	>5.0	>2.0	3.3	>4.5	2.4	<3.0	>4.5
144	2.3	3.5	>4.5	3.4	4.5	>5.0	>2.0	3.3	>4.5	2.4	<3.0	4.5
153	<2.5	3.5	4.5	3.4	4.5	5.0	>2.0	3.3	>4.5	-	-	-
162	2.2	3.6	4.8	3.4	4.5	>5.0	>2.0	3.3	4.8	2.4	2.8	4.5
180	>2.0	3.6	>4.5	3.4	>4.5	>5.0	>2.0	3.5	>4.5	>2.0	3.0	>4.5
189	>2.0	3.7	4.5	3.5	>4.5	5.0	>2.0	3.5	4.5	-	3.2	-
198	>2.0	3.7	4.5	3.5	>4.5	5.0	>2.0	3.6	4.4	-	3.3	-
207	<2.5	3.8	4.3	3.5	>4.5	5.0	>2.0	3.7	4.3	-	-	-
225	<2.5	4.0	4.0	3.6	>4.5	>4.5	>2.0	>3.5	4.0	-	-	-

B - Base proton

Table 5.10(c) : Intranucleotide distances (A°) between base proton H6 and deoxyribose ring protons corresponding to different P and χ values [131].

	χ=-105°			χ= - 150°			χ= - 90°		
P	B-2′	B-2"	B-3′	B-2′	B-2"	B-3′	B-2′	B-2"	B-3′
9°	2.6	3.8	1.5	3.8	4.4	2.6	2.3	3.7	1.6
18°	2.5	3.8	1.8	3.7	4.5	2.8	2.3	3.7	1.8
90°	1.9	3.5	3.6	3.3	4.4	>4.0	<2.0	3.3	3.5
99°	<2.0	3.5	3.8	3.2	4.4	4.5	<2.0	3.3	3.9
117°	1.9	3.4	4.2	3.1	4.3	4.5	<2.0	3.0	>4.0
126°	1.9	3.4	4.2	3.1	4.3	4.5	<2.0	3.0	>4.0
135°	1.9	3.4	>4.0	3.1	4.3	4.7	<2.0	3.0	>4.0
144°	2.0	3.4	>4.0	3.1	4.3	4.8	<2.0	3.0	>4.0
153°	2.0	3.4	>4.0	3.2	4.3	5.0	<2.0	3.0	>4.0
162°	2.0	3.4	4.2	3.1	4.3	5.0	<2.0	3.1	>4.0
180°	2.0	3.5	>4.0	3.2	4.5	5.0	<2.0	3.3	>4.0
207°	2.0	3.7	3.8	3.4	>4.5	4.5	<2.0	3.5	3.8
225°	2.2	3.7	3.5	3.5	>4.5	>4.0	<2.0	3.6	3.5

P	χ= - 60°			χ = -120°		
	B-2′	B-2"	B-3′	B-2′	B-2"	B-3′
9°	<2.0	<3.5	2.5	3.0	4.0	1.6
18°	<2.0	<3.5	2.6	-	-	-
90°	<2.0	2.8	4.5	2.3	3.7	3.3
99°	<2.0	2.7	4.5	2.3	3.7	3.9
117°	2.0	2.5	4.5	-	-	-
126°	2.0	2.5	4.5	-	-	-
135°	2.1	2.5	4.5	2.3	3.6	4.2
144°	2.1	2.5	4.5	2.3	3.6	4.4
153°	2.1	2.5	4.5	2.3	3.6	4.4
162°	2.0	2.5	4.5	2.3	3.6	4.4
180°	<2.0	2.7	4.5	-	-	-
207°	<2.0	3.0	4.5	2.4	3.9	4.0
225°	<2.0	>3.0	3.7	2.5	4.0	3.5

B - Base proton

Table 5.11 : The observed relative intensities of NOE cross peaks in NOESY spectra recorded at τ_m = 75, 150, 200 and 250 ms of d-(TGATCA)$_2$ (Fig. 5.6(a-k)).

Connectivity	τ_m	T1	G2	A3	T4	C5	A6
B-H1′	250	ss	ss	ss	ss	ss	ss
	200	ss	ss	ss	ss	s	ss
	150	-	-	ws	ws	w	ws
	75	-	-	w	w	-	w
B-H2′	250	ss	ss	ss	ss	ss	ss
	200	ss	ss	ss	ss	ss	ss
	150	ss	ss	ss	ss	ss	ss
	75	ss	ss	ss	ss	ss	s
B-H2"	250	s	s	s	s	s	s
	200	s	s	s	s	s	s
	150	s	s	ws	s	s	ws
	75	-	-	-	ws	ws	-
B-H3′	250	ss	ss	ss	-	s	ss
	200	ss	ss	ss	-	s	ss
	150	-	s	ss	-	s	ss
	75	-	-	-	-	-	-

B - base proton, (-) absence of peak, w - weak intensity of peak.

ws - fairly intense. s - intense.

ss very intense.

anti conformation . Hence the relative intensities of cross peaks (Table 5.11) for base H8/H6 - H1′ indicates that T1, G2 residues may have $\chi \simeq -105^{\circ}$ (standard B-DNA values) but A3, T4, C5 and A6 residues are expected to be in high anti conformation.

Considering the base H8/H6 - H2′ distances we find that all residues give very intense cross peaks in NOESY spectra obtained at all mixing times. This distance does not vary much (Fig. 5.14(b, c), Table 5.10(b,c)) with P_S in the range 117° - 162° and therefore it may vary with percentage population of N conformer only. For A3 and G2 residues having extreme values of χ_S i.e. 0.65 and 0.88 the calculated distance is 2.90 and 2.35 A°, respectively for glycosidic bond rotation $\chi = -105^{\circ}$ for major S conformer. An increase in χ to - 90 or - 60°, i.e. high anti conformation will decrease (Fig. 5.14 (b, c)) the base - H2′ distance further. Thus the observation of very intense cross peak for all residues fit into a wide range of χ and does not restrict it to anti or high anti conformation. The base to H2′ distance is infact not really useful in determining glycosidic bond rotation.

Considering the base H8 to H2" distances for G2, A3, A6 residues, we observe intense cross peaks for these at τ_m = 250 (Fig. 5.6(c)), 200 and 150 ms and no peak at τ_m = 75 ms (Table 5.11). The calculated distance using $\chi = -105^{\circ}$ for major S conformer are (3.5 x 0.88 + 4.5 x 0.12) = 3.62 and (3.5 x 0.65 + 4.5 x 0.35) = 3.85 A° for G2 and A3 residues respectively. The observed intense peak for A3 and A6 residues at τ_m = 150 ms therefore, will provide a better fit if χ is increased from - 105°

to high anti values as distance decreases with increase in χ (Fig. 5.14(c)). Thus G2, A3, A6 residues have χ as anti, high anti, high anti respectively. For pyrimidines residues base H6 to H2" distance calculated for P_S = 162°, χ = - 105°, χ_S = 0.75 to 0.80 (that observed for T1, T4 and C5 residues) lie in the range 3.62 - 3.67 A°. If P_S is lower in the range 126° - 153°; the corresponding values of H6-H2" distances lie in the range 3.54 - 3.60 A°. An increase in glycosidic bond rotation from χ = - 105° to high anti values (say χ =-90°) which lowers all the calculated distances considerably, to about 3.31 - 3.37 A°. Since we observed (Table 5.11) fairly intense peaks for T4 and C5 residues at τ_m = 75 ms, it is inferred that these residues are in high anti conformation. Considering the base H8/H6 - H3′ distances, it is known [131] (Fig. 5.14 (b, c), Table 5.10(b, c)) that this distance is > 4.5 A° for all S sugar conformers with P_S in the range 117° - 180°. For P_S = 90° the H8/H6 - H3′ distance ~ 4.0 A°. On the other hand for N conformers H8/H6 - H3′ distance ~ 3.0 A°. Therefore it is expected that the residue having maximum population of N conformer, i.e. A3 residue, will only yield intense peak in NOESY spectra. It is indeed observed that A3 residue gives very intense cross peak (Fig. 5.6 (i) Table 5.11) for H8 - H3′ connectivity. The distance for which is calculated as (4.5 x 0.65 + 3.0 x 0.35) = 3.8 A°. For A6 residue an intense peak is possible only if P_S is lowered from 162° since χ_S = 0.80. This again fits into observed results since P_S = 117°, χ_S = 0.80 for A6. This distance H8 - H3′ is not sensitive to change in χ if major conformation is S conformation i.e. P_S = 126° - 162°.

However for $P_S = 117^\circ$, $\chi_S = 0.80$, lower χ values only fits better. The distance H6 - H3′ (Fig. 5.14 (c)) vary in similar way. The intense peak H6 - H3′ for C5 residue (Fig. 5.6 (c) and Table 5.11) suggests high anti conformation.

Hence all the observed relative intensities of NOE cross peaks for base to sugar distances suggest anti conformation for T1 and G2 residue and perhaps a high anti conformation for A3, T4, C5 and A6 residues.

INTERACTION OF DAUNOMYCIN WITH DEOXYHEXANUCLEOTIDE d-(TGATCA)$_2$

Interaction of daunomycin with deoxyhexanucleotide d-(TGATCA)$_2$ is investigated using one-dimensional and two-dimensional proton NMR techniques. Titration studies on daunomycin-d-(TGATCA)$_2$ complex are carried out by adding 10 μl of daunomycin in steps from a stock solution of 32.66 mM concentration to 0.4 ml of d-(TGATCA)$_2$ sample of 3.68 mM concentration . In the final step, 90 μl of drug is added so that the drug to hexamer duplex concentration ratio is 2:1. Figs. 6.1 (a-g) show the 1D NMR spectra recorded at various drug/DNA ratios in D_2O at 295 K. The chemical shifts of some of the daunomycin and hexamer protons are plotted as a function of drug/DNA (duplex) concentration ratio (Figs. 6.2 (a,b)). The expansions of particular regions of 1D NMR spectra of 2:1 daunomycin-d-(TGATCA)$_2$ complex at different temperatures are shown in Figs. 6.3 (a-d). Chemical shifts of some of the hexamer and daunomycin protons as a function of temperature are shown in Figs. 6.4 (a,b). 2D phase-sensitive double quantum filter COSY spectra is recorded on this complex but due to broad signals present in 1D NMR spectra it could not resolve amongst them and thus is not helpful in spectral assignment. 2D phase-sensitive NOESY spectra on 2:1 daunomycin-d-(TGATCA)$_2$ complex are recorded with different mixing times (τ_m) i.e. 350, 200, 150, 75 and 50 ms at 295 K in D_2O.

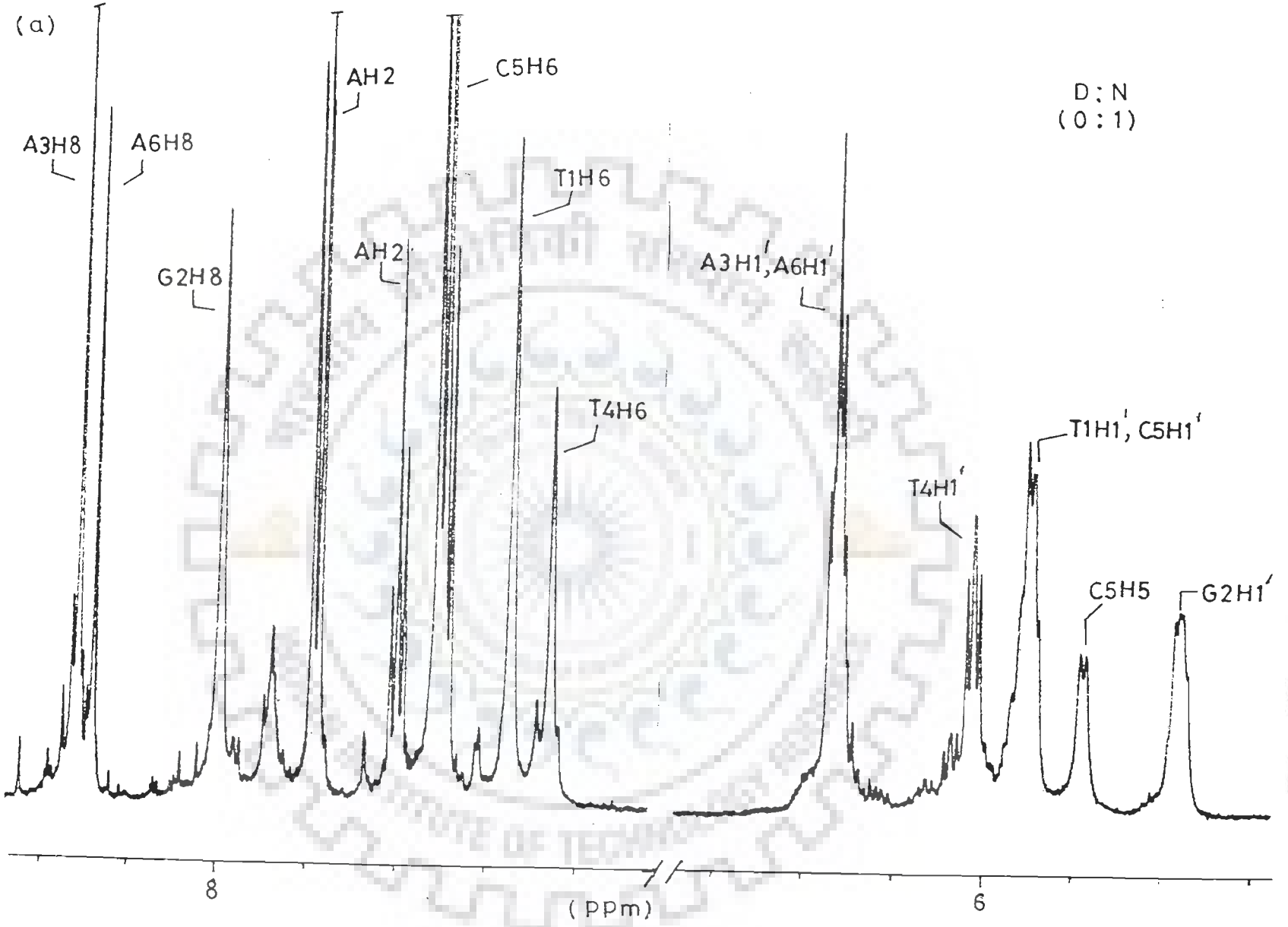

Fig. 6.1(a-g) : 1D proton NMR spectra of d-$(TGATCA)_2$ + daunomycin complex in D_2O at various drug/ DNA (D/N) ratios (295 K).

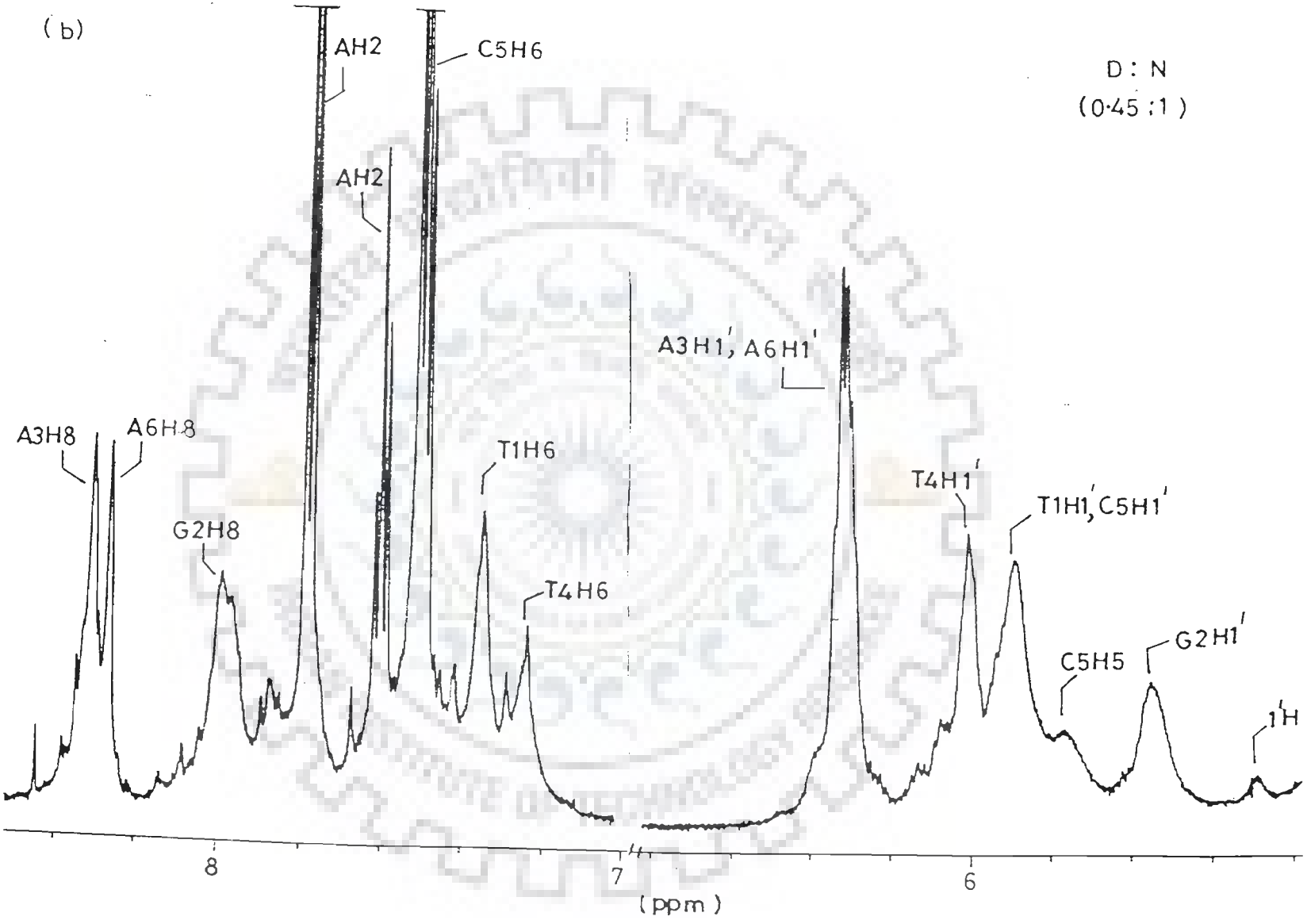
(b)
AH2
C5H6
AH2
D : N
(0·45 : 1)
A3H1', A6H1'
A3H8
A6H8
T1H6
T4H1'
T1H1', C5H1'
G2H8
T4H6
C5H5
G2H1'
1'H
8
7
6
(ppm)

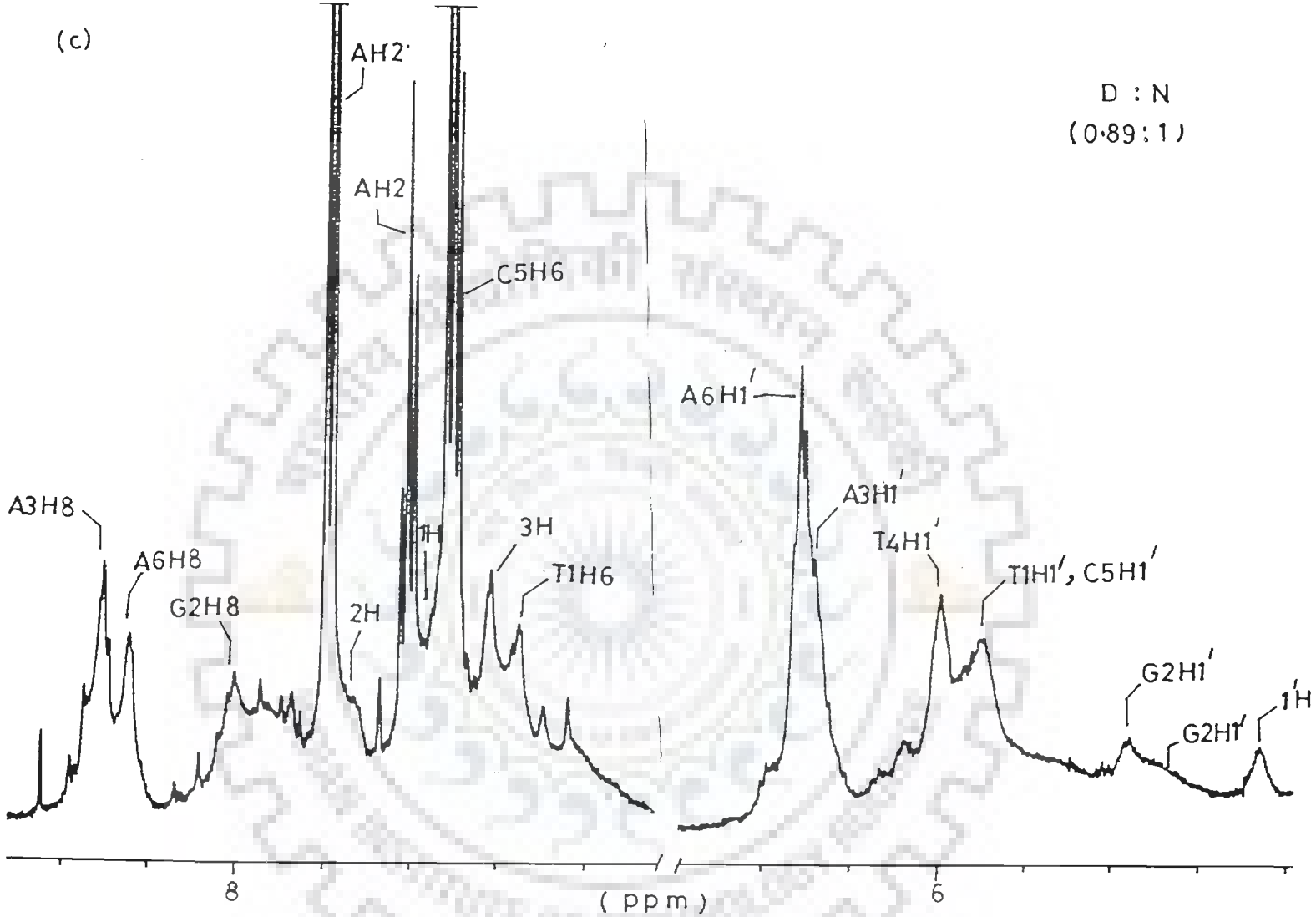
(c)
D : N
(0·89 : 1)
AH2'
AH2
C5H6
A6H1'
A3H8
A6H8
G2H8
2H
1H
3H
T1H6
A3H1'
T4H1'
T1H1', C5H1'
G2H1'
G2H1'
1'H
8
(ppm)
6

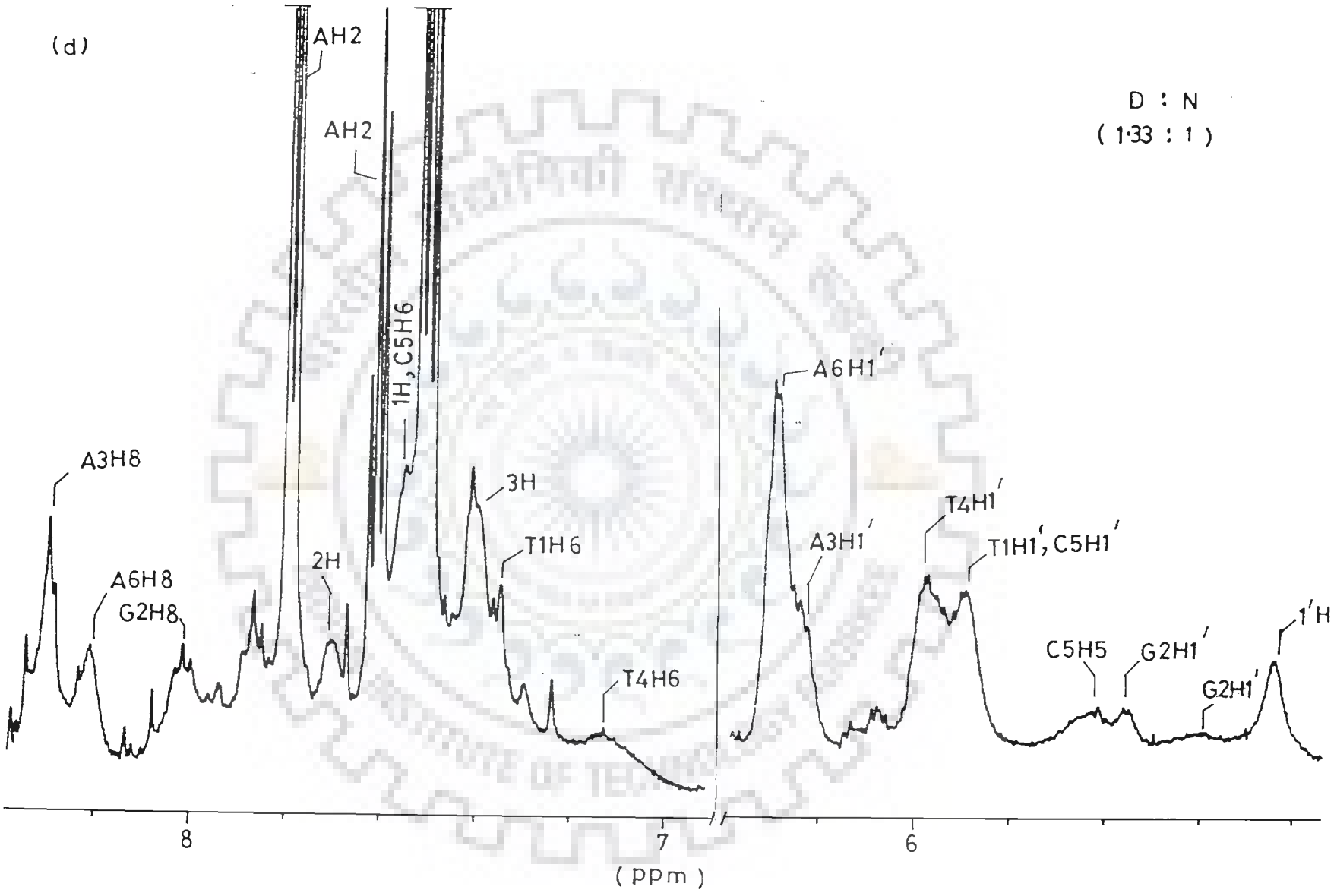
(d)
AH2
AH2
1H, C5H6
D : N
(1·33 : 1)
A6H1′
A3H8
3H
T4H1′
A3H1′
T1H6
T1H1′, C5H1′
2H
A6H8
G2H8
1′H
C5H5
G2H1′
G2H1′
T4H6
8
7
6
(ppm)

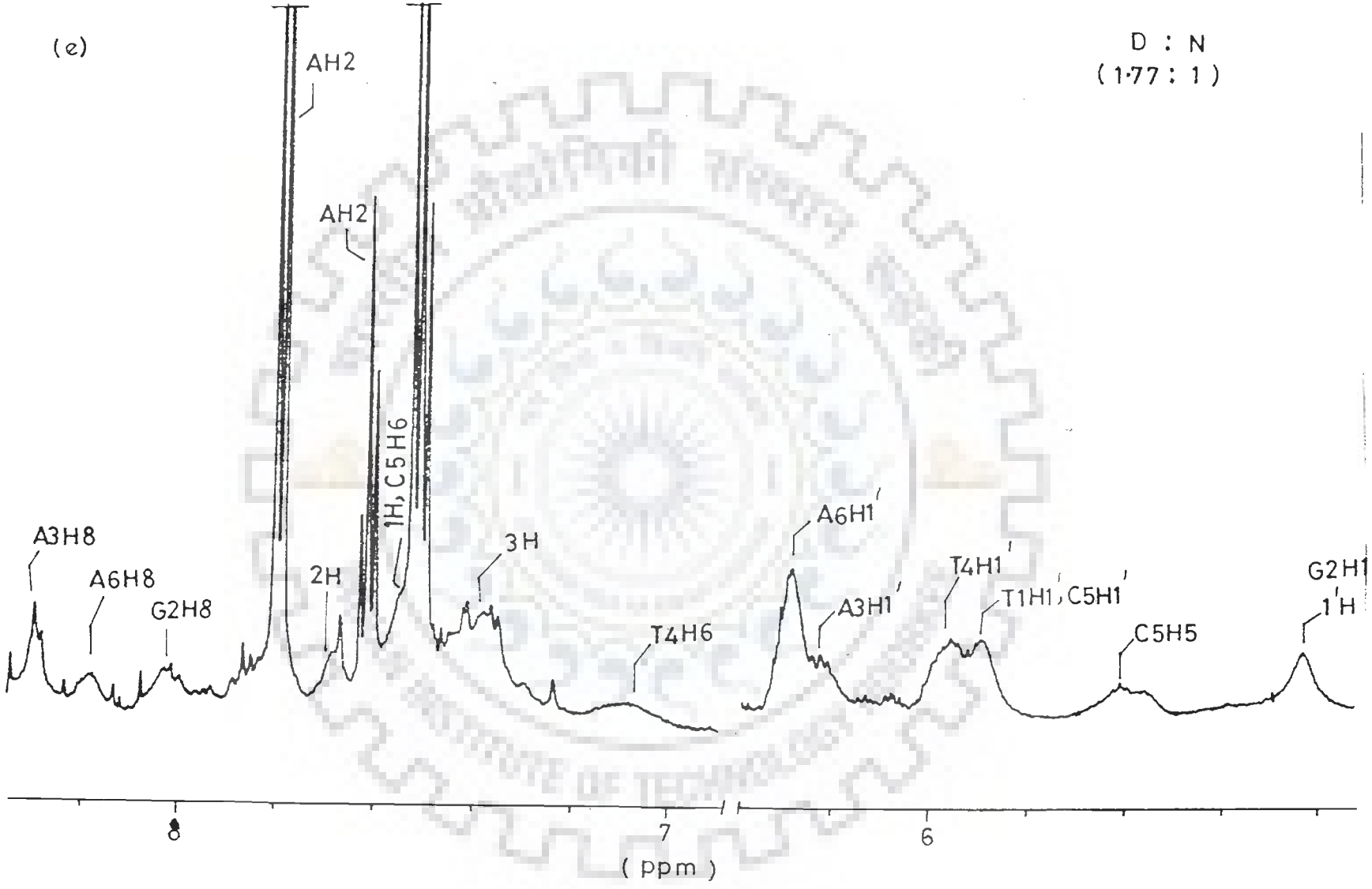
(e)
D : N
(1·77 : 1)
AH2
AH2
1H, C5H6
A3H8
A6H8
G2H8
2H
3H
A6H1'
T4H1'
A3H1'
T1H1', C5H1'
C5H5
G2H1'
1'H
T4H6
8
7
6
(ppm)

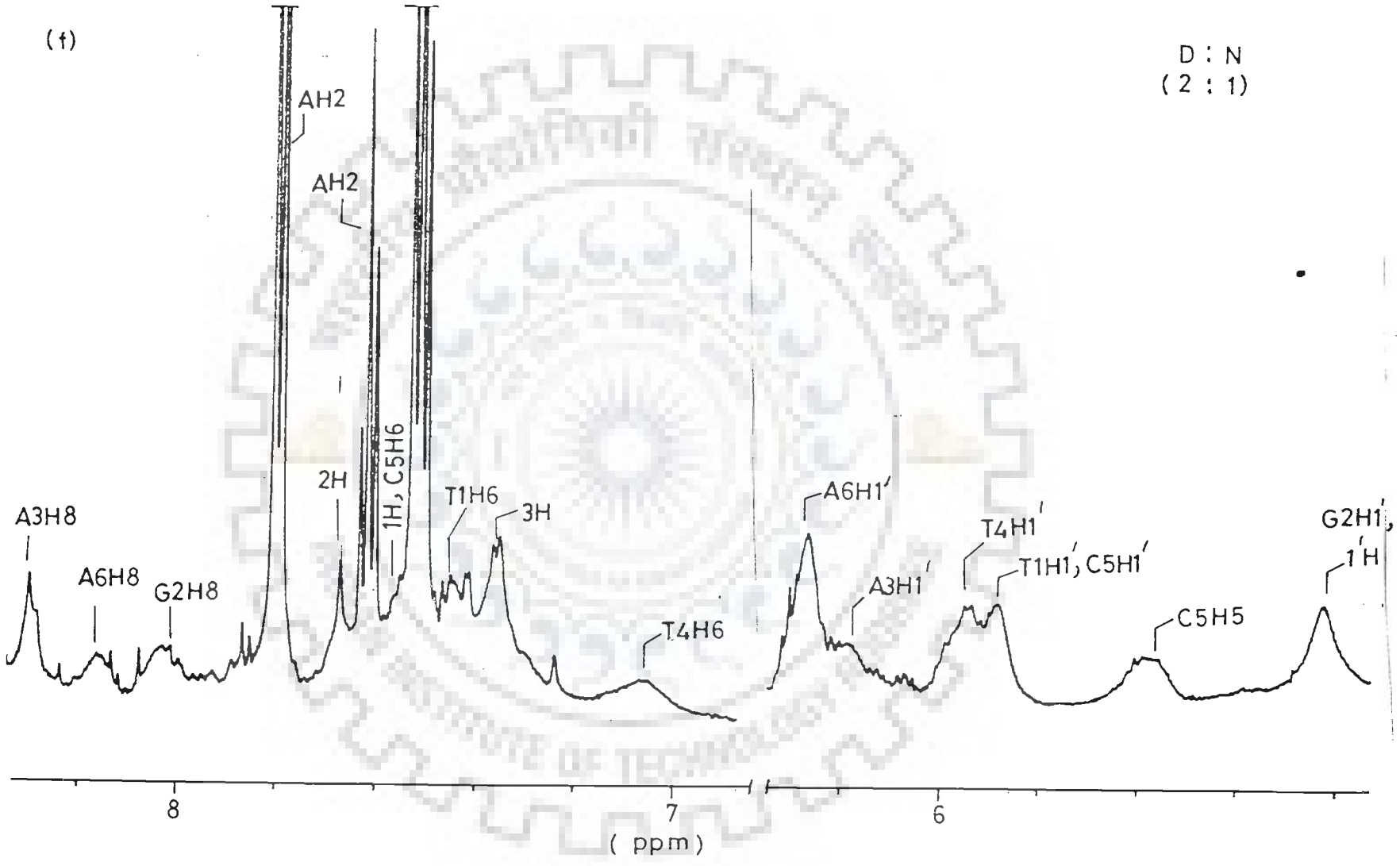
(f)
D : N
(2 : 1)
AH2
AH2
2H
1H, C5H6
T1H6
3H
A3H8
A6H8
G2H8
T4H6
A6H1'
A3H1'
T4H1'
T1H1', C5H1'
C5H5
G2H1',
1'H
8
7
6
(ppm)

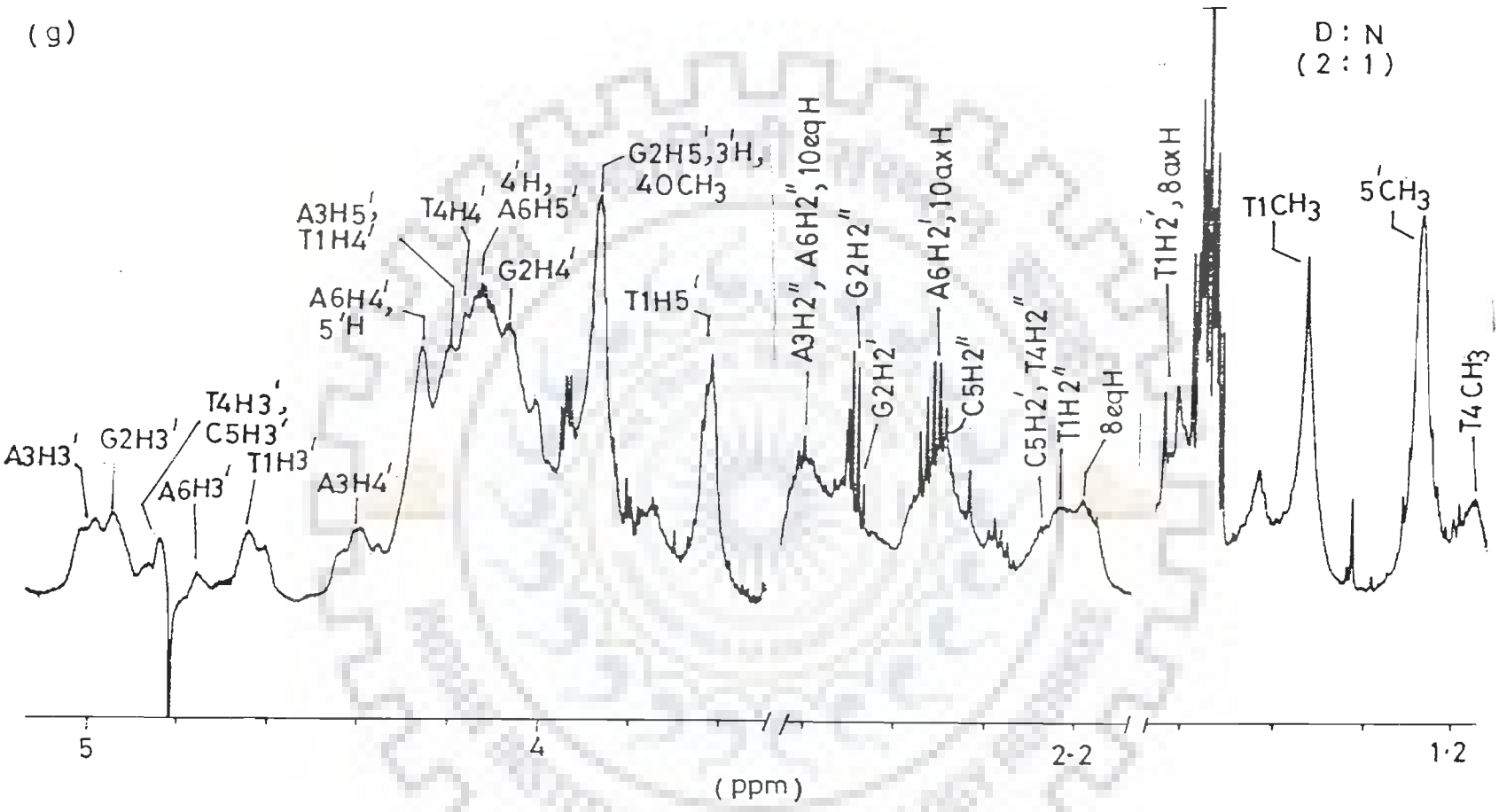
(g)
D : N
(2 : 1)
A3H3'
G2H3'
A6H3'
T4H3',
C5H3'
T1H3'
A3H4'
A3H5',
T1H4'
T4H4'
4'H,
A6H5'
G2H4'
A6H4',
5'H
T1H5'
G2H5',3'H,
4OCH3
A3H2'', A6H2'', 10eqH
G2H2''
G2H2'
A6H2',10axH
C5H2''
C5H2', T4H2''
T1H2''
8eqH
T1H2', 8axH
T1CH3
5'CH3
T4CH3
5
4
2·2
1·2
(ppm)

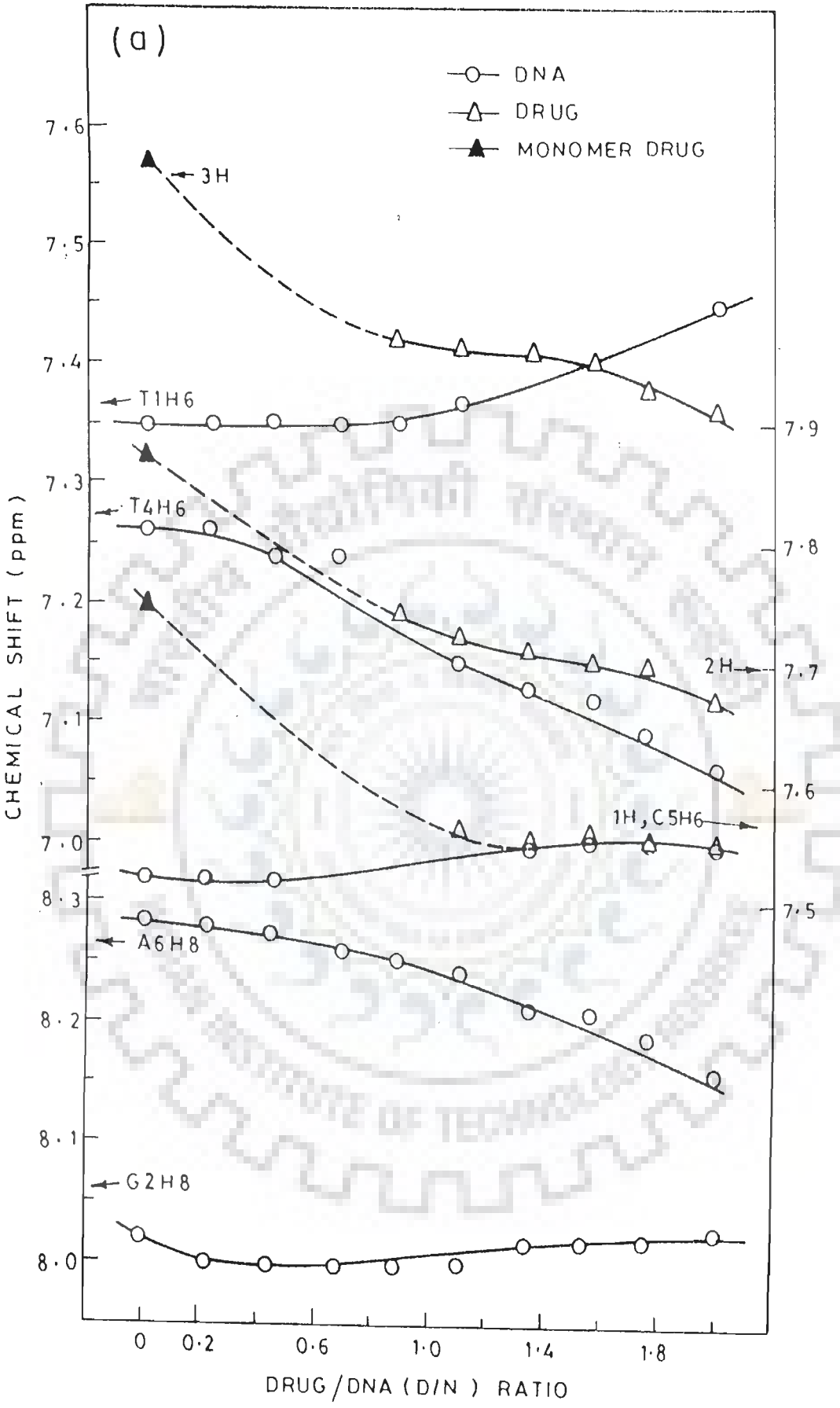

Fig. 6.2(a,b) : Chemical shift of various protons of d-$(TGATCA)_2$ and daunomycin at various drug/DNA (D/N) ratios.

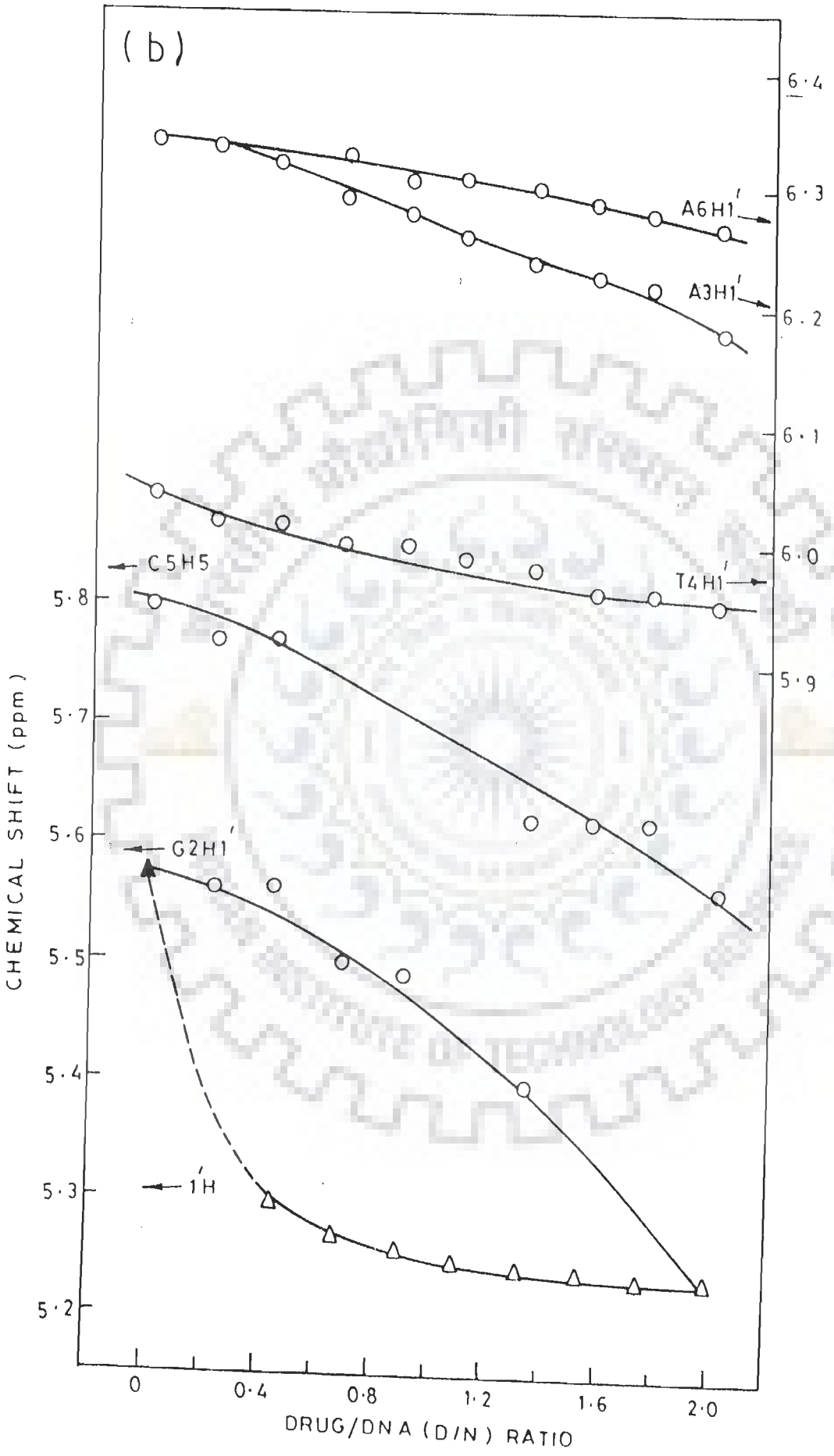
(b)
A6H1'
A3H1'
C5H5
T4H1'
G2H1'
1'H
6·4
6·3
6·2
6·1
6·0
5·9
5·8
5·7
5·6
5·5
5·4
5·3
5·2
CHEMICAL SHIFT (ppm)
0
0·4
0·8
1·2
1·6
2·0
DRUG/DNA (D/N) RATIO

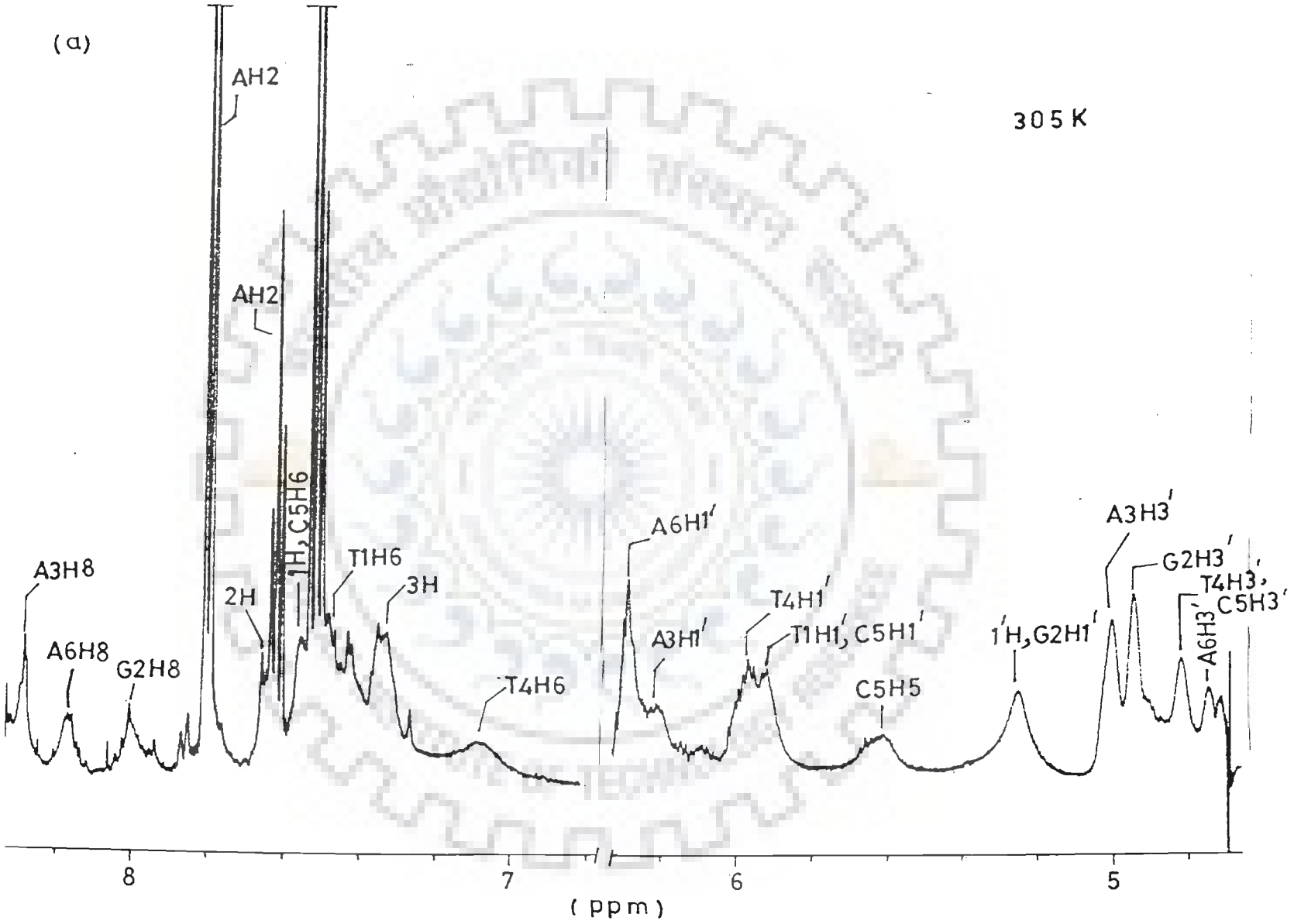

Fig. 6.3 (a-d) : 1D proton NMR spectra of d-$(TGATCA)_2$ + daunomycin complex (2:1) in D_2O at different temperatures.

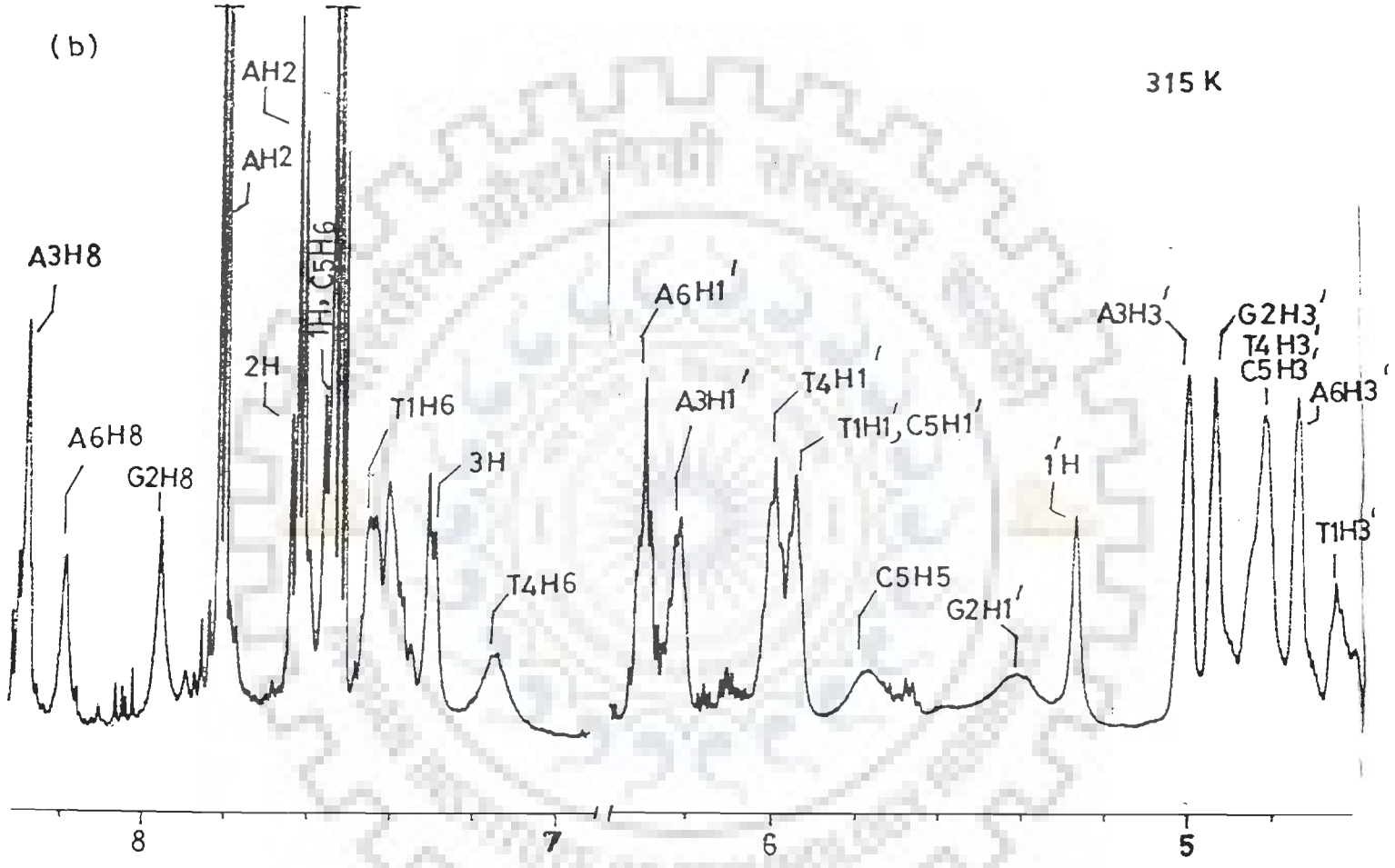
(b)
315 K
AH2
AH2
A3H8
1H, C5H6
2H
A6H8
G2H8
T1H6
3H
T4H6
A6H1'
A3H1'
T4H1'
T1H1', C5H1'
C5H5
G2H1'
1'H
A3H3'
G2H3'
T4H3',
C5H3'
A6H3'
T1H3'
8
7
6
5
(ppm)

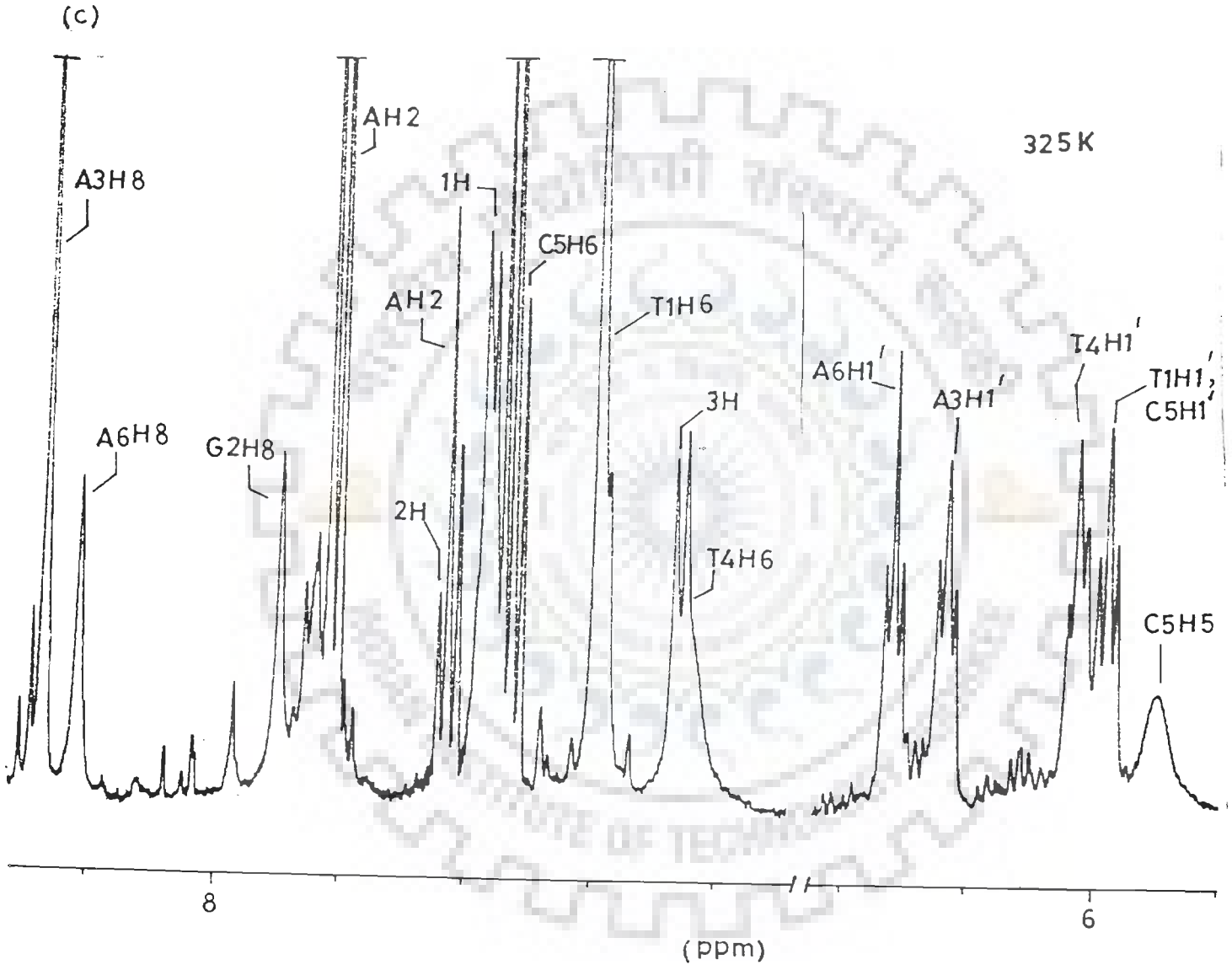
(c)
325 K
A3H8
A6H8
G2H8
AH2
AH2
2H
1H
C5H6
T1H6
3H
T4H6
A6H1'
A3H1'
T4H1'
T1H1',
C5H1'
C5H5
8
6
(ppm)

(d) 325K

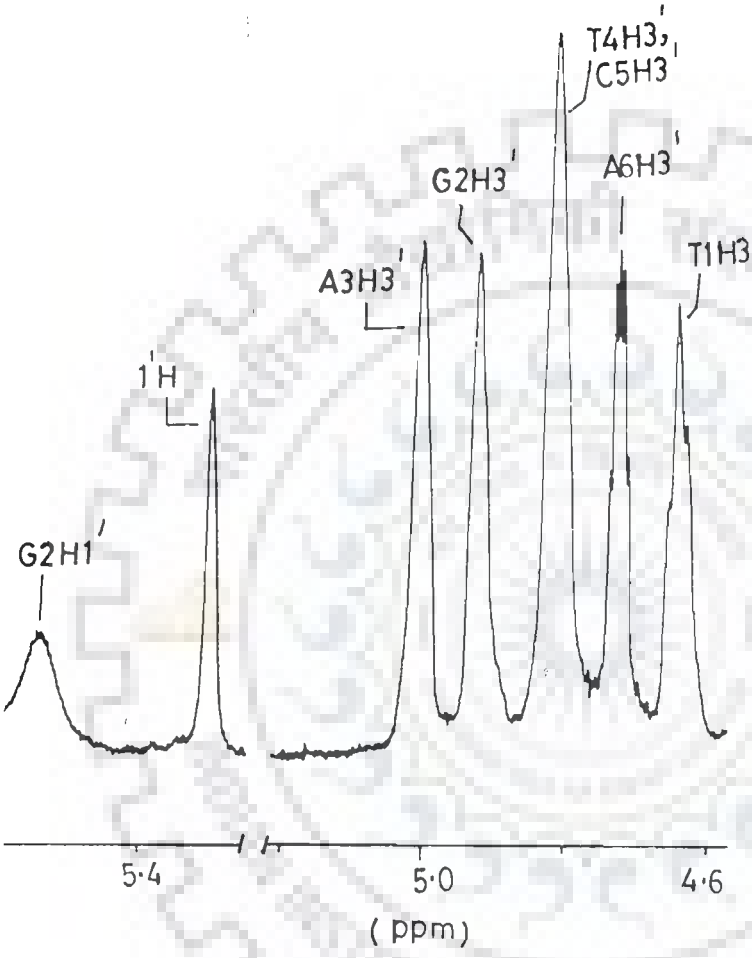

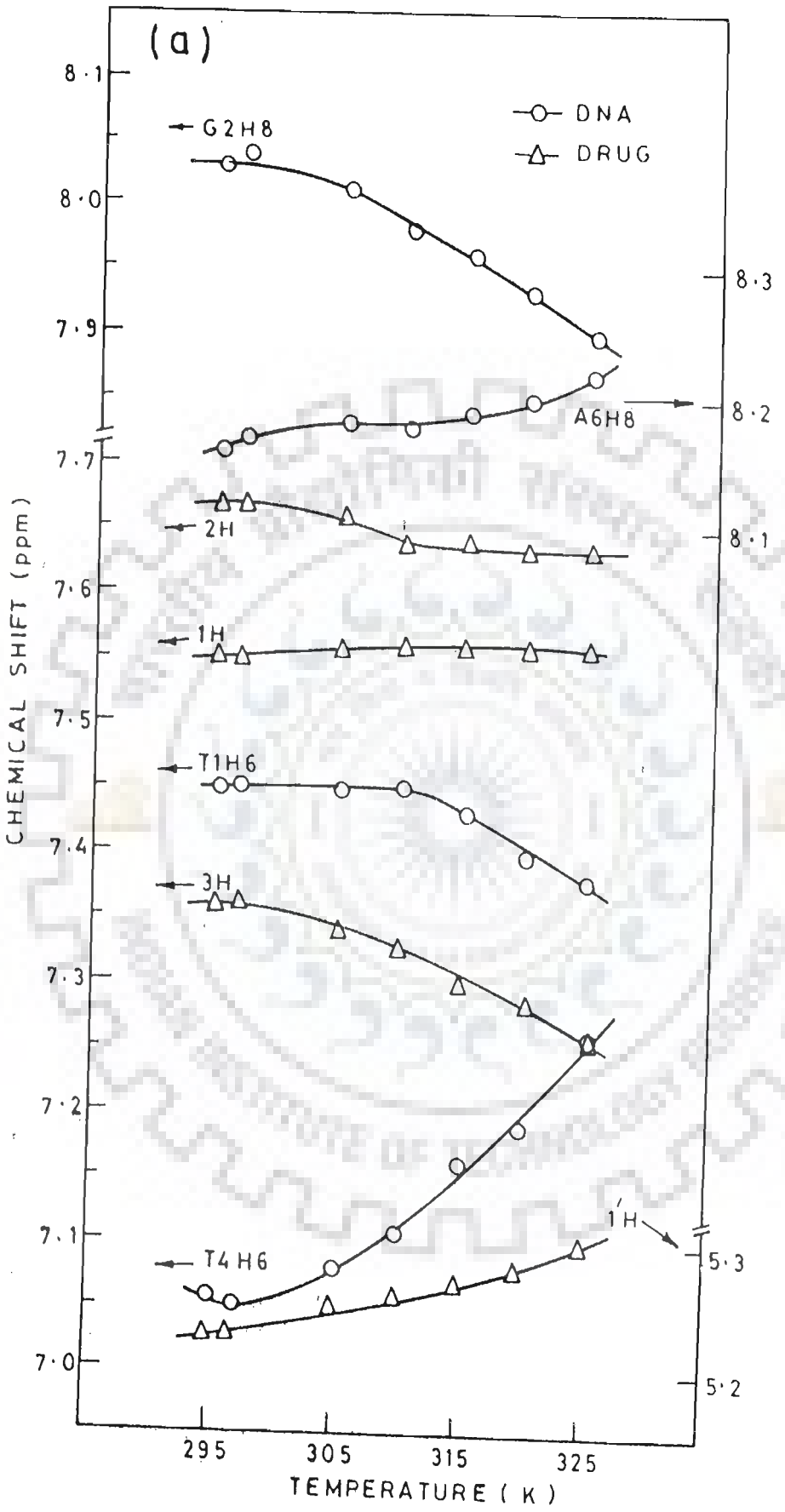

Fig. 6.4(a,b) : Chemical shift of various protons of d-$(TGATCA)_2$ and daunomycin at different temperatures in the range (295 K-325 K)

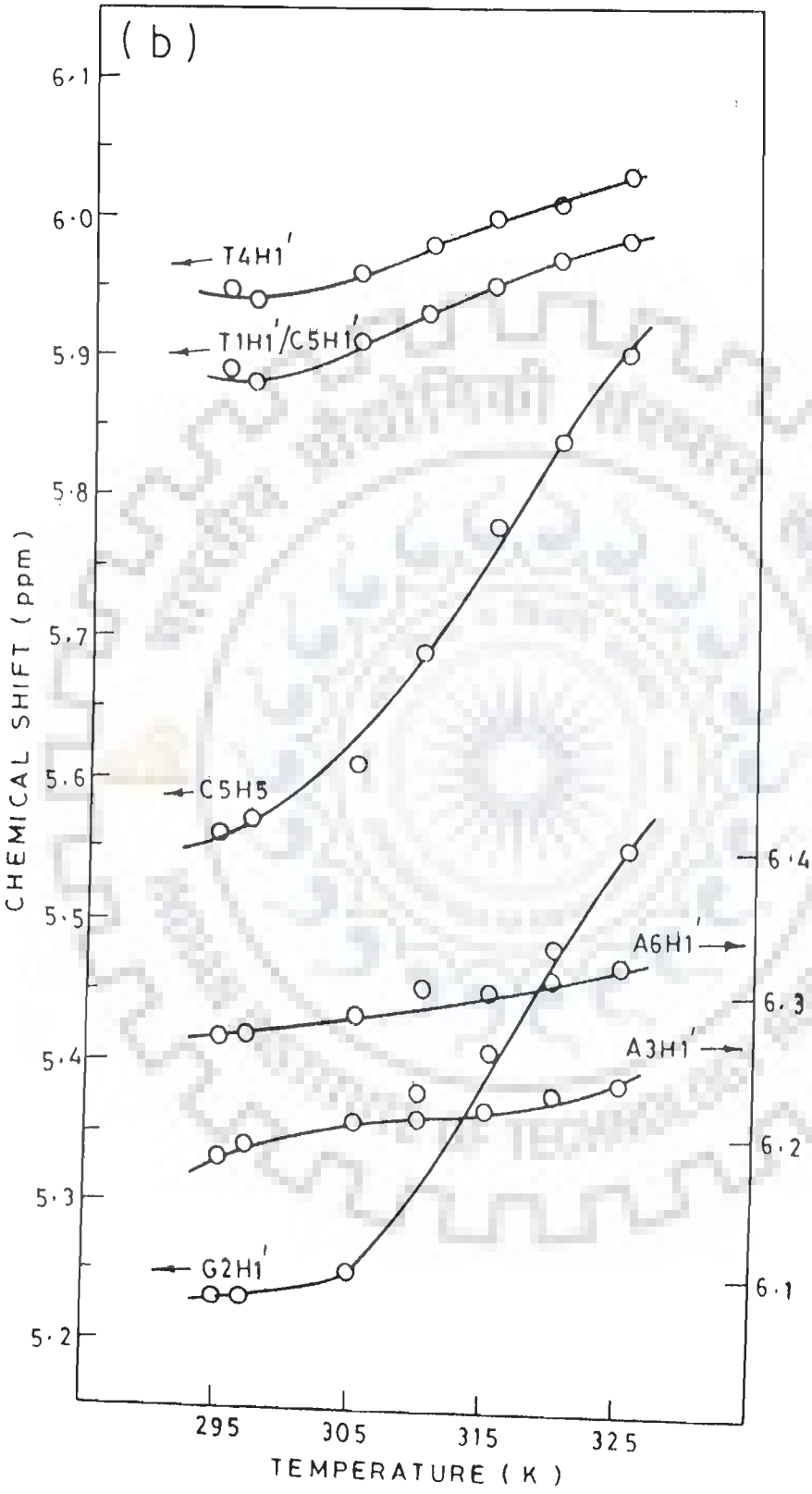
(b)
6·1
6·0
5·9
5·8
5·7
5·6
5·5
5·4
5·3
5·2
CHEMICAL SHIFT (ppm)
T4H1'
T1H1'/C5H1'
C5H5
A6H1'
A3H1'
G2H1'
6·4
6·3
6·2
6·1
295
305
315
325
TEMPERATURE (K)

Figs. 6.5 (a-g) show the expansions of various regions of 350 ms NOESY spectra of daunomycin-d-$(TGATCA)_2$ complex.

SPECTRAL ASSIGNMENT

Spectral Assignment of d-$(TGATCA)_2$

The resonance positions of different hexamer protons are assigned using standard strategies available in literature [33,44,50,65,75,114] for sequential assignment in right handed B-DNA geometry. The base protons H8, H6 appear in the range 7.0 - 8.4 ppm (Fig. 6.1 (f)). The H1′ resonances are observed between 5.2 - 6.4 ppm and the H3′, H4′, H5′, H5", H2′, H2", CH_3 protons resonate in the range 1.2 - 5.1 ppm (Fig. 6.1(g)).

Fig. 6.5(b) shows all the six sets of H2′ - H2" NOE connectivities. Their corresponding H1′ and H3′ resonances are identified by H1′ - H2′, H2" and H3′ - H2′, H2" connectivities, respectively (Fig. 6.5 (c)). The H3′ protons show NOE cross peaks with their corresponding H4′ proton and H4′ is further coupled to its corresponding H5′ proton (Fig. 6.5(d)). Thus, six sets of sugar proton resonances are assigned. Several additional intra sugar NOE connectivities are observed such as H1′ - H4′, H1′ - H3′, H2′ - H4′ and H2" - H4′ (Figs. 6.5(c,d)) for some of the residues, which are used in further analysis. The base resonance at 7.57 ppm gives intense NOE cross peak with proton resonating at 5.58 ppm and are therefore assigned to C5H6 and C5H5 protons, respectively (Fig. 6.5(d)). Two methyl resonances at 1.55 and 1.20 ppm give intense NOE cross peaks with the base protons at

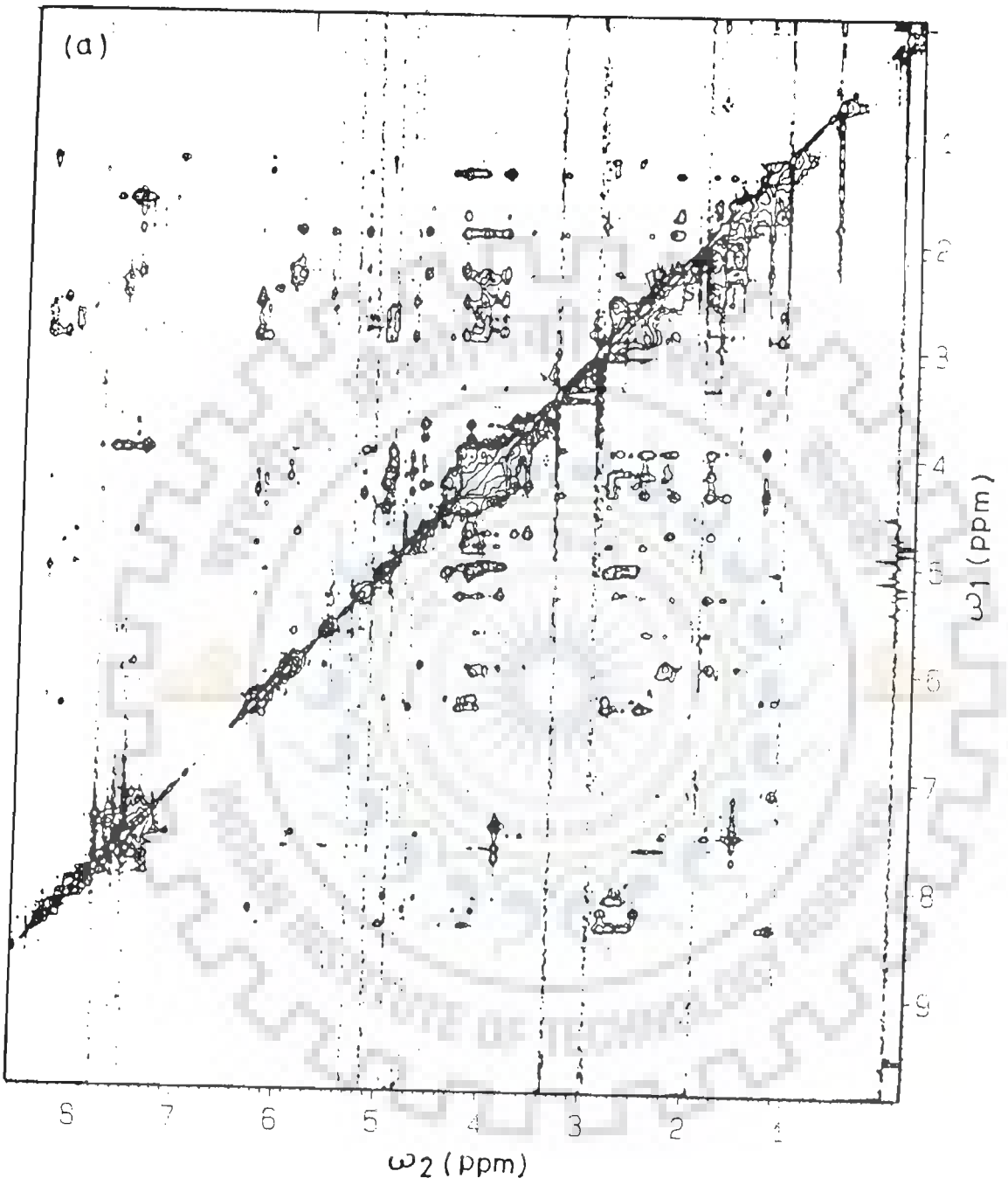

Fig. 6.5(a-g) : Phase-sensitive NOESY spectrum (at τ_m 350 ms) of d-$(TGATCA)_2$ + daunomycin complex highlighting specific NOE connectivities in D_2O at 295 K.

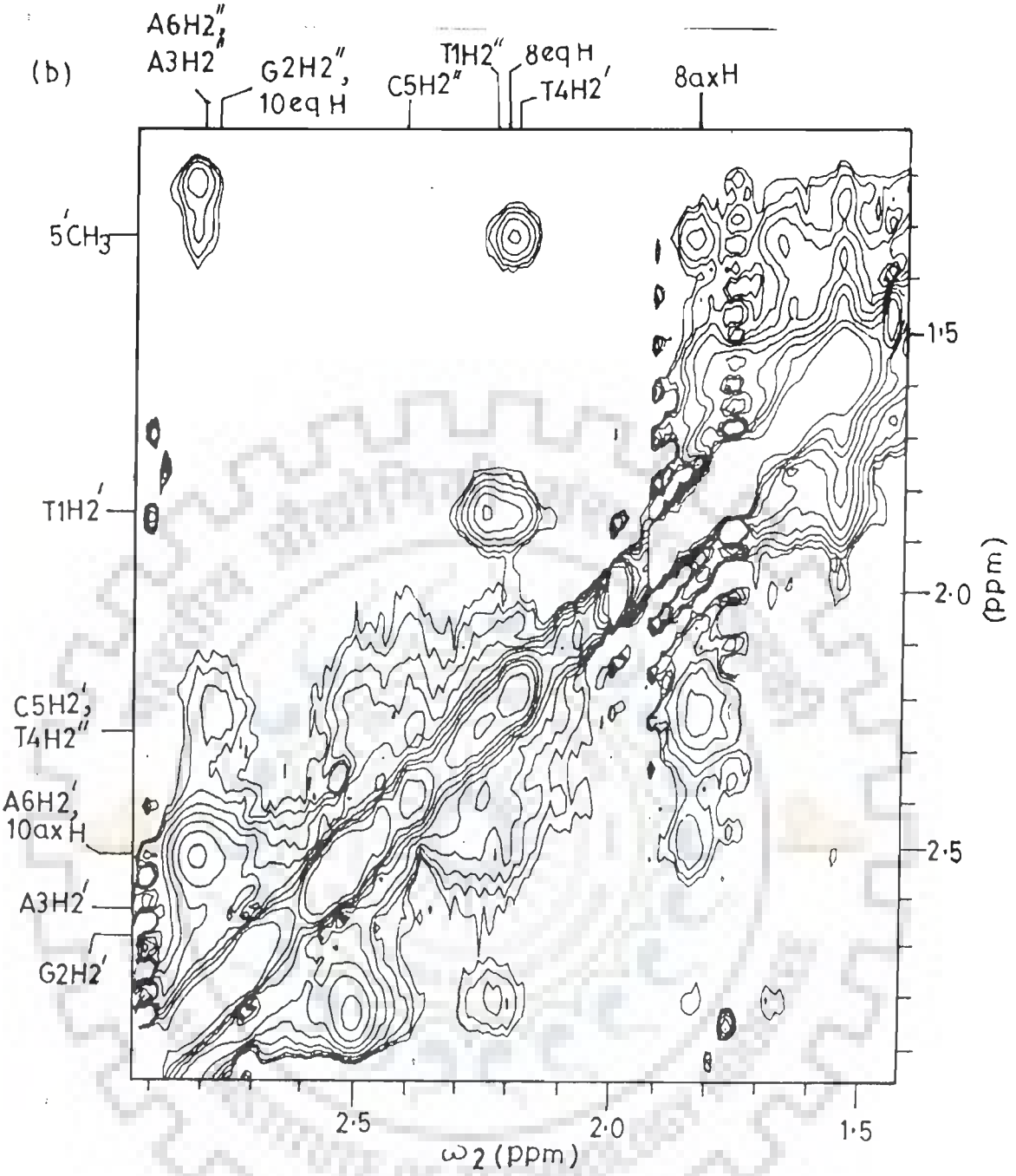
(b)
A6H2″, A3H2
G2H2″, 10eq H
C5H2″
T1H2″
8eq H
T4H2′
8axH
5′CH3
T1H2′
C5H2′, T4H2″
A6H2′, 10ax H
A3H2′
G2H2′
1·5
2·0
2·5
(ppm)
2·5
2·0
1·5
ω2 (ppm)

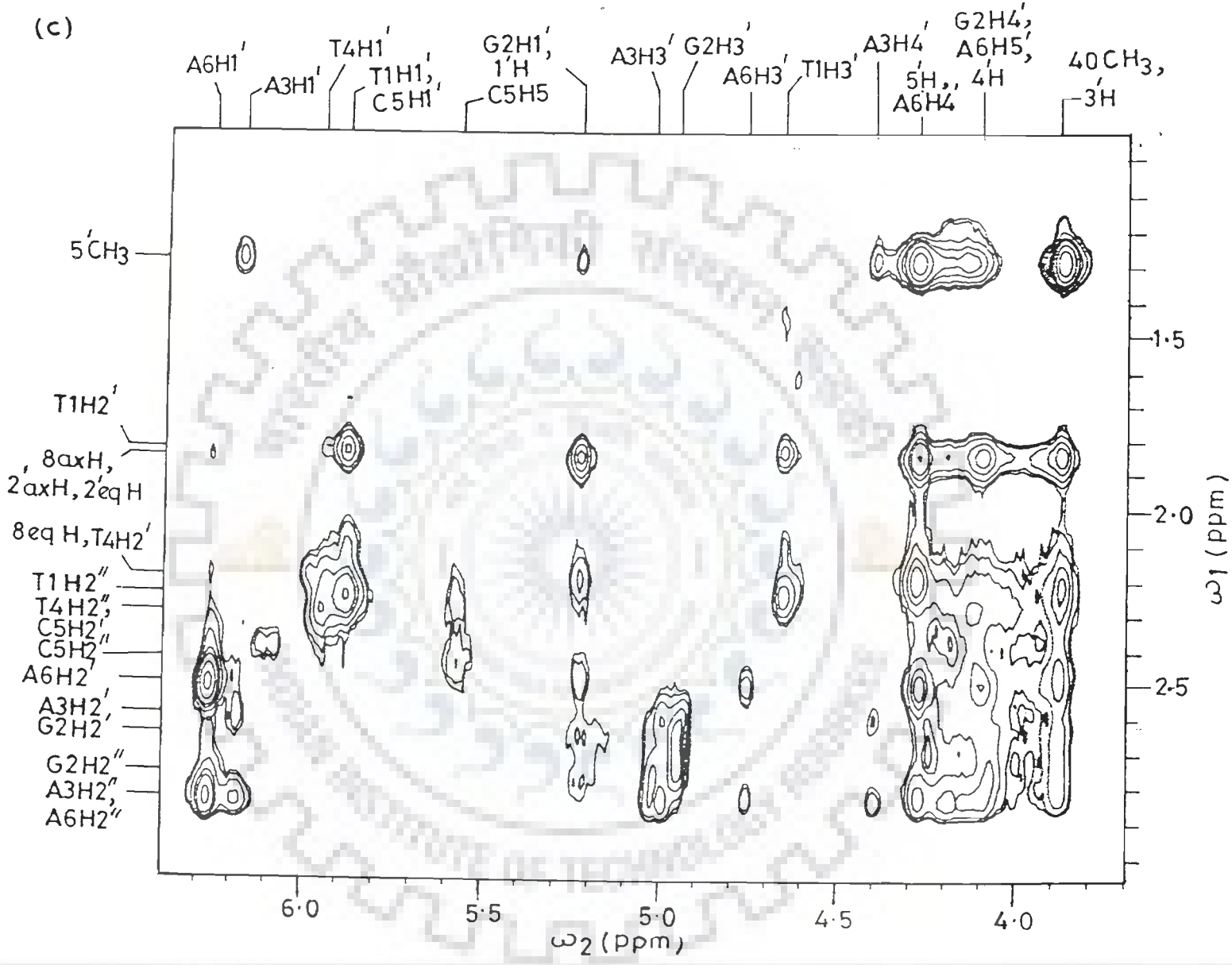
(c)
A6H1'
A3H1'
T4H1'
T1H1', C5H1'
G2H1', 1'H C5H5
A3H3'
G2H3'
A6H3'
T1H3'
A3H4'
5'H, A6H4
G2H4', A6H5', 4'H
40CH3, 3'H
5'CH3
T1H2'
, 8axH, 2'axH, 2'eq H
8eq H, T4H2'
T1H2''
T4H2'', C5H2'
C5H2''
A6H2'
A3H2', G2H2'
G2H2''
A3H2'', A6H2''
6·0
5·5
5·0
4·5
4·0
ω2 (ppm)
1·5
2·0
2·5
ω1 (ppm)

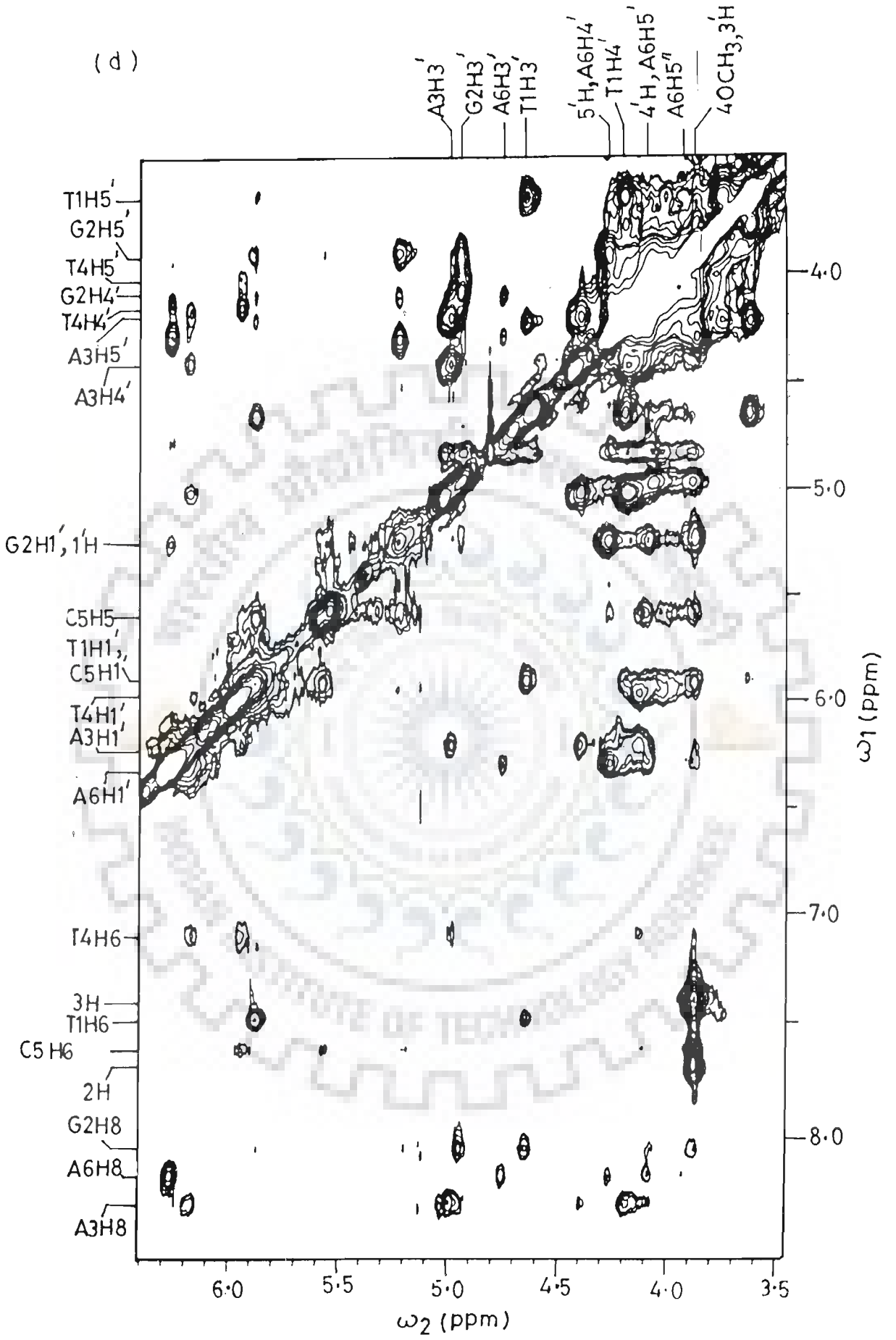
(d)
A3H3′
G2H3′
A6H3′
T1H3′
5′H,A6H4′
T1H4′
4′H,A6H5′
A6H5″
4OCH3,3′H
T1H5′
G2H5′
T4H5′
G2H4′
T4H4′
A3H5′
A3H4′
G2H1′,1′H
C5H5
T1H1′,
C5H1′
T4H1′,
A3H1′
A6H1′
T4H6
3H
T1H6
C5H6
2H
G2H8
A6H8
A3H8
4·0
5·0
6·0
7·0
8·0
ω1 (ppm)
6·0
5·5
5·0
4·5
4·0
3·5
ω2 (ppm)

7.46 and 7.07 ppm, respectively. These are assigned to thymine methyl and H6 protons (Figs. 6.5(e,f)).

The sets of sugar protons so identified are assigned to their respective bases in sequence on the basis of base - H2′, H2" NOE connectivities. Each base proton is expected to give intranucleotide cross peaks with its corresponding H2′/H2" and internucleotide cross peaks with H2′/H2" protons of the preceeding residue. The thymine resonance at 7.46 ppm gives NOE connectivity with one pair of H2′, H2" sugar protons and is therefore assigned to the T1 residue i.e. the terminal one at 5′ end. The other thymine resonance at 7.07 ppm gives intranucleotide cross peak with its H2" proton and internucleotide cross peaks with H2′, H2" protons of the preceeding residue i.e A3 (Figs. 6.5(e,f), Table 6.1). The three H8 resonances correspond to the base protons of the G2, A3 and A6 residues. The A3H8 gives NOE cross peak with T4CH_3 showing its proximity (Figs. 6.5(e,f)). The A3H8 gives internucleotide NOE connectivities with H2′, H2" pair of G2 residue. Thus resonance at 8.07 ppm gets assigned to G2H8 and the remaining H8 resonance is assigned to A6H8 (Figs. 6.5 (e,f)).

It may be noted that although all resonances have been assigned unambiguously we did not observe the following internucleotide NOE connectivities :

G2H8 - T1H2′

G2H8 - T1H2"

A6H8 - C5H2′

A6H8 - C5H2"

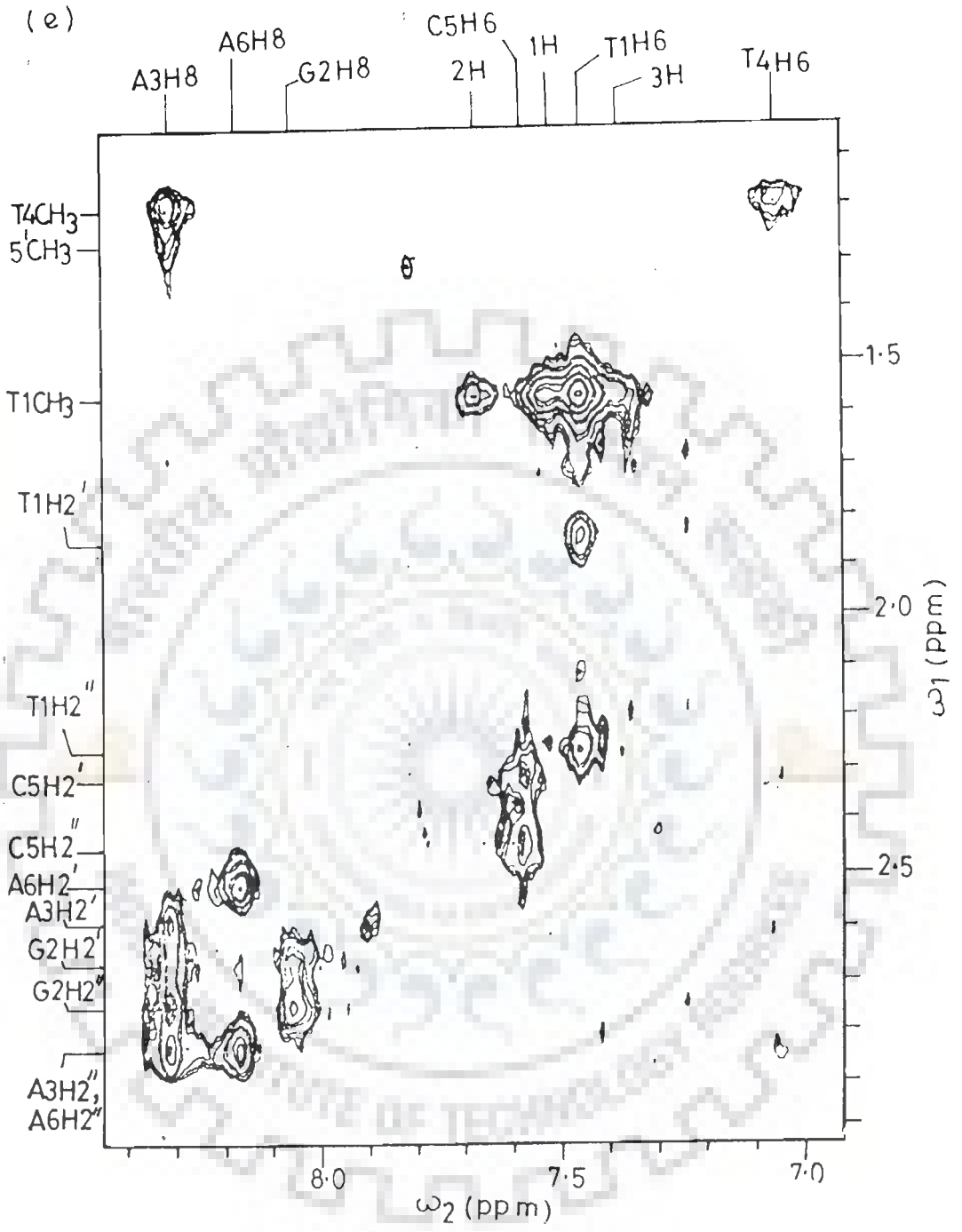
(e)
A3H8
A6H8
G2H8
C5H6
2H
1H
T1H6
3H
T4H6
T4CH3
5'CH3
T1CH3
T1H2'
T1H2''
C5H2'
C5H2''
A6H2'
A3H2'
G2H2'
G2H2''
A3H2'',
A6H2''
1·5
2·0
2·5
ω1 (ppm)
8·0
7·5
7·0
ω2 (ppm)

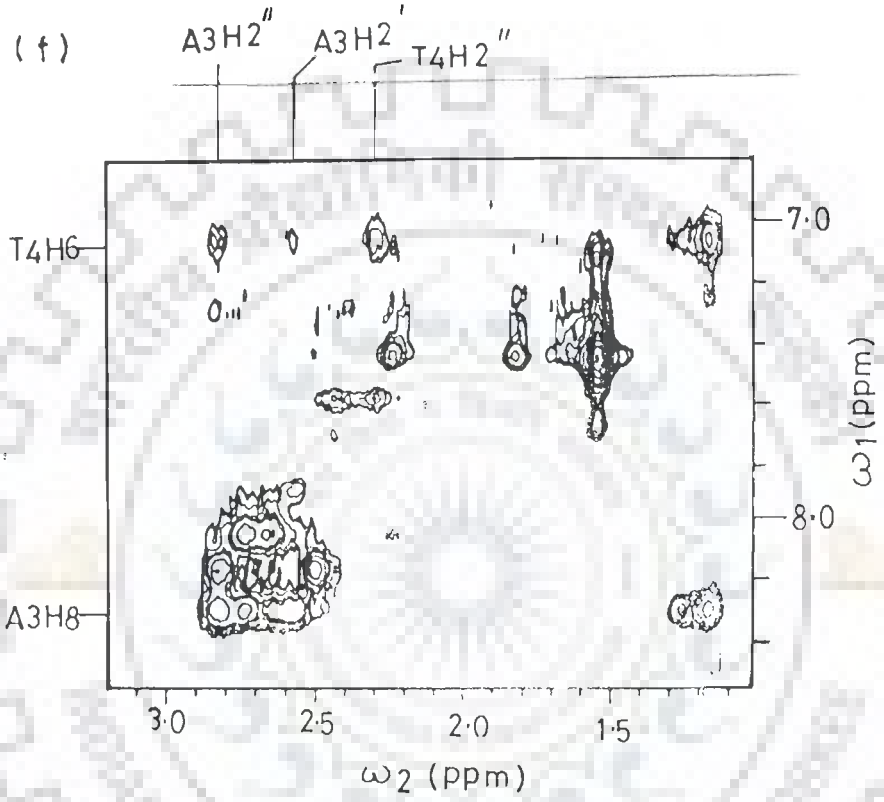
(f)
A3H2''
A3H2'
T4H2''
T4H6
A3H8
7·0
8·0
ω1(ppm)
3·0
2·5
2·0
1·5
ω2 (ppm)

(g)

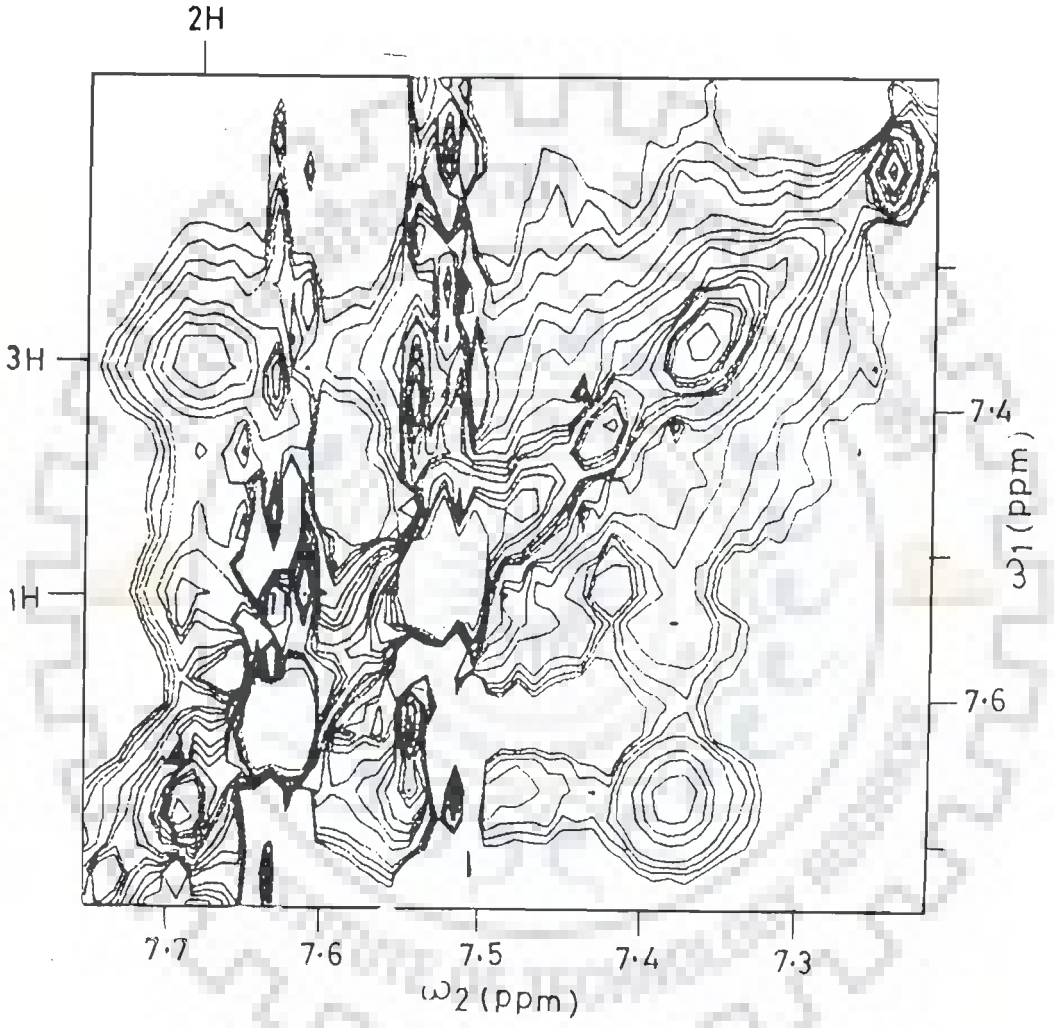

(h)

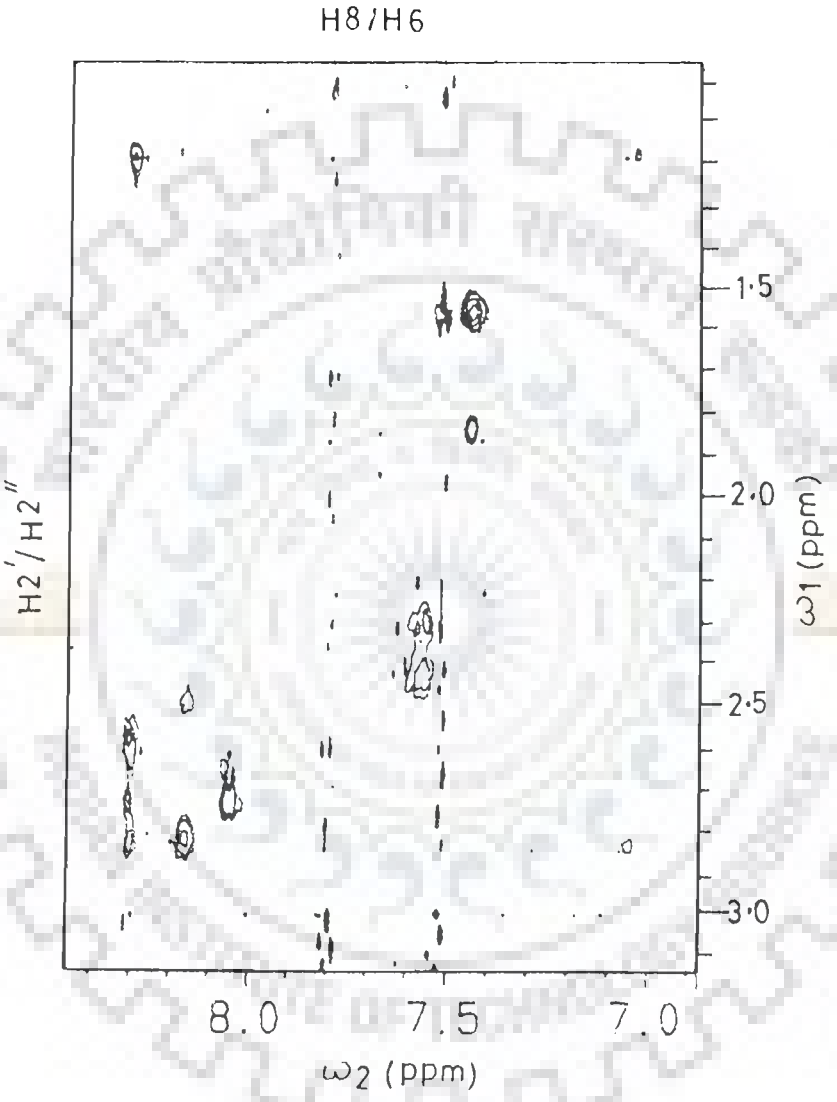

Fig. 6.5 (h) : Phase-sensitive NOESY spectrum (at τ_m 75 ms) of d-$(TGATCA)_2$ + daunomycin complex showing intra and inter-residue base -H2'/H2" NOE connectivites.

Table 6.1 : Presence of inter-residue (sequential) NOE cross peaks of d-$(TGATCA)_2$ on complex formation as observed in phase - sensitive NOESY spectra (τ_m = 350 ms).

C5H6 - T4H1′
C5H5 - T4H4′
C5H5 - T4H5′
T4H6 - A3H2′
T4H6 - A3H2"
T4H6 - A3H1′
T4H6 - A3H3′
$T4CH_3$ - A3H8
A3H8 - G2H2′
A3H8 - G2H2"
A3H8 - G2H3′
G2H8 - T1H3′

This may be due to intercalation of daunomycin at 5′ - TpG - 3′ site.

Several additional inter residue base - H3′, base - H1′, base - H4′ and base - H5′ connectivities are also observed which further confirm the assignment (Fig. 6.5(d)). The chemical shift positions of all protons thus unambiguously assigned are listed in Table 6.2.

Spectral assignment of daunomycin protons

The resonances of 1H, 2H and 3H protons of ring D of daunomycin are expected in the range 7.30 - 7.70 ppm. The proton at 7.69 ppm gives two NOE cross peaks with the resonances at 7.55 and 7.36 ppm and is thus assigned to 2H proton (Fig. 6.5(g)). Further the resonances at 7.55 and 7.36 ppm are assigned to 1H and 3H protons, respectively. The 1H, 2H and 3H protons are expected to give NOE cross peaks with $4OCH_3$ protons of ring D. Fig. 6.5(d) shows that 2H and 3H give NOE with a resonance at 3.88 ppm which is therefore assigned to $4OCH_3$ protons.

Daunosamine sugar protons 1′H and $5'CH_3$ are easily recognisable due to their very different resonating positions than other protons. The intense signal at 1.29 ppm gives NOE cross peak with the resonance at 4.27 ppm which are assigned as $5'CH_3$ and 5′H protons, respectively (Fig. 6.5(c)). The 5′H proton is coupled to resonance at 4.10 ppm which is assigned to 4′H proton of daunosamine sugar (Fig. 6.5(d)). The 4′H resonance is coupled to 3′H proton which is further coupled to 2′axH and 2′eqH protons.

Table 6.2 : The chemical shift δ (in ppm) of various protons of d-$(TGATCA)_2$ on complexation with daunomycin in D_2O at 295 K.

Proton	T1	G2	A3	T4	C5	A6
H6/H8	7.46	8.07	8.32	7.07	7.57	8.18
H1′	5.88	5.22	6.18	5.97	5.88	6.27
H2′	1.83	2.66	2.59	2.19	2.28	2.50
H2"	2.24	2.74	2.83	2.28	2.44	2.83
H3′	4.64	4.94	5.00	4.84	4.84	4.75
H4′	4.20	4.09	4.41	4.13	-	4.27
H5′	3.63	3.89	4.19	4.01	-	4.10
H5"	-	-	-	-	-	3.94
H5/H2/CH_3	1.55	-	-	1.20	5.58	-

This interconnected pathway assigns the resonances at 4.10, 3.88, 1.83 and 1.83 ppm to 4'H, 3'H, 2'axH and 2'eqH protons, respectively (Fig. 6.5(c)). The 2'axH and 2'eqH protons also give NOE connectivities with the 1'H proton of daunosamine sugar resonating at 5.22 ppm. (Fig. 6.5(c)). Thus, all the resonances of daunosamine sugar protons are assigned.

The 5'H and 5'CH_3 protons are found to give NOE cross peaks with two protons resonating at 2.19 and 1.83 ppm (Figs. 6.5(b,c)) which give intense NOE cross peak with each other (Fig. 6.5(b)). These protons are thus assigned to 8axH and 8eqH protons of ring A. Fig. 6.5(b) shows the NOE cross peaks 10axH - 8eqH, 10eqH - 8eqH which assign the protons resonating at 2.50 and 2.78 ppm to 10axH and 10eqH protons of ring A, respectively. The 7H and 9$COCH_3$ protons of ring A could not be assigned specifically. These resonances expected ~ 2.4 ppm and 4.7 ppm appear to be broadened due to interaction of daunomycin with d-$(TGATCA)_2$. The assignment of various resonances to drug protons are further confirmed from 1D NMR spectra recorded on gradual addition of drug during titration studies. Table 6.3 lists the chemical shifts of various protons of daunomycin in D_2O at 295 K in 2:1 daunomycin + d-$(TGATCA)_2$ complex.

TITRATION STUDIES

Expanded regions of one-dimensional proton NMR spectra of daunomycin-d-$(TGATCA)_2$ complex at various drug/DNA concentration ratio showing base H8, H6, H5, drug and H1' resonances are shown in Figs. 6.1 (a-f). It is observed that on addition of 10 μl of

Table 6.3 : The chemical shift δ (in ppm) of daunomycin protons in d-$(TGATCA)_2$ - daunomycin complex at 295 K in D_2O and changes in chemical shift ($\Delta\delta$) (in ppm) on complex formation in daunomycin protons with respect to its monomer position (δ at 355 K)*.

Proton	δ	$\Delta\delta$
1H	7.55	0.20
2H	7.69	0.18
3H	7.36	0.21
4OCH_3	3.88	0.21
10axH	2.50	0.47
10eqH	2.78	0.33
8axH	1.83	0.44
8eqH	2.19	0.22
1'H	5.22	0.35
2'axH	1.83	0.30
2'eqH	1.83	0.30
3'H	3.88	-0.12
4'H	4.10	-0.16
5'H	4.27	0.09
5'CH_3	1.29	0.14

* Monomer position (δ at 355 K, refer to Table 4.2)

(-ve) Sign refers to downfield shift.

(+ve) Sign refers to upfield shift.

daunomycin to DNA hexamer in the first step, i.e. at drug/DNA (duplex) concentration ratio of 0.22:1, several resonances of DNA protons are broadened (spectra not shown here). A new signal due to 5'CH_3 resonance of daunomycin appears at 1.36 ppm. In the complex containing drug to DNA concentration ratio 0.45:1 (Fig. 6.1(b)), the effect of line broadening in several resonances is more pronounced. The G2H8 broadens significantly and the change in C5H6 could not be monitored due to thepresence of an intense spurious peak close to it. The T1H6, T4H6, T4H1', T1H1' and C5H1' protons are also broadened. However, A3H1' and A6H1' resonances still exist as relatively sharp peaks . The C5H5 is the resonance which broadens most in this experiment. Two peaks appear at 7.40 and 5.30 ppm which are found to grow gradually in later experiments as more and more drug is added. These resonances are of 3H and 1'H protons of daunomycin, respectively. A significant observation is the broadening of T4CH_3 spectral line at 1.46 ppm and an increase in the intensity of peak at 1.33 ppm which is due to 5'CH_3 protons of daunomycin (region not shown). In the complex having 0.67 :1 drug to DNA concentration ratio the A3H8, A6H8, T1H6 and T4H6 proton resonances broaden further. The multiplet structure of all H1' resonances, including A3H1', A6H1' also disappear (spectra not shown). The C5H5 proton broadens beyond recognition. The intensity of 1'H and 3H protons of daunomycin has increased further. The 2H proton of daunomycin also starts emerging at 7.75 ppm as a shoulder of AH2 resonance. In the complex containing 0.89:1 drug to DNA concentration ratio further

broadening in resonances of DNA hexamer is observed (Fig. 6.1 (c)). Two signals at 5.56 and 5.49 ppm corresponding to H1' proton of G2 residue are seen. The 1H proton of daunomycin is evident at 1.10 : 1 drug to DNA concentration ratio. It is notable that 1H, 2H and 3H protons of ring D of daunomycin are more pronounced at drug/DNA concentration ratio of 1.33 : 1 (Fig. 6.1(d)).

On increasing the concentration of drug further, broadening in all protons of DNA is observed. Figs. 6.1 (f,g) show the 1D spectra of 2 : 1 daunomycin + d-$(TGATCA)_2$ complex. 2D phase-sensitive NOESY spectra recorded on this 2 : 1 drug to DNA complex are shown in Figs. 6.5(a-h) in which all the protons have been assigned independently as discussed earlier. It is noted that serveral new signals such as 1'H, 1H, 2H, 3H etc. are found to grow on gradual addition of drug and these are assigned on the basis of NOE connectivities to their respective daunomycin protons. However, several other less intense signals such as those at 7.93 and 8.24 ppm, which are also found to grow as more and more drug is added, are not observed in 2D NOESY spectra and hence could bot be assigned. At 2 : 1 drug to DNA concentration ratio, we observe that all signals are very broad. This could be due to presence of several resonances of each proton having almost similar resonating positions and which may correspond to two types of complexes. However, slow exchange takes place between them on NMR time scale which results in broadening of all signals. As a result the 2D DQF-COSY spectra on this complex could not be characterized.

Considering the protons of daunomycin, the ring D protons 1H, 2H and 3H are found to shift upfield by 0.20, 0.18 and 0.21 ppm, respectively (Figs. 6.2(a,b), Table 6.3) with reference to their chemical shift positions at 355 K in unbound daunomycin (chemical shift of monomeric daunomycin, Table 4.2). Similar changes in chemical shifts of ring D protons 1H, 2H and 3H on complex formation with DNA are reported in literature [14,86,92-94,96]. The upfield shifts in 1H, 2H, and 3H protons are ascribed to intercalation of daunomycin chromophore, within the base pairs of DNA (Table 6.3). The 8axH and 10axH protons of ring A also experience large upfield shifts in the range 0.22 - 0.47 ppm due to stacking. The upfield shifts in 1'H, 2'axH, 2'eqH, 5'H and 5'CH_3 protons and downfield shifts in 3'H and 4'H protons of (Table 6.3) daunosamine may be attributed to conformational adjustment within drug molecule on complexation. The T1H6, G2H8 and C5H6 protons of DNA hexamer are shifted downfield by 0.05 - 0.11 ppm, while A3H8, A6H8, T4H6 and C5H5 protons shift upfield by 0.01-0.22 ppm on complexation (Table 6.4, Figs. 6.2(a,b)). The T1CH_3, T4CH_3 and C5H5 protons also shift upfield by 0.18, 0.29 and 0.22 ppm on complex formation (Table 6.4). Such changes in chemical shifts of DNA protons due to interaction of daunomycin are also reported in literature [92-94,96] and are discussed in detail later.

CHANGES WITH TEMPERATURE

The 1D NMR spectra of 2:1 drug to DNA complex obtained as a result of last titration is monitored as a function of temperature

Table 6.4 : Changes in chemical shift $\Delta\delta$ (in ppm) of various protons of d-$(TGATCA)_2$ on formation of complex at 295 K in D_2O.

Proton	T1	G2	A3	T4	C5	A6
H6/H8	-0.11	-0.05	0.01	0.19	-0.05	0.10
H1′	0.02	0.35	0.16	0.07	0.02	0.07
H2′	-0.07	0.13	0.17	-0.17	-0.29	0.26
H2"	0.01	0.05	0.13	0.09	-0.14	-0.30
H3′	0.01	0.06	0.06	0.02	-0.04	-0.01
H4′	-0.13	0.26	0.11	0.07	-	0.13
H5′	0.02	0.18	0.06	-	-	0.0
H5/H2/CH_3	0.18	-	-	0.29	0.22	-

(-ve) sign refers to downfield shift.

(+ve) sign refers to upfield shift.

in the range 295-325 K. Figs. 6.3(a-d) show expansions of 1D NMR spectra at 305, 315 and 325 K showing H8, H6, H1′ and H3′ resonances. The chemical shifts of some of the drug and DNA protons are plotted as a function of temperature and are shown in Figs. 6.4(a,b). It is observed that 3H proton of ring D of daunomycin resonating at 7.36 ppm at 295 K shifts upfield with increase in temperature to 7.26 ppm at 325 K. The position of this proton in self - associated and monomeric state (i.e chemical shift of daunomycin at 297 K and 355 K, refer to Table 4.2 of chapter IV) are at 7.37 ppm and 7.75 ppm, respectively. It has been shown [6,92-94,96] that an increase in temperature results in downfield shift of 1H, 2H, 3H and $4OCH_3$ protons due to dissociation of complex. However, our results are contrary to that reported in literature. [6,92-94,96] i.e. 3H is found to be shifted further upfield with temperature. It may be noted that its position is shifted upfield by 0.49 ppm with respect to the corresponding monomer state of unbound daunomycin (Table 4.2) and by 0.20 ppm (δ at 325 K, Table 4.2) to that of partially destacked drug. This shows that increase in temperature from 295 K to 325 K does not result in dissociation of complex. Similarly upfield shift has been observed for 2H proton with temperature. The ring D 1H proton does not shifts significantly while daunosamine 1′H proton shifts downfield with temperature. Thus, perhaps the resonating positions of drug protons at 325 K refer to that of a

complex (and not drug alone) which may have a structure some what different from that at 295 K, resulting in altered chemical shift positions.

The base protons T1H6 and G2H8 shift upfield with temperature (Figs. 6.4 (a,b)). The resonance positions of these protons in complex at 325 K are different from the corresponding positions in unbound DNA at 295 K (i.e. duplex DNA) as well as to those at 325 K (i.e. single stranded DNA, Table 5.2). No significant change is observed in the chemical shifts of A6H8, C5H6, and A3H8 protons. The T4H6 and C5H5 protons shift downfield with temperature. Thus, DNA as well as drug are, in complexed state at 295 K and 325 K with the structure of complex being different at these two temperatures.

INTERACTIONS OF DRUG WITH DNA

The conformational features of the drug-DNA complex are investigated primarily on the basis of 2D NOESY spectra. Since the signals in 1D NMR are quite broadened and DQF - COSY could not be used, it was not possible to carry out rigorous analysis of the conformation of deoxyribose sugar of the complexed DNA based on spin-spin coupling constants. For five residues i.e. A3, A6, T4, T1 and C5, ΣH1′ and spin-spin coupling constants could be ascertained at 325 K. We observed several NOEs corresponding to intra sugar and base to sugar proton connectivities which are listed in Table 6.5 and Table 6.6, respectively. Some of the NOEs have been used to analyse the C3′-endo ⇆ C2′-endo equilibrium in

sugar pucker as well as in glycosidic bond rotation (χ) (Table 6.6). Several NOEs observed amongst protons of the daunomycin show changes in conformation of drug (Table 6.7). Besides these several intermolecular NOEs are observed (Table 6.8) which are used to analyse the interaction of drug with DNA to arrive at a specific geometry of the complex.

The research group of Alexander Rich and Olga Kennard have extensively studied the structure of complexes of daunomycin and adriamycin with d-CGATCG, d-CGTACG, d-TGATCA and d-TGTACA [34,73,85,126] by x-ray crystallography techniques. We have used the structure obtained by them as a reference, to start with, in order to understand the conformation of drug-DNA complex. Fig. 6.6 shows the schematic drawing of the intercalation geometry of daunomycin chromophore within base pairs of DNA hexamer. Two daunomycin molecules intercalate their aglycon chromophores between the 5'-3'(pyr-pur) i.e. TpG/CpG sites at both ends of the hexamer duplex. The DNA unwinds to accommodate the drug chromophore resulting in change in the orientations of adjacent base pairs. The ring D hangs out in the solvent region while the daunosamine sugar occupies the space in minor groove with its hydrophilic (hydroxyl and amino) functional groups pointing away from the DNA molecule and projecting into the solvent region. We have analysed the observed results regarding structural details of drug-DNA complex in the following way :

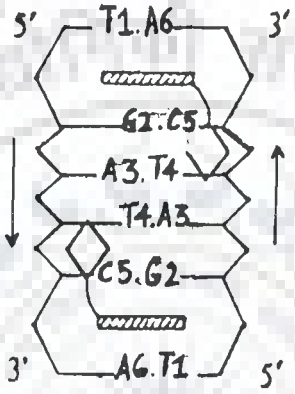

Fig. 6.6 : Schematic drawing of the daunomycin-d-$(TGATCA)_2$ complex. The aglycon chromophores of the daunomycin are shown as hatched bars, which are intercalated between the TpG sequences. The nucleotides are numbered T1 to A6 along each 5'-3' strand.

(i) Change in conformation of d-$(TGATCA)_2$ in order to allow intercalation due to alterations in backbone torsional angles, sugar pucker etc. which will be reflected as change in C3′-endo ⇆ C2′-endo equilibrium, pseudorotation (P) of major conformer and glycosidic bond rotation (χ) :

The sugar resonances are broadened at 295 K and did not allow measurement of J(H1′ - H2′), J(H1′ - H2") or sums of couplings. At 325 K, the H1′ resonances of five of the residues are sharp peaks. The ΣH1′ and J values are read directly from 1D NMR spectra as follows :

	BOUND DNA					UNBOUND DNA	
	ΣH1′ (Hz)	ΣH3′* (Hz)	J(H1′-H2′) (Hz)	J(H1′-H2") (Hz)	χ_S	ΣH1′ (at 325 K)	ΣH1′ (at 305 K)
A6	13.4	~14	6.7	6.6	0.64	14.3	14.5
A3	13.9	~14	6.8	7.1	0.71	13.3	13.6
T4	14.1	~13	7.6	6.5	0.75	13.9	14.5
G2	-	~13	-	-	-	14.5	14.9
T1	~ 14.4	~13	~7.3	~7.2	~0.80	14.2	14.6
C5	~14.4	~13	~7.3	~7.2	~0.80	13.7	14.1

*ΣH3′ includes J(H3′-^{31}P) coupling.

G2H1′ is unusually broad even at 325 K (Fig.6.3(d)) which may be due to implication of this residue in binding as discussed later.

The mole fraction of major S conformer is calculated using the analysis of Van Wijk et al. [123]. It has been observed that

the mole fraction of major S conformer decreases (~0.05) with temperature in unbound d-$(TGATCA)_2$. The A6 residue therefore may have χ_S somewhat higher than 0.64 at 295 K however an average value of ~0.65 ± 0.05 is considered reasonable. The observed values of J(H1′ - H2′) and J(H1′ - H2") couplings in A6 residue show that pseudorotation of the S conformer is either 108° - 117° or 180° - 189° (some of the calculated values for χ_S = 0.65 are listed in Table 5.6). The lower P_S value leads to ΣH3′ = 18.0 Hz while for the higher p_S of 180°, ΣH3′ = 13.0 Hz (Table 5.4(c)). Since the observed value of ΣH3′ at 325 K (Fig. 6.3(d))) ~14.0 - 5.8 ($J(H3'-^{31}P)$) = 8.2 Hz, it is inferred from the Table 5.4(c) and Table 5.6 that χ_S = 0.65 - 0.75 and P_S ~180° - 189° for the A6 residue. A mixture of two S conformers with P = 108°/117° and 180°/189° may be present but it is not possible to confirm the same and obtain mole fraction of each of the S conformer from the limited data available. It is observed that for A3, T1 and C5 residues, the J(H1′ - H2′) and J(H1′ - H2") are nearly equal, χ_S = 0.70 - 0.80 and ΣH3′ being comparatively low the P_S lies in the range 180° - 198°. For T4 residue, the values of J(H1′ - H2′) and J(H1′-H2") are 7.6 and 6.5 Hz, respectively, implying that P_S is in the range 162° - 180°. Comparing ΣH3′ values in complex with the corresponding values obtained in unbound d-$(TGATCA)_2$, it is notable that ΣH3′ values are fairly low in all residues i.e. in the range 7 - 8 Hz (in unbound form ΣH3′ values are in the range 9 -15 Hz). A close look at Table 5.4(c) shows that this is possible only if major conformer is in the P_S range 153° - 225°.

Thus analysis of the data shows that P_S of the major conformer for T1, A3, C5, T4 and G6 are in the range 162°-180° for T4 and 180° - 198° for T1, A3, C5 and G6 residues.

Table 6.5 shows the relative intensities of cross peaks for intra sugar protons observed in the NOESY spectra of the complex recorded at τ_m = 350 ms (Figs. 6.5(a-d)). Intense cross peaks are observed for H1′ - H2′, H1′ - H2", H2′ - H3′ connectivites for all the residues. These NOE connectivities are not expected to differentiate between different pseudorotation values as they vary over a narrow range (Table 5.8, Fig. 5.13). The H2" - H3′ NOE cross peak is least intense for A6 residue implying that it may have maximum fraction of N conformer. The H3′ - H4′ cross peak for A6 residue is also least intense as compared to other residues (Table 6.5). Since the standard distance H3′ - H4′ is largest for P_N = 18° and decreases with increase in P value (Table 5.8), this observation also leads to the conclusion that A6 residue has maximum amount of mixing of two sugar conformers. Further it is observed from relative intensities of H3′ - H4′ cross peaks that the distance H3′ - H4′ increases in the order A3, G2 < T1 < A6. If mole fraction of S conformer is practically same for A3, G2, T1 residues, a lesser distance for A3, G2 than T1 residue will imply that pseudorotation values of A3, G2 are higher than that for T1.

However, it is the H1′ - H4′ distance which can be used as a marker since it varies over a large range, 2.2 A° to 3.65 A°. But the H1′- H4′ distance cannot distinguish between C3′-endo $\leftrightharpoons$ C2′-endo equilibrium since for both P_N = 18° and P_S = 162°

Table 6.5 : Observed relative intensities of intra-sugar NOE cross peaks of d-$(TGATCA)_2$ on complexation in NOESY spectra recorded at τ_m = 350 ms in D_2O at 295 K.

Connectivities	T1	G2	A3	T4	C5	A6
H1'-H2'	ss	ss	ss	ss	ss	ss
H1'-H2"	ss	ss	ss	ss	-	ss
H2'-H3'	ss	ss	ss	-	-	s
H2"-H3'	ss	ss	ss	-	-	ws
H3'-H4'	s	ss	ss	-	-	ww
H1'-H3'	w	w	w	-	-	ww
H1'-H4'	ww	-	w	w	-	s
H2'-H4'	-	-	ws	-	-	ws
H2"-H4'	-	-	w	-	-	w

ss- very intense. s- intense.

ws- fairly intense. w- weakly intense.

ww- very weak.

distance is ~3.0 A°. The variation in H1′ - H4′ distance increases in the order A6 < A3, T4 < T1 < G2. The distance is least for P_S = 90° - 99° (Table 5.8, Fig. 5.13). Since A6 residue has χ_S/χ_N as 0.65/0.35, a comparatively low distance is possible only if another S conformer of P_S in the range 90°-108° exists in solution. Similarly lower distance of A3, T4 as compared to T1 and G2 residues indicates that they also have a fraction of S conformer with P_S lesser than that for T1 and G2 residues.

Maximum variation is seen in H2" - H4′ distance which increases from a distance of 2.29 A° for P_N = 18° to 3.93 A° for P_S = 216° (Table 5.8). Weakly intense cross peak is observed for A3, A6 residues while no cross peak corresponding to this connectivity is seen for other residues. This may be inferred as presence of relatively large percentage of N conformer in A6 residue as well as presence of S conformer having low P_S i.e. in the range 90° - 117° as compared to that for other residues. The variation in H2′ - H4′ as well as H1′ - H3′ distance is rather low and they cannot be used to obtain P values.

Thus the relative intensities corresponding to intrasugar distances show that :

(i) A6 residue has maximum N conformer.

(ii) A6, A3 residues have S conformer with P_S in the range 90°-117°.

(iii) T4 residue has P_S lesser than G2 and T1 residues.

These conclusions regarding P_S values of all residues are consistent with the limited data of spin-spin coupling constants, ΣH1′ and ΣH3′ values.

In the x-ray crystal structure of daunomycin-d-(TGATCA) complex [85] it has been observed that P_S values in residues from 5′-3′end are 138°, 165°, 151°, 125°, 179° and 177°. Similar results were obtained for the crystal structure of other daunomycin -hexamer complexes [34,73,126]. These are not really comparable with the present solution structure, it is not expected, since in our case the P_S value refers to that of major S conformer while that in x-ray structures average values were observed.

The relative intensities of NOE cross peaks corresponding to base-H1′ connectivity (Fig. 6.5(d), Table 6.6) are used to get a range of a value of glycosidic bond rotation using data of interproton distances available for standard A-DNA and B-DNA geometries (Table 5.10(a)), Fig. 5.14(a),) [131]. Among the purines, the base-H1′ distance increases in the order A6 < A3 < G2 which may be interpreted as presence of maximum amount of N conformer and/or a high value of χ, such as -60°, in A6 residue. Among pyrimidines, the distance for T1, T4 residues is lesser than that for C5 residue. The base-H1′ distance in standard B-DNA are lower for pyrimidines than that for purines (Table 5.10 (a)). The intensities of cross peaks (Fig. 6.5(d),Table 6.6) show that distance among all the residues increase in the order A6 < T1, T4 < A3 < G2, C5 and the distance in A6 residue is even lesser than

Table 6.6 : The relative intensities of intra-residue NOE connectivities as observed in phase - sensitive NOESY spectra at τ_m 350 ms and 75 ms.

	B-H2′		B-H2"		B-H1′	
τ_m	350	75	350	75	350	75
T1	s	ws	s	-	s	-
G2	s	w	s	ws	-	-
A3	ss	ws	ss	w	s	-
T4	-	ws	s	-	s	-
C5	s	ws	s	ws	-	-
A6	ss	w	ss	s	ss	-

B - base proton. ss - very intense.

s - intense. ws - fairly intense.

w - weakly intense. (-)- absence of peak.

that for pyrimidines. The observed intensity of cross peak for A6 residue does not reflect a distance of (3.72 x 0.35 + 3.88 x 0.65 = 3.82A°) which is expected if N and S conformer are present in standard A and B-DNA geometries having χ as -150° and -105°, respectively. Hence the observed result implies that χ is ~ - 60° (± 15°) for A6 residue.

Since the distance of base-H2′ is low and varies over P-χ values in a narrow range (Fig.5.14(b,c), Table 5.10(b,c)). It cannot be used to deduce inference about χ. We observe intense cross peaks for all residues in NOESY spectra recorded at τ_m = 350 ms and fairly intense cross peaks in NOESY spectra recorded at τ_m = 75 ms (Fig. 6.5(h), Table 6.6).

The relative intensities of base - H2" NOE connectivities among pyrimidine residues show that base - H2" distance for C5 residue is lesser than that for T1 and T4 (Figs. 6.5(e,f,h), Table 6.6). Intense peak is seen for C5, T1 and T4 at τ_m = 350 ms. However, at τ_m = 75 ms, weakly intense cross peak is seen for C5 residue implying that distance for base - H2" is lesser for C5 than T1 and T4 residues. The distance increases as χ is varied from -105° to higher values ≃ 60° (Table 5.10(c)). The fairly intense peak (at τ_m= 75 ms, Fig. 6.5 (h), Table 6.6) for C5 residue reflects base - H2" distance to be in the range 2.4 - 3.2 A°. If χ = - 105° for major S conformer in C5 residue then base - H2" distance is expected to be in the range 3.7 - 4.4 A° (Fig. 5.14(c), Table 5.10(c)). Therefore the χ value is likely to be

higher and lie in the range $-60^{\circ} \pm 15^{\circ}$ for C5 residue. For T1 and T4 residues χ is comparatively lower.

Among purines the base - H2" distance increases in the order A6 < G2 < A3. The weakly intense or intense cross peak is observed at even τ_m = 75 ms (Fig. 6.5(h), Table 6.6) for all three residues implying that base - H2" distance for these residues may be in the range 2.4 - 3.4 A°. For χ value of -105°, P_S in the range 90°-198° and χ_S = 0.65 - 0.80, the calculated distances of base -H2" would be $\simeq$ 3.9 A° (Table 5.10(b)). Since relatively intense cross peaks are seen which indicate that χ for all purines is higher and may be in the range $\sim -60^{\circ}$ for A6 residue and $\simeq -90^{\circ} \pm 15^{\circ}$ for A3 residue.

Thus we conclude that the χ for T1, A3, T4, C5 and A6 residues are -90°, -90°, -90°, -60°, -60° (to an accuracy of $\pm 15^{\circ}$), respectively. We are unable to ascertain the range of χ for G2 residue in the absence of a knowledge of mole fraction of S and N conformer.

We observe that glycosidic bond rotation (χ) changes from anti for T1, G2 and high anti for A3, T4, C5 and A6 residues (in unbound form) to high anti for all residues on complex formation. In x-ray crystal structure of daunomycin-d-(TGATCA) complex [85] χ was found as anti for G2, C5 and A6 residues while in the present case all residues adopts high anti conformation. This reflects greater flexibility in solution structure.

(iii) Changes in conformation of daunomycin due to binding which would be reflected in interproton distances and changes in chemical shifts :

We observe changes in chemical shifts of various protons of daunomycin (Table 6.3) as well as in relative intensities of various cross peaks within daunomycin molecule on complexation (Figs. 6.5 (a-g), Table 6.7). The observed upfield shifts for ring A, ring D and 1'H protons are in the range 0.18 - 0.47 ppm (Table 6.3) These are best understood in terms of stacking with base pairs and are discussed later. The changes in chemical shift ($\Delta\delta$) of daunosamine sugar protons, in the range -0.16 to 0.30 ppm (-ve refers to downfield shift while +ve sign refers to upfield shifts), could be due to alterations in sugar conformation as well as its proximity to DNA. Some of the interproton distances, the range of which is inferred from relative intensities of cross peaks in NOESY spectra in bound daunomycin, are found to be different from the corresponding distances in unbound daunomycin. Within the sugar moiety, the interproton distances, 1'H - 3'H, 1'H - 5'CH_3 and 3'H - 5'CH_3 are different from the corresponding values obtained in unbound drug. Intense cross peaks are observed for 1'H - 3'H and 3'H - 5'CH_3 connectivites which reflect interproton distances of the order of 2.4 - 3.0 A° as compared to the corresponding distances of 3.9 and 4.0 A°, respectively in the unbound state (Table 4.4 of chapter IV). Within ring A, the NOE

Table 6.7 : **Observed relative intensities of intra molecular NOE cross peaks of daunomycin on complexation.**

Connectivities		Connectivities	
1'H-2'axH	ss(O)	3'H-5'H	ss
1'H-2'eqH	ss(O)	3'H-5'CH_3	ss
2'axH-2'eqH	(O)	4'H-2'axH	ss(O)
3'H-2'axH	ss(O)	4'H-2'eqH	ss(O)
3'H-2'eqH	ss(O)	10axH-8axH	-
3'H-4'H	(O)	10axH-8eqH	w
4'H-5'H	(O)	10eqH-8axH	-
5'H-5'CH_3	ss	7H-1'H	-
4'H-5'CH_3	ss	7H-3'H	-
1H-2H	(O)	7H-4'H	-
2H-3H	ss	7H-5'H	-
1H-4OCH_3	-	7H-5'CH_3	-
2H-4OCH_3	s	1'H-8axH	s(O)
3H-4OCH_3	ss	3'H-8axH	s(O)
7H-8axH	-	4'H-8axH	ss(O)
7H-8eqH	-	8axH-5'H	ss(O)
8axH-8eqH	(O)	8axH-5'CH_3	ss(O)
10axH-10eqH	(O)	1'H-8eqH	s
10eqH-8eqH	s	3'H-8eqH	s
1'H-3'H	ss	4'H-8eqH	-

1'H-4'H	ws	5'H-8eqH	ss (O)
1'H-5'H	ss	5'CH_3-8eqH	ss(O)
1'H-5'CH_3	w		

O - Overlap. ss - very intense. s - intense. ws - fairly intense. w - weakly intense. (-) - absence of peak.

cross peaks 10axH - 8axH and 10eqH - 8axH are not observed (Fig. 6.5(b), Table 6.7) which implies that the corresponding interproton distances are more than 4.0 A°, while these distances in unbound state are observed as 2.50 and 2.71 A°, respectively. Among the NOE connectivities of ring A protons with daunosamine sugar protons, the interproton distances 3'H - 8eqH and 4'H - 8eqH are altered on binding (Table 6.7). An intense cross peak for 3'H - 8eqH NOE connectivity implies distance of the order of 2.4 - 2.8 A°, which is lesser than the corresponding distance of 3.5 A° in unbound state (Table 4.4 of chapter IV). The 4'H - 8eqH cross peak is not observed on complexation which reflects this distance to be more than 4.0 A° as compared to a distance of 3.0 A° in unbound daunomycin.

Thus the distance of 3'H from 1'H and 5'CH_3 are altered on binding. The positions of 8eqH with respect to 10axH and 10eqH have also altered resulting in a change in conformation of daunomycin.

In crystal structures of daunomycin with DNA hexamers [34,73,85,126] it has been shown that conformation of ring A changes on binding. In particular the change in relative position of C8 and C9 atoms was observed. We observe a significant change in 8axH - 10axH and 10eqH - 8axH distances which are increased from the value of 2.50 and 2.71 A°, respectively in unbound state, to greater than 3.5 A° on interaction with DNA.

(iii) Structure of drug-DNA complex reflecting the interaction between drug and DNA molecule, are grouped into four parts as follows :

(a) Stacking interactions between base protons and drug chromophore due to intercalation of aglycon chromophore in the 5′ TpG- 3′ step (T1pG2), i.e. between base pairs T1.A6 and G2.C5 :

The upfield shifts in daunomycin protons 1H, 2H and 3H indicate intercalation of drug chromophore as also observed by several workers [6,92-94,96]. We observe NOEs between non-exchangeable base protons of T1 and C5 residues with ring D protons (Table 6.8). The T1CH_3 proton gives NOE with 1H, 2H and 3H protons of ring D and their relative intensity decreases in the order 1H > 2H > 3H. The 4OCH_3 protons give relatively weak NOE with C5H6 and C5H5 protons (serial no. 1-5, Table 6.8). These NOEs are direct proof of intercalation of drug chromophore and suggests specific positioning of ring D protons with respect to first (T1.A6) and second (G2.C5) base pairs :

In order to have an idea of geometry of intercalation of daunomycin, we consider intercalation of daunomycin between first two base pairs with aglycon chromophore oriented perpendicular to the base pairs in a geometry of d-(TGATCA) + daunomycin complex obtained by x-ray crystallography [85]. It is seen that T1CH_3 is closest to 1H proton of ring D and 4OCH_3 is close to C5H6 and C5H5 protons (Fig. 6.7) [85]. This geometry is likely to result in NOEs observed by us. Ring B and C overlap to a larger extent with

Table 6.8 : Relative intensities of intermolecular NOE connectivities observed on complexation of d-$(TGATCA)_2$ with daunomycin using phase - sensitive NOESY spectra (τ_m 350 ms).

S.No.	Connectivities	Relative intensities
1.	T1CH_3 - 3H	ws
2.	T1CH_3 - 2H	s
3.	T1CH_3 - 1H	ss
4.	C5H5 - 4OCH_3	ws
5.	C5H6 - 4OCH_3	ws
6.	A6H1' - 4OCH_3	ws
7.	A6H3' - 4OCH_3	ws
8.	A6H2' - 4OCH_3	s
9.	A6H5' - 1'H	ws
10.	A6H5' - 2'eqH	s
11.	C5H1' - 2'eqH	s
12.	C5H5 - 1'H	ws
13.	T4H1' - 4'H	w
14.	T4H1' - 3'H	w
15.	A3H8 - 5'CH_3	ws
16.	A3H1' - 5'CH_3	ws
17.	A3H4' - 5'CH_3	ws
18.	A3H2" - 4'H	ss

ss - very intense. s - intense.

ws - fairly intense. w - weakly intense.

(a)

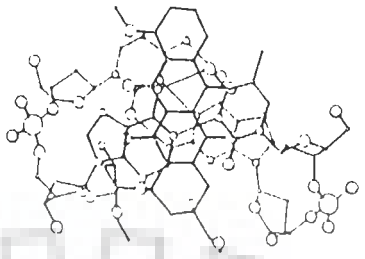

(b)

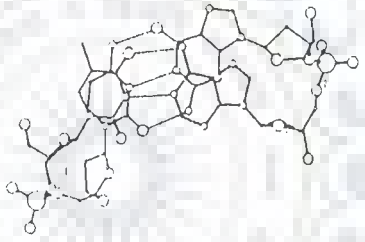

Fig. 6.7 : Spectroscopic drawings of the base-stacking interactions observed in d-$(TGATCA)_2$ on intercalation of daunomycin at TpG step. (a) Daunomycin and its intercalation site base pairs. (b) Base-base overlap of G2pT3 step [85].

base pairs, however there are no non-exchangeable protons to monitor this. It is observed that ring A protons are closer to A6 and G2 residues. This geometry would lead to upfield shifts in ring D and ring A protons due to anisotropic ring current effects from the adjacent base pairs. We have tried to assess the effect of ring currents due to T1.A6 and G2.C5 base pairs on ring A and D protons in the geometry of the d-(TGATCA) + daunomycin complex obtained by Nunn et al. [85]. Using the standard upfield shifts ($\Delta\delta$) due to anisotropic ring currents of T.A and G.C base pairs available in literature [39a], we have obtained the expected values of changes in chemical shifts. The upfield shifts obtained for 1H, 2H, 3H and $4OCH_3$ protons are lesser than 0.1 ppm. However, the experimentally observed values for changes in chemical shifts for the corresponding protons are 0.20, 0.18, 0.21 and 0.21 ppm, respectively (Table 6.3). There are significant differences between the observed and expected values. In order to explain the large upfield shifts observed we may consider that ring D protrudes less towards solvent and shows more overlap with T1.A6 and G2.C5 base pairs in the same configuration i.e. aglycon chromophore perpendicular to the base pairs. The ring A will then move further away and will result in lesser overlap of ring A protons with adjacent base pairs resulting in lesser upfield shifts on complexation. Since we observed large upfield shifts of both ring D as well as ring A protons, it is suggested that aglycon chromophore is some what tilted and is not perpendicular.

The changes in chemical shifts of base protons of T1.A6 and G2.C5 base pairs due to binding are a result of destacking of adjacent base pairs as they move apart to a distance of 6.8 A° and stackingof aglycon chromophore with each base pair. Destacking of base pairs is expected to induce downfield shifts while stacking of drug chromophore is expected to induce upfield shifts in base protons. The net effect will be an upfield or downfield shift. Weobserve$\Delta\delta$ = - 0.05 to + 0.29 ppm in base protons of T1, G2, C5 and A6 residues (Table 6.4).

(b) Stacking interactions in G2pA3 step, that is, between G2.C5 and A3.T4 base pairs due to alterations in base to base overlap on binding of drug to DNA :

Due to interaction of drug with DNA, the base pairs of DNA have to move apart in order to accommodate the drug molecule. It has been shown in literature that on complexation of daunomycin with d-(CGATCG) [73] and d-(TGATCA) [85], the helix axis of the DNA is not in the same position in two base pairs as would be expected for a perfect B-DNA conformation, and the G2.C5 base pair is translated towards the major groove relative to A3.T4 base pair by about 1.3 A°. This results in alteration in relative base stacking between G2.C5 and A3.T4 base pairs (Fig. 6.7 (b)) [85]. The overlap between G2.C5 and A3.T4 base pairs is reduced. A greater overlap occurs for the guanine six membered ring and adenine N-6 as compared to that in complexes with d-CGATCG [73] and d-CGTACG [126]. Such changes in overlap gemoetry are expected to induce changes in chemical shift of corresponding protons. We

do observe large changes in third base pairs on complexation i.e ≃ 0.29 ppm in T4CH_3, 0.19 ppm in T4H6, 0.16 ppm in A3H1′ and 0.35 ppm in G2H1′ protons (Table 6.4).

(c) Stacking interaction in A3pT4 step, that is, between A3.T4 and T4.A3 base pairs due to alterations, if any, in base to base overlap on binding of drug to DNA :

It has been shown in literature that A3.T4 and T4.A3 base pairs show typical stacking of pyrimidine-purine sequences like B-DNA in complexes of daunomycin + d-(CGATCG) and daunomycin + d-(TGATCA) [73,85]. Assuming the stacking of A3.T4 and T4.A3 base pairs to be similar in soultion, we do not expect any change in chemical shift of corresponding protons. Therefore the observed large upfield shifts in T4H6, A3H1′ and T4CH_3 protons on binding, may be attributed to relative change in overlap geometry of G2.C5 with respect to A3.T4 base pair on complexation.

(d) Proximity of daunosamine sugar to DNA protons :

Several intermolecular NOEs are observed between daunosamine sugar protons and d-$(TGATCA)_2$ protons on complexation. Table 6.8 gives a list of intermolecular contacts being observed. These contacts suggest proximity of the daunosamine sugar with A3, T4, C5 and A6 residues. Wang et al. [126] have studied the complex of daunomycin with d-(CGTACG) and have reported some of the van der Waals contacts as well as NOEs expected in their crystal structure. However, we observe several additional NOEs showing the proximity of corresponding residues with daunosamine sugar.

The A6H1', A6H2' and A6H3' protons are positioned close to $4OCH_3$ protons. These NOEs are not listed in the x-ray crystal structure of daunomycin + d-(CGTACG) complex [126] although they are feasible in the crystallographic structure with slight alterations in the geometry of intercalation of daunomycin. The NOEs C5H1' - 2'eqH, A6H5' - 1'H and A6H5' - 2'eqH (serial no. 9-11, Table 6.8) are seen in the complex. The cross peaks A6H5' - 2'eqH and C5H1' - 2'eqH are more intense than A6H5' - 1'H. In the crystal structure of daunomycin + d-(CGTACG) obtained by Wang et al. [126] these three distances i.e. A6H5' - 1'H, A6H5' - 2'eqH and C5H1' - 2'eqH are 1.99, 2.23 and 2.41 A°, respectively and are obviously expected to give NOEs. Thus existence of these three NOEs (serial no. 9-11, Table 6.8) are in accord with the x-ray crystal structure. Besides these we observe seven other NOEs between daunosamine sugar protons and protons of A3, T4 and C5 residues (serial no. 12-18, Table 6.8). A3H2" - 4'H NOE connectivity is very intense. This interproton contact may be compared with the van der Waals contact T3O2 - 4'H having distance of 2.61 A° in daunomycin + d-(CGTACG) x-ray crystal structure [126]. Since in our case third residue is adenine in place of thymine it is likely that postioning of H8 and H1' etc. of A3 residue is close to 4'H and $5'CH_3$ protons.

In the x-ray structure it has also been seen that C2', C3' and C4' atoms of daunosamine sugar are at a distance of 2.3 - 2.47 A° from adjacent C5 residue and A3.T4 base pair resulting in a more tight fit in daunomycin + d-(CGATCG) [73] complex as compared

to daunomycin + d-(CGTACG) complex [126]. These contacts are comparable to the osberved NOEs C5H5 - 1'H, T4H1' - 3'H and T4H1' - 4'H (Table 6.8).

Hence we find that the amino sugar of daunomycin molecule is positioned in a way similar to that in x-ray crystal structure i.e. in minor groove of hexamer duplex [34,73,85,126]. In order to allow van der Waal contacts due to daunosamine sugar placed in the minor groove, its conformation is likely to change. This change in daunosamine sugar is reflected as a significant change in 3'H - 5'CH_3 distance, which gets reduced from a value of 4.0 A° (in unbound daunomycin, Table 4.4) to about 2.6 A° in bound state. It is notable that we did not observe the resonances of 7H and 9$COCH_3$ even at 325 K whereas all other resonances give sharp peak at this temperature. Therefore direct NOE contacts involving 7H, 9$COCH_3$ and DNA protons are not observable. These resonances are severely broadened beyond recognition even at 325 K which implies that they are directly involed in anchoring of the drug to DNA in the complex [34,73,85,126]. The resonance G2H1' is broadened to a much greater extent than the corresponding H1' resonances of other five residues both at 295 K and 325 K which may imply immobilization of G2 residue in the complex. These results are consistent with the hydrogen bonding of 9OH of ring A with 2-amino group of G2 residue [34,73,85,126].

The significance of the present study on daunomycin-d-$(TGATCA)_2$ complex is that it augments the observation that a right-handed segment of DNA can have significant variations both

in backbone geometry and sugar puckering associated with the accommodation of a large intercalator molecule with an amino sugar. However, we observe greater flexibility in backbone geometry and sugar puckering than that observed in x-ray crystal structures obtained by the research group of Alexander Rich and Olga Kennard [34,73,85,126]. The previously studied x-ray crystal structures of dinucleoside monophosphate complex with simple intercalators raise a question about end effects of such short nucleic acid fragments. Simple C3'-endo (3'-5') - C2'-endo mixed pucker pattern around intercalator site were reported [112,124].

However, the present investigations show that in solution phase even in uncomplexed DNA fragments the deoxyribose sugars are a mixture of both north and south conformers. It is observed that percentage of north conformer (χ_N) has increased on complexation for A3, A6 and T4 residues.

We have carried out an independent study on the complex of d-(CGATCG) + adriamycin (unpublished) and observed variation in terms of backbone geometry, sugar puckering etc. on complexation. This suggests that there are no general rules which can be applied to intercalators. Apparently these suttle variations are specific to the type of drug and specific intercalating base pair (TpG/CpG) selected. It has been shown in literature [24,25,34,73,85,126] that daunomycin and adriamycin prefer guanine base at the second position in the 5'-3' sequence. This is evident in our studies as we observe severe broadening of G2H8.

As discussed earlier, 8axH, 10axH and 9$COCH_3$ groups of ring A are significantly altered on binding. This shows that these groups play an important role in interaction of daunomycin with DNA. Therefore modifications of groups attached to C9 will have profound effects on its binding. The classical example of this is adriamycin, a structural analog of daunomycin. It has 9-$COCH_2OH$ group at C-9 position. We observed considerable differences in the binding of these drugs to DNA in solution.

CONCLUSIONS

The torsional angles and interproton distances reveal the structural details of daunomycin in solution state. There are major differences in some of the interproton distances in the present case as compared to the corresponding distances obtained by x-ray crystallography techniques [73]. These interproton distances are 7H - 1'H, 7H - 3'H, 7H - 4'H, 7H - 5'H and 7H - 8axH. Three of these distances i.e. 7H - 8axH, 5'H - 8axH, 1'H - 7H are also different from the solution structure of n-acetyl daunomycin [72]. The molecular model obtained on the basis of these structural constraints suggest that various torsional angles in the solution structure of daunomycin are different from the corresponding crystal structure by ± 15°. The position of C, N and O atoms is likely to be same but the position of hydrogen atoms is quite different in solution.

Analysis of the structure of deoxyhexanucleotide d-$(TGATCA)_2$ indicates that DNA molecule is not locked in a somewhat rigid structure with the motions of the sugar - ring restricted to a small region of the pseudorotation angle. There appears to be time averaging of two different conformers, one N conformer (observed in A - DNA), one S conformer (close to standard B - DNA) existing in a fast equilibrium in solution. Presence of two S conformers and one N conformer is also suggested by some of the results. The pseudorotation angle of sugar pucker of the major S conformer varies in the range 117° - 180° while the mole fraction

of major S conformer varies between 0.65 - 0.88. The range of χ_S in T1, G2, A3, T4, C5 and A6 residues are 0.78, 0.88, 0.65, 0.77, 0.78 and 0.80, respectively. Considerable flexibility at the 3′ end of hexamer leads to comparatively low P_S value of the order of $\simeq 117^\circ$ in A6 residue. Glycosidic angle is different for purines and pyrimidines and lies in the range -60° to -105°.

The structure of daunomycin-d-TGATCA)$_2$ complex appears to be symmetric with daunomycin aglycon chromophore intercalating at 5′-TpG-3′ step at both ends of DNA hexamer, since one set of DNA protons (major complex) are observed. The pseudorotation angle of several residues changes to $\simeq 180^\circ$ due to interaction with drug while the glycosidic bond rotation (χ) is in high anti conformation (-60° to -90°) for most of the residues. Several NOEs between base protons of T1.A6 and G2.C5 base pairs with 1H, 2H and 3H protons of daunomycin confirm the intercalation of aglycon chromophore of daunomycin between terminal base pairs resulting in upfield shifts in ring A and ring D protons of daunomycin. The relative overlap between G2.C5 and A3.T4 base pairs is also altered on interaction. Some of the intermolecular NOEs between protons of daunosamine sugar and base protons demonstrate proximity of daunosamine sugar to the bases. The geometry of the complex is somewhat different in solution than that obtained by x-ray crystallography [34,85,73,126].

REFERENCES

1. Altona C., Geise H.J. and Romers C. Conformation of non aromatic ring compounds. XXV. Geometry and conformation of ring D in some steroids from x-ray structure determinations. Tetrahedron, 1968, 24, 13.

2. Altona C. and Sundaralingam M. Conformational analysis of the sugar ring in nucleosides and nucleotides. A new description using the concept of pseudo-rotation. J. Am. Chem. Soc., 1972, 94, 8205.

3. Angiulli R., Foresti E., Rivi di S.L., Isaacs N.W., Kennard O., Motherwell W.D.S., Wampler D.L. and Arcamone F. Structure of daunomycin : x-ray analysis of N-Br-Acetyl daunomycin solvate. Nature (London) New Biol., 1971, 234, 78.

4. Arora S.K. Molecular structure, absolute stereochemistry, and interactions of nogalamycin, a DNA-binding anthracycline antitumor antibiotic. J. Am. Chem. Soc., 1983, 105, 1328.

5. Aue W.P., Bartholdi E. and Ernst R.R. Two dimensional spectroscopy : Application to nuclear magnetic resonance. J. Chem. Phys., 1976, 64, 2229.

6. Barthwal R.B., Mujeeb A. and Govil G. Interaction of daunomycin with deoxydinucleotide d-CpG by two dimensional proton magnetic resonance techniques. Archives Biochem. Biophys., 1994, 313, 189.

7. Beraldo H., Suillerot A.G., Tosi L. and Lavelle F. Iron (III) - adriamycin and iron (III) - daunorubicin complexes : physico-chemical characteristics, interaction with DNA, and antitumour activity. Biochemistry, 1985, 24, 284.

8. Bodenhausen G., Freeman R. and Turner D.L. Supression of artifacts in two dimensional spectroscopy. J. Magn. Reson., 1977, 27, 511.

9. Bohner R. and Hagen U. Action of intercalating agents on the activity of DNA polymerase I. Biochim. Biophys. Acta, 1977, 479, 300.

10. Brown D.R., Kurz M., Kearns D.R. and Hsu V.L. Formation of multiple complexes between actinomycin D and a DNA hairpin. Structural characterization by multinuclear NMR. Biochemistry, 1994, 33, 651.

11. Calendi E., Di Marco A., Reggiani M., Scarpinato B. and Valentini L. On physico-chemical interactions between daunomycin and nucleic acids. Biochim. Biophys. Acta, 1965, 103, 25.

12. Capranico G., Isabella P.D., Tinelli S., Bigioni M. and Zunino F. Similar sequence specificity of mitoxantrone and VM-26 stimulation of in vitro cleavage by mammalian DNA topoisomerase II. Biochemistry, 1993, 32, 3038.

13. Celda B., Widmer H., Leupin W., Chazin W., Denny A. and Wuthrich K. Conformational studies of d-$(AAAAATTTTT)_2$ using constraints from nuclear overhauser effects and from

quantitative analysis of the cross peak fine structures in two-dimensional ^{1}H nuclear magnetic resonance spectra. Biochemistry, 1989, 28, 1462.

13(a). Chary K.V.R., Hosur R.V. and Govil G. Sequence specific solution structure of d-GGTACGCGTACC. Biochemistry, 1988, 27, 3858.

13(b). Chary K.V.R., Modi S., Hosur R.V., Govil G., Chen C. and Miles H.T. Quantification of DNA structure from NMR data : Conformation of d-ACATCGATGT. Biochemistry, 1989, 28, 5240.

14. Chaires J.B., Dattagupta N. and Crothers D.M. Self-association of daunomycin. Biochemistry, 1982, 21, 3927.

15. Chaires J.B., Dattagupta N. and Crothers D.M. Studies on interaction of anthracycline antibiotics and deoxyribonucleic acid : Equilibrium binding studies on interaction of daunomycin with deoxyribonucleic acid. Biochemistry, 1982, 21, 3933.

16. Chaires J.B. Daunomycin inhibits the B $\longrightarrow$ Z transition in poly d(G-C). Nucleic Acids Res., 1983, 11, 8485.

17. Chaires J.B., Dattagupta N. and Crothers D.M. Binding of daunomycin to calf thymus nucleosomes. Biochemistry, 1983, 22, 284.

18. Chaires J.B. Long range allosteric effects on the B to Z equilibrium by daunomycin. Biochemistry, 1985, 24, 7479.

19. Chaires J.B. Thermodynamics of the daunomycin-DNA interaction : Ionic strength dependence of the enthalpy and entropy. Biopolymers, 1985, 24, 403.

20. Chaires J.B., Dattagupta N. and Crothers D.M. Kinetics of the daunomycin - DNA interaction. Biochemistry, 1985, 24, 260.

21. Chaires J.B., Fox K.R., Herrera J.E., Britt M. and Waring M. J. Site and sequence specificity of the daunomycin - DNA interaction. Biochemistry, 1987, 26, 8227.

22. Chaires J.B., Herrera J.E. and Waring M.J. Preferential binding of daunomycin to 5′ $\frac{A}{T}$ CG and 5′ $\frac{A}{T}$ GC sequences revealed by footprinting titration experiments. Biochemistry, 1990. 29, 6145.

23. Chen C.W., Knop R.H. and Cohen J.S. Adriamycin inhibits the B to Z transition of poly(dGm^{5}dC).poly(dGm^{5}dC). Biochemistry, 1983, 22, 5468.

24. Chen K.X., Gresh N. and Pullman B. A theoretical investigation on the sequence selective binding of daunomycin to double-stranded polynucleotides. J. Biomol. St. Dyn., 1985, 3, 445.

25. Chen K.X., Gresh N. and Pullman B. A theoretical investigation on the sequence selective binding of adriamycin to double-stranded polynucleotides. Nucleic Acids Res., 1986, 14, 2251.

26. Cieplak P., Rao S.N., Grootenhuis P.D.J., and Kollman P.A. Free energy calculation on base specificity of drug-DNA interactions : Application to daunomycin and acridine intercalation into DNA. Biopolymers, 1990, 29, 717.

27. Cirilli M., Giomini M., Giuliani A.M. and Trota E. A truncated driven overhauser effect study of adriamycin in water : conformation of the glycosidic linkage. Biochimica Acta, 1991, 47A, 759.

28. Courseille C., Busetta B., Geoffre S. and Hospital M. Complex daunomycin-butanol. Acta Cryst., 1979, B35, 764.

29. Dalgleish D.G., Fey G. and Kersten W. Circular dichroism studies of complexes of the antibiotic daunomycin, nogalamycin, chromomycin and mithramycin with DNA Biopolymers, 1974, 13, 1757.

29(a). Davies B.D. Prog. in NMR Spectroscopy, 1978, 12, 135.

30. Derome A.E. In "Modern NMR techniques for chemistry research". Volume 6, Pergamon press, Oxford U.K. (1987).

31. DiMarco A. Cancer chemotherapy Rep., 1975, 6, 91.

32. Feigon J., Wright J.M., Leupin W., Denny W.A. and Kearns D.R. Use of two dimensional NMR in the study of a double-stranded decamer. J. Am. Chem. Soc., 1982, 104, 5540.

33. Frechet D., Cheng D.M., Kan L.S. and Tso P.O.P. Nuclear overhauser effect as a tool for the complete assignment of non-exchangeable proton resonances in short

deoxyribonucleic acid helices. Biochemistry, 1983, 22, 5194.

34. Frederick C.A., Williams L.D., Ughetto G., Van der Marel G.A., Van Boom J.H., Rich A. and Wang A.H.J. Structural comparison of anticancer drug-DNA complexes : adriamycin and daunomycin. Biochemistry, 1990, 29, 2538.

35. Fritzsche H., Triebel H., Chaires J.B., Dattagupta N. and Crothers D.M. Studies on interaction of anthracycline antibiotics and deoxyribonucleic acid : Geometry of interaction of iremycin and daunomycin. Biochemistry, 1982, 21, 3940.

36. Gabbay E.J., Grier D., Fingerle R.E., Reimer R., Levy R., Pearce S.W. and Wilson W.D. Interaction specificity of the anthracyclines with deoxyribonucleic acid. Biochemistry, 1976, 15, 2062.

37. Gale E.F., Candliffe E., Reynolds P.E. and Richmond M.H. (1981) In "The molecular basis of antibiotic action" (Gale, E.F. et al. eds) pp. 258, John Willey and Sons London.

38. Gao X. and Patel D.J. Chromomycin dimer-DNA oligomer complexes. Sequence selectivity and divalent cation specificity. Biochemistry, 1990, 29, 10940.

39. Geierstanger B.H., Jacobsen J.P., Mrksich M., Dervan P.B. and Wemmer D.E. Structural and dynamic characterization of the heterodimeric and homodimeric complexes of distamycin

and 1-methylimidazole-2-carboxamide-netropsin bound to the minor groove of DNA. Biochemistry, 1994, 33, 3055.

39(a) Giessner-Prettre C. and Pullman B. On the atomic or local contributions to chemical shifts due to the anisotropy of the diamagnetic susceptibility of the aromatic side chain of amino acids and of the porphyrin ring. Biochem. Biophys. Res. Commun., 1981, 101, 921.

40. Gilbert D.E. and Feigon J. The DNA sequence at echinomycin binding sites determines the structural changes induced by drug binding : NMR studies of echinomycin binding to $[d(ACGTACGT)]_2$ and $[d(TCGATCGA)]_2$. Biochemistry, 1991, 30, 2483.

41. Gochin M., Zon G. and James T.L. Two-dimensional COSY and two-dimensional NOE spectroscopy of $d(AC)_4$, $d(GT)_4$: Extraction of structural constraints. Biochemistry, 1990, 29, 11161.

42. Gorenstein D.G. and Lai K. ^{31}P NMR spectra of ethidium, quinacrine and daunomycin complexes with poly (adenylic acid). poly (uridylic acid) RNA duplex and calf thymus DNA. Biochemistry, 1989, 28, 2804.

43. Graves D.E. and Krugh T.R. Adriamycin and daunorubicin bind in a cooperative manner to deoxyribonucleic acid. Biochemistry, 1983, 22, 3941.

44. Gronenborn A.M. and Clore G.M. Investigation of the solution structure of short nucleic acid fragments by

means of nuclear overhauser enhancements measurements. Prog. NMR Spec., 1985, 17, 1.

45. Hare D.H., Wemmer D.E., Chou S.H., Drobny G. and Reid B.R. Assignment of the non-exchangeable proton resonances of d-$(CGCGAATTCGCG)_2$ using two dimensional methods. J. Mol. Biol., 1983, 171, 319.

46. Holbrook S.R., Wang A.H.J., Rich A. and Kim S.H. Local mobility of nucleic acids as determined from crystallographic data. III. A daunomycin - DNA complex. J. Mol. Biol., 1988, 199, 349.

47. Henry D.W. Structure-activity relationship among daunorubicin an adriamycin analogs. Cancer Treat. Rep., 1979, 63, 845.

48. Hosur, R.V., Ravikumar M., Roy K.B., Zu-Kun T., Miles H.T. and Govil G. In "Magnetic resonance in biology and medicine" (Eds. Govil G., Khetrapal C.L. and Saran A.) Tata McGraw Hill, New Delhi, pp. 305 (1985).

49. Hosur R.V., Ravikumar M., Chary K.V.R., Sheth A., Govil G. Zu-Kun T. and Miles H.T. Solution structure of d-GAATTCGAATTC by 2D NMR : a new approach to determination of sugar geometries in DNA segments. FEBS Lett., 1986, 205, 71.

50. Hosur R.V., Govil G. and Miles H.T. Application of two dimensional NMR spectroscopy in the determination of solution conformation of nucleic acids. Magn. Reson.

Chem., 1988, 26, 927.

51. Islam S.A., Neidle S., Gandecha B.M., Partridge M., Patterson L.H. and Brown J.R. Comparative computer graphics and solution studies of the DNA interaction of substituted anthraquinones based on doxorubicin and mitoxantrone. J. Med. Chem., 1985, 28, 857.

52. Iwamoto R.H., Lim P. and Bhacca N.S. The structure of daunomycin. Tetrahedron Letters, 1968, 36, 3891.

53. Jeener J. Paper presented at the AMPERE International summer school, Borsko, Polje, Yugoslavia. 1971.

54. Jones M.B., Hollstein U. and Allen F.S. Site specificity of binding of antitumor antibiotics to DNA. Biopolymers, 1987, 26, 121.

55. Karplus M. Contact electron - spin coupling of nuclear magnetic moments. J. Chem. Phys., 1959, 30, 11.

56. Karplus M. Vicinal proton coupling in nuclear magnetic resonance. J. Am. Chem. Soc., 1963, 85, 2870.

57. Keeler J. and Neuhaus D. Comparison and evaluation of methods for two dimensional NMR spectra with absorption mode line shape. J. Magn. Reson., 1985, 63, 454.

58. Kriebardis T., Meng D. and Aktipis S. On the inhibition of the RNA polymerase - catalysed synthesis of RNA by daunomycin. Interference of the inhibition with elongation and pre-longation steps. Biochem. Biophys. Res. Commun., 1984, 123, 914.

59. Krugh T.R., Reinhardt C.G. Evidence for sequence preferences in the intercalative binding of ethidium binding to dinucleoside monophosphates. J. Mol. Biol., 1975, 97, 133.

60. Langlois B.E., Gallois B., Brown T. and Hunter W. The molecular structure of a 4'-epiadriamycin complex with d(TGATCA) at 1.7 A° resolution : comparison with the structure of 4'-epiadriamycin d(TGTACA) and d(CGATCG) complexes. Nucleic Acids Res., 1992, 20, 3561.

61. Leonard G.A., Hambley T.W., Mc Auley Hecht K., Brown T. and Hunter W.N. Anthracycline - DNA interactions at unfavorable base - pairs triplet binding sites: Structures of d(CGGCCG) / daunomycin and d(TGGCCA)/ adriamycin complexes. Acta Cryst., 1993, D49, 458.

62. Lerman L.S. Structural considerations in the interaction of DNA with acridines. J. Mol. Biol., 1961, 3, 18.

63. Levitt M. and Warshell A. Extreme flexibility of the furanose ring in DNA and RNA. J. Am. Chem. Soc., 1978, 100, 2607.

64. Lipscomb L.A., Peek M.E., Zhou F.X., Bertrand J.A., Van Derveer D. and Williams L.D. Water ring structure at DNA interfaces : hydration and dynamics of DNA-anthracycline complexes. Biochemistry, 1994, 33, 3649.

65. Lown J.W., Hanstock C.C., Bleakley R.C., Imbach J.L., Rayner B. and Vasseur J.J. Synthesis, complete ^{1}H

assignment and conformations of the self complementary hexadeoxynucleotide d(CpGpApTpCpG)$_2$ and its fragment by high field NMR. Nucleic Acids Res., 1984, 12, 2519.

66. Lown J.W., Morgan A.R., Yen S.F., Wang Y.H. and Wilson W.D. Characteristics of the binding of the anticancer agents mitoxantrone and related structures to deoxyribonucleic acids. Biochemistry, 1985, 24 4028.

67. Marion D. and Wuthrich K. Application of phase-sensitive two dimensional correlated spectroscopy (COSY) for measurement of ^1H - ^1H spin coupling constants in proteins. Biochem. Biophys. Res. commun., 1983, 113, 967.

68. McLennan I.J., Lenkinski R.E. and Yanuka Y. A nuclear magnetic resonance study of the self-association of adriamycin and daunomycin in aqueous solution. Canadian J. Chem., 1985, 63, 1233.

69. Miller K.J. and Newlin D.D. Intercalation of molecules with nucleic acids. VI. Computer design of chromophoric intercalating agents. Biopolymers, 1982, 21, 633.

70. Momparler R.L., Karon M., Siegel S.E. and Avila, F. Effect of adriamycin on DNA, RNA and protein synthesis in cell-free system and intact cells. Cancer Research, 1976, 36, 2891.

71. Mondelli R., Ragg E., Fronza G. and Arnone A. Nuclear magnetic resonance conformational study of daunomycin and related antitumour antibiotics in solution. The

conformation of ring A. J. Chem. Soc., Perkin Trans, 1987, II, 15.

72. Mondelli R., Ragg E. and Fronza G. Conformational analysis of N-acetyl daunomycin in solution. A transient ^{1}H nuclear. overhauser effect study of the glycosidic linkage geometry. J. Chem. Soc., Perkin Trans., 1987, II, 27.

73. Moore M.H., Hunter W.N., Langlois B.L., Kennard O. DNA-drug interactions. The crystal structure of d(CGATCG) complexed with daunomycin. J. Mol. Biol., 1989, 206, 693.

74. Mujeeb A., Kerwin S.H., Egan W., Kenyan G.L. and James T.L. A potential gene target in HIV-1 : rationale, selection of a conserved sequence and determination of NMR distance and torsion angle constraints. Biochemistry, 1992, 31, 9325.

74(a). Majumdar A. and Hosur R.V. Simulation of 2D NMR spectra for determination of solution conformations of nucleic acids. Prog. in NMR Spectroscopy, 1992, 24, 109.

75. Munt, N.A. and Kearns D.R. Poly (dA-dT) has a right handed B conformation in solution : A two dimensional NMR study. Biochemistry, 1984, 23, 791.

76. Murdock K.C., Child R.G., Fabio P.F., Angier R.B., Wallace R.E., Durr F.E., Citarella R.V. Antitumor agents. 1. 1, 4-bis [(aminoalkyl) amino]-9, 10 anthracenediones. J. Med. Chem., 1979, 22, 1024.

77. Nakata Y. and Hopfinger A.J. An extended conformational analysis of doxorubicin. FEBS Lett., 1980, 117, 259.

78. Nakata Y. and Hopfinger A.J. Predicted mode of intercalation of doxorubicin with dinucleotide dimers. Biochem. Biophys. Res. Commun., 1980, 95, 583.

79. Neidle, S. and Taylor, G.L. Nucleic acid binding drugs : Part IV. The crystal structure of the anticancer agent daunomycin. Biochim. Biophys. Acta, 1977, 479, 450.

80. Neidle S., Achari A., Taylor G.L., Berman H.M., Carrel H.L., Glusker J.P. and Stallings W.C. Structure of a dinucleoside phosphate - drug complex as model for nucleic acid-drug interaction. Nature, 1977, 269, 364.

81. Neidle S. (1978) In "Topics in antibiotic chemistry" (Sammes P.G., ed) pp. 240, John Wiley and Sons, New York.

82. Neidle S. and Taylor G.L. Nucleic acid binding drugs. Some conformational properties of the anti-cancer drug daunomycin and several of its derivatives. FEBS Lett., 1979, 107, 348.

83. Neidle S. and Sanderson M.R. (1983) In "Molecular aspects of anticancer drug action" (Neidle S. and Waring M.J. eds) pp. 35, The Macmillan Press Ltd., London and Basingstoke.

84. Neumann J.M., Cavailles J.A., Herve M., Dinh S.T., Langlois d'Estaintot B., Huynh-Dinh T. and Igolen J. 500 MHz ^{1}H-NMR study of the interaction of daunomycin with B and Z helices of d(CGm^{5}CGCG). FEBS Lett., 1985, 182, 360.

85. Nunn C.M., Van Meervelt L., Zhang S., Moore M.H. and Kennard O. DNA-Drug Interactions. The crystal structures of d(TGTACA) and d(TGATCA) complexed with daunomycin. J. Mol. Biol., 1991, 222, 167.

86. Nuss M.E., James T.L., Apple M.A. and Kollman P.A. An NMR study of the interaction of daunomycin with dinucleotides and dinucleoside phosphates. Biochim. Biophys. Acta, 1980, 609, 136.

87. Pachter J.A., Huang C.H., Du Vernay V.H., Prestayko A.W. and Crooke S.T. Viscometric and fluorometric studies of deoxyribonucleic acid interactions of several new anthracyclines. Biochemistry, 1982, 21, 1541.

88. Paoletti, J. and Le Pecq J.B. Resonance energy transfer between ethidium bromide molecules bound to nucleic acids. J. Mol. Biol., 1971, 59, 43.

89. Paoletti J. and Le Pecq J.B. The change of the torsion of the DNA helix caused by intercalation. I - A discussion of the two different possibilities, winding or unwinding. Biochimie, 1971, 53, 969.

90. Patel D.J. and Canuel L.L. Ethidium bromide $(dC\text{-}dG\text{-}dC\text{-}dG)_2$ complex in solution : Intercalation and sequence specificity of drug binding at the tetranucleotide duplex level. Proc. Natl. Acad. Sci., 1976, 73, 3343.

91. Patel D.J. and Canuel L.L. Sequence specificity of mutagen- nucleic acid complexes in solution : Intercalation and mutagen-base pair overlap geometries for proflavine binding to dC-dC-dG-dG and dG-dG-dC-dC self-complementary complexes. Proc. Natl. Acad. Sci., 1977, 74, 2624.

92. Patel D.J. and Canuel L.L. Anthracycline antitumor antibiotic. Nucleic-acid interactions. Structural aspects of the daunomycin. poly (dA-dT) complex in solution. Eur. J. Biochem., 1978, 90, 247.

93. Patel D.J. Helix-Coil transition of the dG-dC-dG-dC self - complementary duplex and complex formation with daunomycin in solution. Biopolymers, 1979, 18, 553.

94. Patel D.J., Kozlowski S.A. and Rice J.A. Hydrogen bonding, overlap geometry and sequence specificity in anthracycline antitumor antibiotic. DNA complexes in solution. Proc. Natl. Acad. Sci., 1981, 78, 3333.

95. Pettit G.R., Einck J.J., Herald C.L., Ode R.H., Von Dreele R.B., Brown P., Brazhnikova M.G. and Gause G.F. The structure of carminomycin I. J. Am. Chem. Soc., 1975, 97, 7387.

96. Phillips D.R. and Roberts G.C.K. Proton nuclear magnetic resonance study of the self-complementary hexanucleotide $d(pTpA)_3$ and its interaction with daunomycin. Biochemistry, 1980, 19, 4795.

97. Piantini U., Sorensen O.W. and Ernst R.R. J. Am. Chem. Soc., 1982, 104, 6800.

98. Pigram W.J., Fuller W. and Hamilton L.D. Stereochemistry of intercalation : Interaction of daunomycin with DNA. Nature New Biol. 1972, 235, 17.

99. Plumbridge T.W. and Brown, J.R. Spectrophotometric and fluorescence polarization studies of the binding of ethidium, daunomycin and mepacrine to DNA and to poly (I.C). Biochim. Biophys. Acta, 1977, 479, 441.

100. Pohle W., Bohl M., Flemming J. and Bohlig H. Subsidiary hydrogen bonding of intercalated anthraquinone anticancer drugs to DNA phosphate. Biophysical Chemistry, 1990, 35, 213.

101. Quigley G.J., Wang A. H.J., Ughetto G., Marel G.V., Boom J.H.V. and Rich A. Molecular structure of an anticancer drug - DNA complex : Daunomycin plus d(CpGpTpApCpG). Proc. Natl. Acad. Sci., 1980, 77, 7204.

102. Ragg E., Mondelli, R., Battistini C., Garbesi A. and Colona F.P. ^{31}P NMR study of daunorubicin-d(CGTACG) complex in solution. FEBS Lett., 1988, 236, 231.

103. Ravikumar M., Hosur R.V., Roy K.B., Miles H.T. and Govil G. Resonance assignment of the 500 MHz proton NMR spectrum of self complementary dodecanucleotide d-GGATCCGGATCC : Altered conformation at Bam HI cleavage sites. Biochemistry, 1985, 24, 7703.

104. Redfield A.G., Kunj S. and Ralph E.K. Quadrature fourier NMR detection, simple multiplex for dual detection and discussion. J. magn. Reson., 1975, 19, 116.

105. Reid B.R., Baukes K., Flynn P. and Nerdal W. NMR distance measurements in DNA duplexes : sugar and bases have the same correlation times. Biochemistry, 1989, 28, 10001.

106. Remeta D.P., Mudd C.P., Berger R.L. and Breslauer K.J. Thermodynamic characterization of daunomycin-DNA interactions : Microcalorimetric measurements of daunomycin - DNA binding enthalpies. Biochemistry, 1991, 30, 9799.

107. Rinkel L.J. and Altona C. Conformational analysis of the deoxyribofuranose ring in DNA by means of sums of proton-proton coupling constants : A graphical method. J. Biomol. St. Dyn., 1987, 4, 621.

108. Robinson H., Liaw Y.C., Marel G.A.V., Boom J.H.V. and Wang A.H.J. NMR studies on the binding of antitumor drug nogalamycin to DNA hexamer d(CGTACG). Nucleic Acids Res., 1990, 18, 4851.

109. Roche C.J., Thomson J.A. and Crothers D.M. Site selectivity of daunomycin. Biochemistry, 1994, 33, 926.

110. Roche C.J., Berkowitz D., Sulikowski G.A., Danishefsky S.J. and Crothers D.M. Binding affinity and site selectivity of daunomycin analogues. Biochemistry, 1994, 33, 936.

111. Saenger W. (1984) In 'Principles of nucleic acid structure (Cantor C.R. ed.) pp. 9, R.R. Donnelley & Sons, Springer-Verlag New York.

112. Sakore T.D., Jain S.C., Tsai C.C. and Sobell H.M. Mutagen-nucleic acid intercalative binding : structure of a 9-aminoacridine:5-iodocytidylyl (3'-5') guanosine crystalline complex. Proc. Natl. Acad. Sci., 1977, 74, 188.

113. Saucier J.M., Festy B. and Le Pecq J.B. The change of the torsion of the DNA helix caused by intercalation. II - Measurement of the relative change of torsion induced by various intercalating drugs. Biochimie, 1971, 53, 973.

114. Scheek R.M., Russo N., Boelens R., Kaptein R. and Van Boom J.H. Sequential resonance assignments in DNA ^{1}H NMR spectra by two dimensional NOE spectroscopy. J. Am. Chem. Soc., 1983, 105, 2914.

115. Schmitz U., Zon G. and James T.L. Deoxyribose conformation in $[d(GTATATAC)]_2$: Evaluation of sugar pucker by simulation of double quantum filtered COSY cross peaks. Biochemistry, 1990, 29, 2357.

115(a). Schmitz U., Sethson I., Egan W.M. and James T.L. Solution structure of a DNA octamer containing the Pribnow box via restrained molecular dynamics simulation with distance and torsion angle constraints derived fron two-dimensional nuclear magnetic resonance spectral fitting. J. Mol.

Biol., 1992, 227, 510.

116. Scott E.V., Zon G., Marzilli L.G. and Wilson W.D. 2D NMR investigation of the binding of the anticancer drug actinomycin D to duplexed d(ATGCGCAT) : conformational features of the unique 2:1 adduct. Biochemistry, 1988, 27, 7940.

117. Searl M.S., Hall J.G., Denny W.A. and Wakelin L.P.G. NMR studies of the interaction of the antibiotic nogalamycin with hexadeoxyribonucleotide duplex d-$(GCATGC)_2$. Biochemistry, 1988, 27, 4340.

118. Shafer R.H. Spectroscopic studies of the interaction of daunomycin with transfer RNA. Biochem. Pharmacol., 1977, 26, 1729.

119. Skorobogaty A., White R.J., Phillips D.R. and Reiss J.A. The 5'-CA DNA-sequence preference of daunomycin. FEBS Lett., 1988, 227, 103.

120. States D.J., Haberkorn R.A. and Reuben D.J. A two dimensional overhauser experiment with pure absorption phase in four quadrants. J. Magn. Reson., 1982, 48, 286.

121. Sundaralingam M. The concept of a conformationally rigid nucleotide and its significance in polynucleotide conformational analysis. Jerus. Symp. Quant. Chem. Biochem., 1973, 5, 417.

122. Sundaralingam M. Principles governing nucleic acid and polynucleotide conformations. In "Structure and

conformation of nucleic acids and protein-nucleic acid interactions". (Sundaralingam, M. and Rao, S.T., eds.), University Park Press, Baltimore, 1975, 487.

123. Van Wijk J., Huckriede B.D., Ippel J.H. and Altona C. Furanose sugar conformations in DNA from NMR coupling constants. Methods in enzymology, 1992, 211, 286.

123(a). Van de Van F.J.M. and Hilbers C.W. Nucleic acids and nuclear magnetic resonance. Eur. J. Biochem., 1988, 178, 1.

124. Wang A.H.J., Nathans J., Marel G.V., Boom J.H.V. and Rich A. Molecular structure of a double helical DNA fragment intercalator complex between deoxy-CpG and a terpyridine platinum compound. Nature, 1978, 276, 471.

125. Wang A.H.J., Ughetto G., Quigley G.J., Hakoshima T., Van der Marel G.A., Van Boom J.H. and Rich A. The molecular structure of a DNA-Triostin A complex. Science, 1984, 225, 1115.

126. Wang A.H.J., Ughetto G., Quigley G.J. and Rich A. Interaction between an anthracycline antibiotic and DNA. Molecular structure of daunomycin complexed to d(CpGpTpApCpG) at 1.2 A° resolution. Biochemistry, 1987, 26, 1152.

127. Wang A.H.J., Gao Y.G., Liaw Y.C. and Li Y.K. Formaldehyde cross-links daunorubicin and DNA efficiently : HPLC and x-ray diffraction studies. Biochemistry, 1991, 30, 3812.

128. Waring M. Variation of the supercoils in closed circular DNA by binding of antibiotics and drugs : Evidence for molecular models involving intercalation. J. Mol. Biol., 1970, 54, 247.

129. Widmer H. and Wuthrich K. Simulated two-dimensional NMR cross-peak fine structures for ^{1}H spin systems in polypeptides and polydeoxynucleotides. J. Magn. Reson., 1987, 74, 316.

129(a). Widmer H. and Wuthrich K. J. Magn. Reson., 1986, 70, 270.

130. Williams L.D., Frederick C.A., Ughetto G. and Rich A. Ternary interactions of spermine with DNA : 4'-epiadriamycin and other DNA :anthracycline complexes. Nucleic Acids Res., 1990, 18, 5533.

131. Wuthrich, K. (1986) In 'NMR of proteins and nucleic acids', John Wiley, New York.

132. Xodo L.E., Manzini G., Ruggiero J. and Quadrifoglio F. On the interaction of daunomycin with synthetic alternating DNAs : Sequence specificity and polyelectrolyte effects on the intercalation equilibrium. Biopolymers, 1988, 27, 1839.

133. Yang D. and Wang A.H.J. Structure by NMR of antitumor drugs aclacinomycin A and B complexed to d(CGTACG). Biochemistry, 1994, 33, 6595.

134. Zhang X. and Patel D.J. Solution structure of the nogalamycin-DNA complex. Biochemistry, 1990, 29, 9451.

135. Zunino F., Gambetta R., Di Marco A. and Zaccara A. Interaction of daunomycin and its derivatives with DNA. Biochim. Biophys. Acta., 1972, 277, 489.

136. Zunino F., Di Marco A. and Zaccara A. and Luoni G. Chem. Biol. Interactions, 1974, 9, 35.

137. Zunino F., Gambetta R., Di Marco A., Luoni G. and Zaccara A. Effects of the stereochemical configuration on the interaction of some daunomycin derivatives with DNA. Biochim. Biophys. Res. Commun., 1976, 69, 744.